Methods in
Molecular Biology 1944

Springer Protocols

Irit Sagi · Nikolaos A. Afratis *Editors*

Collagen

Methods and Protocols

Humana Press

METHODS IN MOLECULAR BIOLOGY

Series Editor
John M. Walker
School of Life and Medical Sciences
University of Hertfordshire
Hatfield, Hertfordshire, AL10 9AB, UK

For further volumes:
http://www.springer.com/series/7651

Collagen

Methods and Protocols

Edited by

Irit Sagi and Nikolaos A. Afratis

Department of Biological Regulation, Weizmann Institute of Science, Rehovot, Israel

Humana Press

Editors
Irit Sagi
Department of Biological Regulation
Weizmann Institute of Science
Rehovot, Israel

Nikolaos A. Afratis
Department of Biological Regulation
Weizmann Institute of Science
Rehovot, Israel

ISSN 1064-3745 ISSN 1940-6029 (electronic)
Methods in Molecular Biology
ISBN 978-1-4939-9094-8 ISBN 978-1-4939-9095-5 (eBook)
https://doi.org/10.1007/978-1-4939-9095-5

Library of Congress Control Number: 2019930144

© Springer Science+Business Media, LLC, part of Springer Nature 2019
This work is subject to copyright. All rights are reserved by the Publisher, whether the whole or part of the material is concerned, specifically the rights of translation, reprinting, reuse of illustrations, recitation, broadcasting, reproduction on microfilms or in any other physical way, and transmission or information storage and retrieval, electronic adaptation, computer software, or by similar or dissimilar methodology now known or hereafter developed.
The use of general descriptive names, registered names, trademarks, service marks, etc. in this publication does not imply, even in the absence of a specific statement, that such names are exempt from the relevant protective laws and regulations and therefore free for general use.
The publisher, the authors, and the editors are safe to assume that the advice and information in this book are believed to be true and accurate at the date of publication. Neither the publisher nor the authors or the editors give a warranty, express or implied, with respect to the material contained herein or for any errors or omissions that may have been made. The publisher remains neutral with regard to jurisdictional claims in published maps and institutional affiliations.

This Humana Press imprint is published by the registered company Springer Science+Business Media, LLC, part of Springer Nature.
The registered company address is: 233 Spring Street, New York, NY 10013, U.S.A.

Preface

Collagen is the most abundant protein in mammals, making up about 25% of the whole-body protein content. Collagen is involved in many physiological and pathological situations. Specifically, collagen has been shown to be involved either directly or indirectly in the promotion of cell adhesion and differentiation, cell functions that are related to the control of embryonic development and regeneration. However, the uncontrolled synthesis and accumulation of collagen from fibroblasts lead to pathological conditions in fibrotic-related diseases and tumorigenesis.

Collagen is the main structural protein in extracellular matrix and connective tissue. The basic fundamental structure consists of three coiled subunits: two α1(I) chains and one α2 (I). There are at least 26 different types of collagen, and all of them contain three-stranded helical segments of similar structure. The differentiation between each type of collagen is due to segments that interrupt the triple helix and that fold into other kinds of three-dimensional structures. Collagen types I, II, and III consist the 80% of the collagen in the body.

Collagen is widely used in many applications like food, cosmetics, pharmaceuticals, cosmetic surgery, artificial skin, and glue (the name *collagen* comes from the Greek κόλλα (*kólla*), meaning "glue," and suffix -γέν, *-gen*, denoting "producing"). The importance of collagen in health and disease and the interest of the researchers to further investigate the in vitro and in vivo mechanisms of collagen were the objective reasons that motivated us to create this *Collagen: Methods and Protocols* book. This volume compiles a collection of state-of-the-art protocols that will serve not only as recipes for bench scientists but also as accepted methods for the collagen field. Each chapter describes a specific topic and technique by an expert in the field and provides a detailed protocol, which includes some most helpful tips in the Notes section.

The content of the book is separated into four different parts. Specifically, Part I focuses on in vitro models for the characterization of collagen formation. In detail, it describes a mimetic model for mineralization of type-I collagen fibrils, cross-linked collagen scaffolds, and methods to clone, mutate, and isolate collagen. Part II highlights a large-scale analysis of collagen with mass spectrometry in order to elucidate the proteomics, degradomics, interactomes, and cross-linking of collagen. It also presents the triple-helix hydroxylation of collagen by solid-state NMR spectroscopy.

Furthermore, Part III describes high-resolution imaging approaches for collagen by the use of scanning electron microscopy and multiphoton imaging. In addition, a new tool for degraded and denatured collagen histopathology and collagen-binding integrin analysis is presented. Finally, Part IV introduces the role of collagen during physiological and pathological conditions and provides an overview of collagenous matrix in tumor microenvironment. The reader will find protocols to analyze the collagen levels from primary fibroblasts, to produce collagen-based peptides for inhibition of matrix metalloproteinases, and to assess collagen deposition during aging and liver fibrosis.

We hope that this volume on collagen will be a useful tool for the scientists working in the field and will inspire them to develop new techniques and models that will create the next generation of collagen protocols. We would also like to thank all the authors and co-authors that participated on this book for their tremendous contributions. It was a great pleasure to work with all of them, and we believe that their effort was critical for the high quality and repeatability of the research protocols.

Rehovot, Israel

Irit Sagi
Nikolaos A. Afratis

Contents

Preface . . . . . *v*
Contributors . . . . . *ix*

PART I IN VITRO MODELS FOR COLLAGEN CHARACTERIZATION

1 Cloning and Mutagenesis Strategies for Large Collagens 3
Olivier Bornert and Alexander Nyström

2 Multi-well Fibrillation Assay as a Tool for Analyzing Crosslinking and Stabilization of Collagen 17
Venkat Raghavan Krishnaswamy

3 Production and Characterization of Chemically Cross-Linked Collagen Scaffolds 23
Ignacio Sallent, Héctor Capella-Monsonís, and Dimitrios I. Zeugolis

4 A Biomimetic Model for Mineralization of Type-I Collagen Fibrils 39
Shasha Yao, Yifei Xu, Changyu Shao, Fabio Nudelman, Nico A. J. M. Sommerdijk, and Ruikang Tang

PART II PROTEOMICS ANALYSIS OF COLLAGEN

5 Investigation of Triple-Helix Collagen Hydroxylation by Solid-State NMR Spectroscopy 57
Wing Ying Chow

6 Measurement of Collagen Cross-Links from Tissue Samples by Mass Spectrometry 79
Amar Joshi, Amna Zahoor, and Alberto Buson

7 Mass Spectrometry-Based Proteomics to Define Intracellular Collagen Interactomes 95
Ngoc-Duc Doan, Andrew S. DiChiara, Amanda M. Del Rosario, Richard P. Schiavoni, and Matthew D. Shoulders

8 Exploring Extracellular Matrix Degradomes by TMT-TAILS N-Terminomics 115
Elizabeta Madzharova, Fabio Sabino, and Ulrich auf dem Keller

PART III IMAGING APPROACHES FOR COLLAGEN

9 Sample Preparation of Extracellular Matrix of Murine Colons for Scanning Electron Microscopy 129
Elee Shimshoni and Irit Sagi

10 In Situ Detection of Degraded and Denatured Collagen via Triple Helical Hybridization: New Tool in Histopathology 135
Yang Li and S. Michael Yu

11 Combination of Traction Assays and Multiphoton Imaging to Quantify Skin Biomechanics 145
Stéphane Bancelin, Barbara Lynch, Christelle Bonod-Bidaud, Petr Dokládal, Florence Ruggiero, Jean-Marc Allain, and Marie-Claire Schanne-Klein

12 Analysis of Collagen-Binding Integrin Interactions with Supramolecular Aggregates of the Extracellular Matrix 157
Uwe Hansen

PART IV COLLAGEN IN HEALTH AND DISEASE

13 Assessing Collagen Deposition During Aging in Mammalian Tissue and in *Caenorhabditis elegans* 169
Alina C. Teuscher, Cyril Statzer, Sophia Pantasis, Mattia R. Bordoli, and Collin Y. Ewald

14 Procollagen C-Proteinase Enhancer 1 (PCPE-1) in Liver Fibrosis 189
Efrat Kessler and Eyal Hassoun

15 Tumorigenic Interplay Between Macrophages and Collagenous Matrix in the Tumor Microenvironment 203
Chen Varol

16 FACS Analysis of Col1α Protein Levels in Primary Fibroblasts 221
Noam Cohen and Neta Erez

17 Methods for the Construction of Collagen-Based Triple-Helical Peptides Designed as Matrix Metalloproteinase Inhibitors 229
Gregg B. Fields

Index *253*

Contributors

Jean-Marc Allain • *Laboratoire de Mécanique des Solides (LMS), Ecole Polytechnique, CNRS, Université Paris-Saclay, Palaiseau, France; Inria, Université Paris-Saclay, Palaiseau, France*

Ulrich auf dem Keller • *Department of Biotechnology and Biomedicine, Technical University of Denmark, Kongens Lyngby, Denmark*

Stéphane Bancelin • *Laboratoire d'Optique et Biosciences (LOB), Ecole Polytechnique, CNRS, INSERM, Université Paris-Saclay, Palaiseau, France; Institut Interdisciplinaire de Neurosciences, CNRS, Université de Bordeaux, Bordeaux, France*

Christelle Bonod-Bidaud • *Institut de Génomique Fonctionnelle de Lyon, ENS-Lyon, CNRS UMR 5242, Université de Lyon, Lyon, France; Tissue Biology and Therapeutic Engineering Unit, LBTI, CNRS UMR 5305, Univ. Lyon, Université Claude Bernard Lyon 1, Lyon, France*

Mattia R. Bordoli • *Department of Biology, Institute of Molecular Health Sciences, Eidgenössische Technische Hochschule (ETH) Zürich, Zürich, Switzerland*

Olivier Bornert • *Department of Dermatology, Faculty of Medicine, Medical Center, University of Freiburg, Freiburg, Germany*

Alberto Buson • *Pharmaxis Drug Discovery, Frenchs Forest, NSW, Australia*

Héctor Capella-Monsonís • *Regenerative, Modular and Developmental Engineering Laboratory (REMODEL), National University of Ireland Galway (NUI Galway), Galway, Ireland; Science Foundation Ireland (SFI) Centre for Research in Medical Devices (CÚRAM), National University of Ireland Galway (NUI Galway), Galway, Ireland*

Wing Ying Chow • *Leibniz-Forschungsinstitut für Molekulare Pharmakologie (FMP), Berlin, Germany*

Noam Cohen • *Department of Pathology, Sackler School of Medicine, Tel Aviv University, Tel Aviv, Israel*

Amanda M. Del Rosario • *Koch Institute, Massachusetts Institute of Technology, Cambridge, MA, USA*

Andrew S. DiChiara • *Department of Chemistry, Massachusetts Institute of Technology, Cambridge, MA, USA*

Ngoc-Duc Doan • *Department of Chemistry, Massachusetts Institute of Technology, Cambridge, MA, USA*

Petr Dokládal • *Centre for Mathematical Morphology, MINES ParisTech, PSL Research University, Fontainebleau, France*

Neta Erez • *Department of Pathology, Sackler School of Medicine, Tel Aviv University, Tel Aviv, Israel*

Collin Y. Ewald • *Department of Health Sciences and Technology, Institute of Translational Medicine, Eidgenössische Technische Hochschule (ETH) Zürich, Zürich, Switzerland*

Gregg B. Fields • *Department of Chemistry and Biochemistry, Florida Atlantic University, Jupiter, FL, USA; Department of Chemistry, Scripps Research, Jupiter, FL, USA*

Uwe Hansen • *Institute of Musculoskeletal Medicine, University Hospital Münster, Münster, Germany*

Eyal Hassoun • *Clinical Biochemistry and Pharmacology Institute, Tel Aviv Sourasky Medical Center, Tel Aviv, Israel*

Amar Joshi • *Pharmaxis Drug Discovery, Frenchs Forest, NSW, Australia*
Efrat Kessler • *Maurice and Gabriela Goldschleger Eye Research Institute, Sheba Medical Center, Sackler Faculty of Medicine, Tel Aviv University, Tel-Hashomer, Israel; Clinical Biochemistry and Pharmacology Institute, Tel Aviv Sourasky Medical Center, Tel Aviv, Israel*
Venkat Raghavan Krishnaswamy • *Department of Biological Regulation, Weizmann Institute of Science, Rehovot, Israel*
Yang Li • *Department of Bioengineering, University of Utah, Salt Lake City, UT, USA; 3Helix Inc., Salt Lake City, UT, USA*
Barbara Lynch • *Laboratoire de Mécanique des Solides (LMS), Ecole Polytechnique, CNRS, Université Paris-Saclay, Palaiseau, France; L'Oréal Research and Innovation, Aulnay-sous-Bois, France*
Elizabeta Madzharova • *Department of Biotechnology and Biomedicine, Technical University of Denmark, Kongens Lyngby, Denmark*
Fabio Nudelman • *School of Chemistry, University of Edinburgh, Edinburgh, UK*
Alexander Nyström • *Department of Dermatology, Faculty of Medicine, Medical Center, University of Freiburg, Freiburg, Germany*
Sophia Pantasis • *Department of Biology, Institute of Molecular Health Sciences, Eidgenössische Technische Hochschule (ETH) Zürich, Zürich, Switzerland*
Florence Ruggiero • *Institut de Génomique Fonctionnelle de Lyon, ENS-Lyon, CNRS UMR 5242, Université de Lyon, Lyon, France*
Fabio Sabino • *Department of Biotechnology and Biomedicine, Technical University of Denmark, Kongens Lyngby, Denmark*
Irit Sagi • *Department of Biological Regulation, Weizmann Institute of Science, Rehovot, Israel*
Ignacio Sallent • *Regenerative, Modular and Developmental Engineering Laboratory (REMODEL), National University of Ireland Galway (NUI Galway), Galway, Ireland; Science Foundation Ireland (SFI) Centre for Research in Medical Devices (CURAM), National University of Ireland Galway (NUI Galway), Galway, Ireland*
Marie-Claire Schanne-Klein • *Laboratoire d'Optique et Biosciences (LOB), Ecole Polytechnique, CNRS, INSERM, Université Paris-Saclay, Palaiseau, France*
Richard P. Schiavoni • *Koch Institute, Massachusetts Institute of Technology, Cambridge, MA, USA*
Changyu Shao • *Department of Chemistry, Center for Biomaterials and Biopathways, Zhejiang University, Hangzhou, Zhejiang, China*
Elee Shimshoni • *Department of Biological Regulation, Weizmann Institute of Science, Rehovot, Israel*
Matthew D. Shoulders • *Department of Chemistry, Massachusetts Institute of Technology, Cambridge, MA, USA*
Nico A. J. M. Sommerdijk • *Laboratory of Materials and Interface Chemistry, Department of Chemical Engineering and Chemistry, Center for Multiscale Electron Microscopy, Eindhoven University of Technology, Eindhoven, The Netherlands; Institute for Complex Molecular Systems, Eindhoven University of Technology, Eindhoven, The Netherlands*
Cyril Statzer • *Department of Health Sciences and Technology, Institute of Translational Medicine, Eidgenössische Technische Hochschule (ETH) Zürich, Zürich, Switzerland*
Ruikang Tang • *Department of Chemistry, Center for Biomaterials and Biopathways, Zhejiang University, Hangzhou, Zhejiang, China*

ALINA C. TEUSCHER • *Department of Health Sciences and Technology, Institute of Translational Medicine, Eidgenössische Technische Hochschule (ETH) Zürich, Zürich, Switzerland*

CHEN VAROL • *The Research Center for Digestive Tract and Liver Diseases, Sourasky Medical Center, Sackler School of Medicine, Tel Aviv University, Tel Aviv, Israel; Department of Clinical Microbiology and Immunology, Sackler School of Medicine, Tel Aviv University, Tel Aviv, Israel*

YIFEI XU • *Laboratory of Materials and Interface Chemistry, Department of Chemical Engineering and Chemistry, Center for Multiscale Electron Microscopy, Eindhoven University of Technology, Eindhoven, The Netherlands; Institute for Complex Molecular Systems, Eindhoven University of Technology, Eindhoven, The Netherlands*

SHASHA YAO • *Department of Chemistry, Center for Biomaterials and Biopathways, Zhejiang University, Hangzhou, Zhejiang, China*

S. MICHAEL YU • *Department of Bioengineering, University of Utah, Salt Lake City, UT, USA; Department of Pharmaceutics and Pharmaceutical Chemistry, University of Utah, Salt Lake City, UT, USA*

AMNA ZAHOOR • *Pharmaxis Drug Discovery, Frenchs Forest, NSW, Australia*

DIMITRIOS I. ZEUGOLIS • *Regenerative, Modular and Developmental Engineering Laboratory (REMODEL), National University of Ireland Galway (NUI Galway), Galway, Ireland; Science Foundation Ireland (SFI) Centre for Research in Medical Devices (CÚRAM), National University of Ireland Galway (NUI Galway), Galway, Ireland*

Part I

In Vitro Models for Collagen Characterization

Chapter 1

Cloning and Mutagenesis Strategies for Large Collagens

Olivier Bornert and Alexander Nyström

Abstract

The size and relatively high GC content of cDNAs are challenges for efficient targeted engineering of large collagens. There are both basic biological and therapeutic interests in the ability to modify collagens, as this would allow for studies precisely describing interactions of collagens with specific interaction partners, addressing consequences of individual disease-causing mutations, and assessing therapeutic applicability of precision medicine approaches. Using collagen VII as an example, we will here describe a strategy for rapid and simple modification of cDNAs encoding large collagens. The method is flexible and can be used for the creation of point mutations, small or large deletions, and insertion of DNA.

Key words Collagen VII, Gibson assembly, Dystrophic epidermolysis bullosa, Collagenopathy, Exon skipping

1 Introduction

Size, repetitive sequences, and GC-rich content are factors that pose challenges for cloning and targeted modification of large collagens [1]. The ability to recombinantly express collagens with specific point mutations and small or large deletions is an important tool that can be used for addressing a multitude of biological and clinical questions surrounding individual collagens or a group of them. These questions encompass understanding of the specific interactome of a collagen, understanding of disease mechanisms underlying specific mutations causing a collagenopathy, and the potential therapeutic applicability of collagens shortened by targeted deletion [2–5]. Multiple strategies are available that can be applied to successfully mutate or delete parts in long, complex cDNAs. However, a majority of these strategies involve multiple cloning steps with cutting and pasting out and in of different vectors. We and others have previously used such approaches to successfully clone and express recombinant wild-type collagen VII or collagen VII variants with targeted deletions [2, 3,

Irit Sagi and Nikolaos A. Afratis (eds.), *Collagen: Methods and Protocols*, Methods in Molecular Biology, vol. 1944, https://doi.org/10.1007/978-1-4939-9095-5_1, © Springer Science+Business Media, LLC, part of Springer Nature 2019

5–7]. By incorporating enzymatic assembly of overlapping DNA fragments developed by Gibson and co-workers [8, 9] in our workflow of mutating, expressing, and purifying modified recombinant collagen VII, we have been able to minimize the steps needed for this, leading to a significantly streamlined process with higher fidelity.

We focus our work on collagen VII. Collagen VII is a large collagen with a length and molecular weight close to 400 nm and 1 MDa, respectively [10]. It has a big N-terminal non-collagenous (NC1) domain, followed by the largest uninterrupted collagenous domain in mammalian, and a short C-terminal NC2 domain, which is essential for antiparallel dimerization [10, 11]. Outside the cell, two collagen VII molecules align in a tail-to-tail fashion; processing of the NC2 domain by astacin-like family proteases allows for the formation of disulfide bonds between two molecules leading to the creation of stable antiparallel dimers [12–14]. Lateral aggregation of the dimers produces electron-dense structures that loop through the lamina densa down to the superficial papillary dermal matrix—these structures are known as anchoring fibrils. The anchoring fibrils confer dermal stability through high affinity to laminin-332 and collagen IV in the epidermal basement membrane and physical entrapment of collagen fibrils in the dermal loops [11]. In addition to skin stability, collagen VII is essential for correct epidermal and dermal healing after wounding by aiding organization of the epidermal basement membrane and regulating fibroblast activation [15]. Genetically evoked loss of abundance or function of collagen VII causes the skin blistering disease dystrophic epidermolysis bullosa (DEB), which in its most severe forms is a severely debilitating disease [16]. There are active research efforts toward improving the treatment of DEB. One feature that can be exploited for therapy which collagen VII also shares with most fibrillar collagens is that the majority of its exons is in frame and ends with a full codon [2, 17]. Skipping or deletion of exons carrying mutations could be used as one means to correct the mRNA, resulting in a shorter but still functional protein [17]. Indeed, multiple reports of naturally occurring skipping of mutated exons have shown that this can lead to a milder DEB phenotype [18–21]. Preclinical studies have also shown that targeted permanent deletion or antisense oligonucleotide-mediated exon skipping on the pre-mRNA level can increase the abundance of collagen VII molecules, which are slightly shortened but retain sufficient functionality to restore dermal-epidermal cohesion [2, 22–25]. However, studies on other diseases suggest that in some cases exon skipping worsen the phenotype [26] and thus the functionality of proteins resulting from exon skipping cannot be generalized. Accordingly, clinical applicability of these approaches has to be assessed on an exon-to-exon-based basis, to determine the functionality of protein variants lacking the amino acids encoded by specific exons.

We will here present our new optimized workflow for precision engineering of large collagens. The approach is rapid and flexible, allowing for direct cDNA creation of point mutations, insertion of DNA, and deletion of small to large regions. It can also be applied for other large proteins or proteins encoded by GC-rich genes.

2 Materials

2.1 Polymerase Chain Reaction (PCR)

1. Phusion® high-Fidelity PCR master mix with high-fidelity buffer.
2. 10 mM DNA primers in ultrapure water.
3. Thermocycler.
4. 1% Agarose gel: Dissolve 1 g of agarose in 100 ml of Tris-acetate-EDTA (TAE) buffer (40 mM Trizma® base, 40 mM acetate, 1 mM EDTA pH 8.0) by boiling the solution. Add 2 μl GelRed® fluorescent nucleic acid dye and cast the gel with the appropriate gel comb.
5. 6× loading dye.
6. Amersham imager 600.
7. GeneJET Extraction Kit.
8. NanoDrop™ 1000 Spectrophotometer.

2.2 Gibson Reaction and Bacterial Transformation

1. NEBuilder® HiFi DNA Assembly Cloning Kit.
2. Thermocycler.
3. Luria broth (LB)-ampicillin agar plates: dissolve 3.7 g of LB agar MILLER in 100 ml of ultrapure water. After sterilization of the medium with an autoclave, 100 μg/ml of ampicillin is added to the medium when the temperature of the mixture is lower than 50 °C. Pour the solution into petri dish plates until it covers the bottom.
4. NEB® 10-alpha competent *E. coli* bacteria.
5. Water bath at 42 °C.
6. Incubator at 37 °C.
7. LB medium: Dissolve 2.5 g of LB medium in 100 ml of ultrapure water, and sterilize the medium with an autoclave.
8. 100 mg/ml ampicillin.
9. 15 ml round-bottom tube.
10. 500 ml Erlenmeyer flask.
11. PCR products and plasmids purification kit, e.g., GeneJET plasmid Miniprep Kit.
12. HiSpeed Plasmid Maxi Kit.
13. Incubator at 37 °C with shacking plate.

2.3 Recombinant Expression of Collagen VII

1. Human Embryonic Kidney (HEK) 293 cells.
2. DMEM/F12 medium: Dulbecco's Modified Eagle medium/F12 supplemented with 10% Bovine Serum Albumin, 1% penicillin–streptomycin, 1% antibiotic–antimycotic, and 1% L-glutamine.
3. Lipofectamine® 2000.
4. Opti-MEM Reduced Serum Medium.
5. 20 mg/ml phleomycin
6. 10 cm cell culture dish
7. Blue sample buffer (BSB) 4×: 4 M Urea, 0.5 M Trizma® base, 0.05% bromophenol blue, 10% SDS, 50% glycerol, 0.25 M DTT, pH 6.8.
8. 7.5% Mini-PROTEAN® TGX precast gels (*see* **Note 1**)
9. Mini-PROTEAN® Tetra Vertical Electrophoresis cell.
10. TGS electrophoresis buffer: 25 mM Trizma® base, 192 mM glycine, 0.1% SDS, pH 8.3.
11. Criterion™ blotter.
12. Transfer buffer: 1× Tris-borate (TB) buffer, 50 mM Trizma® base, and 50 mM boric acid (*see* **Note 2**).
13. Amersham Protran nitrocellulose membrane.
14. Antibodies: Rabbit polyclonal antibody directed against the epitope of the mouse monoclonal LH7.2 antibody (homemade and verified to be specific for collagen VII [27], the epitope is in the NC1 domain of collagen VII) and rabbit polyclonal ProC7 antibody (homemade, raised against the end of the NC2 domain of collagen VII; specific for the pro-form of collagen VII) (*see* **Note 3**).
15. Tris-buffered saline-Tween 20 (TBS-T): 50 mM Trizma® base, 150 mM NaCl, 0.05% Tween 20, pH 7.4.
16. Blocking buffer: TBS-T + 5% nonfat dry milk.
17. Enhanced chemiluminescence detection reagent, e.g., ECL™ Prime.
18. Developing system, e.g., Amersham™ imager 600.
19. 1× Phospho-buffered saline (PBS).
20. 50 μg/ml L-Ascorbic acid.
21. 50 ml Falcon Conical Centrifuge Tube.
22. 1 mM Pefabloc.
23. 500 mM EDTA pH 8.0.
24. Collagen IV.
25. 100 ng laminin-332.

3 Methods

3.1 Strategy Design and Generation of DNA Fragments with Overlapping Ends

1. First, a strategy that will be used to modify the DNA sequence of the target cDNA has to be designed. As an example, we will describe a procedure to remove a specific DNA region (from a few amino acids to deletion of large sequences) from *COL7A1* cDNA cloned into the vector pcDNA3.1 (Fig. 1).
2. The strategy is based on the use of PCR dividing the target cDNA and vector, in this case *COL7A1* and pcDNA3.1, into fragments. In order to allow efficient amplification of the fragments by PCR, dividing the mother sequence into fragments of 2.5 to 3 kb maximum is recommended.
3. As shown in Fig. 1, the strategy described here can be used to delete a specific region of DNA. Not described here, by using

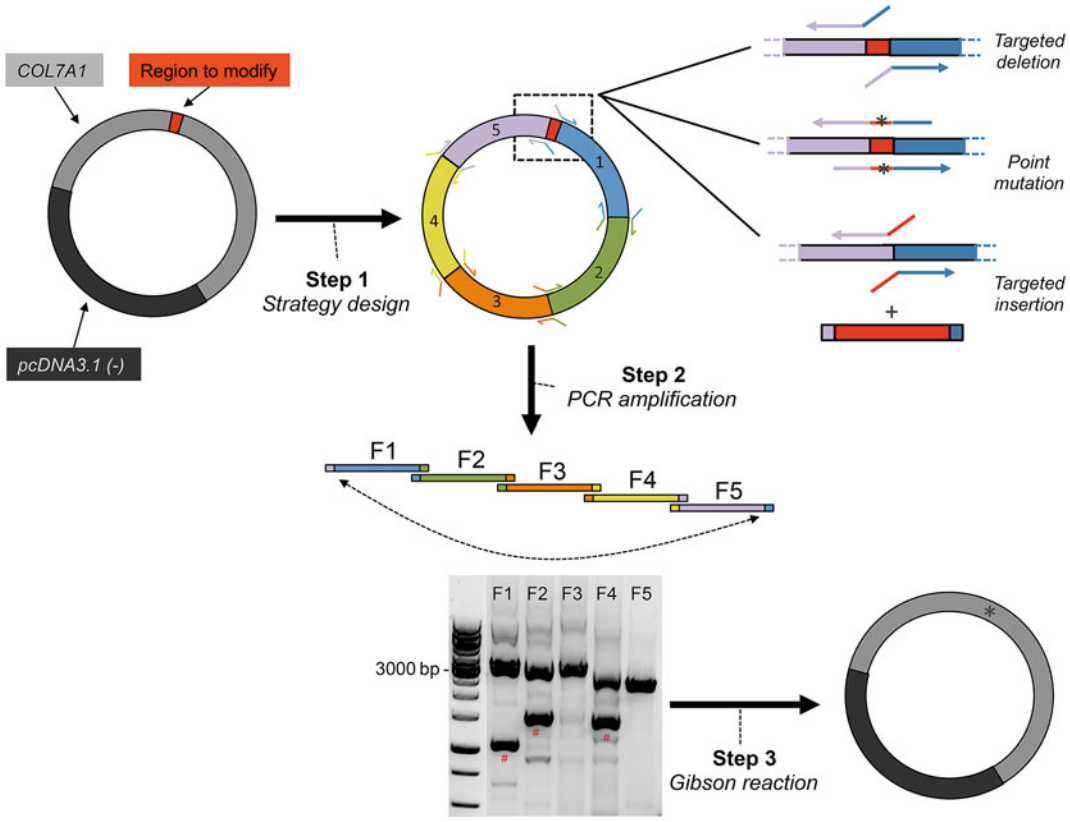

Fig. 1 Mutagenesis of *COL7A1* using Gibson cloning. This figure presents an overview of the strategy used to modify the *COL7A1* cDNA sequence in the pcDNA3.1 vector by Gibson assembly. In step 1, specific pairs of primers with overlapping sequence are designed to ensure reconstitution of the mother DNA construct, as well as excision of a specific DNA sequence in *COL7A1*. These primers are then used to amplify selected regions of the mother DNA construct (step 2). Finally, through Gibson reaction (step 3), the fragments are assembled together in order to create a new DNA construct lacking the target DNA sequence

Table 1
Primers used for amplification of *COL7A1* and deletion of exon73. Primers used to delete exon73 are shown in red. Overlap is indicated with lower case

Primer name	Sequence (5' to 3')	Location (bp)
Ex73_F1_fwd	aatcaggggaTAACGCAGGAAAGAACATGTGAG	Cloning vector
Ex73_F1_rev	agtgcatccaGGCCGAACTCTGTCCGTG	COL7A1 (299-326)
Ex73_F2_fwd	gagttcggccTGGATGCACTTGGCTCTG	COL7A1 (307-334)
Ex73_F2_rev	tccaggacccTCCTCGTAGCCTCCGCAC	COL7A1 (3239-3266)
Ex73_F3_fwd	gctacgaggaGGGTCCTGGAGCGTCTGG	COL7A1 (3247-3274)
Ex73_F3_rev	cccgttctccCTCCTTGCCTGGGGGGCC	COL7A1 (5998-6015.....6216-6225)
Ex73_F4_fwd	aggcaaggagGGAGAACGGGGAGAGAAAG	COL7A1 (6008-6015.....6216-6235)
Ex73_F4_rev	ataccccctagagCCCCAGCTGGTTCTTTCC	Cloning vector
Ex73_F5_fwd	ccagctggggCTCTAGGGGGTATCCCCAC	Cloning vector
Ex73_F5_rev	tcctgcgttaTCCCCTGATTCTGTGGATAAC	Cloning vector

overlapping primer containing point mutations, one or more nucleotides in a DNA sequence can be modified. Insertion of DNA is also possible by in vitro synthesis or PCR amplification of a piece of DNA with ends that overlap with the region where it should be inserted.

4. To illustrate the approach, we have chosen to present deletion of the nucleotides corresponding to exon73 from *COL7A1* cDNA. Listed in Table 1 are the primers used to achieve this; the overlap and specific sequences are shown by lower case and capital letters, respectively. The primers designed to delete exon73 are shown in red (Table 1).
5. PCR primers that will be used to amplify the DNA fragments must contain an overlap sequence of 10 nucleotides from the adjacent fragments together with a specific sequence for the region to be amplified (15–25 nucleotides) (Table 1). Even though the design of the primers can be done manually [9], we recommend to use the online tool, NEBuilder® assembly tool, available at nebuilder.neb.com.
6. On ice, add 0.05 mM of each primer together with 1 ng of the vector pcDNA3.1 containing COL7A1 cDNA to a 1.5 ml Eppendorf tube. Increase volume to 10 μl with ultrapure sterile water. Then, combine 10 μl of Phusion® High-Fidelity PCR Master Mix with high-fidelity buffer to the mixture.
7. The following thermocycling conditions are commonly used by us to amplify the DNA fragments:

Initial denaturation	98 °C	2 min	1 cycle
Denaturation Annealing[a] Extension[a]	98 °C 60 °C 72 °C	30 s 30 s 1 min	35 cycles
Final extension	72 °C	5 min	1 cycle
Hold	4 °C		

[a] *See* **Note 4**

8. After amplification, add 4 μl of loading dye to the PCR reaction. Load samples on a 1% agarose gel, and perform migration at 120 V for approximately 1 h in TAE buffer. PCR products can be visualized using Amersham™ imager 600 equipped with a UV lamp. Next, bands corresponding to the desired products are cut out from the gel using a scalpel. The DNA fragments are then extracted from the gel and purified using GeneJET Extraction Kit. The concentration of the extracted DNA fragments can be determined using a NanoDrop™ 1000 Spectrophotometer (*see* **Note 5**).
9. As assembly of more than four fragments using Gibson cloning is challenging, we recommend a minimal concentration of 20 ng/μl in a volume of at least 20 μl for the DNA fragments. PCR can be repeated if the quantity is not sufficient.

3.2 Gibson Assembly and Bacterial Transformation

1. Mix 50 ng of each PCR product together in a PCR tube. For optimal reaction, the total volume should not exceed 20 μl (*see* **Note 6**). Add a 1:1 volume of NEBuilder® HiFi DNA assembly 2× Master Mix to the mixture. A control reaction lacking one of the fragments is highly recommended to assess the efficacy and specificity of the reaction.
2. Incubate reactions in a thermocycler at 50 °C for 60 min. Figure 2 provides a detailed step-by-step illustration of the Gibson assembly® strategy [9]. Following incubation, samples can be used directly or stored at −20 °C for subsequent transformation.
3. Thaw on ice NEB 10-alpha (*see* **Note 7**) Competent *E. coli* bacteria, and incubate 2 μl of the assembled product with 50 μl the bacteria for 30 min on ice. Heat shock the samples at 42 °C during 45 s, and cool down on ice for 2 min. Resuspend the transformed bacteria in 200 μl Super Optimal broth with Catabolite repression (SOC) medium, and plate the mixture on a LB-agar-ampicillin petri dish. Incubate the plate at 37 °C overnight.
4. Select ten clones for analysis, and resuspend them individually in 3 ml of LB medium with 100 μg/ml ampicillin in a 15 ml

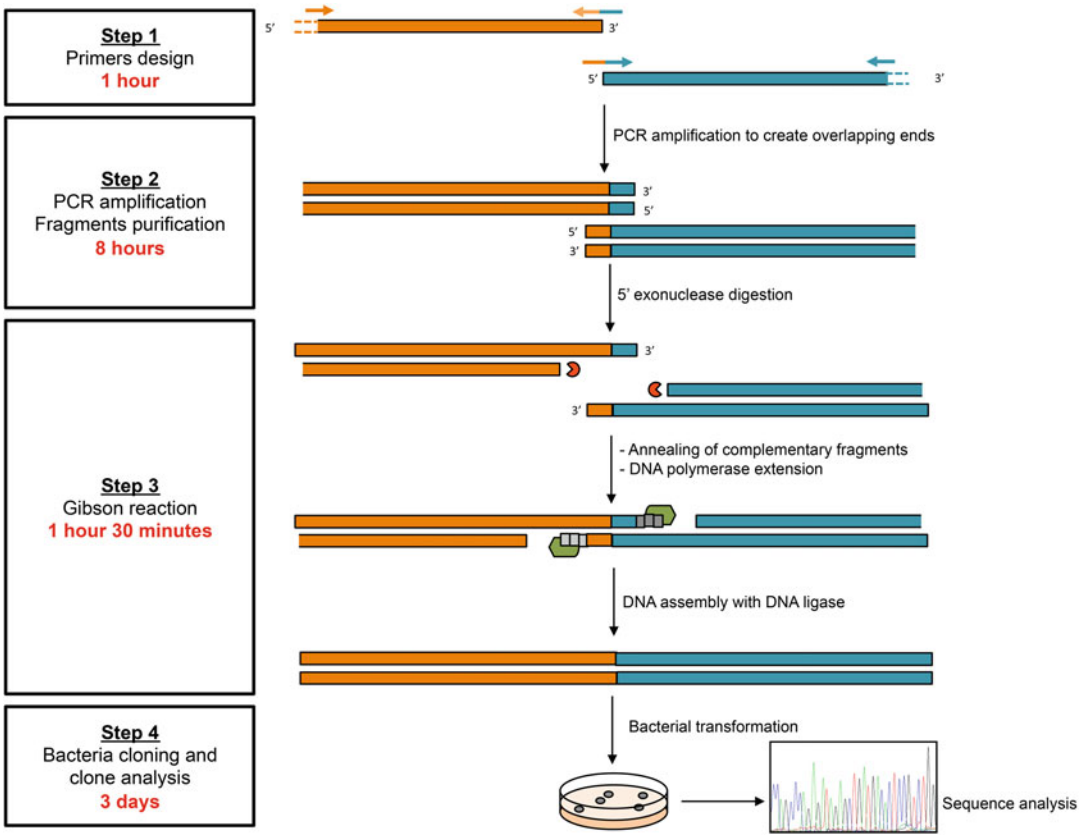

Fig. 2 Gibson cloning in detail. In order to assemble two pieces of DNA together using Gibson assembly, it is necessary to design primers containing a sequence that binds to the mother sequence and an overlapping end, which correspond to the second DNA fragment. After amplification by PCR, the 5′ end will be digested with a 5′ exonuclease. Then, complementary DNA sequences will anneal together, and a DNA polymerase will be used to extend the fragment. After sealing of the gaps with a DNA ligase, the construct can be used to transform bacteria. Finally, the newly generated product can be analyzed by sequencing

round-bottom tube. Incubate the mixture at 37 °C overnight under vigorous shacking (230 rpm).

5. Purify plasmids from the bacteria by using GeneJET Plasmid Miniprep Kit, and perform analysis by DNA sequencing (*see* **Note 8**).
6. Positive clone(s) can be resuspended in 100 ml of LB medium with 100 μg/ml ampicillin in a 500 ml Erlenmeyer flask. Incubate at 37 °C overnight under vigorous shacking (230 rpm).
7. Purify DNA plasmid by using HiSpeed Plasmid Maxi Kit, and store the construct at −20 °C.

3.3 Collagen VII Expression in HEK293 Cells

1. HEK293 cells in DMEM/F12 medium are grown until a confluence of 70% and then transfected with Lipofectamine® 2000 with purified plasmids in a 10 cm cell culture dish. First,

mix 74 μl of Lipofectamine® 2000 with 500 μl of Opti-MEM medium (tube A). In a second tube (tube B), add 24 μg of plasmid DNA to 500 μl of Opti-MEM medium. Then, transfer mixture in tube B to tube A, and incubate the reaction for 5 min at room temperature (RT) after mixing.

2. Dropwise add the transfection reaction to the cell culture dish containing HEK293 cells, and incubate for 2 days at 37 °C with 5% CO_2.
3. To select cells that have been transfected with the construct, change the medium, and add phleomycin to a final concentration of 100 μg/ml (*see* **Note 9**). Change the medium every other day, and add phleomycin to the fresh medium at 100 μg/ml. Keep selecting the cells for 2 weeks.
4. Synthesis of collagen VII can be detected by Western blotting directly of the medium. Add 5 μl of BSB 4× to 15 μl of conditioned medium, and heat the mixture for 5 min at 98 °C.
5. Place 7.5% mini-PROTEAN® TGX precast gels into a mini-PROTEAN® Tetra Vertical Electrophoresis tank previously filled with TGS electrophoresis buffer. Load sample, and perform migration at 110 V until dye front exit the gel (*see* **Note 1**).
6. Transfer proteins on a nitrocellulose membrane by using a Criterion™ blotter. Migration is performed at 4 °C with ice-cold transfer buffer (we prefer to transfer large proteins with TB buffer) at 300 mA during at least 2 h (*see* **Note 2**).
7. Incubate membrane in blocking buffer for 1 h at 4 °C. Then, incubate the membrane at 4 °C overnight under gentle agitation with rabbit polyclonal LH7.2 or ProColVII antibody diluted 1000 times in blocking buffer (*see* **Note 10**).
8. After extensive wash with TBS-T, incubate the membrane with HRP-conjugate goat anti-rabbit for 2 h at 4 °C (1:10.000 in blocking buffer). Finally, wash the membrane four times with 50 ml of TBS-T for 5 min at RT.
9. Collagen VII single α1 chains can then be revealed with ECL and visualized by using Amersham™ 600 imager (Fig. 3).

3.4 First Assessment of Functionality of Engineered Collagen VII Variants

1. Seed selected HEK293 cells carrying the construct of interest on poly-L-lysine-coated 10 cm tissue culture plates, and grow the cells to confluence.
2. Wash the plates three times with 3 ml PBS.
3. Add 10 ml serum-free DMEM and 50 μg/ml L-ascorbic acid (*see* **Note 11**).
4. Next day add an additional 50 μg/ml L-ascorbic acid.
5. After 2 days harvest the medium, and add it to a Falcon 50 ml Conical Centrifuge Tube, and centrifuge at 1000 × *g* for 5 min

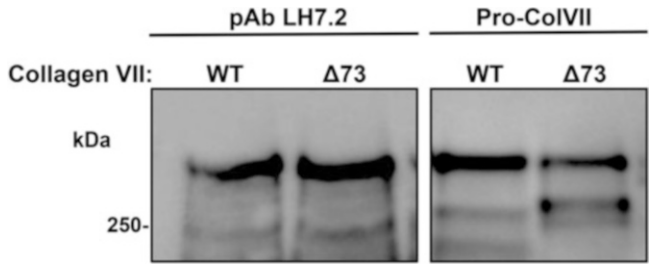

Fig. 3 Analyses of mutated collagen VII. Western blot for collagen VII on conditioned medium from HEK293 cells expressing wild-type (WT) or collagen VII with an internal deletion (the nucleotides corresponding to exon73 have been deleted (Δ73)). The modified collagen VII has a deletion of 201 bp in the central region of the *COL7A1* cDNA (bp 6015 to 6216). As the deletion is small in comparison to the large size of collagen VII, no significant difference in size can be seen by Western blot. Usage of polyclonal LH7.2 and ProColVII antibodies allows ensuring that the collagen VII is produced in full, as these antibodies, respectively, bind the NC1 and the NC2 domains of collagen VII

to remove cells and debris (*see* **Note 12**). Add the medium to a fresh 50 ml Falcon tube.

6. Cool the medium to 4 °C, and add ammonium sulfate to a saturation of 20%.
7. Precipitate the medium for 1 h at 4 °C by rotating the tube head over head.
8. Centrifuge 6000 × *g* for at 4 °C for 20 min.
9. Discard the supernatant and dissolve the pellet in 200 μl TBS. Optional, if the protein is not to be used for limited trypsin digestion, add 1 mM Pefabloc and 5 mM EDTA.
10. Limited trypsin digestion can be performed to give quick information of correct folding of collagen VII (for a detailed protocol please *see* [6]). The functionality of the protein can further be assessed by determining binding to 100 ng immobilized laminin-332 or collagen IV, as described in detail in ref. 2.

4 Notes

1. Mini-PROTEAN® TGX precast gels are suitable for routine analyses. For optimized results it is recommended to cast SDS-polyacrylamide gels with a polyacrylamide percentage that allows the best separation while keeping the sharpness of the bands of the protein of interest. For analysis of collagen VII, we routinely use 4–12% polyacrylamide gradient gels.

2. To transfer large and complex proteins, we prefer to use TB buffer. Standard transfer buffer consisting of 25 mM Trizma® base, 192 mM glycine, and 20% methanol can also be used; however, the transfer efficiency of collagens is increased by supplementing this buffer with 0.1–0.25% SDS.
3. Multiple commercial antibodies exist that detects the NC1 domain in Western blots, e.g., the mouse monoclonal LH7.2 antibody and a rabbit antihuman collagen VII from Millipore [28]. We are unfortunately not aware of any good commercially available antibodies that recognize the NC2 domain.
4. As annealing temperature is dependent on each pair of primer, optimal annealing temperature needs to be determined individually. Nevertheless, primers designed with NEBuilder® Assembly Tool (nebuilder.neb.com) are usually suitable to be used with an annealing temperature of 60 °C. Also, the extension time can be increased or decreased based on the length of the fragment to amplify. An extension of 1 min is ideal for a 3 kb fragment.
5. As shown in Fig. 1, additional bands may appear after PCR amplification (label with #). These bands are not problematic if they are far enough from the desired product and if they are not predominantly amplified. Optimization of the PCR is required if this is not the case.
6. In order to ensure an optimal Gibson reaction in a volume suitable for subsequent bacteria transformation, the total volume of the reaction needs to be lower than 40 μl. Then, a minimal concentration of 20 ng/μl of purified PCR product is mandatory. As an example, 50 ng of each fragment is necessary for a five-fragment Gibson reaction. With a concentration of 20 ng/μl, 2.5 μl of each fragment will be used. The volume will be then 12.5 μl. In this case 12.5 μl of NEBuilder HiFi DNA Assembly 2× Master Mix will be added to the mixture.
7. We recommend to use NEB 10-alpha competent *E. coli* bacteria as these bacteria show increased transformation ability of large DNA construct than others in our hands.
8. It is important to take care when designing the internal primers in the cDNA used for sequencing. In some cases the primers used for fragment amplification can also be used for sequencing.
9. In this protocol phleomycin is used to select transfected cells as the pcDNA3.1 plasmid used here has a Zeocin selectable marker.
10. It is often sufficient to incubate the primary antibody for 1 h at RT.

11. Ascorbic acid is essential for synthesis of hydroxyproline and hydroxylysine and thus formation of stable collagen triple helices.
12. It is not recommended to filter the medium as collagen VII sticks to the filter leading to significantly reduced yield of purified collagen VII.

Acknowledgments

Part of the work was financed by a research collaboration with ProQR, Netherlands. AN's research was supported by grants from the German Research Foundation, DFG (grants NY90/2-1, NY90/3-2, SFB850-B11 to AN, BR1475/12-1 to LBT), and from the Dystrophic Epidermolysis Bullosa Research Association (DEBRA) (grant Nystrom Bruckner-Tuderman 1) to AN.

References

1. Phillips CL, Lever LW, Pinnell SR et al (1991) Construction of a full-length murine pro alpha 2(I) collagen cDNA by the polymerase chain reaction. J Invest Dermatol 97:980–984
2. Bornert O, Kühl T, Bremer J et al (2016) Analysis of the functional consequences of targeted exon deletion in COL7A1 reveals prospects for dystrophic epidermolysis bullosa therapy. Mol Ther J Am Soc Gene Ther 24:1302–1311. https://doi.org/10.1038/mt.2016.92
3. Chmel N, Bornert O, Hausser I et al (2018) Large deletions targeting the triple-helical domain of collagen VII Lead to mild Acral dominant dystrophic Epidermolysis Bullosa. J Invest Dermatol 138:987–991. https://doi.org/10.1016/j.jid.2017.11.014
4. Nyström A, Bornert O, Kühl T et al (2018) Impaired lymphoid extracellular matrix impedes antibacterial immunity in epidermolysis bullosa. Proc Natl Acad Sci U S A 115: E705–E714. https://doi.org/10.1073/pnas.1709111115
5. Chen M, Costa FK, Lindvay CR et al (2002) The recombinant expression of full-length type VII collagen and characterization of molecular mechanisms underlying dystrophic epidermolysis bullosa. J Biol Chem 277:2118–2124. https://doi.org/10.1074/jbc.M108779200
6. Nyström A, Bruckner-Tuderman L, Kern JS (2013) Cell- and protein-based therapy approaches for epidermolysis bullosa. Methods Mol Biol Clifton NJ 961:425–440. https://doi.org/10.1007/978-1-62703-227-8_29
7. Fritsch A, Spassov S, Elfert S et al (2009) Dominant-negative effects of COL7A1 mutations can be rescued by controlled overexpression of normal collagen VII. J Biol Chem 284:30248–30256. https://doi.org/10.1074/jbc.M109.045294
8. Gibson DG (2011) Enzymatic assembly of overlapping DNA fragments. Methods Enzymol 498:349–361. https://doi.org/10.1016/B978-0-12-385120-8.00015-2
9. Gibson DG, Young L, Chuang R-Y et al (2009) Enzymatic assembly of DNA molecules up to several hundred kilobases. Nat Methods 6:343–345. https://doi.org/10.1038/nmeth.1318
10. Ricard-Blum S (2011) The collagen family. Cold Spring Harb Perspect Biol 3:a004978. https://doi.org/10.1101/cshperspect.a004978
11. Varki R, Sadowski S, Uitto J, Pfendner E (2007) Epidermolysis bullosa II. Type VII collagen mutations and phenotype-genotype correlations in the dystrophic subtypes. J Med Genet 44:181–192. https://doi.org/10.1136/jmg.2006.045302
12. Chen M, Keene DR, Costa FK et al (2001) The carboxyl terminus of type VII collagen mediates antiparallel dimer formation and constitutes a new antigenic epitope for epidermolysis Bullosa acquisita autoantibodies. J Biol Chem 276:21649–21655. https://doi.org/10.1074/jbc.M100180200
13. Rattenholl A, Pappano WN, Koch M et al (2002) Proteinases of the bone morphogenetic

protein-1 family convert procollagen VII to mature anchoring fibril collagen. J Biol Chem 277:26372–26378. https://doi.org/10.1074/jbc.M203247200

14. Moali C, Font B, Ruggiero F et al (2005) Substrate-specific modulation of a multisubstrate proteinase. C-terminal processing of fibrillar procollagens is the only BMP-1-dependent activity to be enhanced by PCPE-1. J Biol Chem 280:24188–24194. https://doi.org/10.1074/jbc.M501486200
15. Nyström A, Velati D, Mittapalli VR et al (2013) Collagen VII plays a dual role in wound healing. J Clin Invest 123:3498–3509. https://doi.org/10.1172/JCI68127
16. Bruckner-Tuderman L (2010) Dystrophic epidermolysis bullosa: pathogenesis and clinical features. Dermatol Clin 28:107–114. https://doi.org/10.1016/j.det.2009.10.020
17. Nyström A, Bernasconi R, Bornert O (2018) Therapies for genetic extracellular matrix diseases of the skin. Matrix Biol 71–72:330–347. https://doi.org/10.1016/j.matbio.2017.12.010
18. McGrath JA, Ashton GH, Mellerio JE et al (1999) Moderation of phenotypic severity in dystrophic and junctional forms of epidermolysis bullosa through in-frame skipping of exons containing non-sense or frameshift mutations. J Invest Dermatol 113:314–321. https://doi.org/10.1046/j.1523-1747.1999.00709.x
19. Schwieger-Briel A, Weibel L, Chmel N et al (2015) A COL7A1 variant leading to in-frame skipping of exon 15 attenuates disease severity in recessive dystrophic epidermolysis bullosa. Br J Dermatol 173:1308–1311. https://doi.org/10.1111/bjd.13945
20. Cserhalmi-Friedman PB, McGrath JA, Mellerio JE et al (1998) Restoration of open reading frame resulting from skipping of an exon with an internal deletion in the COL7A1 gene. Lab Investig J Tech Methods Pathol 78:1483–1492
21. Koga H, Hamada T, Ishii N et al (2011) Exon 87 skipping of the COL7A1 gene in dominant dystrophic epidermolysis bullosa. J Dermatol 38:489–492. https://doi.org/10.1111/j.1346-8138.2010.01008.x
22. Goto M, Sawamura D, Nishie W et al (2006) Targeted skipping of a single exon harboring a premature termination codon mutation: implications and potential for gene correction therapy for selective dystrophic epidermolysis bullosa patients. J Invest Dermatol 126:2614–2620. https://doi.org/10.1038/sj.jid.5700435
23. Wu W, Lu Z, Li F et al (2017) Efficient in vivo gene editing using ribonucleoproteins in skin stem cells of recessive dystrophic epidermolysis bullosa mouse model. Proc Natl Acad Sci U S A 114:1660–1665. https://doi.org/10.1073/pnas.1614775114
24. Turczynski S, Titeux M, Tonasso L et al (2016) Targeted exon skipping restores type VII collagen expression and anchoring fibril formation in an in vivo RDEB model. J Invest Dermatol 136:2387–2395. https://doi.org/10.1016/j.jid.2016.07.029
25. Bremer J, Bornert O, Nyström A et al (2016) Antisense oligonucleotide-mediated exon skipping as a systemic therapeutic approach for recessive dystrophic Epidermolysis Bullosa. Mol Ther Nucleic Acids 5:e379. https://doi.org/10.1038/mtna.2016.87
26. Toh ZYC, Thandar Aung-Htut M, Pinniger G et al (2016) Deletion of Dystrophin in-frame exon 5 leads to a severe phenotype: guidance for exon skipping strategies. PLoS One 11:e0145620. https://doi.org/10.1371/journal.pone.0145620
27. Kühl T, Mezger M, Hausser I et al (2015) High local concentrations of intradermal MSCs restore skin integrity and facilitate wound healing in dystrophic Epidermolysis Bullosa. Mol Ther J Am Soc Gene Ther 23:1368–1379. https://doi.org/10.1038/mt.2015.58
28. Wullink B, Pas HH, Van der Worp RJ et al (2018) Type VII collagen in the human accommodation system: expression in Ciliary body, Zonules, and lens capsule. Invest Ophthalmol Vis Sci 59:1075–1083. https://doi.org/10.1167/iovs.17-23425

Chapter 2

Multi-well Fibrillation Assay as a Tool for Analyzing Crosslinking and Stabilization of Collagen

Venkat Raghavan Krishnaswamy

Abstract

Collagen is the most widely used substratum in cell culture and biomaterials applications. In this chapter, we describe a simple procedure to isolate collagen, which can be employed to a wide range of tissue sources, and subsequently use it to study the collagen crosslinking and stabilization abilities of various compounds. The protocol is designed for a multi-well format assay and thus can be used for simultaneous assessment of multiple number of compounds and can be easily adapted to a high-throughput screening setup.

Key words Collagen, Crosslinking, Extracellular matrix, Fibrillation, Quarter staggered structure

1 Introduction

Collagen is the most abundant protein in the human body and plays a vital role in several physiological and pathological conditions [1–3]. It is used in several biomedical applications and holds a central role in treating a myriad of abnormalities such as abnormal wound healing, cancer, etc. [4]. Because of its wide presence and diverse functions, isolation and characterization of collagen are important aspects in biomaterials preparation and understanding the molecular mechanisms of various diseases. One of the intriguing properties of the isolated collagen fibrils, in vitro, is its ability to arrange into an quarter-staggered structure in physiological conditions resembling the in vivo fibril formation [5]. This property can be utilized to comprehend the influence of molecules on the three-dimensional spatial organization of collagens, which are crucial in dictating the cellular behavior.

Irit Sagi and Nikolaos A. Afratis (eds.), *Collagen: Methods and Protocols*, Methods in Molecular Biology, vol. 1944, https://doi.org/10.1007/978-1-4939-9095-5_2, © Springer Science+Business Media, LLC, part of Springer Nature 2019

2 Materials

All solutions should be prepared using analytical grade reagents. Follow all safety precautions and waste disposal regulations diligently.

2.1 Collagen Isolation

This protocol can be employed to isolate collagen from a variety of sources including skin and tendon. The most commonly used source is rat tail tendon which is almost entirely made up of collagen type I. The isolation of tendon from rat tail is explained by Rajan et al. [6].

1. Wash buffer 1: Mix three volumes of methanol with one volume of chloroform. Store the solution in an airtight bottle at 4 °C.
2. Wash buffer 2: Prepare 0.5 M sodium acetate by dissolving 41.02 g of sodium acetate in 1 L of deionized water.
3. Extraction reagent: Make up 28.73 mL of pure glacial acetic acid to 1 L with deionized water to prepare 0.5 M acetic acid. Store at 4 °C.
4. Precipitating solution: To prepare 2.8 M sodium chloride, dissolve 163.6 g of sodium chloride in 800 mL, and make up the volume to 1 L using extraction reagent, store at 4 °C.
5. Dialysate: Make up 1.14 mL of pure glacial acetic acid to 1 L with deionized water to prepare 0.02 M acetic acid. Store at 4 °C.

2.2 Collagen Fibrillation

2.2.1 Fibrillation Buffer

1. Sodium phosphate buffer (component a): To prepare 0.2 M sodium phosphate buffer, dissolve 35.61 g of disodium hydrogen phosphate dihydrate ($Na_2HPO_4 \cdot 2H_2O$) and 27.6 g of sodium dihydrogen phosphate monohydrate ($NaH_2PO_4 \cdot H_2O$) separately in 800 mL of deionized water. Make up the volumes to 1 L. Store these stock solutions at 4 °C. Before the assay, mix 770 mL of $Na_2HPO_4 \cdot 2H_2O$ and 230 mL of $NaH_2PO_4 \cdot H_2O$; adjust the pH to 7.2 if necessary.
2. Sodium chloride (component b): To prepare 2 M sodium chloride, dissolve 116.88 g of sodium chloride in 800 mL, and the make up the volume to 1 L using deionized water, store at 4 °C.
3. Sodium hydroxide (component c): To prepare 1.25 N sodium hydroxide, dissolve 50 g of sodium hydroxide in 800 mL, and the make up the volume to 1 L using deionized water.

For 1 mL collagen, mix 100 and 75 μL of components a and b respectively. The volume of component c may vary for each batch of collagen (*see* **Note 6**). The mixing of the fibrillation buffer components is always done on the day of the assay.

3 Methods

3.1 Collagen Isolation

1. After harvesting the tissue, remove the unwanted tissues like soft tissue, clotted blood, etc. that are present. Wash the samples twice thoroughly with cold deionized water.
2. Wash the tissue samples with wash buffer 1. Repeat two more times, and ensure all the fat particles are removed.
3. Wash the samples once with wash buffer 2.
4. Wash the samples extensively with extraction reagent, and incubate the tissue in at least 10 volumes of extraction solution for 48 to 72 h (*see* **Note 1**).
5. Homogenize the samples in a blender with extraction reagent. Centrifuge the samples at 14,000 × *g* for 30 min at 4 °C. Save the supernatant, and re-extract the collagen once from the pellet by repeating the homogenization. Pool both the supernatants (*see* **Note 2**).
6. For 750 mL of collagen supernatant, gradually add 250 mL of precipitating solution with mild stirring overnight at 4°C.
7. Centrifuge the solution at 6000 × *g* for 10 min at 4 °C. Discard the supernatant, and collect the pellet.
8. Dissolve the pellet in a suitable volume of cold extraction reagent.
9. Dialyze the collagen solution extensively against dialysate at least for 24–48 h (*see* **Note 3**).
10. Freeze the samples as a thin layer on a lyophilized flask by rotating the flask with the sample on an ice-salt slurry. Freeze the collagen coated flasks at −80 °C for a minimum of 12–16 h.
11. Freeze dry the samples thoroughly. Store the samples at −80 °C in an airtight container.
12. Dissolve a portion of the lyophilized sample in the dialysate, and estimate the collagen content using standard procedures. The purity of the collagen can be assessed by a standard sodium dodecyl sulfate-polyacrylamide gel electrophoresis (*see* **Note 4**) (Fig. 1).

3.2 Collagen Fibrillation

1. Prepare 0.5 mg mL^{-1} collagen solution by dissolving the required amount of lyophilized collagen in the dialysate with mild stirring at 4 °C (*see* **Note 5**).
2. Add required volume of fibrillation buffer in different wells of a multi-well plate (*see* **Note 6**).
3. Mix the test compounds to the fibrillation buffer at this stage by replacing with the same volume of sodium phosphate buffer.

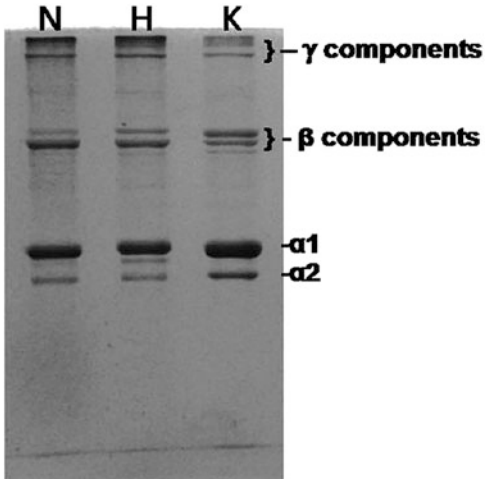

Fig. 1 The electrophoretic mobility of collagen isolated from normal (N), hypertrophic scar (H), and keloid (K) skin tissue using the present method [7]

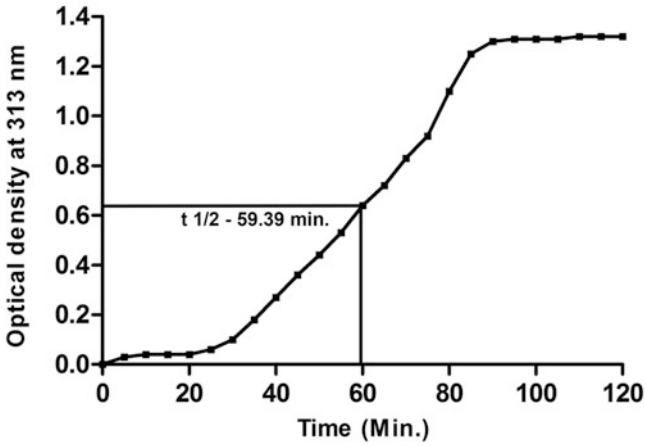

Fig. 2 Representative graph showing typical pattern of the collagen fibrillation

4. Switch on the plate reader, and pre-warm the plate chamber to 37 °C.
5. Add 200 μL of collagen to all the tubes mix gently with the pipette to make a uniform solution. Set up controls in parallel (*see* **Note 7**).
6. Quickly spin the contents of the tube to collect any solution on the walls and to remove air bubbles, if any.
7. Measure the absorbance kinetics at 313 nm for at least 120 min.
8. Calculate the $T_{1/2}$, which is the time taken to reach half the value of the plateau. Compare the $T_{1/2}$ of treated and untreated samples to understand the effect of the treated compounds (Fig. 2).

4 Notes

1. If isolating from skin, remove the epidermis using a scalpel blade. Care must be taken not to expose the tissue for a long period at room temperature. One easy way is to perform this step after soaking the tissue in extraction reagent which would loosen up the epidermis. After washing, record the wet weight of the samples.
2. Place the blending jar at 4 °C for at least 6 h before using it. The pulse blending option should be used rather than continuous mode to prevent heating of the samples. The acid soluble collagen in the supernatant and the insoluble portion in the pellet can be separated at this point. The insoluble pellet can be further digested using pepsin (1 mg per 100 mg of wet weight). The fibrillation assay can be performed with both the collagens; typically pepsin-solubilized atelocollagen has a slower rate of fibril formation as they lack the terminal telopeptides.
3. Proper removal of salts is important for downstream applications of collagen. The volume of the dialysate should be 250 times the sample volume. In cases of large sample volumes, the dialysate can be changed every 24 h, and the dialysis timing can be increased. The dialysate pH can be measured to assess the efficiency of dialysis.
4. Hydroxyproline assay is a reliable method for quantification of the collagen content. However, dye-based assay kits with simple colorimetric estimation are now commercially available. Weighing the lyophilized collagen before dissolving helps in assessing the concentration of the entire batch.
5. Obtaining a homogeneous solution is important. The lyophilized collagen should be weighed and transferred as quickly as possible. Using pre-chilled acetic acid is essential.
6. The pH of the final solution is very critical for proper fibril formation. Therefore, for each batch of collagen, run a trial to determine the volume of fibrillation buffer component "c" required to adjust the pH to 7.2. As temperature greatly influences pH, after mixing all the components, warm the solution to 37 °C and check pH quickly. Once pH is adjusted, leave the tube at 37 °C in a water bath, and note the time taken for the fibrillation. Alternatively, an aliquot of it can be transferred to a microplate and read at 313 nm till the optical density reaches plateau. This will also indicate whether the collagen concentration is optimum.

7. Use multichannel pipette to dispense collagen simultaneously to multiple wells. Do not introduce air bubble as it interferes with the reading. Set controls (without test compounds), positive controls (50 μM glutaraldehyde or other known crosslinking agents) and negative controls (replace collagen with dialysate) in parallel for comparison.

References

1. Prockop DJ, Kivirikko KI (1995) Collagens: molecular biology, diseases, and potentials for therapy. Annu Rev Biochem 64:403–434. https://doi.org/10.1146/annurev.bi.64.070195.002155
2. Mienaltowski MJ, Birk DE (2014) Structure, physiology, and biochemistry of collagens. Adv Exp Med Biol 802:5–29. https://doi.org/10.1007/978-94-007-7893-1_2
3. Myllyharju J, Kivirikko KI (2001) Collagens and collagen-related diseases. Ann Med 33(1):7–21
4. Lee CH, Singla A, Lee Y (2001) Biomedical applications of collagen. Int J Pharm 221 (1–2):1–22
5. Chung HJ, Steplewski A, Chung KY, Uitto J, Fertala A (2008) Collagen fibril formation. A new target to limit fibrosis. J Biol Chem 283 (38):25879–25886. https://doi.org/10.1074/jbc.M804272200
6. Rajan N, Habermehl J, Cote MF, Doillon CJ, Mantovani D (2006) Preparation of ready-to-use, storable and reconstituted type I collagen from rat tail tendon for tissue engineering applications. Nat Protoc 1(6):2753–2758. https://doi.org/10.1038/nprot.2006.430
7. Krishnaswamy VR, Lakra R, Korrapati PS (2014) Keloid collagen–cell interactions: structural and functional perspective. RSC Adv 4 (45):23642–23648. https://doi.org/10.1039/C4RA01995D

Chapter 3

Production and Characterization of Chemically Cross-Linked Collagen Scaffolds

Ignacio Sallent, Héctor Capella-Monsonís, and Dimitrios I. Zeugolis

Abstract

Chemical cross-linking of collagen-based devices is used as a means of increasing the mechanical stability and control the degradation rate upon implantation. Herein, we describe techniques to produce cross-linked with glutaraldehyde (GTA; amine terminal cross-linker), 4-arm polyethylene glycol succinimidyl glutarate (4SP; amine terminal cross-linker), diphenyl phosphoryl azide (DPPA; carboxyl terminal cross-linker), and 1-ethyl-3-(3-dimethylaminopropyl)carbodiimide (EDC; carboxyl terminal cross-linker) collagen films. In addition, we provide protocols to characterize the biophysical (swelling), biomechanical (tensile), and biological (metabolic activity, proliferation and viability using human dermal fibroblasts and THP-1 macrophages) properties of the cross-linked collagen scaffolds.

Key words Collagen cross-linking, Biophysical characterization, Biomechanical properties, Cytotoxicity, Macrophage response

1 Introduction

Collagen is the most abundant extracellular matrix (ECM) protein in mammals. Fibril-forming collagens (type I, II, III, V, XI) represent 90% of the total collagen content in the body, while their fibrous structure empower containing tissues with their specific viscoelastic properties [1]. Collagen type I comprises of two $\alpha 1$ (I) and one $\alpha 2$(I) polypeptide chains that tangle up in a triple-helix conformation [1, 2]. It is stabilized via two cross-links in the helical region and one more in each telopeptide region (N- and C-terminal), through the action of lysyl oxidase [3, 4], sugar-mediated [5, 6], and transglutaminase [7] cross-linking. These cross-links are responsible for the quarter-staggered arrangement of collagen molecules in lateral and head-to-tail fashion, resulting in the formation of cross-striated fibrils with exceptional mechanical properties [8, 9].

Irit Sagi and Nikolaos A. Afratis (eds.), *Collagen: Methods and Protocols*, Methods in Molecular Biology, vol. 1944, https://doi.org/10.1007/978-1-4939-9095-5_3, © Springer Science+Business Media, LLC, part of Springer Nature 2019

Considering its abundance in native ECM supramolecular assemblies and its cell recognition signals, collagen type I is favored for tissue engineering and drug delivery applications [10]. However, collagen type I extraction from animal tissues involves breakage of the native cross-links and consequent loss of its mechanical integrity/stability [11, 12]. Thus, reconstituted forms of collagen need to be exogenously cross-linked, through chemical, physical, or biological approaches [12–14] to tune the mechanical properties and the degradation rate of the produced scaffolds upon implantation [15–17]. Although physical (e.g., dehydrothermal [18, 19], ultraviolet irradiation [20, 21]) and biological (e.g., microbial [22, 23] or tissue type II [24, 25] transglutaminase) cross-linking methods have been assessed, the resultant cross-linking is weak. To this end, amine or carboxyl terminal chemical cross-linking methods are preferred. However, customarily employed chemical cross-linkers, such glutaraldehyde (GTA, amine terminal) and 1-ethyl-3-(3-dimethylaminopropyl)carbodiimide (EDC, carboxyl terminal), are often associated with cytotoxicity [26–29], foreign body response [30, 31], and macrophage pro-inflammatory response [32–34]. Although alternative cross-linkers, such as 4-arm polyethylene glycol succinimidyl glutarate (4SP; amine terminal) [35–38] and diphenyl phosphoryl azide (DPPA; carboxyl terminal) [39, 40], have been proposed and have shown promise, they have yet to be directly compared.

We have previously described assays to characterize collagen and to quantify thermal and biochemical properties of collagen-based preparations, biomaterials, and tissue specimens [41–45]. Herein, we provide protocols to fabricate cross-linked with GTA, 4SP, EDC, and DPPA collagen type I films and to characterize the effect of the cross-linking treatment on the biophysical (swelling), biomechanical (tensile), and biological (metabolic activity, proliferation, and viability using human dermal fibroblasts and THP-1 macrophages) properties of the resultant scaffolds.

2 Materials

2.1 Collagen Cross-Linking and Film Preparation

1. 1 M sodium hydroxide (NaOH) in water.
2. 1 M hydrochloric acid (HCl) in water.
3. 1× and 10× phosphate-buffered saline (PBS).
4. 6 mg/ml collagen type I stock solution: Dissolve 180 mg of freeze-dried collagen type I in 30 ml of 0.05 M acetic acid.
5. 0.625% GTA cross-linker solution: Dilute 6.25 μl of 25% GTA in 244 μl of PBS 1× (*see* **Note 1**).
6. 20 mM 4SP cross-linker solution: Dissolve 50 mg of 4SP-SG in 0.25 ml PBS 1×. Vortex thoroughly until the powder dissolves.

7. 1% DPPA cross-linker solution: Dilute 2.5 μl of DPPA in 0.25 ml of 2% dimethylformamide (DMF) (*see* **Note 1**).
8. 1000 mM EDC cross-linker solution: Dissolve 98 mg of 2-(*N*-morpholino)ethanesulfonic acid (MES) in 10 ml of distilled water, and adjust the pH to 5.5. Dissolve 115 mg of *N*-hydroxysuccinimide (NHS) in 5 ml of MES buffer. Dissolve 48 mg of *N* (3-dimethylaminopropyl)-*N*′-ethylcarbodiimide (EDC) hydrochloride in 0.25 ml of the MES + NHS solution (*see* **Note 1**).
9. Silicon or PDMS nonadherent mold (3 × 4 cm).
10. 15 ml screw-cap tubes.
11. Benchtop vortex.
12. Laminar flow hood.

2.2 Swelling Assay

1. 1× phosphate-buffered saline (PBS).
2. Tweezers.
3. Laboratory digital milligram scale.

2.3 Tensile Test

1. Scalpel and blades.
2. Ruler.
3. Cutting board.
4. 1× phosphate-buffered saline (PBS).
5. Tweezers.
6. Digital caliper.
7. Tensile test machine with 10 N load cell (Zwick Roell).

2.4 Cell Culture

1. Primary human dermal fibroblasts (DF; ATCC).
2. Human-derived leukemic monocyte cells (THP-1; ATCC).
3. Culture media for DF: DMEM—High glucose supplemented with 10% fetal bovine serum (FBS) and 1% penicillin and streptomycin.
4. Culture media for THP-1: RPMI-1640 supplemented with 10% fetal bovine serum (FBS) and 1% penicillin and streptomycin.
5. Phorbol 12-myristate 13-acetate (PMA).
6. Lipopolysaccharides from *Escherichia coli* O55:B5 (LPS).
7. Cell culture silicone rings to fix the films on the plates: 18.6 mm of diameter ace O-rings.
8. Sterile 24-well plates.

2.5 Cell Proliferation and Morphology Assay

1. 4′,6-diamidino-2-phenylindole (DAPI): 1:3000 dilution in PBS 1× from 1 mg/ml stock.
2. Optional: Rhodamine phalloidin, 1:150 dilution in PBS 1× from 0.2 mg/ml stock.

3. 4% paraformaldehyde (PFA).
4. 1× Phosphate-buffered saline (PBS).
5. Triton-X 100 solution in 0.2% PBS.

2.6 Metabolic Activity Assay (alamarBlue®)

1. 1× sterile phosphate-buffered saline (PBS).
2. alamarBlue® solution in 10% PBS.

2.7 Cell Viability Assay

1. Dimethyl sulfoxide (DMSO).
2. Phosphate-buffered saline 1× (PBS).
3. 4 mM calcein AM in DMSO.
4. 2 mM ethidium homodimer-1 in DMSO.

3 Methods

3.1 Collagen Cross-Linking and Film Preparation

All steps detailed in this paragraph need to be performed on ice to avoid denaturation of collagen and prevent its premature gelation. The temperature of the centrifuge, if possible, should be set to 4 °C before starting the procedure. The following instructions describe the production of a film of 3 × 4 cm dimensions, for other mold dimensions the volume of the reagents need to be scaled up.

1. Mix 0.42 ml of PBS 10× with 0.2 ml of 1 M NaOH in a 15 ml screw-cap tube using a benchtop vortex.
2. Add 4.2 ml of the collagen stock solution to the mixture, and mix thoroughly with the vortex.
3. Use the pH meter and 1 M NaOH to neutralize the solution (pH 7.2–7.4).
4. Add the 0.25 ml of the chosen cross-linker, and mix with the benchtop vortex (*see* **Note 2**).
5. Centrifuge the solution at 2000 rpm for 10 s to remove the bubbles.
6. Pour 4 ml of the solution on the nonadherent mold (3 × 4 cm).
7. Incubate the sample (mold and collagen) at 37 °C for 1 h.
8. Dry the sample in the flow hood at room temperature (RT) for at least 24 h.
9. Use tweezers to peel off the collagen film from the nonadherent surface.
10. Store the films in a dark and dry environment until use.

3.2 Swelling Assay

1. Use a blade and a scalpel to cut five pieces ($n = 5$) from the collagen film, and record their dry weight using a laboratory scale (*see* **Note 3**).

2. Incubate the samples in PBS 1× at RT overnight.
3. Blot the samples with filter paper to remove the excess surface water.
4. Weigh the samples in the laboratory scale, and record their wet weight.
5. Calculate the swelling ratio (%) as follows: [(wet weight − dry weight)/dry weight] × 100%.

3.3 Tensile Test

1. Use a scalpel with a sharp blade and a ruler to cut the collagen film in three stripes of 1 × 4 cm (*see* **Note 4**).
2. Hydrate the samples overnight in PBS 1× at 37 °C (*see* **Note 5**).
3. Blot the samples with filter paper to remove the excess surface water.
4. Using the calipers, take five measurements of the thickness of the sample in the middle region (*see* **Note 6**).
5. Insert the sample into the upper grip of the tensile tester, and tighten (*see* **Note 7**).
6. Bring the crosshead into an appropriate range for the sample and affix the sample to the lower grip (*see* **Note 8**).
7. Set up the software from the mechanical tester to the following tensile test parameters: Preload, 0.01 N; preload speed, 5 mm/min; test speed, 10 mm/min.
8. Initiate the test, and export the results to excel.
9. Calculate the following parameters: stress at break (MPa), strain at break (%) and Young's modulus (MPa), using the width and the thickness of the samples. Stress at break = force at break/original cross-sectional area of the sample, Young's modulus = slope of the linear region of the stress (MPa)/strain (no units) curve (*see* **Note 8**) (Table 1).

Table 1
Swelling ratio, thickness, and mechanical data of the produced collagen films

Cross-linking agent	Swelling ratio (%)	Thickness (μm)	Stress at break (MPa)	Strain at break (%)	Young's modulus (MPa)
NC	100 ± 16	178 ± 4	0.03 ± 0.01	8.33 ± 3.00	0.20 ± 0.04
GTA	21 ± 9 #	67 ± 6 #	0.19 ± 0.04 #	4.19 ± 2.82	1.95 ± 0.33 #
4SP	80 ± 9	232 ± 33	0.07 ± 0.03 #	13.28 ± 3.13	0.38 ± 0.04
EDC	125 ± 7	185 ± 39	0.03 ± 0.01	15.78 ± 3.08	0.10 ± 0.03
DPPA	91 ± 23	83 ± 12 #	0.05 ± 0.01	18.22 ± 1.89 #	0.22 ± 0.01

GTA significantly decreased water absorption. GTA and DPPA significantly reduced thickness. GTA induced the highest stress at break. DPPA induced the highest strain at break. GTA induced the highest modulus. # indicates statistically significant difference ($p < 0.05$)

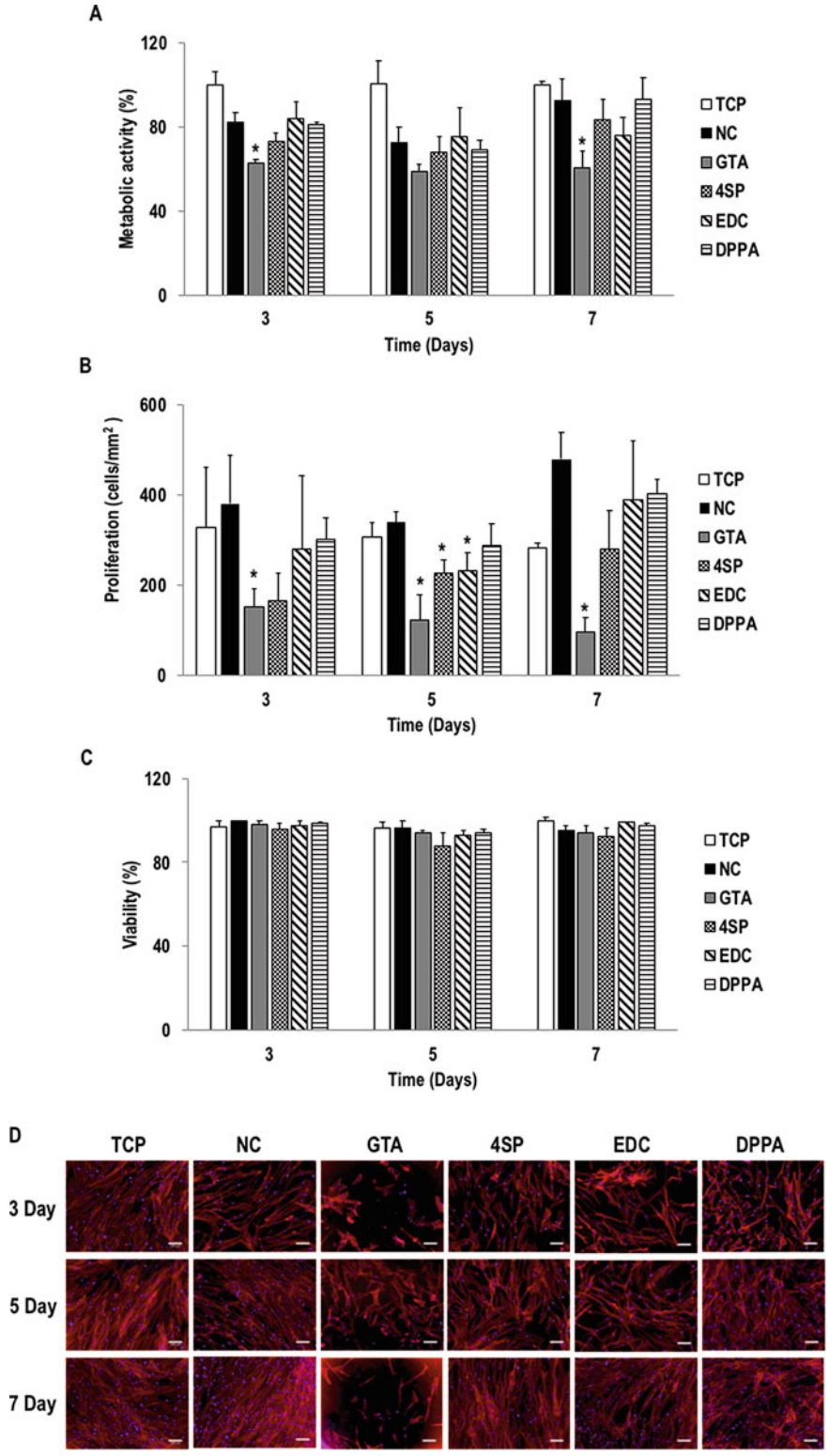

Fig. 1 Metabolic activity (**a**), proliferation (**b**), viability (**c**), and rhodamine phalloidin (red) and DAPI (blue) images (**d**) of DF seeded onto the collagen scaffolds. DF on GTA cross-linked scaffolds presented reduced

3.4 Cell Culture

3.4.1 Scaffold Preparation

1. Using a scalpel with a blade cut the collagen films into 1 × 1 cm squares.
2. In the laminar flow hood, place the films in 24-well plates (*see* **Note 9**).
3. Use the UV from the laminar flow hood for 1 h to partially sterilize the collagen scaffolds in the plates. Keep the lid of the plates open during the process.
4. Fix the collagen films to the bottom of the plates with the help of autoclaved tweezers and silicone rings.
5. Remove the excess of cross-linker by washing the films three times with sterile PBS 1× for 20 min.
6. Sterilize the films with 0.5 ml of 70% ethanol for 30 min.
7. Wash the films three times in sterile PBS 1×.

3.4.2 DF Seeding

1. Incubate the sterilized films at 37 °C and 5% CO_2 overnight with specific media for the DF cells.
2. Discard the media, and seed the DF onto the various samples at 20×10^3 cells/cm^2 with 0.5 ml of fresh DMEM supplemented media. Incubate the fibroblast for 3, 5, and 7 days at 37 °C and 5% CO_2. Change media every 3–4 days (Fig. 1).

3.4.3 THP-1 Seeding

1. Incubate the sterilized films at 37 °C and 5% CO_2 with 1 ml cell-specific media for THP-1 cells for 3 days.
2. Collect the RPMI supplemented media incubated with the scaffolds (preconditioned media), and filter it through 0.2 μm sterile filters. Keep it at 37 °C in the water bath until further use.
3. Seed THP-1 into new 24-well plates and onto the scaffolds at 26×10^3 cells/cm^2 with THP-1 complete media supplemented with 100 ng/ml of PMA to induce adherent mature macrophage-like state for 6 h.
4. Wash off nonattached cells with sterile PBS 1×.
5. Add 0.5 ml of the filtered preconditioned media to the macrophages attached to the 24-well plates TCP and 0.5 ml of fresh RPMI supplemented media to the macrophages attached to the scaffolds. Create a positive control for macrophage

Fig. 1 (continued) metabolic activity at day 3 and 7 and reduced proliferation at all three time points in comparison to the NC samples. None of the cross-linking treatments significantly affected DF viability (**c**). DF adopted a spindle-shaped morphology in all the groups except for GTA, on which cells spread in all directions (**d**). Treatments: non-cross-linked collagen films (NC), collagen films cross-linked with glutaraldehyde (GTA), 4-arm PEG succinimidyl glutarate (4SP), 1-ethyl-3-(3-dimethylaminopropyl)carbodiimide (EDC), and diphenylphosphoryl azide (DPPA). Tissue culture plastic (TCP) was used as control. Significance compared to *NC group ($p < 0.05$)

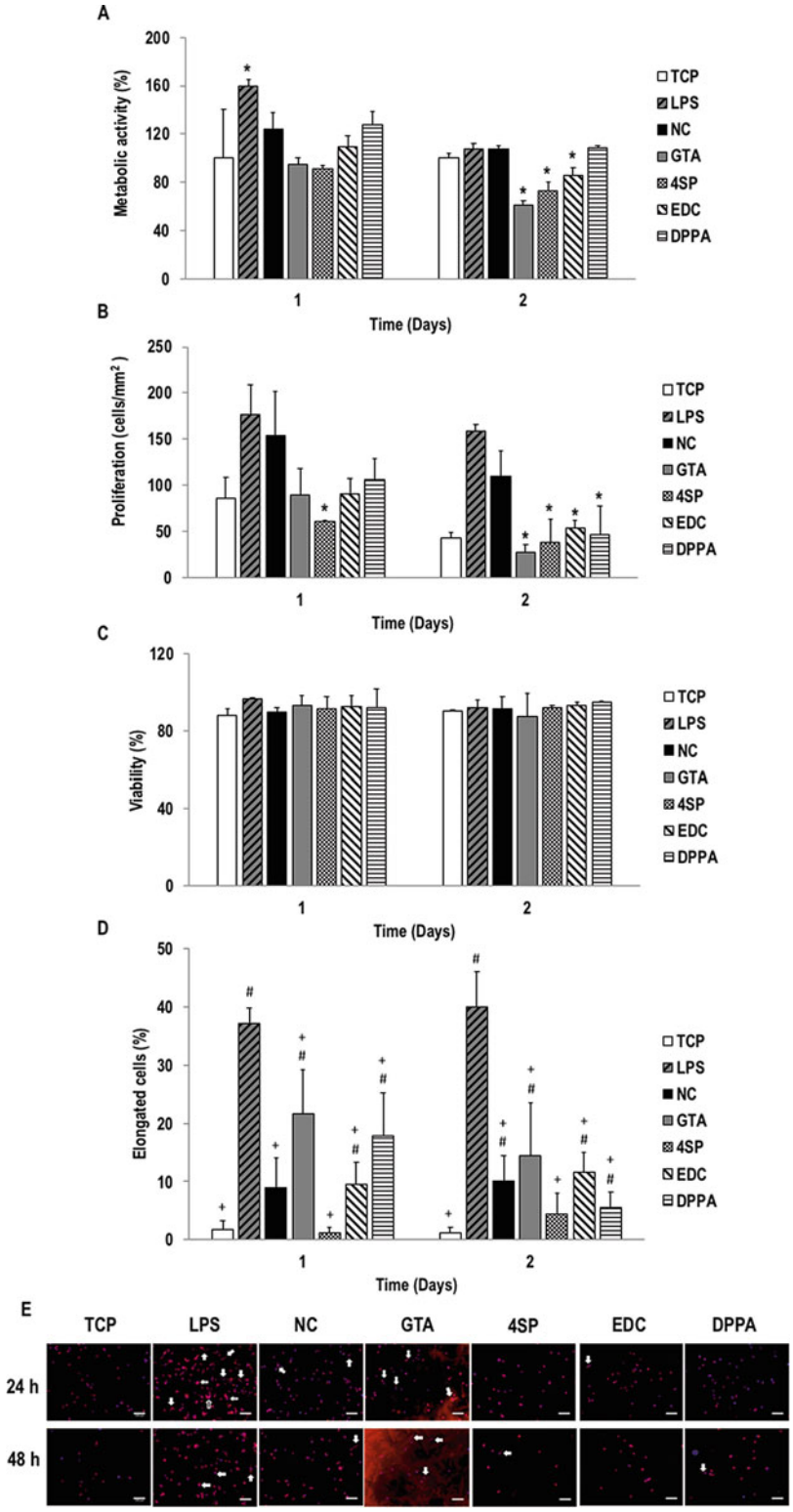

Fig. 2 Metabolic activity (**a**), proliferation (**b**), viability (**c**), elongated cells proportion (**d**), and rhodamine phalloidin (red) and DAPI (blue) images (**e**) of THP-1 seeded onto the collagen scaffolds. By day 1, LPS significantly increased THP-1 metabolic activity (**a**); and 4SP significantly reduced THP-1 proliferation (**b**) in

inflammatory response by culturing TCP-seeded macrophages with 100 ng/ml of LPS in RPMI complete media and a negative control with only complete media. Incubate macrophages for 24 h and 48 h at 37 °C and 5% CO_2 (Figs. 2 and 3).

3.5 Cell Proliferation and Morphology Assay

1. At the appropriate time point remove media from cells.
2. Gently wash scaffolds with PBS 1×.
3. Add 0.5 ml of 4% PFA, and allow the sample to fix for 30 min at RT (*see* **Note 10**).
4. Wash the sample with 1× PBS.
5. Incubate the samples with 0.2 ml of 0.2% Triton-X solution for 5 min.
6. Wash the sample with PBS 1×.
7. Add rhodamine-phalloidin solution enough to cover the bottom of the well and/or scaffolds (around 150 μl).
8. Incubate 1 h at RT. Protect the samples from the light during this procedure and in subsequent manipulations.
9. Wash the sample with PBS 1×.
10. Add 150 μl of DAPI solution, and incubate for 5 min at RT.
11. Wash the sample three times with PBS 1× (*see* **Note 11**).
12. Image the samples in a fluorescence or confocal microscope using a 10× objective and an excitation/emission wavelength of 358/461 nm for DAPI and 540/565 nm for rhodamine phalloidin.
13. Take 4–5 representative images of every sample.
14. Use ImageJ or other software for an automated counting of the nuclei per image (*see* **Note 12**) and for morphology assessment (*see* **Note 13**).
15. Graph the number of cells per area to evaluate cell proliferation.

Fig. 2 (continued) comparison to the NC samples. By day 2, GTA, EDC, and 4SP significantly reduced THP-1 metabolic activity (**a**); and all the cross-linking treatments significantly reduced THP-1 proliferation (**b**) in comparison to the NC. None of the cross-linking treatments significantly affected macrophage viability (**c**). All treatments elicited a significant lower proportion of elongated cells than LPS, whereas THP-1 in GTA, EDC and DPPA presented a significant higher number of elongated cells than TCP at both time points, likewise NC at day 2 (**d**). THP-1 adopted a rounded morphology, independently of the treatment and time in culture. Some elongated macrophages (white arrows) were observed predominantly in LPS- and GTA-treated samples, whereas cell clusters (black arrows) were mainly observed in LPS condition (**e**). Treatments: non-cross-linked collagen films (NC), collagen films cross-linked with glutaraldehyde (GTA), 4-arm PEG succinimidyl glutarate (4SP), 1-ethyl-3-(3-dimethylaminopropyl)carbodiimide (EDC), and diphenylphosphoryl azide (DPPA). Tissue culture plastic (TCP) and lipopolysaccharides in TCP (LPS) were used as controls. Significance compared to *NC group, compared to #TCP and compared to +LPS group ($p < 0.05$)

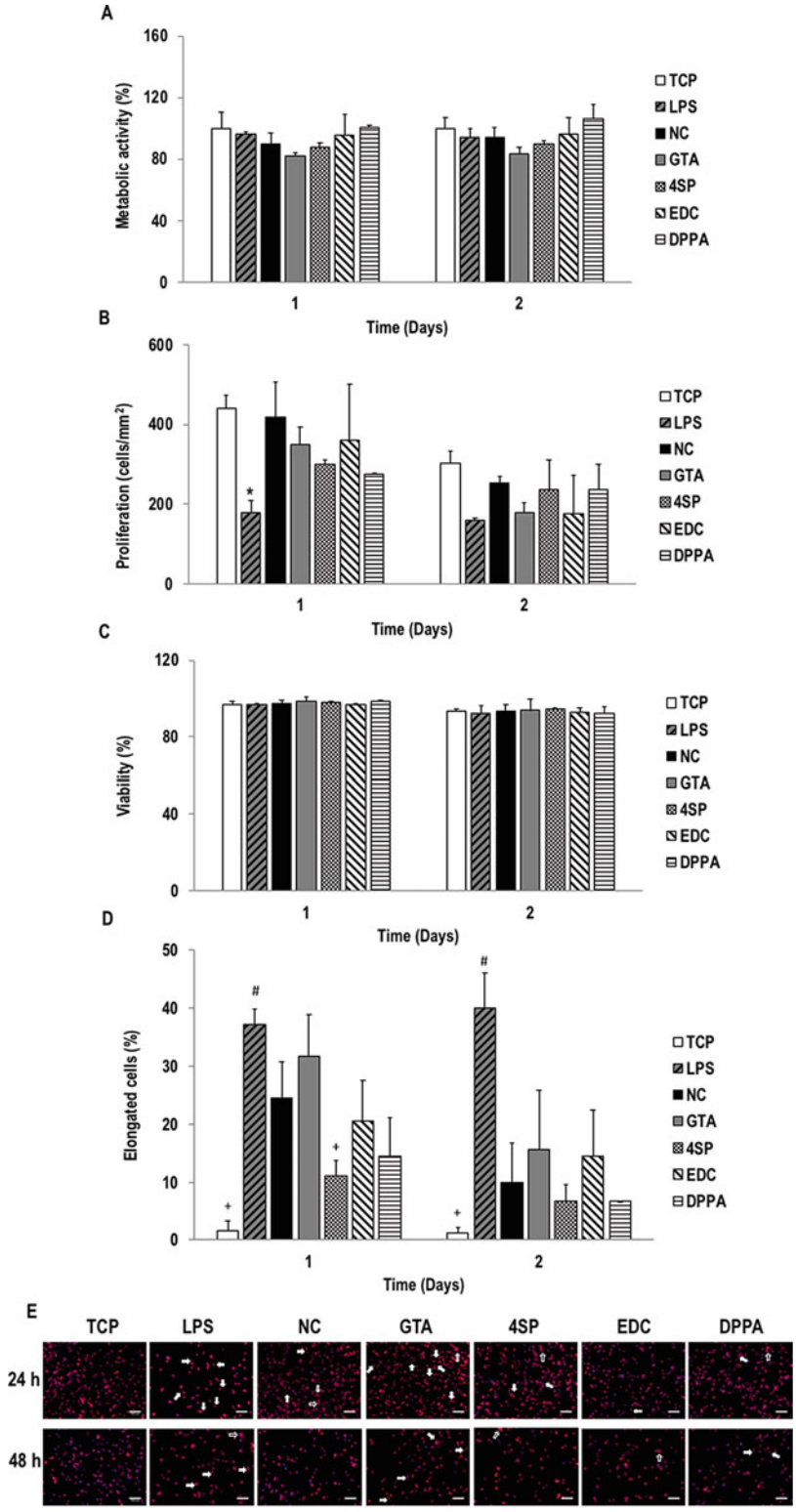

Fig. 3 Metabolic activity (**a**), proliferation (**b**), viability (**c**), elongated cells proportion (**d**), and rhodamine phalloidin (red) and DAPI (blue) images (**e**) of THP-1 cultured with preconditioned media from the cross-linked

3.6 Cell Metabolic Activity Assay (alamarBlue®)

1. Cell metabolic activity can be assessed by the incubation of the cells with 10% alamarBlue® for 2 h on the day of the time point, as per manufacturer's protocol (*see* **Note 14**).
2. Cell metabolic activity is expressed as % of reduced alamarBlue® and normalized to the activity of cells in TCP.

3.7 Cell Viability Assay

1. Prepare staining solution by diluting 1:1000 the calcein AM and the ethidium homodimer-1 stock solutions with PBS 1×.
2. Add 150 μl of DMSO to a well with cells alone (no scaffold) to create a negative control with dead cells. Place the plate in the incubator for 20 min.
3. Remove culture medium from the wells, and wash cells with PBS.
4. Add 150 μl of staining solution to each scaffold.
5. Incubate at 37 °C, 5% CO_2 for 30 min.
6. Wash the sample with PBS 1× (*see* **Note 11**).
7. Image the samples in a fluorescence or confocal microscope using a 10× objective and an excitation/emission wavelength of 495/515 nm and 528/617 nm for Calcein AM and ethidium homodimer-1, respectively.
8. Take 3–5 images of every sample.
9. Count viable (green) and dead (red) cells with ImageJ or another software.
10. Calculate cell viability (%) by dividing the number of alive cells by the total number of cells.

Fig. 3 (continued) collagen films. None of the cross-linking treatments significantly affected THP-1 metabolic activity (**a**). Only cells treated with LPS showed a decreased proliferation in comparison with the NC samples (**b**). None of the cross-linking treatments significantly affected macrophage viability (**c**). LPS showed a higher number of elongated cells than TCP at both times points. All treatments showed values higher than TCP and lower than LPS. Significant differences were found between LPS and TCP at both time points, whereas only 4SP showed a significant difference with LPS at day 1 (**d**). THP-1 adopted a rounded morphology, independently of the treatment and time in culture. Some elongated macrophages were observed (white arrows) predominantly in LPS-, NC-, and GTA-treated samples. Some cell clusters were observed (black arrows) in all the conditions except for TCP (**e**). Treatments: non-cross-linked collagen films (NC), collagen films cross-linked with glutaraldehyde (GTA), 4-arm PEG succinimidyl glutarate (4SP), 1-ethyl-3-(3-dimethylaminopropyl) carbodiimide (EDC), and diphenylphosphoryl azide (DPPA). Tissue culture plastic (TCP) and lipopolysaccharides (LPS) in TCP were used as controls. Significance compared to *NC group, compared to #TCP and compared to +LPS group ($p < 0.05$)

4 Notes

1. For safety reasons, prepare these cross-linking solutions in the chemical hood. GTA, DPPA, and EDC are toxic if swallowed, inhaled, or in contact with eyes or skin. Use personal protective equipment (PPE) when manipulating these samples outside the fume hood.
2. After the addition of the cross-linker, collagen gelation will take place within 1–5 min (depending on the cross-linker used). To avoid collagen gelling in the tube, the next two steps (centrifugation and pouring of the solution on the mold) need to be performed rapidly. Alternatively, devices like dual syringes or 3-way stopcocks might be used to mix the collagen solution with the cross-linker, followed by direct pouring of the resulting mixture on the PDMS molds (skip the centrifugation step).
3. For an accurate estimation of the swelling of the collagen samples, the minimum recommended weight per sample piece is 10 mg.
4. When cutting the collagen film in stripes for tensile testing, caution must be taken not to damage the middle region of the sample (test region). Any defects in that region should result in automatic rejection of the sample. If possible, samples cut in the dog bone shape are preferred, as a narrower than the edges middle area promotes stress concentration in the middle of the sample (this may not be possible in very fragile samples). Tensile test assays are typically carried out in quintuplicate ($n = 5$), meaning that in this case at least two collagen films (3×4 cm) per condition are needed to obtain an accurate measurement of the scaffolds' mechanical properties.
5. C-shaped sample holders made of water-resistant materials can be used to maintain the collagen films in a stretched position preventing the samples from folding over onto themselves when incubated in PBS 1×, which facilitates sample thickness measurement and loading in the tensile test machine. Bench protector sheets made of paper and a laminated waterproof polyethylene layer can be used to make these sample holders. Dry collagen stripes can be glued at their ends to two sample holders in a "sandwich" conformation. After affixing the sample in the tensile test machine, sample holders need to be cut in their middle region to negate potential bias during testing.
6. Two glass panes can be used to give a consistent thickness measurement for the samples: Use the calipers to measure the thickness of the glass panes alone, and then repeat the measurement with the sample inserted between the panes.

7. It is essential to ensure that the placement of the sample is at 90° angle to the grip so as to negate potential bias upon test.
8. Young's modulus should be extracted from the linear region of the stress/strain curve in between the toe and the failure regions typical of collagen materials.
9. The number of technical replicates (wells per condition) typically ranges between 3 and 5. The number of plates to consider depends on the number of time points and experiments planned.
10. To minimize the toxicity risks associated with PFA, the fixation step should be performed in the chemical hood.
11. GTA cross-linking can lead to the autofluorescence of the collagen scaffolds when imaged with 358, 495, 528, and 540 nm wavelengths. Washing the scaffolds thoroughly with PBS 1× diminishes the effect of this phenomenon.
12. Automated counting with ImageJ in confluent cells can lead to inaccuracies. If cells are confluent or over-confluent (nuclei superposition), manual counting is recommended.
13. Elongation degree of THP-1cells can be employed to assess the immune reaction in vitro. To do so, using ImageJ manually describe the shape of 25–50 cells per image and measure the shape features aspect ratio, circumference, and roundness. Consider as elongated cells those with an aspect ratio higher than 3.0 or with an aspect ratio superior to 2 and circumference and roundness lower than 0.5. Calculate the percentage of elongated cells in 4–5 images for each condition. The presence of a high number of clusters (aggregates of 5 or more cell) can also be assessed as an indication of inflammatory reaction.
14. When assessing the metabolic activity of cells on scaffolds, these must be moved to new wells with the help of sterile tweezers to prevent the action of cells attached to surrounding TCP.

Acknowledgments

This work has been supported by the Science Foundation Ireland, Career Development Award Programme (grant agreement number: 15/CDA/3629); Science Foundation Ireland and the European Regional Development Fund (grant agreement number: 13/RC/2073); and EU H2020, ITN award, Tendon Therapy Train Project (grant agreement number: 676338).

References

1. Gelse K, Poschl E, Aigner T (2003) Collagens–structure, function, and biosynthesis. Adv Drug Deliv Rev 55(12):1531–1546
2. Brodsky B, Ramshaw JA (1997) The collagen triple-helix structure. Matrix Biol 15 (8–9):545–554
3. Smith-Mungo LI, Kagan HM (1998) Lysyl oxidase: properties, regulation and multiple functions in biology. Matrix Biol 16 (7):387–398
4. Yamauchi M, Taga Y, Hattori S, Shiiba M, Terajima M (2018) Analysis of collagen and elastin cross-links. Methods Cell Biol 143:115–132. https://doi.org/10.1016/bs.mcb.2017.08.006
5. Fu MX, Wells-Knecht KJ, Blackledge JA, Lyons TJ, Thorpe SR, Baynes JW (1994) Glycation, glycoxidation, and cross-linking of collagen by glucose. Kinetics, mechanisms, and inhibition of late stages of the Maillard reaction. Diabetes 43(5):676–683
6. Reddy GK (2004) Cross-linking in collagen by nonenzymatic glycation increases the matrix stiffness in rabbit achilles tendon. Exp Diabesity Res 5(2):143–153. https://doi.org/10.1080/15438600490277860
7. Greenberg CS, Birckbichler PJ, Rice RH (1991) Transglutaminases: multifunctional cross-linking enzymes that stabilize tissues. FASEB J 5(15):3071–3077
8. Bailey AJ, Light ND, Atkins ED (1980) Chemical cross-linking restrictions on models for the molecular organization of the collagen fibre. Nature 288(5789):408–410
9. Orgel JP, Irving TC, Miller A, Wess TJ (2006) Microfibrillar structure of type I collagen in situ. Proc Natl Acad Sci U S A 103 (24):9001–9005. https://doi.org/10.1073/pnas.0502718103
10. Glowacki J, Mizuno S (2008) Collagen scaffolds for tissue engineering. Biopolymers 89 (5):338–344. https://doi.org/10.1002/bip.20871
11. Cliche S, Amiot J, Avezard C, Gariepy C (2003) Extraction and characterization of collagen with or without telopeptides from chicken skin. Poult Sci 82(3):503–509. https://doi.org/10.1093/ps/82.3.503
12. Friess W (1998) Collagen-biomaterial for drug delivery. Eur J Pharm Biopharm 45 (2):113–136
13. Charulatha V, Rajaram A (2003) Influence of different crosslinking treatments on the physical properties of collagen membranes. Biomaterials 24(5):759–767
14. Zeugolis DI, Paul GR, Attenburrow G (2009) Cross-linking of extruded collagen fibers -- a biomimetic three-dimensional scaffold for tissue engineering applications. J Biomed Mater Res A 89(4):895–908. https://doi.org/10.1002/jbm.a.32031
15. Weadock K, Olson RM, Silver FH (1983) Evaluation of collagen crosslinking techniques. Biomater Med Devices Artif Organs 11 (4):293–318
16. Jorge-Herrero E, Fernandez P, Turnay J, Olmo N, Calero P, Garcia R, Freile I, Castillo-Olivares JL (1999) Influence of different chemical cross-linking treatments on the properties of bovine pericardium and collagen. Biomaterials 20(6):539–545
17. van Wachem PB, Zeeman R, Dijkstra PJ, Feijen J, Hendriks M, Cahalan PT, van Luyn MJ (1999) Characterization and biocompatibility of epoxy-crosslinked dermal sheep collagens. J Biomed Mater Res 47(2):270–277
18. Haugh MG, Jaasma MJ, O'Brien FJ (2009) The effect of dehydrothermal treatment on the mechanical and structural properties of collagen-GAG scaffolds. J Biomed Mater Res A 89(2):363–369. https://doi.org/10.1002/jbm.a.31955
19. Wess TJ, Orgel JP (2000) Changes in collagen structure: drying, dehydrothermal treatment and relation to long term deterioration. Thermochim Acta 365(1-2):119–128. https://doi.org/10.1016/S0040-6031(00)00619-5
20. Weadock KS, Miller EJ, Bellincampi LD, Zawadsky JP, Dunn MG (1995) Physical cross-linking of collagen fibers: comparison of ultraviolet irradiation and dehydrothermal treatment. J Biomed Mater Res 29 (11):1373–1379. https://doi.org/10.1002/jbm.820291108
21. Torres DS, Freyman TM, Yannas IV, Spector M (2000) Tendon cell contraction of collagen-GAG matrices in vitro: effect of cross-linking. Biomaterials 21(15):1607–1619
22. Chen RN, Ho HO, Sheu MT (2005) Characterization of collagen matrices crosslinked using microbial transglutaminase. Biomaterials 26(20):4229–4235. https://doi.org/10.1016/j.biomaterials.2004.11.012
23. Stachel I, Schwarzenbolz U, Henle T, Meyer M (2010) Cross-linking of type I collagen with microbial transglutaminase: identification of cross-linking sites. Biomacromolecules 11 (3):698–705. https://doi.org/10.1021/bm901284x

24. Zeugolis DI, Panengad PP, Yew ES, Sheppard C, Phan TT, Raghunath M (2010) An in situ and in vitro investigation for the transglutaminase potential in tissue engineering. J Biomed Mater Res A 92(4):1310–1320. https://doi.org/10.1002/jbm.a.32383
25. Orban JM, Wilson LB, Kofroth JA, El-Kurdi MS, Maul TM, Vorp DA (2004) Crosslinking of collagen gels by transglutaminase. J Biomed Mater Res A 68(4):756–762. https://doi.org/10.1002/jbm.a.20110
26. Moshnikova AB, Afanasyev VN, Proussakova OV, Chernyshov S, Gogvadze V, Beletsky IP (2006) Cytotoxic activity of 1-ethyl-3-(3-dimethylaminopropyl)-carbodiimide is underlain by DNA interchain cross-linking. Cell Mol Life Sci 63(2):229–234. https://doi.org/10.1007/s00018-005-5383-x
27. Speer DP, Chvapil M, Eskelson CD, Ulreich J (1980) Biological effects of residual glutaraldehyde in glutaraldehyde-tanned collagen biomaterials. J Biomed Mater Res 14(6):753–764. https://doi.org/10.1002/Jbm.820140607
28. Gough JE, Scotchford CA, Downes S (2002) Cytotoxicity of glutaraldehyde crosslinked collagen/poly(vinyl alcohol) films is by the mechanism of apoptosis. J Biomed Mater Res 61(1):121–130. https://doi.org/10.1002/jbm.10145
29. Hass V, Luque-Martinez IV, Gutierrez MF, Moreira CG, Gotti VB, Feitosa VP, Koller G, Otuki MF, Loguercio AD, Reis A (2016) Collagen cross-linkers on dentin bonding: stability of the adhesive interfaces, degree of conversion of the adhesive, cytotoxicity and in situ MMP inhibition. Dent Mater 32(6):732–741. https://doi.org/10.1016/j.dental.2016.03.008
30. Delgado LM, Bayon Y, Pandit A, Zeugolis DI (2015) To cross-link or not to cross-link? Cross-linking associated foreign body response of collagen-based devices. Tissue Eng Part B 21(3):298–313. https://doi.org/10.1089/ten.TEB.2014.0290
31. Brown BN, Londono R, Tottey S, Zhang L, Kukla KA, Wolf MT, Daly KA, Reing JE, Badylak SF (2012) Macrophage phenotype as a predictor of constructive remodeling following the implantation of biologically derived surgical mesh materials. Acta Biomater 8(3):978–987. https://doi.org/10.1016/j.actbio.2011.11.031
32. McDade JK, Brennan-Pierce EP, Ariganello MB, Labow RS, Michael Lee J (2013) Interactions of U937 macrophage-like cells with decellularized pericardial matrix materials: influence of crosslinking treatment. Acta Biomater 9(7):7191–7199. https://doi.org/10.1016/j.actbio.2013.02.021
33. Orenstein SB, Qiao Y, Klueh U, Kreutzer DL, Novitsky YW (2010) Activation of human mononuclear cells by porcine biologic meshes in vitro. Hernia 14(4):401–407. https://doi.org/10.1007/s10029-010-0634-7
34. Witherel CE, Graney PL, Freytes DO, Weingarten MS, Spiller KL (2016) Response of human macrophages to wound matrices in vitro. Wound Repair Regen 24(3):514–524. https://doi.org/10.1111/wrr.12423
35. Delgado LM, Fuller K, Zeugolis DI (2017) Collagen cross-linking: biophysical, biochemical, and biological response analysis. Tissue Eng Part A 23(19–20):1064–1077. https://doi.org/10.1089/ten.TEA.2016.0415
36. Lotz C, Schmid FF, Oechsle E, Monaghan MG, Walles H, Groeber-Becker F (2017) Cross-linked collagen hydrogel matrix resisting contraction to facilitate full-thickness skin equivalents. ACS Appl Mater Interfaces 9(24):20417–20425. https://doi.org/10.1021/acsami.7b04017
37. Monaghan M, Browne S, Schenke-Layland K, Pandit A (2014) A collagen-based scaffold delivering exogenous microRNA-29B to modulate extracellular matrix remodeling. Mol Ther 22(4):786–796. https://doi.org/10.1038/mt.2013.288
38. Sanami M, Sweeney I, Shtein Z, Meirovich S, Sorushanova A, Mullen A, Miraftab M, Shoseyov O, O'Dowd C, Pandit A, Zeugolis D (2016) The influence of poly(ethylene glycol) ether tetrasuccinimidyl glutarate on the structural, physical, and biological properties of collagen fibers. J Biomed Mater Res B 104(5):914–922
39. Marinucci L, Lilli C, Guerra M, Belcastro S, Becchetti E, Stabellini G, Calvi EM, Locci P (2003) Biocompatibility of collagen membranes crosslinked with glutaraldehyde or diphenylphosphoryl azide: an in vitro study. J Biomed Mater Res A 67A(2):504–509. https://doi.org/10.1002/jbm.a.10082
40. Petite H, Frei V, Huc A, Herbage D (1994) Use of diphenylphosphorylazide for cross-linking collagen-based biomaterials. J Biomed Mater Res 28(2):159–165. https://doi.org/10.1002/Jbm.820280204
41. Capella-Monsonís H, Coentro J, Graceffa V, Wu Z, Zeugolis D (2018) An experimental toolbox for characterization of mammalian collagen type I in biological specimens. Nat Protoc 13(3):507–529

42. Coentro J, Capella-Monsonís H, Graceffa V, Wu Z, Mullen A, Raghunath M, Zeugolis D (2017) Collagen quantification in tissue specimens. Methods Mol Biol 1627:341–350
43. Lareu R, Zeugolis D, Abu-Rub M, Pandit A, Raghunath M (2010) Essential modification of the Sircol collagen assay for the accurate quantification of collagen content in complex protein solutions. Acta Biomater 6(8):3146–3151
44. Zeugolis D, Li B, Lareu R, Chan C, Raghunath M (2008) Collagen solubility testing, a quality assurance step for reproducible electro-spun nano-fibre fabrication. A technical note. J Biomater Sci Polym Ed 19(10):1307–1317
45. Zeugolis D, Raghunath M (2010) The physiological relevance of wet versus dry differential scanning calorimetry for biomaterial evaluation: a technical note. Polym Int 59(10):1403–1407

Chapter 4

A Biomimetic Model for Mineralization of Type-I Collagen Fibrils

Shasha Yao, Yifei Xu, Changyu Shao, Fabio Nudelman, Nico A. J. M. Sommerdijk, and Ruikang Tang

Abstract

The bone and dentin mainly consist of type-I collagen fibrils mineralized by hydroxyapatite (HAP) nanocrystals. In vitro biomimetic models based on self-assembled collagen fibrils have been widely used in studying the mineralization mechanism of type-I collagen. In this chapter, the protocol we used to build a biomimetic model for the mechanistic study of type-I collagen mineralization is described. Type-I collagen extracted from rat tail tendon or horse tendon is self-assembled into fibrils and mineralized by HAP in vitro. The mineralization process is monitored by cryoTEM in combination with two-dimensional (2D) and three-dimensional (3D) stochastic optical reconstruction microscopy (STORM), which enables in situ and high-resolution visualization of the process.

Key words Bone, Type-I collagen, Calcium phosphate, CryoTEM, STORM

1 Introduction

Type-I collagen is the main organic constitution of the hard tissues of vertebrates, e.g., the dentin and bone [1–3]. The type-I collagen fibrils are assembled by ~300-nm-long triple helix molecules which are ~1.5 nm in diameter [4]. Recent X-ray study indicates that in type-I collagen fibrils, subunit called "microfibrils" is formed by five 1D staggered and twisted collagen molecules [5]. These microfibrils pack into superstructures with triclinic symmetry (P1, $a \approx 40.0$ Å, $b \approx 27.0$ Å, $c \approx 678$ Å, $\alpha \approx 89.2°$, $\beta \approx 94.6°$, $\gamma \approx 105.6°$) and form larger collagen fibrils which display a ~67 nm periodical structure. Each ~67 nm unit contains a less dense gap region and an overlap region, which are, respectively, ~37 nm and ~30 nm long [5], while the values vary slightly depending on the sources of the collagen [6]. The type-I collagen

Shasha Yao and Yifei Xu contributed equally to this work.

Irit Sagi and Nikolaos A. Afratis (eds.), *Collagen: Methods and Protocols*, Methods in Molecular Biology, vol. 1944, https://doi.org/10.1007/978-1-4939-9095-5_4, © Springer Science+Business Media, LLC, part of Springer Nature 2019

fibrils in bone are embedded by ~4-nm-thick-carbonated hydroxyapatite (HAP) nanoplatelets with their c-axis oriented along the fibril axis [7, 8], which significantly improves the mechanical performances of the fibrils [9, 10]. The formation mechanism of the intrafibrillar HAP crystals has long been an attractive research topic. Due to the difficulty of in vivo study of bone formation process, the majority of the studies on collagen mineralization was performed in vitro based on biomimetic models, using demineralized collagen from the bone or dentin [11, 12], collagen sponge [8, 13], but most commonly self-assembled collagen fibrils [14–17]. Type-I collagen molecules could self-assemble in vitro at pH = 7 to 10 at temperatures from 20 to 37° with the presence of electrolytes (e.g., KCl) [18, 19], forming fibrils with ~67 nm periodical structures similar to those found in vivo. It has been shown that collagen could be intrafibrillarly mineralized in vitro by HAP platelets oriented in *c*-axis [8–15], with electron diffraction pattern indistinguishable to mineralized collagen fibrils found in bones. Charged macromolecules mimicking the acidic non-collagenous proteins (NCP) [20] in bone or dentin such as polyaspartic acid (pAsp) [8, 15], polyacrylic acid (pAA) [17], fetuin [15, 21], and poly (allylamine) hydrochloride (pAH) [16] were found to be essential for the in vitro mineralization of the type-I collagen fibrils. This is probably related to their ability to stabilize amorphous calcium phosphate (ACP) precursor and inhibit the formation of HAP. Recently we have found that charged small biomolecules, such as citrate, could further promote the type-I collagen mineralization by reducing the interfacial energy between collagen and the ACP precursor [14]. In summary, the in vitro biomimetic models have been shown to be a powerful tool which provide profound insight into the collagen mineralization process [22]. However, these models were often based on different collagen sources and different methods to obtain and mineralize the collagen fibrils, which brings uncertainty for interpreting and comparing experimental results.

In this chapter we describe the protocol we used for assembling and mineralizing type-I collagen fibrils [14, 15]. In a typical procedure, a type-I collagen (from rat tail tendon or horse tendon) stock solution was mixed with an assembling buffer solution and then dripped onto transmission electron microscopy (TEM) grids to assemble the collagen fibrils on the grids. The grids were then exposed to the mineralization solution to induce the HAP mineralization. After mineralization, the products were visualized using a conventional cryogenic TEM (cryoTEM) in combination with 2D/3D STORM images in order to examine the intrafibrillar and extrafibrillar HAP mineralization of type-I collagen fibrils in situ with nano-level accuracy. We hope our method will contribute for establishing a standard experimental model, which will benefit all the researchers in this field.

2 Materials

1. Type-I collagen stock solution (3 mg ml^{-1}) from rat tail tendon was purchased from Gibco-Invitrogen (USA). Type-I collagen extract from horse tendon was kindly provided by Dr. Giuseppe Falini (Department of Chemistry, University of Bologna, Italy).
2. Assembling buffer: 0.3754 g glycine and 1.481 g KCl were dissolved in 100 ml of deionized water and ultrasonicated for 20 min at room temperature to obtain an assembling buffer solution containing 50 mM glycine and 200 mM KCl. The pH value was adjusted to 9.2 with 1 M NaOH solution. The assembling buffer solution was kept at 4 °C prior to use.
3. Mineralization solution: 2 ml of 3.34 mM $CaCl_2$ was dripped into a 10 ml petri dish, and then 0 to 240 μl of 10 mg ml^{-1} pAsp (27 kDa) stock solutions was added into the calcium solution. 2 ml phosphate solution containing 19 mM Na_2HPO_4 and 300 mM NaCl was then mixed with the above solution to obtain the mineralization solution.
4. Imaging buffer: 1.6 mg ml^{-1} glucose oxidase, 50 mM Tris, 10 mM NaCl, 50 mM cysteamine, 10% (w/v) glucose, 32 μg ml^{-1} catalase, and 1% (v/v) β-mercaptoethanol. The pH of the imaging buffer was tuned to 8 by 1 M NaOH and HCl solution.
5. Assembling buffer for cryoTEM study: 10 mM Hepes (pH = 7.4), 200 mM NaCl, and 30 mM KH_2PO_4 (*see* **Note 1**).
6. Hepes buffer: 10 mM Hepes (pH 7.4), 150 mM NaCl.
7. Mineralization solution C1: 10 mM Hepes (pH = 7.4), 5.4 mM $CaCl_2$.
8. Mineralization solution C2: 2.7 mM K_2HPO_4, 10 mM Hepes, 20 mg l^{-1}pAsp (Mw =2000~11,000 Da).
9. APTES solution: Dissolve 0.5 ml (3-aminopropyl) triethoxysilane (APTES) into 9.5 ml anhydrous ethanol.
10. The blocking buffer and the washing buffer were purchased from Beyotime (Product Code, P0023B, China).
11. The type-I collagen rabbit anti-mouse antibody (1:50) and mouse anti-rabbit Cy3B-conjugated secondary antibodies (1:100) were supplied by Proteintech (USA).
12. Deionized water and all the solutions were filtered through 0.22 μm Millipore films prior to use.

3 Methods

3.1 Conventional TEM Experiments

3.1.1 Self-Assembly of Type-I Collagen Fibrils

1. In order to assemble the collagen on TEM grids, 8.33 μl of type-I collagen stock solution from rat tail tendon was dripped into 0.5 ml of assembling buffer solution and incubated at 37 °C for 20 min with stirring (*see* **Note 2**).
2. 200-mesh gold TEM grids (*see* **Note 3**) coated by carbon films were glow discharged for 40 s using a Cressington 208 carbon coater and then transferred into a glass petri dish.
3. 3 μl of incubated type-I collagen solution was gently dripped into the carbon film face of the TEM grids (*see* **Note 4**).
4. Sealed TEM grids were incubated at 37 °C for 12 h (*see* **Note 5**) and then gently rinsed with deionized water.
5. The type-I collagen fibrils were further cross-linked with 0.05% glutaraldehyde for 2 h and gently rinsed with deionized water and air-dried.
6. To increase the contrast of the periodical structure within the type-I collagen fibrils, 2% (w/v) uranyl acetate staining solution was dripped onto the TEM grids loaded with type-I collagen fibrils and then washed after 15 s with deionized water and air-dried.

3.1.2 Collagen Mineralization

1. 8 μl of 5% (w/v) NaN_3 was added to the mineralization solution to retard bacterial growth. The solutions should be mixed quickly, and the as-prepared mineralization solution should be colorless and transparent. Slow mixing would lead to a light blue-colored, cloudy dispersion (Fig. 1).
2. TEM grids loaded with type-I collagen fibrils were floated upside down on the mineralization solution at 37 °C for designated times.
3. After mineralization, the TEM grids were taken out and washed in sequence by deionized water, 25% ethanol, 50% ethanol, and 100% ethanol.

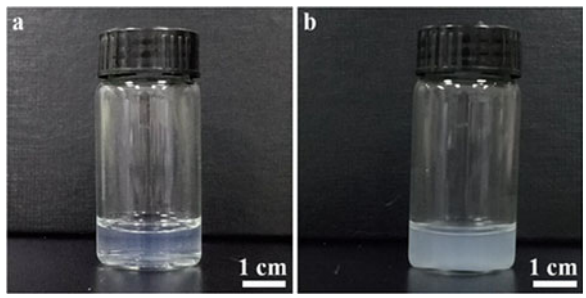

Fig. 1 Photos showing the effect of mixing speed on preparing the mineralization solution. (**a**) The colorless and transparent mineralization solution obtained by fast mixing. (**b**) The light blue-colored, cloudy dispersion obtained by slow mixing

3.1.3 TEM Imaging and Mineralization Degree Calculation

The assembled (Fig. 2), stained (Fig. 3), and mineralized (Figs. 4 and 5) type-I collagen fibrils were visualized by TEM operating at 100 kV or 200 kV. The mineralization degree increased with increasing the pAsp concentration from 0 to 240 μg ml^{-1} (Fig. 4) and increasing the mineralization time from 6 h to 24 h (Fig. 5).

The mineralization degree (*m.d.*) was calculated by first splitting the pixel intensity histogram of the TEM images into three Gaussian distributions (Fig. 6), which correspond to the

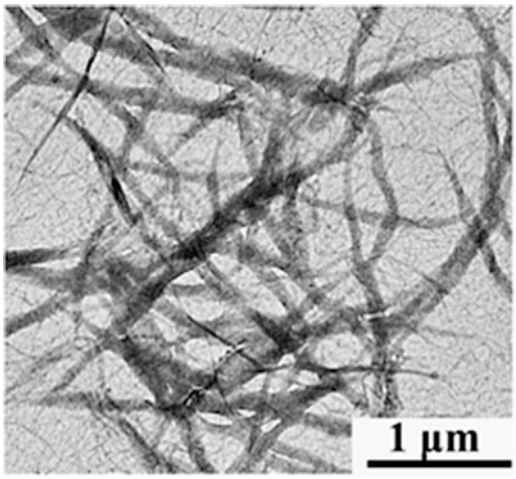

Fig. 2 Conventional TEM image of the assembled type-I collagen fibrils

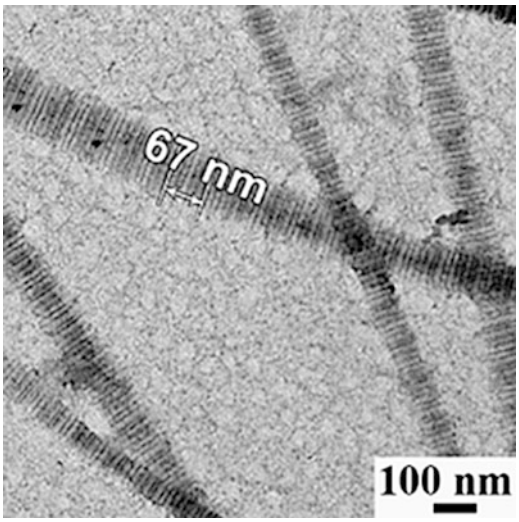

Fig. 3 Conventional TEM image of the assembled type-I collagen fibrils after uranyl acetate positive staining, displaying the ~67 nm periodical structures together with fine band structures. Reproduced with permission [14]. Copyright 2018, Wiley-VCH

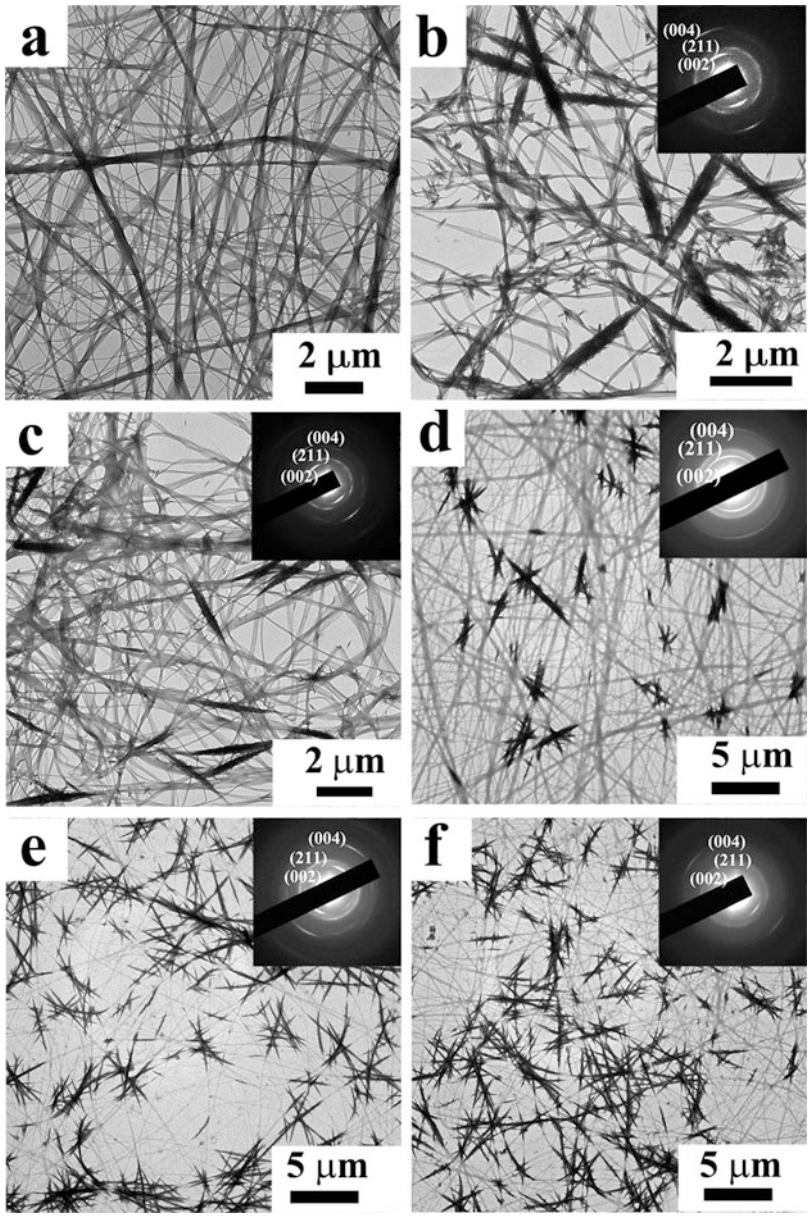

Fig. 4 Conventional TEM images of the mineralized collagen-I fibrils in the presence of 0 (**a**), 10 (**b**), 15 (**c**), 50 (**d**), 120 (**e**), and 240 (**f**) μg ml^{-1} pAsp. Insets: selected area electron diffraction (SAED) patterns of the samples, which match with the HAP diffractions and indicate the oriented crystallization. Reproduced with permission [14]. Copyright 2018, Wiley-VCH

background, collagen fibrils, and mineralized collagen fibrils, respectively. The thresholds (T) between the three areas are determined by $T = \bar{I} - 2\sigma$ [23], where $\bar{I}$ is the mean pixel intensity of each Gaussian distribution and σ is the standard. The areas corresponding to all of the collagen fibrils (S1) and the mineralized

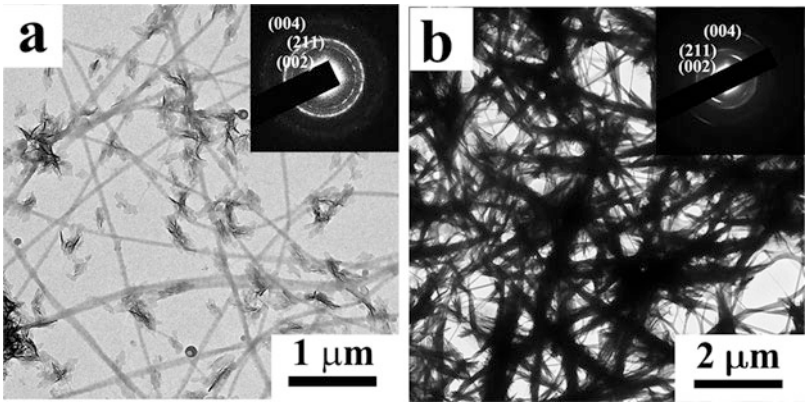

Fig. 5 Conventional TEM images of the collagen-I fibrils mineralized at 6 h (**a**) and 24 h (**b**). Insets: SAED patterns indicating HAP mineralization. Reproduced with permission [14]. Copyright 2018, Wiley-VCH

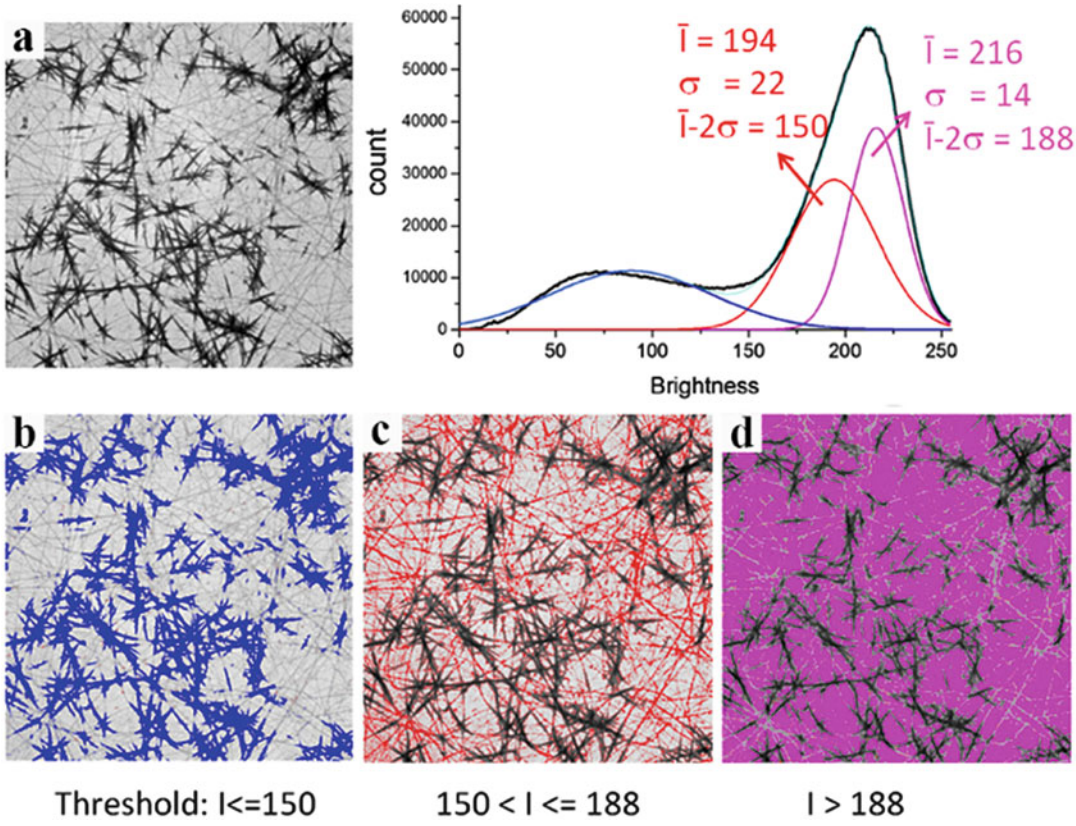

Fig. 6 Mineralization degree calculation. (**a**) Segmentation thresholds determined by analyzing the pixel intensity histogram of the TEM image and splitting the histogram into three Gaussian distributions. Determination of the regions of the mineralized collagen-I fibrils (**b**), unmineralized collagen-I fibrils (**c**), and the background (**d**). Reproduced with permission [14]. Copyright 2018, Wiley-VCH

part of the collagen fibrils (S2) could then be segmented from the image, and *m.d.* could then be given by comparing S1 and S2

$$m.d. = \frac{S1}{S2}$$

For each analysis, at least five samples were examined to obtain the mean value and standard deviation of *m.d.*

3.2 CryoTEM Experiments

3.2.1 Self-Assembly of Type-I Collagen Extracted from Rat Tail Tendon

1. 3 mg ml^{-1} of type-I collagen stock solution from rat tail was mixed with the assembling buffer for cryoTEM study in a 1:29 ratio. 300 μl of as-prepared incubation solution was applied on a parafilm.
2. Gold Quantifoil grids were floated upside down on the incubation solution droplet (Fig. 7). The parafilm was then covered by a glass petri dish and incubated for 200 min.
3. After incubation, the grids were transferred to the Vitrobot (FEI, Mark III) in 100% humidity (*see* **Note 6**), blotted for 5 s by filter papers, and then vitrified in liquid ethane to visualize the collagen fibrils or transferred to the mineralization solution (*see* Subheading 3.2.3).

3.2.2 Self-Assembly of Type-I Collagen Extracted from Horse Tendon

1. 1 g of type-I collagen extracted from horse tendon was mixed overnight with 10 ml of 50 mM aqueous acetic acid, pH 2.5, centrifuged at 3500 × *g* for 10 min, and the supernatant was collected and stored at 4 °C.
2. CryoTEM grids were laid on a 15 μl drop of collagen solution for 10 s. The excess of collagen solution was manually blotted, and the grids were transferred to a 15 μl drop of Hepes buffer, for 30 min. This procedure was performed inside a glove box, where temperature and humidity are controlled at 22 °C and 100% relative humidity.
3. The grids were then vitrified as described in Subheading 3.2.1 or transferred to the mineralization solution (*see* Subheading 3.2.3).

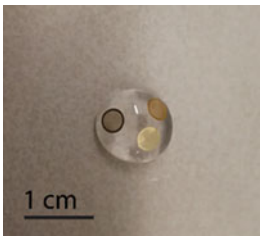

Fig. 7 Photo of the gold Quantifoil TEM grids floating on a droplet of buffer solution applied on a parafilm

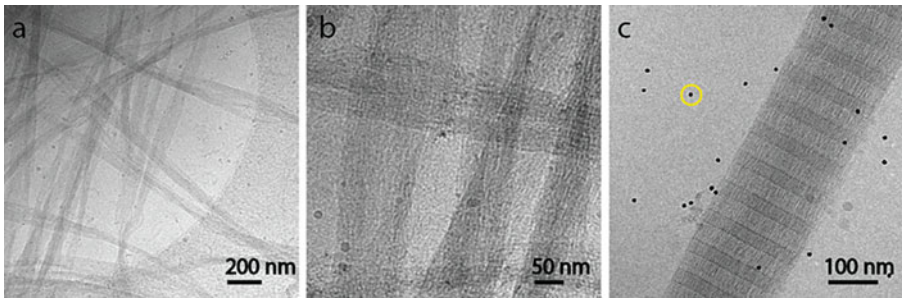

Fig. 8 CryoTEM image of assembled type-I collagen fibrils. (**a**) Rat tail type-I collagen fibrils, which are 60–80 nm thick. (**b**) Zoom-in image of the fibrils showing no periodical structure. (**c**) A horse tendon type-I collagen fibril, which is ~300 nm thick and clearly shows the ~67 nm periodical structure. The 10 nm particles highlighted by yellow circle are gold fiducial markers used for tomography

3.2.3 Collagen Mineralization

1. Mineralization solutions C1 and C2 were mixed 1:1 to prepare the final mineralization solution in a glass petri dish.
2. The gold Quantifoil grids were rinsed in two 300 μl water droplets applied on parafilm for 1 min each immediately after collagen assembly to remove the residual salts and then transferred into the petri dish containing the mineralization solution.
3. The petri dish was then sealed by parafilm and heated at 37 °C for 72 h for mineralization.
4. After mineralization, the grids were transferred to the Vitrobot (FEI, Mark III) in 100% humidity, blotted for 5 s by filter papers, and then vitrified in liquid ethane.

3.2.4 CryoTEM Imaging

1. CryoTEM imaging of the assembled (Fig. 8 and *see* **Note 7**) and then mineralized (Fig. 9) collagen was performed under ~3 μm defocus on a FEI Titan cryoTEM equipped with a field emission gun (FEG) and operating at 300 kV or a FEI Tecnai 20 (Type Sphera) TEM equipped with a LaB_6 filament operating at 200 kV and a Gatan cryo-holder operating at −170 °C.
2. Images were recorded in FEI Titan using a 2 k × 2 k Gatan CCD camera equipped with a post-column Gatan energy filter (GIF) or in FEI Tecnai using a 1 k × 1 k Gatan CCD camera. The electron dose used is 10 e $Å^{-2}$ per image (*see* **Note 8**).

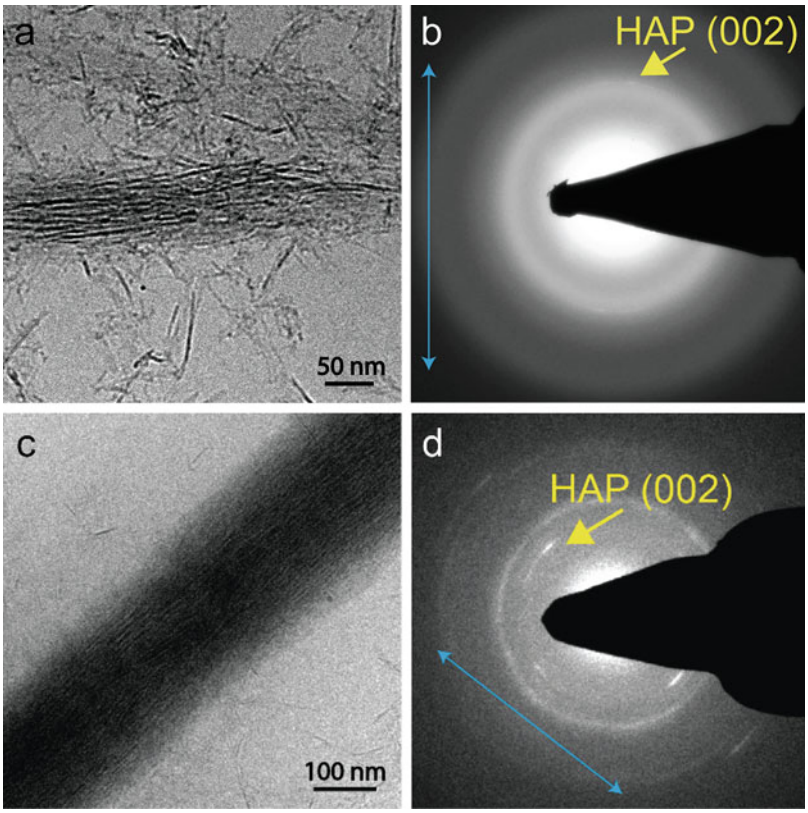

Fig. 9 CryoTEM image of mineralized type-I collagen fibrils. (**a**) Image showing a mineralized rat tail type-I collagen fibril, displaying stacks of HAP platelets. (**b**) SAED pattern of the mineralized rat tail collagen fibril, which shows a narrow but very weak HAP (002) diffraction arc in the collagen fibril axis direction as highlighted by the yellow arrow. (**c**) Image showing a mineralized horse tendon type-I collagen fibril. The fibril is completely impregnated with HAP platelets, and therefore the ~67 nm periodical structures are not distinguishable. (**d**) SAED pattern of the mineralized horse tendon type-I collagen fibril, which clearly shows the HAP (002) diffraction arc in the collagen axis as highlighted by the yellow arrow. The collagen fibril axis directions in (**c**) and (**d**) are highlighted by the blue arrows

3.3 STORM Experiments

3.3.1 Modification of the Laser Confocal Culture Dish (LCCD) and Self-Assembly of Type-I Collagen Fibrils

1. Type-I collagen fibrils (rat tail) were immobilized on the amino-silanized LCCD. In the experiments, 200 μl APTES was dripped onto a LCCD substrate avoiding the light. The APTES solution was then removed and dried in an oven at 100 °C prior to use (*see* **Note 9**).
2. 100 μl of 50 μg ml^{-1} type-I collagen (rat tail) solution was dripped on the modified LCCD substrate and incubated at 37 °C for 12 h and then gently rinsed with deionized water.
3. The type-I collagen fibrils were further cross-linked with 0.05 wt% glutaraldehyde for 2 h and then gently rinsed with deionized water (*see* **Note 10**).

3.3.2 Staining and Mineralization of the Type-I Collagen Fibrils

The immunofluorescent staining was performed according to the following steps:

1. The type-I collagen (rat tail) fibrils were incubated with blocking buffer for 1 h and then incubated with the type-I collagen rabbit anti-mouse antibody at 37 °C for another 2 h.
2. The samples were washed by the washing buffer for three times (10 min each) and incubated with mouse anti-rabbit Cy3B-conjugated secondary antibodies for 1 h at 37 °C.
3. The samples were washed by three extra times in the washing buffer (10 min each) and mineralized with the mineralization solution.

The mineralization process was as follows:

1. 2 ml of 3.34 mM $CaCl_2$ solution and 48 μl of 10 mg ml^{-1} pAsp solution were dropped into a LCCD which was loaded with immunofluorescence-stained collagen.
2. 2 ml of solution containing 19 mM Na_2HPO_4 and 300 mM NaCl was mixed into the solution.
3. The samples were mineralized in the as-prepared mineralization solution at 37 °C for 24 h and rinsed with deionized water for three times.
4. The mineralized type-I collagen fibrils were labeled by 2 ml of 10 μM calcein which specifically bind with HAP for 20 min at room temperature. Residual calcein was removed by washing using deionized water.

3.3.3 STORM Imaging

The type-I collagen (rat tail) fibrils were immersed in the imaging buffer before STORM imaging.

1. 2D STORM imaging experiments were performed on inverted optical microscope. For *z*-stack images of the mineralized type-I collagen fibrils, the images were recorded, processed, and analyzed using the Imaris software.
2. 3D STORM imaging experiments were performed on a Nikon N-STORM microscope equipped with a 100 × oil immersion objective and an Andor camera [24].
3. To identify the zone of interest, a low-magnification fluorescence image was acquired prior to STORM imaging.
4. After switching to higher magnification (100× objective), conventional fluorescence images were first acquired. STORM data acquisition was then started using imaging cycles at one frame of activation laser illumination (405 nm laser) followed by five frames of imaging laser illumination (561 nm laser). The integration time of the camera was set to the one frame mode with an EM gain of 305,000–10,000 cycles per channel, which was

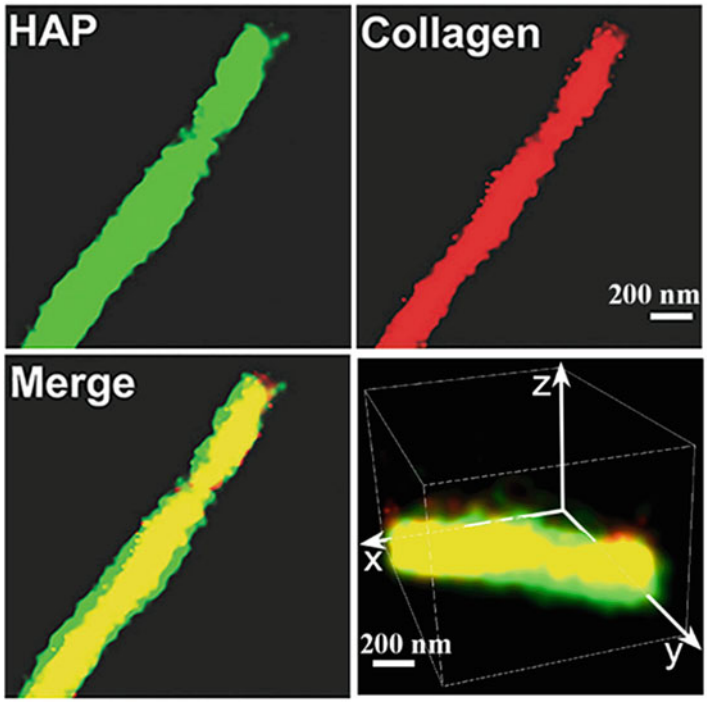

Fig. 10 The xy projects of the 2D STORM images of the mineralized collagen-I fibrils, with collagen labeled by Cy3B and showing red fluorescence. The HAP was labeled with calcein, which emitted green fluorescence. Reproduced with permission [14]. Copyright 2018, Wiley-VCH

used for the reconstruction of each 3D super-resolution image. The STORM images confirm the intrafibrillar mineralization of type-I collagen fibrils.

5. In the 2D images, the type-I collagen fibrils were labeled before mineralization, which emitted red fluorescence. After mineralization, the HAP was labeled with calcein, which emitted fluorescence with the wavelength of green light. The data showed that the ACP infiltrated into the type-I collagen fibrils and transformed into HAP inside the type-I collagen fibrils (Fig. 10).
6. The *z*-slice of the 3D STORM images of the mineralized type-I collagen fibrils indicated the mineralization of HAP inside and outside the type-I collagen fibrils. Besides, the HAP was homogeneously dispersed in the type-I collagen fibrils (Fig. 11).

4 Notes

1. This buffer solution induces a faster assembly of rat tail type-I collagen, which benefits the cryoTEM study.

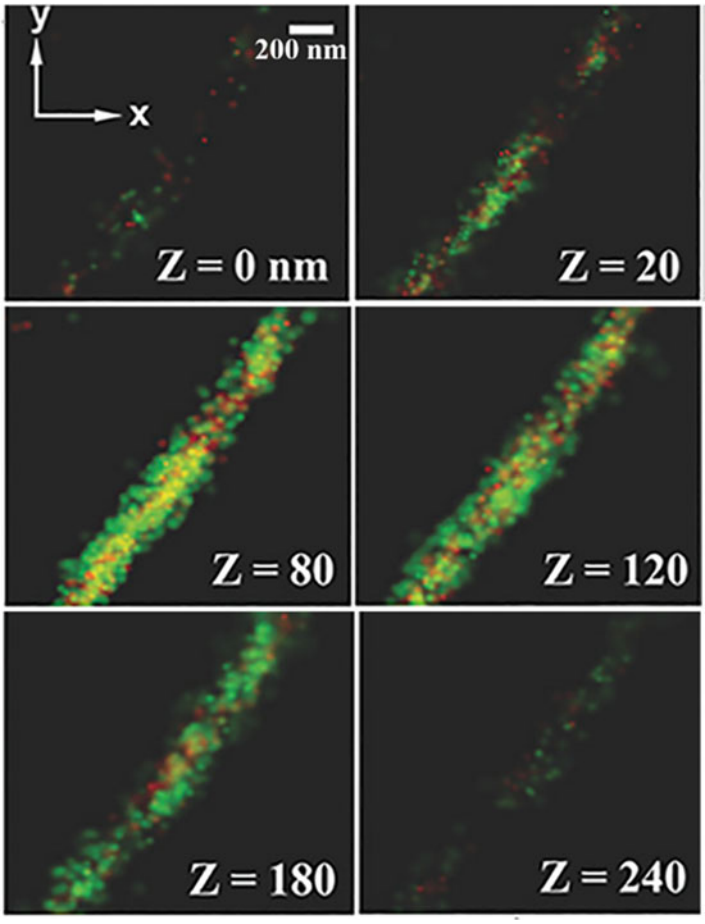

Fig. 11 The *z*-slices of the STORM image of the mineralized collagen-I fibrils, indicating that the mineralization of HAP inside and on the surface of the collagen-I fibrils. Reproduced with permission [14]. Copyright 2018, Wiley-VCH

2. Incubation time less than 20 min will lead to an inhomogeneous dispersion of the type-I collagen fibrils on the TEM grid (Fig. 12).
3. The mineralization experiment could not work on copper grids because of copper leaching in the solution which inhibits the crystallization of HAP [25].
4. 3 μl is the optimal volume which neither dries very quickly (less than 4 h) nor leads to overflow of the TEM grids.
5. The mineralization solution was replaced each 6 h to keep the supersaturation constant.
6. The solution left between the tweezers has to be carefully removed by filter paper before the grids were transferred into Vitrobot, in order to prevent the tweezers from being frozen during the vitrification process.

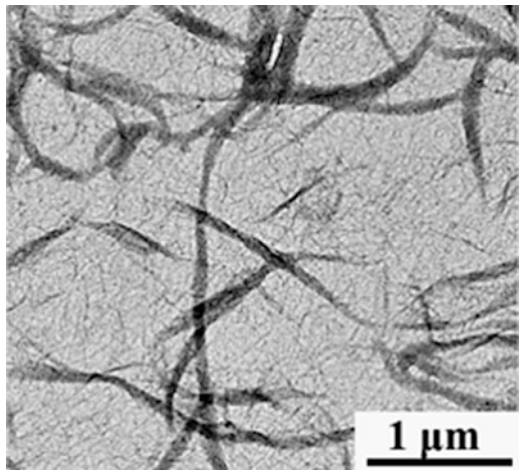

Fig. 12 Conventional TEM image of the TEM grid inhomogeneously covered by collagen-I fibrils

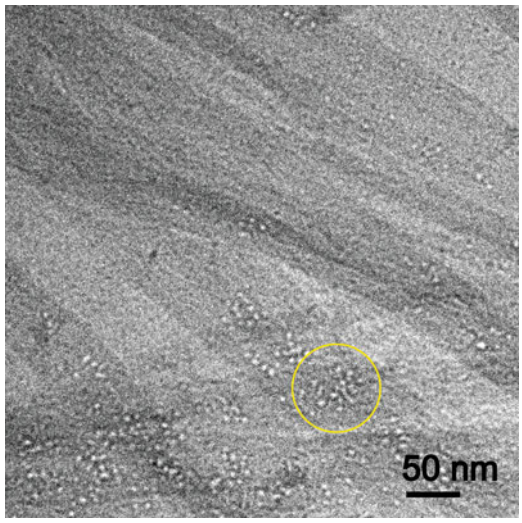

Fig. 13 CryoTEM image of collagen fibrils after exposure of 200 e/Å^2, showing the beam damage (white spots, as highlighted by the yellow circle)

7. No ~67 nm periodical structure could be visualized without staining for the assembled rat tail collagen fibrils, while the horse tendon collagen fibrils clearly show the periodical structure. This is due to the fact that these rat tail collagen fibrils (60–80 nm in diameter) are much thinner than the horse tendon collagen fibrils (~300 nm in diameter).
8. Collagen fibril is very sensitive to the electron beam, and beam damage could be clearly observed after the fibril was exposed to 200 e/Å^2 (Fig. 13).

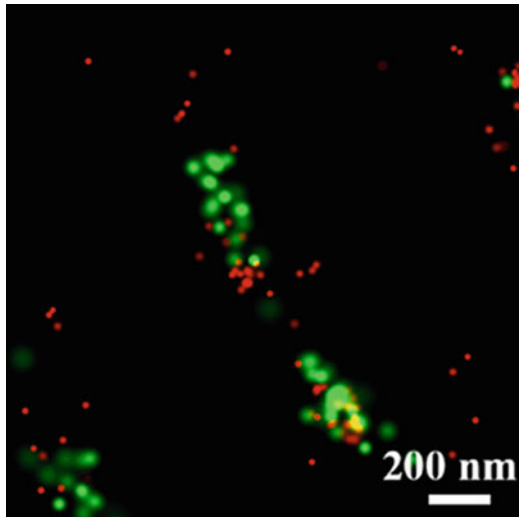

Fig. 14 2D STORM image of the nonhomogeneous stained collagen-I fibrils

9. The LCCD must be fresh and clean prior to use. After the removal of the APTES solution, the modified LCCD was ultrasonicated with anhydrous ethanol and deionized water for 20 min, respectively, to remove the physical absorbed chemicals. 50 μg ml^{-1} of type-I collagen solution was obtained by mixing 5 μl of type-I collagen stock solution with 295 μl of assembling solution and then incubating the mixed solution at room temperature for 20 min. After 12 h, the LCCD was gently rinsed with deionized water for at least three times to remove unassembled type-I collagen.
10. Incubation times of antibodies less than 2 h or calcein labeling time less than 20 min would lead to inhomogeneous stained type-I collagen samples (Fig. 14). The labeling process should avoid the light.

References

1. Weiner S, Traub W, Wagner HD (1999) Lamellar bone: structure-function relations. J Struct Biol 126:241–255
2. Beniash E, Traub W, Veis A, Weiner S (2000) A transmission electron microscope study using vitrified ice sections of predentin: structural changes in the dentin collagenous matrix prior to mineralization. J Struct Biol 132:212–225
3. Goldberg M, Kulkarni AB, Young M, Boskey A (2011) Dentin: structure, composition and mineralization. Front Biosci (Elite Ed) 3:711–735
4. Hodge AJ (1963) Recent studies with the electron microscope on ordered aggregates of the tropocollagen macromolecule. In: Ramachandran GN (ed) Aspects of protein structure. Academic Press, New York, pp 289–300
5. Orgel JPRO, Irving TC, Miller A, Wess TJ (2006) Microfibrillar structure of type I collagen in situ. Proc Natl Acad Sci U S A 103:9001–9005
6. Quan BD, Sone ED (2013) Cryo-TEM analysis of collagen fibrillar structure. Methods Enzymol 532:189–205

7. Weiner S, Traub W (1986) Organization of hydroxyapatite crystals within collagen fibrils. FEBS Lett 206:262–266
8. Olszta MJ et al (2007) Bone structure and formation: A new perspective. Mater Sci Eng R Rep 58:77–116
9. Gao HJ, Ji BH, Jager IL, Arzt E, Fratzl P (2003) Materials become insensitive to flaws at nanoscale: Lessons from nature. Proc Natl Acad Sci U S A 100:5597–5600
10. Nair AK, Gautieri A, Chang S-W, Buehler MJ (2013) Molecular mechanics of mineralized collagen fibrils in bone. Nat Commun 4:1724
11. Chen J, Burger C, Krishnan CV, Chu B, Hsiao BS, Glimcher MJ (2005) In vitro mineralization of collagen in demineralized fish bone. Macromol Chem Phys 206:43–51
12. Wang J et al (2013) Remineralization of dentin collagen by meta-stabilized amorphous calcium phosphate. CrystEngComm 15:6151–6158
13. Olszta M, Douglas E, Gower L (2003) Scanning electron microscopic analysis of the mineralization of type I collagen via a polymer-induced liquid-precursor (PILP) process. Calcif Tissue Int 72:583–591
14. Shao C et al (2018) Citrate improves collagen mineralization via interface wetting: a physicochemical understanding of biomineralization control. Adv Mater 30:1704876
15. Nudelman F et al (2010) The role of collagen in bone apatite formation in the presence of hydroxyapatite nucleation inhibitors. Nat Mater 9:1004–1009
16. Niu LN et al (2017) Collagen intrafibrillar mineralization as a result of the balance between osmotic equilibrium and electroneutrality. Nat Mater 16:370–378
17. Wang Y et al (2012) The predominant role of collagen in the nucleation, growth, structure and orientation of bone apatite. Nat Mater 11:724
18. Jiang F, Hörber H, Howard J, Müller DJ (2004) Assembly of collagen into microribbons: effects of pH and electrolytes. J Struct Biol 148:268–278
19. Williams BR, Gelman RA, Poppke DC, Piez KA (1978) Collagen fibril formation. Optimal in vitro conditions and preliminary kinetic results. J Biol Chem 253:6578–6585
20. George A, Veis A (2008) Phosphorylated proteins and control over apatite nucleation, crystal growth, and inhibition. Chem Rev 108:4670–4693
21. Price PA, Toroian D, Lim JE (2009) Mineralization by inhibitor exclusion the calcification of collagen with fetuin. J Biol Chem 284:17092–17101
22. Nudelman F, Lausch AJ, Sommerdijk NAJM, Sone ED (2013) In vitro models of collagen biomineralization. J Struct Biol 183:258–269
23. Smeets PJM et al (2017) A classical view on nonclassical nucleation. Proc Natl Acad Sci U S A 114:E7882–E7890
24. Bates M, Jones SA, Zhuang X (2013) Stochastic optical reconstruction microscopy (STORM): a method for superresolution fluorescence imaging. Cold Spring Harb Protoc 2013(6):498–520 pdb.top075143
25. Nudelman F, Bomans PH, George A, Sommerdijk NA (2012) The role of the amorphous phase on the biomimetic mineralization of collagen. Faraday Discuss 159:357–370

Part II

Proteomics Analysis of Collagen

Chapter 5

Investigation of Triple-Helix Collagen Hydroxylation by Solid-State NMR Spectroscopy

Wing Ying Chow

Abstract

Solid-state nuclear magnetic resonance spectroscopy (ssNMR) is an emerging technique in structural methods of studying collagen proteins, capable of identifying features on an atomic length scale in tissues and protein samples without extensive extraction or purification. Hydroxylation is a key posttranslational modification of collagen that gives rise to distinctive signals in the ssNMR spectrum of collagen proteins. Here we outline the type of information that ssNMR can provide and describe the procedures involved in a ssNMR structural study, with particular focus on using dynamic nuclear polarization to enhance sensitivity for detecting hydroxylysine residues by ssNMR.

Key words Solid-state nuclear magnetic resonance spectroscopy, NMR, Proline, Lysine, Hydroxylation, Hydroxyproline, Hydroxylysine, Isotopic enrichment/labelling, Dynamic nuclear polarization

1 Introduction

Hydroxylation is an important posttranslational modification (PTM) for all families of collagen proteins, contributing to the stability of the triple helix [1] and also providing sites for glycosylation and cross-linking [2]. Mass spectrometry-based studies can yield highly sensitive and quantitative information on the extent and location of modification, yet the information of the structural role of the hydroxylated species is lost in the extraction and purification processes required. Solid-state NMR, X-ray crystallography, solution-state NMR, and more recently cryo-electron microscopy are the key techniques to generate atomic-level structural information on biomolecules. Compared to other techniques, ssNMR has the advantage that it can be directly applied to highly heterogeneous and solid samples, such as tissue and extracellular matrix (ECM) samples.

Irit Sagi and Nikolaos A. Afratis (eds.), *Collagen: Methods and Protocols*, Methods in Molecular Biology, vol. 1944, https://doi.org/10.1007/978-1-4939-9095-5_5, © Springer Science+Business Media, LLC, part of Springer Nature 2019

1.1 NMR Overview

Nuclear magnetic resonance spectroscopy [3–5] relies on the fact that nuclei have a quantum property called *spin*. Spin arises from the number of protons and neutrons in the nuclei, taking values of 0, 1/2, 1, 3/2, and so on; certain nuclei (e.g., ^{1}H, ^{13}C) have a value of spin >0, and these nuclei can be detected by NMR, i.e., they are NMR-active. For elements with different isotopes, the nuclei of these isotopes often have different values of spin. For example, of the isotopes of carbon, the most abundant (^{12}C) has zero spin and hence cannot be detected by NMR. On the other hand, ^{1}H and ^{31}P, both highly abundant, have spin and can be detected by NMR. Almost all of the nuclei that are used for detection in NMR are stable (i.e., nonradioactive) isotopes.

In most biomolecular NMR, the focus is on experiments that involve spin-1/2 nuclei, commonly ^{1}H, ^{13}C, ^{15}N, and ^{31}P. These nuclei have the property of having two quantum states which have different energies when placed in a magnetic field. There are applications detecting NMR of higher-spin nuclei such as ^{2}H (spin-1), ^{14}N (spin-1), ^{17}O (spin-5/2), ^{23}Na (spin-3/2), and ^{43}Ca (spin-7/2); however, these often give rise to more complicated NMR spectra and therefore are beyond the scope of this chapter.

Transitions between the two states of a spin-1/2 nuclei in a magnetic field occur at a frequency that is determined by an intrinsic property of the nuclei and by the strength of the magnetic field. It is therefore necessary to note which nuclei is being detected, as at 9.4 T, the ^{1}H (proton) frequency is 400 MHz, while ^{13}C would have a frequency of 100 MHz and ^{15}N would have a frequency of 40 MHz. It is common to refer to NMR spectrometers by the ^{1}H frequency, so a 9.4 T magnet is commonly called a 400 MHz spectrometer and an 18.8 T magnet, an 800 MHz spectrometer.

A key part of NMR equipment is the probe head, which sits in the core of the magnet and plays several important roles: firstly, it places the sample in the region of the magnet with the most homogeneous magnetic field; secondly, it regulates the sample temperature; thirdly, for solid-state NMR, the probe head contains the stator, which can be adjusted to the magic angle and regulates the spinning of the rotor, necessary for producing resolved spectra (*see* below); fourthly and perhaps most importantly, a coil in the stator surrounds the sample and converts magnetic behavior of the spins to an electric current, which is amplified and can be detected by the resonant circuits. The circuits can be tuned to the specific characteristic frequency for ^{1}H and other nuclei to deliver radio-frequency (RF) pulses to manipulate the spin transitions; the combination of the number, timing, spacing, length, and power of the pulses is what makes up different NMR experiments by selecting for specific spin interactions.

Since the magnetic behavior of the spins occur at specific frequencies, the electric current induced and measured also shows an oscillating behavior over time, which has an overall decrease in

signal due to relaxation and is called the free induction decay (FID). Generally, the FID is not analyzed directly but instead subjected to Fourier transform which provides a spectrum with a frequency axis. Fourier transform procedures are routine on modern spectrometers and computers and are therefore not further described in this chapter.

1.2 Chemical Shift

One of the key advantages of NMR is its sensitivity to small variations in chemical structure. Differences in the number and types of bonds lead to relatively small (parts per million level) changes in the transition frequency. The simplest NMR spectra, so-called 1D spectra, are plots of the intensity of transition frequencies of one particular type of nuclei, giving insight into the types of different chemical environments for these nuclei in the sample.

The transition frequency scales with the external applied magnetic field. Therefore, the spectrum is commonly presented with a frequency scale called the *chemical shift* (δ), which is relative to parts per million (ppm) of the transition frequency of the nuclei in a reference sample, rather than the directly measured frequencies in MHz. The chemical shift scale has the useful property of enabling direct comparison of spectra obtained on spectrometers with different magnetic field strengths.

While the method of referencing the chemical shift scale can seem like a technical detail, it is important for accurate reporting and correct comparisons to literature-reported chemical shift values. For ^{1}H and ^{13}C NMR, the chemical shift ppm scale is referenced by setting the signal of TMS (tetramethylsilane) or DSS (2,2-dimethyl-2-silapentane-5-sulfonic acid) to zero ppm. TMS is used by publications in synthetic chemistry as per IUPAC recommendations [6], while DSS is more commonly used in biomolecular NMR spectroscopy due to its better water solubility [7]. For ^{13}C, the DSS-referenced chemical shift values are greater than the TMS-referenced values by approximately 2.7 ppm, so it is important to take this conversion factor into account when comparing to literature values.

In solution-state NMR, referencing is often carried out using the solvent signal. However, this is not the recommended approach in solid-state NMR due to the highly variable amount of solvent, the wider temperature range, and the potential inhomogeneity in solvent distribution, all of which can lead to shifting or broadening of the solvent signal, complicating attempts to reference and/or reproduce the spectra. Instead, DSS is sometimes added to wet pellet protein samples as an internal reference or external referencing is used where DSS or TMS is not added to the sample but measured separately. In this chapter, we use an external referencing scheme based on TMS, as we would prefer to facilitate comparisons with synthetic compounds that model collagen glycosylation [8].

Using 1D NMR spectra and chemical shifts alone, it is possible to quickly identify the components present in the tissue or collagen sample. In particular, solid samples containing a high proportion of collagen should show ^{13}C signals at 42.5 ppm (glycine Cα), 70 ppm (hydroxyproline Cγ), and a broad signal around 170.5 ppm (amide C′) with a shoulder at 169–170 ppm (glycine C′). Representative spectra of collagen-containing samples are shown in Subheading 3.

NMR is highly sensitive to hydroxylation of proline and lysine, as hydroxylation leads to a large change of the chemical shift of the carbon signal. Proline Cγ is found at 25 ppm, but hydroxyproline Cγ is found at 70 ppm. Similarly, lysine Cδ is found at 28 ppm, but hydroxylysine Cδ is found at 70 ppm. While we can distinguish between the unmodified and the hydroxylated forms, we see that both hydroxyproline and hydroxylysine have a ^{13}C signal at 70 ppm, and indeed, in a 1D NMR spectrum, it is not possible to determine whether the signal arises from a hydroxylated proline or lysine without other prior knowledge, such as by selectively labelling one of these amino acids.

Multidimensional NMR spectra can improve resolution and enable signals that overlap in 1D to be more clearly identified and assigned, thus allowing more structural information to be extracted. Such spectra provide information on correlations between pairs or a series of nuclei, usually in a distance- or bond-dependent manner. The nuclei correlated can be the same type (e.g., ^{13}C–^{13}C), or different (e.g., ^{13}C–^{15}N). In the specific case of hydroxylated residues in collagen, it is possible to distinguish hydroxyproline and hydroxylysine since the closest carbons have different chemical shifts (Fig. 1), meaning that crosspeaks are resolved from each other in 2D ^{13}C–^{13}C spectra. Another method to distinguish between the two is to find correlations between the hydroxylysine sidechain nitrogen and Cγ in 2D ^{13}C–^{15}N spectra, as the ^{15}N chemical shift of the lysine and hydroxylysine side chain is very different from that of the backbone amide.

While there is mathematically no limit to the number of dimensions and the length of NMR-active nuclei series thus detected, with more transfers/dimensions leading generally to better resolution, NMR phenomena are subject to relaxation, and there is a sensitivity loss for each additional dimension. While it is useful to have multiple dimensions for separating overlapping signals, in this chapter we will only cover experiments up to two dimensions which are routinely achievable.

1.3 Solid-State NMR and Magic Angle Spinning

The lack of tumbling motion of the sample in solid-state NMR complicates the spectra compared to those of solution-state NMR. Since the interaction of the nuclei and the magnetic field is anisotropic and depends on the orientation of surrounding atoms and bonds, the signals in solid-state NMR spectra of static noncrystalline samples are greatly broadened. Moreover, through-space

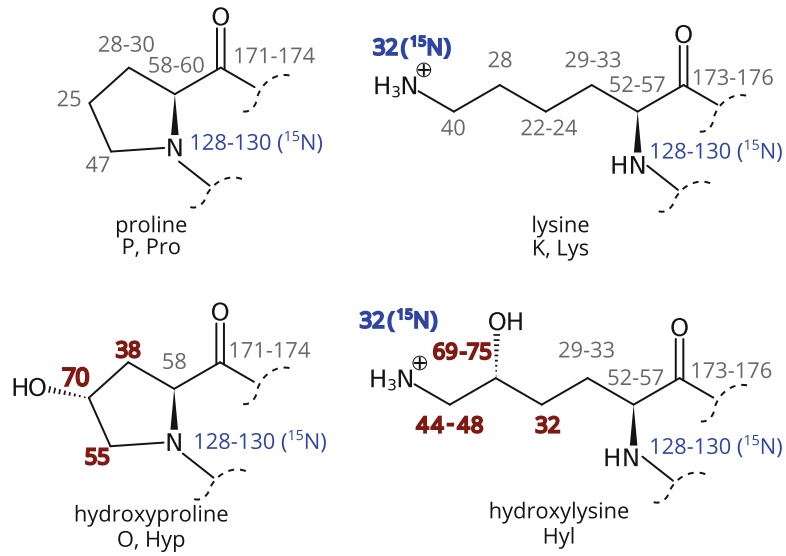

Fig. 1 Typical ^{13}C and ^{15}N chemical shifts of proline, hydroxyproline, lysine, and hydroxylysine. For proline, hydroxyproline, and lysine, variations are usually less than 2 ppm. For hydroxylysine, variations of up to 5 ppm are possible due to structural changes induced by glycosylation, glycation, and cross-linking. Changes due to hydroxylation are shown in bold text. Chemical shift values are referenced to TMS to enable easy comparison to the synthetic chemistry literature on various hydroxylysine modifications

dipolar interactions between nuclei are also highly anisotropic and further broaden and distort the NMR signals. Magic angle spinning (MAS) is a key technique for overcoming these anisotropic effects. By rotating the sample in a rotor that is oriented along the magic angle (54.7°) at thousands or tens of thousands of rotations per second, it is possible to average out the effect of these anisotropic interactions, significantly reducing the line-broadening effects and enabling us to recover the isotropic chemical shifts that are routinely observed in solution-state NMR experiments.

The effectiveness of MAS depends on the strength of the interaction and the inherent frequency distribution arising from chemical structures. It is possible to record well-resolved ^{13}C and ^{15}N spectra with a modest 8 Hz MAS rate, but it is not possible to recover well-resolved ^{1}H spectra even at a 60 Hz MAS rate, due to the much stronger homonuclear ^{1}H–^{1}H dipolar interactions. Therefore, in this chapter, we will focus on obtaining solid-state NMR spectra detected on ^{13}C.

When the MAS rate is lower than or not significantly higher than the strength of the interaction, spinning sidebands are observed as smaller intensity signals located at multiples of the spinning rate from the centerband in the spectrum. Sidebands can be easily recognized by changing the MAS rate, as sidebands would

change location while the centerband would not. In proteins, the aliphatic signals (5–65 ppm) generally do not give rise to significant spinning sidebands above a MAS rate of 5Hz, while the amide carbon signals (168–175 ppm) can give spinning sidebands. Some MAS rates are suggested in the Notes to avoid placing amide carbon spinning sidebands in the aliphatic carbon region.

It is important to ensure that the rotor containing solid samples are packed in a balanced manner, with the sample mass evenly distributed through the rotor, to enable stable MAS. In the case of imbalance, the sample can fail to spin faster than 1 Hz and can also lead to unstable spinning and, in the worst case, a rotor crash. Apart from destroying the sample, rotor crashes often also damage the NMR equipment. If in doubt, the sample should be repacked before attempting MAS.

1.4 Sensitivity of NMR Experiments

NMR spectroscopy at room temperature can be rather insensitive. The insensitivity, in the case of biomolecules, is due to two factors: firstly, the low natural abundance of NMR-active nuclei and, secondly, the physics of NMR phenomena. Here we outline strategies to overcome both of these issues.

1.4.1 Isotopic Enrichment

To overcome the challenge of low natural abundance of NMR-active nuclei, the common strategy is to produce isotopically enriched samples, particularly in ^{13}C and ^{15}N. These types of samples are frequently referred to as "labelled" in NMR literature. In biomolecular NMR, the standard protocol is to overexpress the protein of interest in *E. coli*, and supplement the culture medium with ^{13}C-enriched glucose and ^{15}N ammonium salts [9]. While a recombinant collagen analogue can be produced by bacteria [10], successful production of native triple-helical collagen protein generally requires PTMs that are not found in bacterial expression systems. We have previously shown that it is possible to generate isotopically enriched collagen-containing ECM for ssNMR both by using mammalian cell culture and by feeding mice with a suitable diet [11, 12], based on the stable isotope labelling with amino acid (SILAC) methodology used in mass spectrometry [13].

It is important to define the amino acids of interest at the outset of the study, prior to any sample preparation, in order to select the most cost-effective labelling scheme. Since solid-state NMR reveals all labelled species within the sample, it is important to ensure that samples are not contaminated with other labelled metabolites.

For the case of tissue samples, care should be taken so that a homogeneous sample of a single tissue type is dissected. Ideally, the tissue type investigated should be predominantly collagen, even better if it is one particular type of collagen. In the case of cell culture samples, it is ideal to select a culture that produces ECM rich in a single type of collagen. Currently, it is challenging to use ssNMR to study completely heterogeneous protein samples where

collagen is only a minor component, as signals from other proteins are likely to overlap with those arising from collagen. However, there is an inherent advantage in studying hydroxylation of prolines and lysines, which are PTMs exclusively found in collagen proteins. Even if collagen is a minor component of the tissue, the methods described in this chapter should be able to detect these types of residues and identify the presence of collagen.

Prolines are nonessential. When supplemented in the medium/diet, it does not show a large degree of conversion into other amino acids apart from generating hydroxyproline. Samples labelled with ^{13}C-proline show ssNMR signals from both proline and hydroxyproline under routine ssNMR conditions.

Lysines are essential for mammals. Therefore, in order to achieve isotope enrichment of lysine residues, it is necessary to provide lysine as ^{13}C-only or ^{13}C, ^{15}N labelled amino acids in the cell culture media for generating labelled ECM or in the diet for generating labelled tissue. In our experience, lysine labelling of mammalian ECM/tissues is generally clean, i.e., with essentially no transfer or scrambling of the isotope label to other non-lysine residues or sugars. During collagen biosynthesis, a small part of labelled lysine is converted to labelled hydroxylysine, at a level of less than 2% of the collagen triple helix. At this level, even with labelling, routine ssNMR is unable to detect lysine, and further signal enhancement is required, such as by dynamic nuclear polarization.

1.4.2 Dynamic Nuclear Polarization in Solid-State NMR

The detectable signal in NMR phenomena is based on population differences between the spin quantum states, which is termed the polarization. The energy differences between spin quantum states are much smaller than thermal energy at room temperatures, which leads to a very small population difference, a very small polarization, and consequently a very small detectable signal. One of the techniques to improve polarization in solid-state NMR is dynamic nuclear polarization (DNP) [14], which has undergone commercialization and rapid development in the recent years. DNP enhancement relies on the transfer of polarization from electrons to nuclei, either directly or through a spin diffusion process, thereby achieving signal enhancement up to a theoretical limit of 660 for ^{1}H (and even larger for other nuclei). Assuming no loss of sensitivity via depolarization effects, the time saving is equal to the signal enhancement squared. In other words, when an enhancement factor of 10 is obtained relative to some reference spectrum, an experiment with the same signal-to-noise ratio as the reference spectrum can be conducted in 1/100th of the time. Signals that would take weeks of signal averaging before accumulating sufficient intensity above the noise level under routine ssNMR conditions can be observed in hours with sufficient DNP enhancement.

DNP enhancement requires three main components: one or more unpaired electron(s) that is in close proximity to the nuclear spins of interest, a microwave source to enable the polarization transfer, and a temperature of below 200 K to ensure the efficiency of the transfer. Unpaired electrons are generally provided in the form of a small molecule containing stable radicals, and biradicals were found to be effective as they can produce DNP enhancement via a cross effect mechanism involving two electron spins and one nuclear spin, with water-soluble nitroxide-based biradicals being the current conventional choice for biological samples. The current commercial implementation of equipment for DNP enhancement uses a gyrotron as the microwave source, with a low temperature MAS cabinet that can achieve running temperatures of 100 K. In general, DNP enhancement improves by lowering the temperature; therefore, we recommend that experiments be conducted at the lowest stable temperature whenever possible.

There are a few drawbacks of the DNP enhancement procedure. Firstly, due to the low temperatures required, molecular motion is significantly slowed down. The lack of molecular motion means that molecules are trapped in a range of conformations, all with slightly different chemical shifts, thus leading to broadening of the signals and a reduction in the resolution. Fortunately, the resolution loss in DNP is not a significant issue for detecting hydroxylated residues in collagen since the unmodified and the hydroxylated forms have such different chemical shifts (45 ppm difference) that there is effectively no chance of overlap. Secondly, as a stable biradical is doped into the sample, DNP-enhanced ssNMR cannot be considered a completely nondestructive technique where the sample can be cleanly and easily recovered, unlike normal ssNMR.

2 Materials

2.1 NMR Equipment

1. A solid-state NMR spectrometer equipped with a MAS probe head tuned to the frequencies of the required nuclei (*see* **Note 1**). For the rest of this chapter, quantities mentioned are specific for a restricted volume 3.2 mm diameter MAS rotor with a volume of 30 μL.
2. For studies involving hydroxylysines or other residues or components that occur at a level less than 2% of the collagen triple helix, DNP enhancement is strongly recommended. A system capable of DNP enhancement includes in addition to the spectrometer:
   (a) A microwave source (usually a gyrotron) at a commensurate electron transition frequency (e.g., 263 GHz gyrotron at 9.7 T for a 400 MHz NMR spectrometer at 9.4 T).

(b) A waveguide from the gyrotron to the DNP probe head.

(c) A cooling cabinet capable of maintaining MAS gas flows at temperatures below 150 K (*see* **Note 2**).

(d) A DNP probe head that permits microwave irradiation and also thermally isolates the cooling gas flows of the sample rotor from the inner bore of the magnet.

The system should provide sufficient stability in MAS and thermal isolation for a minimum of 12 h.

3. Zirconia or sapphire MAS rotors of a commensurate diameter to the stator within the probe (*see* **Note 3**).
4. Vespel or zirconia MAS rotor caps of a commensurate diameter (*see* **Note 4**).

2.2 Solid Biological Samples

While general procedures of preparing samples for DNP NMR experiments on water-soluble proteins, assemblies, and precipitates have been described [21], since most collagen samples are poorly soluble in water, we provide the procedures described below, which were inspired by prior applications of DNP signal enhancement on porous materials [22] and can be applied on a wide range of solid samples. For example, ssNMR experiments have been successfully performed on tissues dissected from patients or model organisms, on protein pellets such as those obtained from cell culture-derived ECM, and on freeze-dried triple-helical peptides obtained from solid-phase peptide synthesis [11, 12]. ^{13}C-enriched material is necessary for studies involving hydroxylysine and recommended for studies involving hydroxyprolines. While this chapter will not provide a full description of isotope enrichment procedures, which can vary greatly depending on the scientific question and the type of samples involved, some general requirements of samples suitable for solid-state NMR experiments are provided below.

1. NMR experiments can be successfully carried out with slightly less than 10 mg of isotope-enriched sample, but more is better for both detection and spinning stability. Up to 30 mg of sample can usually be packed into a 3.2 mm diameter rotor (*see* **Note 5**).
2. Although a high level of isotope enrichment is desirable, a level of 20–50% can be sufficient (*see* **Note 6**).
3. Avoid freeze-drying tissue samples (*see* **Note 7**).
4. Avoid mechanical milling of tissue samples (*see* **Note 8**).
5. The use of fixatives or preservatives are generally not recommended, as these substances can give rise to irrelevant but strong signals in the NMR spectra, especially in the case of natural abundance samples (*see* **Note 9**).
6. If a cell lysis step is carried out, it is recommended to rinse the ECM with phosphate buffered saline (1×) or distilled water to remove any cell debris.

2.3 Stable Radicals for DNP Enhancement

1. Water-soluble binitroxide radicals such as bcTol-M [17] and AMUPol [18]. Store away from light.
2. Heavy water (D_2O).
3. Distilled water (H_2O) (for freeze-dried samples only).

3 Methods

3.1 Preparing the Radical Stock Solution for DNP Enhancement

Carry out this procedure at room temperature. Try to avoid working at a bench which is under direct sunlight, as this can lead to quenching of the radicals.

1. If the sample is hydrated, use D_2O as the solvent. Otherwise, if the sample is freeze-dried, use a mix of D_2O and H_2O in a ratio of 9:1 (v/v) as the solvent. Allow for 4–10 μL of radical solution for each ssNMR sample to estimate the volume of radical stock solution required.
2. If using AMUPol, calculate the mass required for a 30 mM solution. If using bcTol-M, calculate the mass required for a 40 mM solution. Weigh out the mass required using a balance with sufficient accuracy (*see* **Note 10**).
3. Dissolve the solid radical thoroughly with the required amount of water (pure D_2O or mixed D_2O/H_2O). Check carefully for any undissolved crystals and sonicate if necessary. Label, wrap the radical stock solution container with tinfoil to protect from light, and store in the refrigerator until use.

3.2 Packing the ssNMR Rotor

For most collagen-containing samples, this procedure can be carried out at room temperature. In the case of highly temperature-sensitive biological samples, the procedure can be carried out at low temperature. The procedures below are specifically for 3.2 mm diameter rotors.

1. Weigh the empty ssNMR rotor with the cap prior to sample packing.
2. Weigh the sample. If there is more than 30 mg of sample, return the excess to storage.
3. If the sample is solid tissue, cut or break up the sample into pieces that are no larger than 1.5 mm × 1.5 mm × 4 mm, keeping the cut pieces in relatively similar sizes where possible.
4. Fill the sample into the rotor with occasional compaction to ensure an even weight distribution, which is important for successful MAS. Stop filling when the sample height in the rotor is about 3 mm below the top edge of the rotor. When this happens, or when the sample is all filled into the rotor, weigh the packed rotor to determine the mass of sample in the rotor.

5. If there is insufficient sample mass to fill the rotor to this point, check whether the filling length of the sample is centered in the rotor. If not, remove the sample completely from the rotor, and use spacing material below the sample to ensure that the sample is centered lengthwise in the rotor. Weight the rotor to determine the mass of the spacing material.

If DNP enhancement is not required, skip to **step 9** at this point.

6. If less than 12 mg of sample was filled into the rotor, pipette 4 μL of radical solution into the rotor, directly on top of the packed sample (*see* **Note 11**).
7. If more than 12 mg of sample was filled into the rotor, first take out half of the packed sample, and then pipette 4 μL of radical solution into the rotor. Then replace the other half of the sample in the rotor, and pipette another 4 μL of radical solution into the rotor (*see* **Note 12**).
8. Weigh the rotor to ensure that there is a mass increase due to the addition of the radical solution.
9. If there is more than 3 mm of space between the top of the sample and the top edge of the rotor, add a small amount of Teflon as spacing material.
10. Close the rotor with the cap carefully, taking care not to damage the vanes on the cap (*see* **Note 13**).
11. Check the bottom of the rotor for the optical mark (a black line along half the circumference) by which the MAS rate is tracked, ensuring that it is continuous and clear. If not, reinforce it with a black/dark felt-tip pen.

3.3 Inserting Rotor into Magnet and Magic Angle Spinning

3.3.1 Insertion on a Probe Head Without the Option of DNP Enhancement

1. Set the temperature of the NMR probe head to the desired value (*see* **Note 14**).
2. Press "insert" on the MAS control panel.
3. Insert the sample by placing the rotor into the sample transfer line or directly into the opening of the stator within the probe head.

3.3.2 Insertion on a Probe Head with the Option of DNP Enhancement

1. Cool the DNP NMR probe head down to 100 K using the MAS and variable temperature gas flow.
2. Press "eject" on the MAS control panel (*see* **Note 15**).
3. Place the rotor in the sample holder of the sample transfer line.
4. Press "insert" on the MAS control panel (*see* **Note 16**).

3.3.3 Magic Angle Spinning

1. Stop the insertion gas flow.
2. Spin the sample to 5 Hz MAS (*see* **Note 17**).
3. Once the spinning has stabilized, increase MAS rate to the desired rate (*see* **Note 18**).

3.4 Solid-State NMR Experiments

Here we present three experiments that are particularly useful for studying collagen hydroxylation. We assume that the solid-state NMR spectrometer had already been used previously for other $^{13}C/^{15}N$ experiments and therefore does not cover basic spectrometer setup such as setting the magic angle and initial calibration of the RF pulse powers, and we assume that a functional pulse sequence has been installed. For each experiment, some representative spectra are included to aid interpretation and analysis. Please check with the local facility manager to ensure that maximum power levels of the NMR spectrometer are not exceeded.

3.4.1 1D Cross Polarization (CP)

This experiment yields a 1D ^{13}C or ^{15}N NMR spectrum and is the basis of many other ssNMR experiments. Below, the $^{13}C/^{15}N$ nucleus is denoted with X (*see* **Note 19**).

1. Create a new dataset from a previous CP experiment.
2. Optimize the following parameters for maximum signal-to-noise ratio (*see* **Note 20**):
   (a) ^{1}H 90° pulse length
   (b) ^{1}H contact pulse power
   (c) ^{1}H-X contact pulse length
   (d) ^{1}H decoupling sequence pulse power during signal acquisition
3. Signal average the optimized CP experiment for at least 4–10 min. Usually this would equate to a minimum of 128 transients.
4. For measuring DNP signal enhancement, the same CP experiment (with same number of transients and parameters) should be run twice: once with the microwave irradiation switched off and once again with the microwave irradiation switched on. The relative ratio of intensity of the two 1D CP spectra is commonly referred to as the enhancement value (ε). An acceptable value of ε is 10—many experiments are already much more feasible at this level of enhancement. On collagen samples, we have thus far obtained values of ε up to 57.
5. For all other DNP NMR experiments, the microwave irradiation should be switched on prior to the start and kept at the same level throughout the experiment.

If the referenced spectrum contains a ^{13}C signal at 70 ppm, it strongly indicates that the sample contains hydroxylated carbon

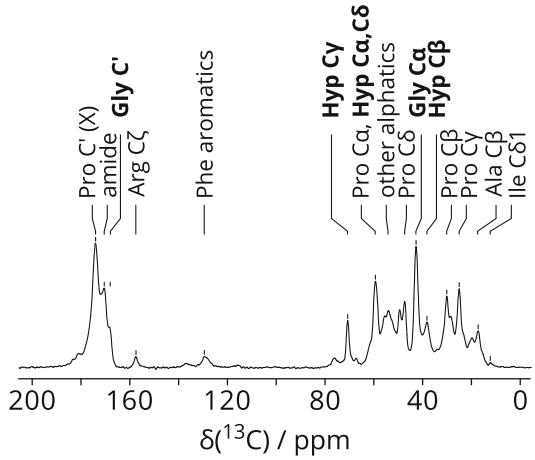

Fig. 2 1D ^{13}C NMR spectra of adult human bone (natural abundance), 297 K, 400 MHz spectrometer, 10 Hz MAS. Residues that feature prominently in collagen-containing samples are labelled in bold text

atoms. By eliminating the possibility of other alcohol or glycerol-like substances, and confirming the presence of other distinctive protein and collagen signals, it is possible to identify collagen hydroxylation within the sample using this experiment. If present in unlabelled or generally isotopically labelled samples, the 70 ppm signal is likely to be dominated by hydroxyproline, unless lysine is specifically ^{13}C labelled. Figure 2a shows a representative 1D ^{13}C ssNMR spectrum, with each signal assigned to the specific types of carbon atoms in specific residues. Figure 2b shows the effect of DNP enhancement by comparing the microwave on/off 1D ^{13}C ssNMR spectra.

3.4.2 2D ^{13}C–^{13}C Correlation

Proton-driven spin diffusion (PDSD) and dipolar-assisted rotary resonance (DARR) are two very similar experiments that can yield informative 2D (usually ^{13}C–^{13}C) spectra and are fairly simple to set up on isotope-enriched samples.

1. Create a new dataset from a previous PDSD/DARR experiment, ensuring that it is a 2D dataset with two ^{13}C dimensions.
2. Transfer the optimized CP parameters to the new dataset.
3. Optimize the ^{13}C 90° pulse length, generally achieved by looking for a zero crossing of the signal when a variable length carbon pulse is applied after the CP step prior to detection.
4. Select the mixing time and pulse power (*see* **Note 21**).
5. Check that the indirect dimension sweep width is sufficiently wide (for ^{13}C, around 250 ppm) to contain the whole ^{13}C chemical shift range, but not so excessively wide that it leads to an unnecessarily long experiment.

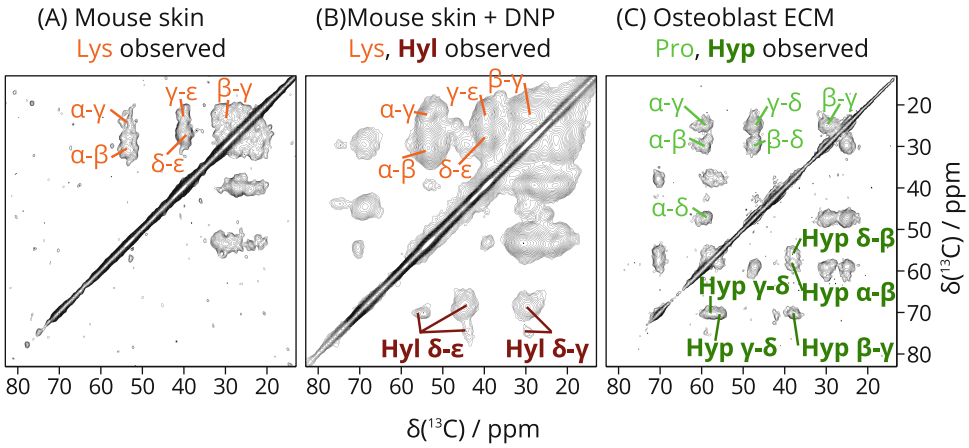

Fig. 3 2D ^{13}C–^{13}C DARR spectra of (**a**) lysine ^{13}C-labelled mouse skin, no DNP enhancement, 285 K, 20 ms mixing time, 600 MHz spectrometer, 13,333 Hz MAS; (**b**) lysine ^{13}C-labelled mouse skin, 110 K, with DNP enhancement (AMUPol, 30 mA microwave current, $\varepsilon = 27$), 5 ms mixing time, 400 MHz spectrometer, 8889 Hz MAS; (**c**) proline and glycine ^{13}C, ^{15}N-labelled fetal sheep osteoblast ECM, 110 K, no DNP enhancement, 20 ms mixing time, 400 MHz spectrometer, 8889 Hz MAS. Annotations indicate signals for unmodified lysine (orange/light gray) and proline (light gray/light gray) residues, and bold-type labels indicate signals for hydroxylysine (dark brown/dark gray) and hydroxyproline (dark green/dark gray). We can see from (**b**) and (**c**) that hydroxylysine and hydroxyproline signals do not overlap with each other; thus, we can use the 2D spectral pattern to distinguish between these two hydroxylated residues

6. Signal average the PDSD/DARR experiment for 5–20 h.

Using this experiment, it is possible to distinguish the signals arising from hydroxyproline and the hydroxylysine in triple-helical collagen. The additional dimension provides the resolution required to separate the signals that normally overlap in a 1D experiment. Figure 3 shows two DARR experiments on lysine ^{13}C-labelled samples acquired without and with DNP enhancement, highlighting the hydroxylysine signals that only appear in the latter. A third DARR spectrum labelled with proline but not lysine illustrates how the crosspeak positions of hydroxyproline are distinct from those of hydroxylysine.

3.4.3 ^{15}N–^{13}C Heteronuclear Correlation

This experiment is also sometimes called a double CP experiment, as the magnetization is first transferred by CP from ^{1}H to ^{15}N, then transferred a second time, again by CP, from ^{15}N to ^{13}C. This experiment requires ^{15}N and ^{13}C labelling and ideally a relatively good DNP enhancement in order to obtain sufficient sensitivity. DNP enhancement is optional for observing hydroxyprolines using this experiment but necessary if hydroxylysines are of interest.

It is possible to transfer the magnetization further, thus overall from H → N → C → C, with the third step mediated by DARR/PDSD. This transfer scheme enables correlations between carbon atoms that are not directly bonded to nitrogen to be detected.

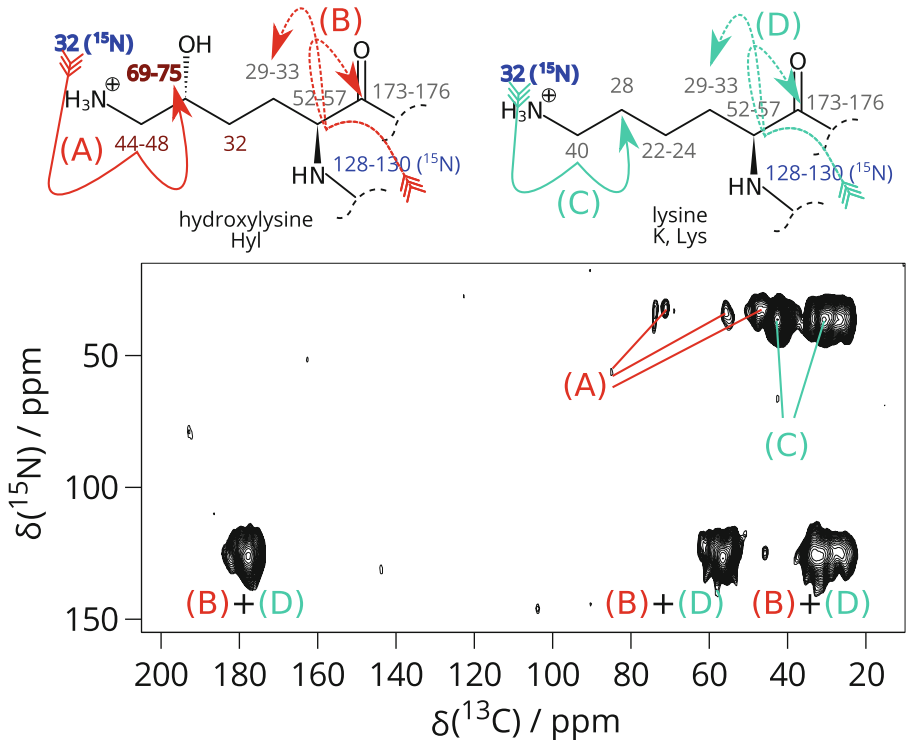

Fig. 4 2D ^{15}N–^{13}C spectra of lysine ^{13}C, ^{15}N-labelled adult bovine vascular smooth muscle cell ECM, 110 K, with DNP enhancement (AMUPol, 30 mA microwave current, $\varepsilon = 57$), 10 ms DARR mixing time, 400 MHz spectrometer, 8889 Hz MAS. The signals specific to hydroxylysine (**a**, **b**; in red/dark gray) and hydroxylysine (**c**, **d**; in teal/light gray) are indicated on the figure. Arrows on the chemical structure indicate the magnetization transfer pathways, omitting the initial ^{1}H to ^{15}N CP step, but starting on ^{15}N and ending on ^{13}C, that give rise to the signals observed. Due to the low number of hydroxylysine residues in the ECM relative to lysine residues, the sidechain signals from the hydroxylysine pathway (**a**) are much weaker than those from the lysine pathway (**c**)

1. Create a new dataset from a previous ^{15}N–^{13}C experiment, ensuring that it is a 2D dataset with a directly detected ^{13}C dimension and an indirect ^{15}N dimension.
2. Transfer the optimized CP and DARR parameters to the new dataset.
3. Calculate the NC(A) contact matching condition. A reasonable set of initial values are:
   (a) ^{13}C pulse power: 1.5× MAS rate with a tangential shape (×1.4 to compensate for power loss during the shaped pulse).
   (b) ^{15}N pulse power: 2.5× MAS rate with a square shape (×1).
   (c) ^{1}H pulse power: use the same power as the ^{1}H decoupling power during acquisition.
   (d) NC contact pulse length: 5 ms.

4. Optimize (a), (c), and (d) on a 1D version of the NC/double CP experiment for maximum signal-to-noise ratio (*see* **Note 22**).
5. Check that the indirect acquisition sweep width is sufficiently wide (for ^{15}N, around 200 ppm) and centered correctly to contain the entire ^{15}N chemical shift range, including the amide signals up to 120 ppm and the lysine sidechain amine signal at around 40 ppm.
6. Signal average the NC experiment for 5–20 h.

Using this experiment, it is possible to identify signals arising from lysine and hydroxylysine due to the distinctive sidechain amine ^{15}N chemical shift. As the amine sidechain and the hydroxylated carbon are not directly bonded, the additional ^{13}C–^{13}C PDSD/DARR step is required in order to generate a spectrum with a Cδ-Nζ correlation that is unique to hydroxylysine. Figure 4 shows a ^{15}N–^{13}C NMR spectrum on ^{13}C, ^{15}N-lysine-labelled vascular smooth muscle cell ECM.

4 Notes

1. For tissue samples, rotor diameters of 3.2 mm, 4.0 mm, and 7.0 mm have all been successfully used to achieve stable spinning. Smaller rotor diameters such as 2.5 mm and 1.9 mm may also be used, but more care is needed to balance the sample.
2. From our experience, the commercial DNP-ssNMR 3.2 mm diameter MAS probe head produced by Bruker requires cooling with approximately 250 L of liquid nitrogen every 24 h when running at a set temperature of 100 K.
3. In the cases where the sample mass is limited, restricted depth rotors should be used to center the sample in the center of the rotor to improve RF pulse homogeneity and experiment sensitivity. Inert spacers made of materials such as Teflon can be used for restricting the sample height to the center of the rotor. Materials low in proton and carbon (where possible) are preferred, as otherwise the spacer material could be observed in the NMR spectra; care should also be taken to avoid materials that show large volume change with temperature variations.
4. For experiments at the low temperature conditions for DNP enhancement (<200 K), zirconia caps are recommended, though Vespel caps have also been successfully used. It is recommended to test shrinkage of the rotor cap by placing the packed rotor into liquid nitrogen and observing whether there is any movement or slippage of the cap before inserting the rotor into the probe head. Use rotors with regular wall

thickness (1 mm) when possible. Some rotors with thin walls (0.5 mm) appear to have looser rotor caps and are more prone to cap slippage.

5. The amount of sample required depends on the proportion of sites of interest within the sample and the degree of isotope enrichment. Due to the sensitivity challenges of NMR, it is advantageous to fill the volume of the rotor with as much sample as possible while maintaining stable magic angle spinning.
6. The isotope enrichment method or labelling scheme depends on the sites of interest. In general, it is better to enrich only the amino acids that would be of interest, to avoid irrelevant signals overlapping with the signals of interest and loss of resolution in the NMR spectra. For example, it is ideal to only ^{13}C-enrich lysine residues by adding ^{13}C lysine to the cell culture media or to the diet if the sites of interest are hydroxylysines. With DNP enhancement, it is possible to detect hydroxylysine sites in tissues with 45% ^{13}C lysine enrichment.
7. While more protein sample can be filled into the rotor after freeze-drying, the procedure can lead to structural damage that manifests as a loss of resolution in the NMR spectra. Whether to sacrifice the resolution for more sensitivity has to be determined on a case-by-case basis. For hydrated samples, excess water can be removed in a more gentle manner by placing the sample between two layers of Parafilm and gently pressing. The water expelled can be removed with a pipette.
8. We have found that cryomilling led to significant loss in resolution in mouse bone ^{13}C spectra, likely due to dehydration. Tissue obtained from small animals may be particularly susceptible. On the other hand, milling may be necessary for mineralized tissues that are significantly larger than the rotor in size. The bone obtained from larger mammals, such as horses and humans, appears to be only minimally affected by cryomilling.
9. If fixatives or preservatives were used, the tissue sample should be soaked for 24 h or more in a significant excess of water to remove any remaining fixative and rinsed prior to use.
10. Ensure that the container containing the stable radical is at room temperature before opening, to avoid buildup of condensation. As a rather small amount of radical mass (under 0.5 mg) is usually required to be weighed out, we often use the tip of a needle for transferring the solid radical from the stock container and carry out the weighing process in the lid of a small Eppendorf tube, which can then be used directly for mixing the radical solution. The concentrations recommended for AMUPol and bcTol-M are different due to the higher solubility of bcTol-M in water.

11. The amount of radical solution has to match the amount of sample in the rotor. Excessive radical concentration will bleach the NMR signal, leading to poor or no enhancement. For DNP enhancement of biomolecules, a concentration of 10 mM is generally recommended. However, it can be difficult to estimate the volume of a solid sample; hence, the procedure here is based on sample mass. If the sample is unexpectedly bulky, such that the rotor volume is full with less than 15 mg of sample, use the procedure in the next step.
12. The aim here is to achieve a final concentration of approximately 10 mM of biradical in the rotor. Assuming that the sample completely fills the volume of the 3.2 mm diameter rotor (30 μL), adding 8 μL 40 mM bcTol-M stock solution results in a final concentration of 10.7 mM. If the sample mass is more than 12 mg but less than 20 mg, reduce the second addition of the radical solution proportionally.
13. If radical solution was added to the rotor, use a tabletop spinner to further distribute the radical solution through the packed sample with several inversions of the rotor. This can help to maximize the wetting of the sample and optimize the DNP enhancement. Check the cap carefully for any signs of damage, and also check to make sure that the rotor cap is flush against the top of the rotor, without any gaps, as otherwise MAS would fail.
14. Generally, a temperature between 0 and 20 °C is selected. Due to air friction during MAS, there can be a difference between the reported and the actual temperatures. For up to 14 Hz MAS, the difference should not be more than 10 °C.
15. Due to the low operating temperature of the DNP probe head, it is important to avoid moisture ingress. Therefore, when the probe head is cold, the eject gas flow must always be enabled prior to opening the sample transfer line.
16. It is recommended to monitor this process via one of two ways: Either set the bearing gas flow to 200–300 mBar, and look for a decrease in the bearing gas flow on insertion of the sample, or display the frequency sweep (Bruker Topspin spectrometer software "wobb" command) and look for a change in the absorption minimum frequency on insertion of the sample. The tendency of the DNP NMR probe to condense moisture from the air leads to a higher chance of the rotor being stuck in the transfer line. In case there is a problem with insertion, test whether the rotor spins; if not, try to eject the rotor; if the rotor fails to eject, warm up the probe head before attempting ejection again. It is possible as well to start with a warm probe, and then carry out one of the two following variations: Spin the sample to the desired MAS rate, and then cool the probe down

to 100 K; or, spin the sample to a moderate rate (e.g., 5 Hz), cool the sample to 100 K, and then increase the MAS rate further. In both of these variations, it is important to increase the cooling gas slowly, as the cooling gas introduces turbulence and destabilizes MAS. If the temperature is changed too suddenly, there is a risk of a rotor crash.

17. If the rotor fails to spin faster than 900–1000 Hz at this stage, it indicates a mass imbalance within the rotor. Sometimes this resolves itself in a few minutes, but at other times, the rotor has to be ejected and the sample repacked or redistributed. If a larger gap has appeared between the top of the sample and the top edge of the rotor, consider adding a small amount of Teflon tape as a spacer.
18. Some suggested MAS rates: For a 400 MHz spectrometer, 8889 Hz MAS; for a 600 MHz spectrometer, 13,333 Hz MAS; and for a 700 or an 800 MHz spectrometer, 11,000 Hz MAS. At these rates, the spinning sidebands of the amide signals do not tend to overlap with the signals arising from hydroxylation.
19. CP is usually carried out by transferring magnetization from ^{1}H to ^{13}C or ^{1}H to ^{15}N and detecting on the X nuclei. This technique has the advantage of increasing the sensitivity of the nuclei being observed, while at the same time increasing sensitivity per unit time as the relaxation behavior follows that of the more abundant (usually ^{1}H) spins and is of the order of several hundred milliseconds, rather than several seconds or more in the case of ^{13}C, thus enabling more transients to be obtained in a shorter time. The CP experiment is quite forgiving, and it is possible to obtain a good 1D spectrum on samples containing collagen even without isotope labelling, provided that a full rotor is used and signal averaging is carried out for 4–12 h (for ^{13}C) and 12–24 h (for ^{15}N). These signal averaging times can be drastically reduced by DNP enhancement, potentially down to 10–30 min. The CP experiment relies on the Hartmann-Hahn matching condition [19] during the contact time, when pulses are simultaneously applied on both channels. We use a ramp on the ^{13}C pulse during the contact pulse to broaden the matching condition [20].
20. For an optimized CP sequence, here are some characteristic parameters obtained from our spectrometers. We do not report the powers as these values are not transferable between different spectrometers. ^{1}H 90° pulse length: 2.5–4 μs and ^{1}H-X contact time: 750–1750 μs.
21. Both the PDSD and DARR experiments correlate pairs of ^{13}C spins that are within a certain distance of each other. As part of the experiment, we can control a time duration (the "mixing

time) where there is either no pulses at all (PDSD) [21] or a low power constant amplitude pulse on the ^{1}H channel (DARR) [22]. In both of these cases, when the mixing time is short (5–20 ms), only pairs of ^{13}C that are within 2 Å would show crosspeaks. However, when the mixing time is long (100+ ms), ^{13}C–^{13}C pairs within 6 Å would show crosspeaks. Due to the low temperature of the DNP enhancement conditions, crosspeaks tend to appear at shorter mixing times. DARR is believed to lead to a quicker buildup than PDSD, though the differences are relatively minor at a 400 MHz spectrometer.

22. Compare the 1D double CP experiment signal intensity with a normal ^{13}C CP acquired with the same number of transients. Due to the extra transfer step, the intensity of the double CP experiment should be around 5–40% of that obtained from a CP. If the double CP intensity is more than 20% of that obtained from a CP, that is a reasonably optimized experiment for collagen-containing samples, and the parameters should yield a good 2D spectrum. If the double CP intensity is less than 5%, then the parameters should be further optimized to try to increase the transfer efficiency.

Acknowledgments

The author thanks Dr. Jonathan Clark from the Babraham Institute for providing the lysine ^{13}C-labelled mouse skin sample, Mr. Rakesh Rajan and Professor Melinda Duer from the University of Cambridge for providing the proline and glycine ^{13}C, ^{15}N-labelled fetal sheep osteoblast ECM sample, Mr. Robert Hayward and Professor Cathy Shanahan at King's College London for providing the lysine ^{13}C, ^{15}N-labelled adult bovine vascular smooth muscle cell ECM sample, and Dr. Kelsey Collier at FMP Berlin for useful discussions and comments.

References

1. Shoulders MD, Raines RT (2009) Collagen structure and stability. Annu Rev Biochem 78:929–958. https://doi.org/10.1146/annurev.biochem.77.032207.120833
2. Yamauchi M, Sricholpech M (2012) Lysine post-translational modifications of collagen. Essays Biochem 52:113–133. https://doi.org/10.1042/bse0520113
3. Levitt MH (2013) Spin dynamics: basics of nuclear magnetic resonance. John Wiley & Sons, New Jersey
4. Cavanagh J, Fairbrother WJ, Palmer AG, Skelton NJ, Rance M (2010) Protein NMR spectroscopy: principles and practice. Elsevier, Amsterdam
5. Keeler J (2011) Understanding NMR spectroscopy. John Wiley & Sons, New Jersey
6. Harris RK, Becker ED, De Menezes SMC, Granger P, Hoffman RE, Zilm KW (2008) International Union of Pure and Applied Chemistry physical and biophysical chemistry division (2008) further conventions for NMR shielding and chemical shifts IUPAC

recommendations. Magn Reson Chem 46:582–598. https://doi.org/10.1002/mrc.2225

7. Wishart DS, Bigam CG, Yao J, Abildgaard F, Dyson HJ, Oldfield E, Markley JL, Sykes BD (1995) ^{1}H, ^{13}C and ^{15}N chemical shift referencing in biomolecular NMR. J Biomol NMR 6:135–140
8. Allevi P, Paroni R, Ragusa A, Anastasia M (2004) Hydroxylysine containing glycoconjugates: an efficient synthesis of natural galactosylhydroxylysine (gal-Hyl) and glucosylgalactosylhydroxylysine (Glu-gal-Hyl) and of their (5S)-epimers. Tetrahedron Asymmetry 15:3139–3148. https://doi.org/10.1016/j.tetasy.2004.08.006
9. LeMaster DM (1994) Isotope labeling in solution protein assignment and structural analysis. Prog Nucl Magn Reson Spectrosc 26:371–419. https://doi.org/10.1016/0079-6565(94)80010-3
10. An B, Kaplan DL, Brodsky B (2014) Engineered recombinant bacterial collagen as an alternative collagen-based biomaterial for tissue engineering. Front Chem 2:40. https://doi.org/10.3389/fchem.2014.00040
11. Chow WY, Rajan R, Muller KH, Reid DG, Skepper JN, Wong WC, Brooks RA, Green M, Bihan D, Farndale RW, Slatter DA, Shanahan CM, Duer MJ (2014) NMR spectroscopy of native and in vitro tissues implicates polyADP ribose in biomineralization. Science 344:742–746. https://doi.org/10.1126/science.1248167
12. Wong VWC, Reid DG, Chow WY, Rajan R, Green M, Brooks RA, Duer MJ (2015) Preparation of highly and generally enriched mammalian tissues for solid state NMR. J Biomol NMR 63:119–123. https://doi.org/10.1007/s10858-015-9977-9
13. Ong S-E, Blagoev B, Kratchmarova I, Kristensen DB, Steen H, Pandey A, Mann M (2002) Stable isotope labeling by amino acids in cell culture, SILAC, as a simple and accurate approach to expression proteomics. Mol Cell Proteomics 1:376–386
14. Lilly Thankamony AS, Wittmann JJ, Kaushik M, Corzilius B (2017) Dynamic nuclear polarization for sensitivity enhancement in modern solid-state NMR. Prog Nucl Magn Reson Spectrosc 102-103:120–195. https://doi.org/10.1016/j.pnmrs.2017.06.002
15. Itin B, Sergeyev IV (2018) Strategies for efficient sample preparation for dynamic nuclear polarization solid-state NMR of biological macromolecules. In: Ghose R (eds) Protein NMR. Methods in Molecular Biology, vol 1688. https://doi.org/10.1007/978-1-4939-7386-6_7
16. Lesage A, Lelli M, Gajan D, Caporini M A, Vitzthum V, Miéville P, Alauzun J, Roussey A, Thieuleux C, Mehdi A, Bodenhausen G, Copéret C, Emsley L (2010) Surface enhanced NMR spectroscopy by dynamic nuclear polarization. J Am Chem Soc 132:15459–61. https://doi.org/10.1021/jacs.5b08423
17. Geiger M-A, Jagtap AP, Kaushik M, Sun H, Stöppler D, Sigurdsson ST, Corzilius B, Oschkinat H (2018) Efficiency of water-soluble Nitroxide Biradicals for dynamic nuclear polarization in rotating solids at 9.4 T: bcTol-M and cyolyl-TOTAPOL as new polarizing agents. Chemistry 24(51):13485–13494. https://doi.org/10.1002/chem.201801251
18. Sauvée C, Rosay M, Casano G, Aussenac F, Weber RT, Ouari O, Tordo P (2013) Highly efficient, water-soluble polarizing agents for dynamic nuclear polarization at high frequency. Angew Chem Int Ed Engl 125:11058–11061. https://doi.org/10.1002/ange.201304657
19. Hartmann SR, Hahn EL (1962) Nuclear double resonance in the rotating frame. Phys Rev 128:2042–2053. https://doi.org/10.1103/physrev.128.2042
20. Metz G, Wu XL, Smith SO (1994) Ramped-amplitude cross polarization in magic-angle-spinning NMR. J Magn Reson A 110:219–227. https://doi.org/10.1006/jmra.1994.1208
21. Szeverenyi NM, Sullivan MJ, Maciel GE (1982) Observation of spin exchange by two-dimensional fourier transform ^{13}C cross polarization-magic-angle spinning. J Magn Reson 47:462–475. https://doi.org/10.1016/0022-2364(82)90213-x
22. Takegoshi K, Nakamura S, Terao T (2001) ^{13}C–^{1}H dipolar-assisted rotational resonance in magic-angle spinning NMR. Chem Phys Lett 344:631–637. https://doi.org/10.1016/s0009-2614(01)00791-6

Chapter 6

Measurement of Collagen Cross-Links from Tissue Samples by Mass Spectrometry

Amar Joshi, Amna Zahoor, and Alberto Buson

Abstract

All tissues contain an extracellular matrix (ECM) which is constantly and dynamically remodeled, either in physiological or pathological processes, such as fibrosis or cancer. One of the key contributors in the establishment of a fibrotic state is the abnormal deposition of extracellular matrix and cross-linked proteins, in particular collagen, leading to tissue stiffening and disruption of organ function. The precise and sensitive measurement of these cross-links by LC-MS/MS is a very powerful tool for providing a quantitative and qualitative analysis of fibrosis and is a key requirement in the study of this state, as well as in the development of drugs for this unmet clinical need.

Key words Collagen, Tissue cross-linking, Immature cross-links, Mature cross-links, Solid phase extraction (SPE), Mass spectrometry

1 Introduction

One of the most relevant hallmarks of a fibrotic state in a tissue is the accumulation of heavily cross-linked collagen fibers, primarily due to the activity of enzymes belonging to the family of the lysyl oxidases, i.e., LOX and lysyl oxidase like 1 through 4 - (LOXL1–LOXL4). The expression of these enzymes is often upregulated in course of diseases such as cancer and fibrotic conditions, resulting in the oxidative deamination of lysine and hydroxylysine residues in collagen precursor proteins and lysine residues in elastin. These residues are modified to reactive aldehydes, which spontaneously further react in various combinations, giving rise to a variety of lysine- and hydroxylysine-derived cross-links [1]. The hydroxylysine residues, in particular, are product of the posttranslational modification of specific lysine residues by members of the lysine hydroxylase family of enzymes and bear a particular importance in terms of stability and mechanical properties of the collagen in the tissue. These modifications are of significant biological importance, since dysregulations of the system lead to disruption of the

Irit Sagi and Nikolaos A. Afratis (eds.), *Collagen: Methods and Protocols*, Methods in Molecular Biology, vol. 1944, https://doi.org/10.1007/978-1-4939-9095-5_6, © Springer Science+Business Media, LLC, part of Springer Nature 2019

physiological homeostasis, with pathological consequences that range from the various syndromes linked to insufficient hydroxylation to the exacerbation of the fibrotic state in case of excessive hydroxylation. The direct quantification of the cross-links generated in the fibrotic process is a key complement to the quantification and localization of total collagen, providing additional information and a more thorough evaluation of the degree of fibrosis of a given tissue. Furthermore, the collagen cross-links dynamically shift from immature to mature, in parallel with the maturation and the mechanical properties of the collagen fibers. The relative content of the immature over the mature cross-links thus provides additional qualitative information on the trajectory and reversibility of the fibrotic state [2]. In the type of measurement, we do in our lab, the tissue undergoes homogenization and reduction steps to obtain a full release of the cross-links, and before the analysis by UHPLC-MS/MS, the samples are purified by a solid phase extraction step. The method can be applied to most tissues, e.g., liver, lung, heart, kidney, skin, and others.

2 Materials

Prepare all solutions using ultrapure water (prepared by purifying deionized water, to attain a sensitivity of 18.2 MΩ-cm at 25 °C) and analytical grade reagents. All reagents should be prepared and stored at room temperature (unless otherwise specified). All waste should be disposed according to proper waste regulations.

2.1 Tissue Sample Preparation

2.1.1 Tissue Preparation

1. Freeze dryer.
2. Weighing scales.
3. 5 mL polystyrene tubes with cell-strainer caps.
4. 2 mL metal bead lysing matrix tubes.
5. Metal spatulas.
6. Benchtop tissue homogenizer.
7. Phosphate buffered saline (PBS).
8. 2 mL acid-/heat-resistant screw cap tubes.
9. Genevac/evaporator.

Tissue Preparation (Skin)

1. 10 mg/mL Collagenase/Dispase: sourced commercially, source is *V. alginolyticus/B. polymyxa*: prepare 10 mg/mL collagenase solution by dissolving 100 mg of collagenase in 10 mL of PBS. Invert gently to mix.

2.1.2 Reduction Step

1. 12 mg/mL sodium borohydride ($NaBH_4$) buffer: the buffer is prepared in 20 mM sodium hydroxide (NaOH) solution. The NaOH stock solution can be prepared at 2 M in water and then diluted to 20 mM with water for $NaBH_4$ buffer preparation (*see* **Note 1**).
2. Neat acetic acid: >99.7% purity.
3. Benchtop centrifuge.
4. Benchtop heat block.
5. 6 M hydrochloric acid (HCL): 12 M HCL sourced commercially is diluted 1:2 to obtain 6 M HCL (*see* **Note 2**).

2.1.3 Sample Cleanup Using Solid Phase Extraction (SPE)

1. Automated SPE machine (e.g., GX-271 ASPEC™ Liquid Handler).
2. Benchtop quick spin.
3. Benchtop shaker.
4. Capless graduated microtubes (1.7 mL).
5. C18 columns (e.g., GracePure™ C18).
6. Solid phase extraction (SPE) strong cation exchange (SCX) columns (e.g., GracePure™ SPE).
7. 5 mL round bottom tubes.
8. Solution 1: 10 mM ammonium formate, 0.1% formic acid, 0.1% heptafluorobutyric acid (HFBA) in water. For a 500 mL solution preparation, weigh 315.3 mg of ammonium formate and transfer to a 500 mL glass bottle. Add 500 μL formic acid, 500 μL HFBA and make up to 500 mL with water. Mix (*see* **Note 2**).
9. Solution 2: 10 mM ammonium formate, 0.1% formic acid, 0.1% HFBA, 40% methanol in water. For a 500 mL solution preparation, weigh 315.3 mg ammonium formate and transfer to a 500 mL Schott glass bottle. Add 500 μL formic acid, 500 μL HFBA, 200 mL methanol and make up to 500 mL with water. Mix (*see* **Note 2**).
10. Solution 3: 25% ammonium hydroxide solution in water (*see* **Note 2**).
11. Solution 4: 0.1% formic acid in water. For a 500 mL solution preparation, add 500 μL formic acid and make up to 500 mL with water. Mix (*see* **Note 2**).
12. HFBA solution: 5% HFBA in water (*see* **Note 2**).
13. SnapStrip 8-strip PCR tubes.
14. High-performance liquid chromatography (HPLC) screw vials (with fixed inserts) and lids.

2.1.4 Sample Normalization

Total protein assay kit.

2.2 Ultrahigh-Performance Liquid Chromatography-Triple Quadrupole Mass Spectrometer (UHPLC-MS/MS) Method

1. Ultrahigh-performance liquid chromatographic (UHPLC) (e.g., Thermo Scientific Dionex ultimate 3000).
2. UHPLC column (e.g., Agilent SB C18 RRHD, 50 × 2.1 mm, 1.8 μm reversed phase column).
3. Triple quadrupole mass spectrometer.
4. Mobile phase A: 10 mM ammonium formate, 0.1% formic acid, 0.12% heptafluorobutyric acid (HFBA) in water. Weigh 630.6 mg of ammonium formate and transfer to the 1 L glass bottle. Add 900 mL of water; add 1 mL of formic acid and 1.2 mL of HFBA. Make up to 1 L with water and mix. Protect the prepared solution from light by preparing it in amber colored bottle, or cover the normal glass bottle with aluminum foil (*see* **Notes 2** and **3**).
5. Mobile phase B: 10 mM ammonium formate, 0.1% formic acid, 0.12% HFBA in LCMS grade methanol. Weigh 315.3 mg of ammonium formate and transfer to the 500 mL glass bottle. Add 400 mL of LCMS grade methanol; add 0.5 mL of formic acid and 0.6 mL of HFBA. Make up to 500 mL with LCMS grade methanol and mix well. Protect the prepared solution from light by preparing it in amber colored bottle, or cover the normal glass bottle with aluminum foil (*see* **Notes 2** and **3**).
6. Autosampler needle wash solution: 20% methanol in water. Take 800 mL of water in a 1 L glass bottle and add 200 mL of LCMS grade methanol. Mix well.
7. Column wash solution A: 0.1% formic acid in water. Take 900 mL of water in a 1 L glass bottle; add 1 mL of formic acid and make up to 1 L with water. Mix well.
8. Column wash solution B: 0.1% formic acid in LCMS grade acetonitrile. Take 900 mL of LCMS grade acetonitrile in a 1 L glass bottle; add 1 mL of formic acid and make up to 1 L with LCMS grade acetonitrile. Mix well.
9. The working standard were dihydroxylysinonorleucine (DHLNL), hydroxylysinonorleucine (HLNL), pyridinoline (PYD) and deoxypyridinoline (DPD) and hydroxyproline. For DHLNL, dissolve 2.5 mg of the working standard in 1 mL of water to obtain a concentration of 2.5 mg/mL, which is equivalent to 8.14 nmol/μL. For HLNL, dissolve 0.5 mg of the working standard in 172 μL water to obtain a concentration of 2.9 mg/mL, which is equivalent to 10 nmol/μL. For hydroxyproline, dissolve 13.1 mg of working standard in 1 mL of water to obtain a concentration of 13.1 mg/mL, which is equivalent to 100 nmol/μL. PYD and DPD are

available as a solution mixture where the concentration labeled on the vial for PYD is 5.88 μg/mL and for DPD is 3.06 μg/mL.

10. Graph Pad Prism software.

3 Methods

Carry out all procedures at room temperature unless otherwise specified.

3.1 Extraction and Purification of Cross-Links

For immature and mature collagen cross-links and hydroxyproline.

3.1.1 Tissue Sample Preparation

Note that this tissue preparation is generic and applies for most soft tissues, except skin (*see* Subheading "Skin Preparation").

1. Weigh out relevant amount of tissue and carry out freeze-drying. Cut the tissue into smaller pieces to increase the surface area for freeze-drying (*see* **Note 4**).
2. Grind the freeze-dried tissue manually using a spatula and then collect 20 mg in a 2 mL metal bead lysing matrix tube (*see* **Note 5**).
3. Homogenize the dry tissue twice. The sample becomes a dry powder.
4. Add 1 mL of PBS and homogenize two more times (*see* **Note 6**).
5. Transfer 500 μL of the homogenate (equivalent to 10 mg dry tissue) into a 2 mL heat/acid resistant screw cap tube (*see* **Note 7**). Tissue preparation is complete for mature collagen and mature elastin cross-links samples.
6. For immature collagen cross-links extraction and hydroxyproline extraction samples, top up with 370 μL of PBS, to gain a total volume of 870 μL.
7. Reduction step (*see* Subheading 3.1.2).

Skin Preparation

1. Weigh out each sample and insert into a 2 mL metal bead lysing matrix tube (*see* **Note 8**).
2. For homogenization of skin samples, add 1 mL of collagenase solution per 10 mg of tissue.
3. Incubate for 24 h at room temperature. During the incubation, the samples should be homogenized intermittently (*see* **Note 9**).

4. Transfer 500 μL of the homogenate (equivalent to 5 mg dry tissue) into a 2 mL acid-/heat-resistant screw cap tube (*see* **Note 7**).
5. Top up with 370 μL PBS, to gain a total volume of 870 μL.
6. Reduction step (*see* Subheading 3.1.2).

3.1.2 Reduction Step

For immature collagen cross-links extraction and hydroxyproline. For mature collagen and elastin cross-links, go straight to **step 5**.

1. Add 30 μL of 12 mg/mL $NaBH_4$ buffer into the 870 μL tissue homogenate (equivalent to a 30× dilution of the buffer). After addition, shake the tubes manually by hand to ensure the reduction reaction can occur.
2. Incubate at room temperature for 30 min.
3. Stop the reaction by adding 50 μL of neat acetic acid, which will bring the pH below 2.5 (*see* **Note 10**).
4. Quick spin the samples to remove liquid contents from the lid.
5. Dry the samples using the Genevac at 60 °C with the aqueous program settings.
6. Add 1600 μL of 6 M HCL to the pellet. Heat at 105 °C to hydrolyse for 24 h (*see* **Note 11**).
7. Dry the HCL using the Genevac at 60 °C with the $H_2O + NH_3$ program settings (*see* **Note 12**).
8. Reconstitute the samples in 200 μL of water, and place on shaker for 10 min at high speed.
9. Spin dow the samples at 20,000 × *g* for 1 min.

3.1.3 Sample Cleanup Using SPE (Automated)

1. Prepare C18 and SCX columns by inserting adaptors onto the columns (*see* **Note 13**).
2. Take 50 μL of the sample hydrolysate (i.e., from **step 8** of the reduction procedure) into 400 μL of solution 1.
3. Load onto a SPE C18 column.
4. Perform **steps 5–9** in a fume hood (*see* **Note 2**).
5. Add 600 μL of solution 1 to the C18 column and elute into a C18-labeled 5 mL round bottom tube.
6. Add 500 μL of solution 2 to the C18 column and elute into the abovementioned 5 mL round bottom tube.
7. Add the C18 eluate (1550 μL total) directly onto a SCX column (which has been pre-rinsed with 2 mL of water and 500 μL of solution 4).
8. Wash the loaded SCX column with 1 mL of water.
9. Elute the SCX cartridge with 3 mL of solution 3 and collect into a SCX-labeled 5 mL round bottom tube.

10. Dry the SCX eluate using the Genevac at 60 °C with the H_2O + NH_3 program settings.
11. Add 500 μL of 5% HFBA solution.
12. Dry the sample using the Genevac at 60 °C with the aqueous program settings.
13. Reconstitute the dried samples in 50 μL of solution 1 and transfer to SnapStrip PCR tubes (*see* **Note 14**).
14. Spin the samples using a benchtop spin at high speed for 5 min.
15. Transfer 40 μL of the supernatant into HPLC vials; take extra care not to disturb the pellet.

3.1.4 Protein Assay

Perform a protein assay on the samples as per instructions detailed in the total protein assay kit (*see* **Note 15**).

3.2 Ultrahigh-Performance Liquid Chromatography-Triple Quadrupole Mass Spectrometer (UHPLC-MS/MS)

3.2.1 Chromatographic Conditions

1. Flow rate: 0.3 mL/min using a multistep gradient method.
2. Gradient method: Hold mobile phase A at 96.2% for 1.0 min and then decrease linearly to 80% within 5 min. Hold mobile phase A at 80% from 5 min to 7 min. Switch the divert valve from ion source to the waste at 7 min. Decrease mobile phase A linearly to 0% from 7 min to 9 min. Bring back mobile phase A concentration from 0% to 96.2% linearly at 9.5 min and hold for the next 1.5 min, i.e., until 12.0 min. At the end of the gradient program, for the duration of 0.2 min from 11.8 to 12.0 min, decrease the flow rate from 0.3 mL/min to 0.05 mL/min.
3. Total run time: 12.0 min.
4. Column oven temperature: 40 °C.
5. Autosampler temperature: Room temperature.
6. Injection volume: 10 μL for the skin, liver, and kidney tissues.

3.2.2 Mass Spectrometry Conditions

Quantitation of the immature cross-links dihydroxylysinonorleucine (DHLNL) and hydroxylysinonorleucine (HLNL), the trivalent mature cross-links pyridinoline (PYD) and deoxypyridinoline (DPD), as well as hydroxyproline (HYP) to determine total collagen in the prepared samples by ultra-performance liquid chromatography-electrospray ionization tandem mass spectrometry (UPLC-ESI-MS/MS).

1. Operate the ESI source as follows: Spray voltage, 4000 V; sheath gas, 35 psi; auxiliary gas, 20 psi; sweep gas, 0 psi; ion transfer tube temperature, 350 °C; vaporizer temperature, 300 °C.
2. The MS acquisition parameters for DHLNL: Radio frequency (RF) lens voltage, 100 V; collision energy, 23 V. Collect data in single reaction monitoring (SRM) mode using retention time

window from 3.19 min to 4.0 min and a transition of precursor ion *m/z* 308.1 to a product ion *m/z* 128.246. The confirmation peak transitions have precursor *m/z* 308.1 to a product ion *m/z* 82.136 with a collision energy as 33 V and *m/z* 308.1 to a product ion *m/z* 146.109 with a collision energy as 25 V.

3. The MS acquisition parameters for HLNL: Radio frequency (RF) lens voltage, 100 V; collision energy, 20.921 V. Collect data in single reaction monitoring (SRM) mode using retention time window from 4.33 min to 5.0 min and a transition of precursor ion *m/z* 292.139 to a product ion *m/z* 128.097. The confirmation peak transitions have precursor *m/z* 292.139 to a product ion *m/z* 130.183 with a collision energy as 19.303 V and *m/z* 292.139 to a product ion *m/z* 229.111 with a collision energy as 20.466 V.
4. The MS acquisition parameters for PYD: Radio frequency (RF) lens voltage, 180 V; collision energy, 30 V. Collect data in single reaction monitoring (SRM) mode using retention time window from 4.7 min to 5.0 min and a transition of precursor ion *m/z* 429.2 to a product ion *m/z* 412.13. The confirmation peak transitions have precursor *m/z* 429.2 to a product ion *m/z* 266.98 with a collision energy as 36 V and *m/z* 429.2 to a product ion *m/z* 367.06 with a collision energy as 30 V.
5. The MS acquisition parameters for DPD: Radio frequency (RF) lens voltage, 140 V; collision energy, 30 V. Collect data in single reaction monitoring (SRM) mode using retention time window from 5.8 min to 8.0 min and a transition of precursor ion *m/z* 413.2 to a product ion *m/z* 267.1. The confirmation peak transitions were having *m/z* 413.2 to a product ion *m/z* 351.12 with a collision energy as 28 V and *m/z* 413.2 to a product ion *m/z* 396.16 with a collision energy as 30 V.
6. The MS acquisition parameters for HYP: Radio frequency (RF) lens voltage, 81 V; collision energy, 13.135 V. Collect data in single reaction monitoring (SRM) mode using retention time window from 0.85 min to 1.5 min and a transition of precursor ion *m/z* 132.2 to a product ion *m/z* 96.125. The confirmation peak transitions have precursor *m/z* 132.2 to a product ion *m/z* 68.389 with a collision energy as 22.236 V and *m/z* 132.2 to a product ion *m/z* 78.214 with a collision energy as 29.618 V.
7. Operate the collision induced gas at 1.5 mTorr.

3.2.3 Calibration Standards Preparation

Carry out all procedures at room temperature unless otherwise specified.

1. Pipette out 650 μL of the PYD/DPD mixture from the vial out of the total volume of 750 μL and transfer it into a plastic test

tube. The concentration of PYD is 3.82 μg/mL equivalent to 8.9 nmol/mL and DPD is 1.99 μg/mL equivalent to 4.8 nmol/mL.

2. Dry the samples using the Genevac EZ-2 plus at 60 °C using the aqueous program.
3. Reconstitute the dried sample with 2 mL of mobile phase A, add 446.5 μL of hydroxyproline stock solution equivalent to 100 nmol/μL, then add 2.74 μL of DHLNL stock solution (8.14 nmol/μL), then add 0.89 μL of HLNL stock solution (10 nmol/μL) and then finally add 2.015 mL of mobile phase A. The final concentrations of the biomarkers in the prepared solution are 100 nmol/10 μL hydroxyproline, 50 pmol/10 μL DHLNL, 20 pmol/10 μL HLNL, 20 pmol/10 μL PYD, and 10 pmol/10 μL DPD. Mix well. Name the solution as "Cross-links Calibration solution 1."
4. Make 2.5 dilutions of Crosslinks Calibration solution 1; take 2060 μL of Cross-links Calibration solution 1 and add into 3090 μL of mobile phase A. The final concentrations of the biomarkers in the prepared solution are 40 nmol/10 μL hydroxyproline, 20 pmol/10 μL DHLNL, 8 pmol/10 μL HLNL, 8 pmol/10 μL PYD, and 4 pmol/10 μL DPD. Mix well. Name the solution as "Cross-links Calibration solution 2."
5. Make 2.5 dilutions of Cross-links Calibration solution 2; take 2060 μL of Cross-links Calibration solution 2 and add into 3090 μL of mobile phase A. The final concentrations of the biomarkers in the prepared solution are 16 nmol/10 μL hydroxyproline, 8 pmol/10 μL DHLNL, 3.2 pmol/10 μL HLNL, 3.2 pmol/10 μL PYD, and 1.6 pmol/10 μL DPD. Mix well. Name the solution as "Cross-links Calibration solution 3."
6. Make 2.5 dilutions of Crosslinks Calibration solution 3; take 2060 μL of Cross-links Calibration solution 3 and add into 3090 μL of mobile phase A. The final concentrations of the biomarkers in the prepared solution are 6.4 nmol/10 μL hydroxyproline, 3.2 pmol/10 μL DHLNL, 1.28 pmol/10 μL HLNL, 1.28 pmol/10 μL PYD, and 0.64 pmol/10 μL DPD. Mix well. Name the solution as "Cross-links Calibration solution 4."
7. Make 2.5 dilutions of Cross-links Calibration solution 4; take 2060 μL of Cross-links Calibration solution 4 and add into 3090 μL of mobile phase A. The final concentrations of the biomarkers in the prepared solution are 2.56 nmol/10 μL hydroxyproline, 1.28 pmol/10 μL DHLNL, 0.512 pmol/10 μL HLNL, 0.512 pmol/10 μL PYD, and 0.256 pmol/10 μL DPD. Mix well. Name the solution as "Cross-links Calibration solution 5."

8. Make 2.5 dilutions of Cross-links Calibration solution 5; take 2060 μL of Cross-links Calibration solution 5 and add into 3090 μL of mobile phase A. The final concentrations of the biomarkers in the prepared solution are 1.024 nmol/10 μL hydroxyproline, 0.512 pmol/10 μL DHLNL, 0.2048 pmol/10 μL HLNL, 0.2048 pmol/10 μL PYD, and 0.1024 pmol/10 μL DPD. Mix well. Name the solution as "Cross-links Calibration solution 6."
9. Make 2.5 dilutions of Cross-links Calibration solution 6; take 2060 μL of Cross-links Calibration solution 6 and add into 3090 μL of mobile phase A. The final concentrations of the biomarkers in the prepared solution are 0.4096 nmol/10 μL hydroxyproline, 0.2048 pmol/10 μL DHLNL, 0.08192 pmol/10 μL HLNL, 0.8192 pmol/10 μL PYD, and 0.04096 pmol/10 μL DPD. Mix well. Name the solution as "Cross-links Calibration solution 7."
10. Make 2.5 dilutions of Cross-links Calibration solution 7; take 2060 μL of Cross-links Calibration solution 7 and add into 3090 μL of mobile phase A. The final concentrations of the biomarkers in the prepared solution are 0.163 nmol/10 μL hydroxyproline, 0.08192 pmol/10 μL DHLNL, 0.0328 pmol/10 μL HLNL, 0.328 pmol/10 μL PYD, and 0.0164 pmol/10 μL DPD. Mix well. Name the solution as "Cross-links Calibration solution 8."
11. Make 2.5 dilutions of Cross-links Calibration solution 8; take 2060 μL of Cross-links Calibration solution 8 and add into 3090 μL of mobile phase A. The final concentrations of the biomarkers in the prepared solution are 0.0655 nmol/10 μL hydroxyproline, 0.0328 pmol/10 μL DHLNL, 0.01312 pmol/10 μL HLNL, 0.01312 pmol/10 μL PYD, and 0.00656 pmol/10 μL DPD. Mix well. Name the solution as "Cross-links Calibration solution 9."
12. Transfer a required amount of the prepared Calibration standards to a HPLC vial and load it into the autosampler for analysis of cross-links samples. Store the remaining amount of the standards at −20 °C and use them further as and when needed.

3.2.4 Sample Acquisition and Data Analysis

1. Start up the LC-MS/MS system (*see* **Note 16**). Perform at least five injections of water onto the column using the cross-links method. This is to equilibrate the column and the mass spectrometer ion source with the cross-link method conditions.
2. Following equilibration, inject a few Cross-links Calibration standard for sensitivity and chromatography check (*see* **Note 17**).
3. Inject all the Cross-links Calibration standards (*see* **Note 18**), followed by injecting the processed tissue samples.

Immediately following tissue samples, inject all the Cross-links Calibration standards again to complete one bracket of the run. Similarly, inject the other tissue samples by bracketing them between the Cross-links Calibration standards.

4. Wash the column and the ion source by injecting water samples using column wash method.
5. Column wash method is as follows: Flow rate, 0.5 mL/min using a multistep gradient method; total run time, 40.0 min. The gradient is as follows: Hold column wash solution B at 5% for 1.0 min, and then increase linearly to 95% within 8 min. Decrease the column wash solution B at 5% within 8.5 min and hold for up to 10 min. Again linearly increase the column wash solution B to 95% within 18 min. Decrease the column wash solution B at 5% within 18.5 min and hold for up to 20 min. Linearly increase the column wash solution B to 95% within 28 min. Decrease the column wash solution B at 5% within 28.5 min and hold for up to 30 min. Linearly increase the column wash solution B to 95% within 38 min. Decrease the column wash solution B at 5% within 38.5 min and hold for up to 40 min.
6. Calibration parameters are as follows: Use "External method" for a standard type method (*see* **Note 19**). Set the Curve type as "Quadratic," Origin as "Ignore," and Weighting as "Equal." Use the averaged out calibration curve from each of the two adjacent calibrator levels. Select the sample type for Calibration standards as "Cal STD," and assign the correct levels to each bracketing Calibration standard (*see* **Note 20**).
7. Units used for analysis of Cross-links Calibration standards: pmols/10 μL.
8. After sample acquisition onto the LC-MS/MS, evaluate the generated chromatographic data of each biomarker individually by observing the Cross-links Calibration standards and tissue samples in terms of peak shape and peak integrity (manually integrate the peak if needed). Also evaluate % CV (coefficient of variance) of peak responses of adjacent calibrators injected before and after the tissue samples to monitor for any drift in peak responses onto the detector and % error of calculated amount of each calibrator on comparing it with its actual amount and the r^2 (coefficient of determination) of the calibration curve.
9. Check the peak responses of the tissue samples and check where they lie on the calibration curve. Use the most relevant calibration levels, which cover the peak response range of the tissue samples and exclude the rest of the calibration points from the analysis (*see* **Note 21**).

10. Once the chromatographic data are finalized, apply the correct conversion factor to the tissue samples. This would give the actual amount of biomarker present in the total volume of hydrolysate sample. Conversion factor is the ratio of the volume of the hydrolysate sample to the volume of the injected sample (e.g., for a 200 μL hydrolysate sample and an injected 10 μL sample onto the column, the conversion factor would be 200/10 = 20).
11. Generate the final LC-MS/MS results summary file into an Excel file for further calculations.
12. The amount generated are in terms of pmols/volume of sample hydrolysate. Convert the amount in terms of pmols/mL.
13. Normalize the amount (pmols/hydrolysate sample) of DHLNL, HLNL, PYD, and DPD against HYP amount (pmols/hydrolysate sample). Normalize the amount (pmols/hydrolysate sample) of all biomarkers against dry tissue weight (mg) and normalize the amount (pmols/mL) of all biomarkers against protein content (mg/mL).
14. Conduct the statistical data analysis on Graph Pad Prism software, version 6 or latest. Use unpaired *t*-test for the comparison of healthy and diseased animal groups. Use one-way ANOVA for all treated groups against the untreated group to compare the effect of one variable at the time (dose or different drugs). Conduct all the Prism analysis on cleaned data by excluding the outliers, using the Rout test, with the *Q* value set at 1%.

4 Notes

1. The $NaBH_4$ buffer is not stable; make it right before the reduction reaction. Use and discard appropriately.
2. To avoid exposure to dangerous fumes, prepare the solutions inside a fume hood.
3. Heptafluorobutyric acid (HFBA) is sensitive, and hence if the solution exposes to light, the concentration of HFBA tends to deteriorate having an adverse impact on the sensitivity of biomarkers and their retention times onto the column.
4. We use 5 mL polystyrene tubes with cell-strainer caps to insert the tissue in for freeze-drying. The tissue samples should be placed on dry ice and allowed to thaw such that they can be easily cut with a blade. Dry ice is a hazard and should be handled carefully in accordance with laboratory guidelines. Freeze-drying results in approximately 70% loss of weight of tissue, and at the end of the procedure, minimum 10 mg dry tissue must be gained; therefore, the initial weighing of the wet

tissue for each sample must be done accordingly (i.e., for liver samples, 300 mg wet weight is a good starting point). After each sample has been weighed out, it must be snap frozen in dry ice (all tubes can be stored at −80 °C for 30 min before being placed on the freeze dryer). It can take up to 2 days for the samples to freeze-dry completely; at the end of the procedure, perform a qualitative (tissue should appear pale and lighter in color) and quantitative (check to see approximately 70% of the weight has been deducted).

5. For the cross-links procedure, 10 mg has been determined to be the ideal amount for the assay (although in some instances 5 mg is used). We usually weigh out 20 mg, add 1 mL PBS, and take 500 μL of the homogenate across to further steps (which is equivalent to 10 mg).
6. For certain tissue types, homogenizing two more times is not sufficient. The tube must be observed thoroughly to ensure an evenly reconstituted homogenate. The homogenization can be performed a number of times (when dissolved evenly, the homogenate usually appears pink). If after 5–6 cycles the powder is not dissolved into the PBS, use a pipette tip to poke at the tissue that may be stuck to the walls of the tube and then homogenize again. Occasionally, the metal beads lead to break of the integrity of the tube, which may in turn lead to leakage of the homogenate. If this occurs midway, stop the machine and reweigh the tissue. A good safety catch is to check the tubes after each homogenization cycle and change the lids if scratches are observed.
7. It is critical the homogenate is evenly reconstituted before transferring. Therefore, pipette up and down carefully before transferring the 500 μL. If any large tissue bits are observed, repeat the homogenization.
8. If the skin sample is in excess of 14 mg or so, then the sample should be divided into two, and both subsections should be taken across in individual metal bead lysing matrix tubes.
9. The homogenization should be performed every 2–3 h (5–6× at every time point) when feasible. Before the end of the 24-h period, the tissue should be entirely homogenized and no skin tissue should be visible.
10. Concentrated acetic acid is corrosive to the skin and must therefore be handled with appropriate care. This step should be performed in a fume hood.
11. If after the 24-h hydrolysis, the procedure cannot be continued straight away, the samples containing HCl can be stored a −20 °C.

12. If the sample cleanup using SPE (i.e., next step) is to be performed later, the dried pellet after the HCl has dried can be stored at 4 °C as these samples are stable.
13. On the automated SPE machine, the columns must have adaptors inserted onto them. Otherwise, the probe will not be able to create pressure in the column during the SPE procedure.
14. The reconstituted sample can be transferred to any tube for a quick spin. However, it is easier to use SnapStrip PCR tubes. The sample should be pipetted up and down 5–6× to ensure the pellet is evenly reconstituted in solution 1 before transferring to the SnapStrip tubes.
15. For cross-links analysis, the data is normalized against different parameters. Protein measurement is one of the parameters used in our laboratory. The protein assay can be conducted at the end of the entire experimental procedure. The sample to be used is the remaining sample after it was reconstituted in 200 μL of water and 50 μL was taken for SPE. If the dry weight initially was 10 mg, a 1 in 100 dilution is to be performed for the assay, and if the initial dry weight was 5 mg, a 1 in 50 dilution is to be performed for the protein assay. Nevertheless, the dilution can be adjusted based on the results obtained. Prepare the samples in this manner, and then 15 μL of each diluted sample can be pipetted into the appropriate wells (**step 4** in the protein assay kit booklet). The plate readout obtained (mg/mL) should be multiplied by the dilution factor used for sample preparation. Protein assay measurements should be reported as mg/mL.
16. Switch on all modules of UHPLC and switch the mass spectrometer from standby mode to scan mode. Allow the ion source temperature to achieve the desired temperature as per the cross-links method and then turn on the solvent delivery pumps.
17. Inject calibrators from the middle range (e.g., Cross-links Calibration solution 5, 4, and 3). Check for the retention time, peak shape, and sensitivity of the standards and compare with the previously injected reference ones. In cases where one of the parameters does not match with the previous results, re-prepare the mobile phase using a new bottle of HFBA. It is critical to procure HFBA in small pack sizes and do not reuse from the same pack for LC-MS/MS analysis.
18. Inject the calibration standards in the reverse order starting from "Cross-links Calibration solution 9" to "Cross-links Calibration solution 1" to avoid any autosampler carry-over effect. Inject a water sample before and after each calibration cycle to monitor contamination and carry-over, if any.

19. Deuterated internal standards of each biomarker are very difficult to synthesis and thus very tough to get. Hence, an external standard method is used to conduct the cross-links analysis.
20. In the method setup section of the LC-MS/MS software, create nine calibration levels for each biomarker. Capture the actual amounts of each calibration standard. Allocate the correct levels to their corresponding calibrators and analyze.
21. The calibration range for each biomarker is very broad, extending beyond the perfectly linear portion of the curve. However, to analyze all the tissue samples in a single run, such broad range is necessary. Hence, use only the relevant calibration levels for the calculations, ignoring the other ones.

References

1. Trackman PC (2016) Enzymatic and non-enzymatic functions of the lysyl oxidase family in bone. Matrix Biol 52-54:7–18
2. van der Slot-Verhoeven AJ, van Dura EA, Attema J, Blauw B, De Groot J, Huizinga TW, Zuurmond AM, Bank RA (2005) The type of collagen cross-link determines the reversibility of experimental skin fibrosis. Biochim Biophys Acta 1740:60–67

Chapter 7

Mass Spectrometry-Based Proteomics to Define Intracellular Collagen Interactomes

Ngoc-Duc Doan, Andrew S. DiChiara, Amanda M. Del Rosario, Richard P. Schiavoni, and Matthew D. Shoulders

Abstract

We present the development, optimization, and application of constructs, cell lines, covalent cross-linking methods, and immunoprecipitation strategies that enable robust and accurate determination of collagen interactomes via mass spectrometry-based proteomics. Using collagen type-I as an example, protocols for working with large, repetitive, and GC-rich collagen genes are described, followed by strategies for engineering cells that stably and inducibly express antibody epitope-tagged collagen-I. Detailed steps to optimize collagen interactome cross-linking and perform immunoprecipitations are then presented. We conclude with a discussion of methods to elute collagen interactomes and prepare samples for mass spectrometry-mediated identification of interactors. Throughout, caveats and potential problems researchers may encounter when working with collagen are discussed. We note that the protocols presented herein may be readily adapted to define interactomes of other collagen types, as well as to determine comparative interactomes of normal and disease-causing collagen variants using quantitative isotopic labeling (SILAC)- or isobaric mass tags (iTRAQ or TMT)-based mass spectrometry analysis.

Key words Collagen proteostasis network, Co-immunoprecipitation, Proteomics, Cross-linking, Mass spectrometry

1 Introduction

Collagen is the molecular scaffold for animal life [1, 2]. In addition to forming the primary proteinaceous component of bone, skin, cartilage, basement membranes, and other tissues, collagen also facilitates diverse phenomena such as cell–cell signaling, wound healing, and cell migration [3]. Proper execution of the folding, modification, and quality control processes required for biogenesis of this complex protein is, therefore, critical [4, 5]. Collagen proteostasis, encompassing all of these factors, can be disrupted by mutations in collagen molecules themselves or by dysfunction of the proteostasis network [6–9], which is the integrated system of intracellular chaperones, quality control factors, and trafficking

Irit Sagi and Nikolaos A. Afratis (eds.), *Collagen: Methods and Protocols*, Methods in Molecular Biology, vol. 1944, https://doi.org/10.1007/978-1-4939-9095-5_7, © Springer Science+Business Media, LLC, part of Springer Nature 2019

mechanisms that addresses cellular protein production challenges [10, 11]. The hierarchical nature of collagenous matrices allows the resulting defects in individual collagen molecules to propagate to the level of tissues [12, 13], engendering a broad category of disease known as the collagenopathies [7, 14]. Current therapies remain inadequate for alleviating pathologic manifestations of these diseases, owing in part to an incomplete understanding of collagen biogenesis.

Developing a molecular-level understanding of intracellular collagen folding, processing, assembly, and quality control requires that we first identify the players. Unfortunately, the lack of an amenable collagen-I expressing cell model system, the absence of high quality immunoprecipitation (IP)-grade collagen antibodies, and the challenges associated with performing molecular biology on a lengthy, GC-rich, and highly repetitive gene had, prior to our work [15], precluded systematic study of the collagen proteostasis network. After addressing practical problems associated with handling collagen genes, we generated panels of fibrosarcoma and osteosarcoma cell lines that inducibly express collagen variants tagged with distinct antibody epitopes to overcome these roadblocks. Covalent cross-linking and selective immunoprecipitation of collagen-I from these cells, followed by mass spectrometry-based proteomic analysis (Fig. 1), yielded the first unbiased map of the wild-type collagen-I proteostasis network (Table 1). Our strategy robustly identified virtually all previously known collagen-I interactors, as well as ~30 putative new players in collagen-I biogenesis. The novel interactors we identified encompass a wide range of proteostasis-relevant endoplasmic reticulum proteins, including co-chaperones, oxidoreductases, and trafficking mechanisms. We validated a number of the newly identified players in collagen-I proteostasis by immunoprecipitations and genetic knockdowns in osteoblast-like cells that natively produce collagen-I. We also discovered a novel collagen-I posttranslational modification, aspartyl hydroxylation, via these interactome studies.

Using our work with wild-type collagen-I as a template for the description of a generalizable strategy, we present a detailed protocol to map collagen interactomes, including approaches for manipulating collagen genes, developing stable cell lines expressing antibody epitope-tagged collagens, optimizing and validating

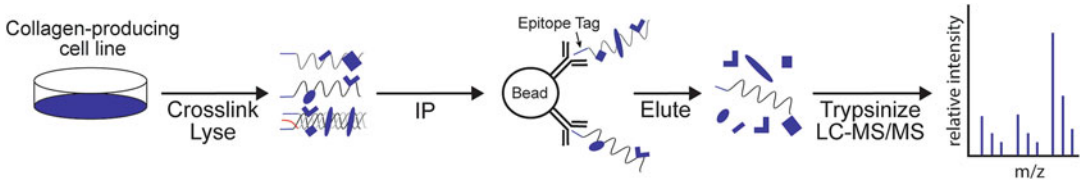

Fig. 1 Schematic representation of collagen interactomics workflow

Table 1
Selected wild-type collagen-I interactors reproducibly identified by mass spectrometry [15]

Protein name	Gene name	Total peptides	Unique peptides
Collagen α1(I) chain	*Col1A1*	915	63
Protein disulfide isomerase	*P4HB*	129	20
Prolyl 4-hydroxylase subunit α2	*P4HA2*	69	15
Prolyl 4-hydroxylase subunit α1	*P4HA1*	68	15
78 kDa glucose-regulated protein (BiP/GRP78)	*HSPA5*	56	15
Collagen α2(I) chain	*Col1A2*	42	13
Endoplasmin (GRP94)	*HSP90B1*	35	12
Prolyl 3-hydroxylase 1	*LEPRE1*	25	9
Peptidyl-prolyl cis-trans isomerase FKBP10	*FKBP10*	19	8
Prelamin-A/C	*LMNA*	14	8
Transitional endoplasmic reticulum ATPase	*VCP*	13	8
Protein disulfide isomerase A3	*PDIA3*	16	7
Fibronectin	*FN1*	11	7
Cytoskeleton-associated protein 4	*CKAP4*	10	7
Peptidyl-prolyl cis-trans isomerase B	*PPIB*	25	6
Procollagen-lysine,2-oxoglutarate 5-dioxygenase 2	*PLOD2*	20	6
Procollagen-lysine,2-oxoglutarate-5-dioxygenase 3	*PLOD3*	17	6
Annexin A2	*ANXA2*	15	6
C-type mannose receptor 2	*MRC2*	12	6
Procollagen-lysine,2-oxoglutarate-5-dioxygenase 1	*PLOD1*	16	5
Cartilage-associated protein	*CRTAP*	14	5
Protein disulfide isomerase A6	*PDIA6*	12	5
Serpin H1 (HSP47)	*SERPINH1*	10	5
Peptidyl-prolyl cis-trans isomerase FKBP9	*FKBP9*	12	4
Protein disulfide isomerase A4	*PDIA4*	8	4
Galectin-3-binding protein	*LGALS3BP*	7	4
Peroxiredoxin-1	*PRDX1*	5	3
Peptidyl-prolyl cis-trans isomerase A	*PPIA*	5	3
Endoplasmic reticulum resident protein 44	*ERP44*	5	3
Calreticulin	*CALR*	5	3
Golgi apparatus protein-1	*GLG1*	4	3

(continued)

Table 1
(continued)

Protein name	Gene name	Total peptides	Unique peptides
Thioredoxin domain-containing protein 5	*TXNDC5*	4	3
Hypoxia up-regulated protein 1	*HYOU1*	3	3
Calnexin	*CANX*	5	2
Polyubiquitin-C	*UBC*	5	2
Reticulocalbin-1	*RCN1*	5	2
Endoplasmic reticulum resident protein 29	*ERP29*	4	2
Golgi integral membrane protein 4	*GOLIM4*	4	2
Thioredoxin domain-containing protein 12	*TXNDC12*	3	2
Calumenin	*CALU*	3	2
DnaJ homolog subfamily B member 11	*DNAJB11*	2	2
Peptidyl-prolyl cis-trans isomerase FKBP4	*FKBP4*	2	2
Reticulocalbin-3	*RCN3*	2	2
Thioredoxin-related transmembrane protein 1	*TMX1*	2	2

mass spectrometry-grade immunoprecipitations and covalent cross-linking reactions, preparing samples for proteomic analysis, and performing mass spectrometry experiments. The protocol should prove useful not just for studying wild-type collagen-I but also for quantitatively evaluating how cells engage misfolding, disease-causing collagen-I variants. Moreover, the protocol is readily adaptable to studying the interactome of any of the other 27 types of collagen [16].

2 Materials

2.1 Molecular Biology and Cell Culture

1. Genes, vectors, and DNA oligomers: Human *Col1A1* and *Col1A2* genes (Origene), pENTR1A vector (Thermo Fisher Scientific), pTRE-Tight vector (Clontech), pLenti.CMV/TO. DEST vectors with assorted resistance cassettes (Addgene) [17], puromycin and hygromycin linear selection markers (Clontech), DNA primers (Sigma), and RRE, REV, and VSVG vectors for lentivirus production (Addgene).
2. Enzymes: Q5 Polymerase, BamHI, EcoRV, NotI, T4 ligase, Antarctic phosphatase (New England BioLabs; NEB), and LR Clonase (Thermo Fisher Scientific).

3. Gel Purification Kit (Omega BioTech).
4. Bacterial cell lines: Sure2 *E. coli* (Agilent) and DH5α electrocompetent and Stbl3 competent *E. coli* (Thermo Fisher Scientific).
5. Human cell lines: Human bone osteosarcoma Saos-2 cells (ATCC), human fibrosarcoma HT-1080 Tet-Off cells that constitutively express the tetracycline (Tet) transactivator (Clontech), and HEK293FT cells (Thermo Fisher Scientific).
6. Cell culture: Dulbecco's Modified Eagle Medium (DMEM), Minimum Essential Medium (MEM), fetal bovine serum (FBS), and trypsin-EDTA (all from Corning Cellgro), tetracycline-free FBS (Clontech), and Opti-MEM media (Thermo Fisher Scientific).
7. Transfection reagents: XFect (Clontech) and Lipofectamine 2000 (Thermo Fisher Scientific).
8. Antibiotics: Penicillin-streptomycin (Thermo Fisher Scientific), puromycin (Corning Cellgro), hygromycin (Enzo Life Sciences), and blasticidin (Sigma).
9. Lenti-X GoStix (Takara).
10. Chemicals: Doxycycline hyclate, L-glutamine, poly-D-lysine, and polybrene (Sigma).
11. Antibodies: anti-HSP47 (ADI-SPA-470; Enzo Life Sciences), anti-HA (sc-7392; Santa Cruz), anti-PDI (sc-20,132; Santa Cruz), anti-Colα1(I) (LF68; Kerafast), anti-Colα2 (I) (SAB4500363; Sigma), and secondary antibodies 800CW goat anti-rabbit, 800CW goat anti-mouse, 680LT goat anti-rabbit, and 680LT goat anti-mouse (LiCor Biosciences).

2.2 Preparation of Protein Samples, Immunoprecipitation, Protein Elution, and Precipitation

All chemicals and supplies used in these protocol steps must be mass spectrometry-grade. RNase-/DNase-free microcentrifuge tubes employed can be from a variety of vendors, but should not be autoclaved prior to use.

1. Radioimmunoprecipitation assay (RIPA) buffer: 50 mM Tris (VWR), 0.5% sodium deoxycholate (Alfa Aesar), 1% Triton (INTEGRA Chemical), 0.1% sodium dodecyl sulfate (SDS; Alfa Aesar), 50 mM NaF (Alfa Aesar), 5 mM β-glycerol phosphate (Sigma), 1 mM sodium metavanadate (Sigma), 5 mM ethylene glycol-bis(β-aminoethyl ether)-N,N,N′,N′-tetraacetic acid (EGTA; STREM Chemicals), 5 mM ethylenediaminetetraacetic acid (EDTA; Aqua Solutions), 100 μM sodium pyruvate (Sigma), 1 mM phenylmethylsulfonyl fluoride (PMSF; Thermo Fisher Scientific), and protease inhibitor mixture (Pierce) at pH 7.4 in dd-H_2O.

2. Lysis buffer: 50 mM Tris, 1% Triton, 1 mM PMSF, 150 mM NaCl, 1.5 mM $MgCl_2$, 1 mM EDTA, and protease inhibitor mixture (Biotool) or tablets (Pierce) at pH 7.4.
3. Phosphate-buffered saline (Corning).
4. Dithiobis(succinimidyl propionate) (DSP; Sigma).
5. Ultrasound processor (Cole Parmer), tube rotator (VWR), refrigerated benchtop centrifuge (Thermo Scientific), vortex mixer (Corning).
6. Anti-HA agarose beads (A2095; Sigma).
7. Elution buffer: 6% SDS in 1 M aqueous Tris buffer at pH 6.8.
8. Solvents: MeOH and $CHCl_3$ (Thermo Fisher Scientific).
9. Vacuum centrifuge dryer (Cole Parmer).

2.3 Preparation of Tryptic Peptides and Mass Spectrometry

All chemicals and supplies used in these protocol steps must be mass spectrometry-grade. RNase-/DNase-free microcentrifuge tubes employed can be from a variety of vendors, but should not be autoclaved prior to use.

1. Chemicals: Iodoacetamide (IAA; Sigma), 1,4-dithiothreitol (DTT; Sigma), urea and formic acid (Fluka).
2. NH_4HCO_3 buffer: 100 mM NH_4HCO_3(aq) at pH 8.0.
3. TFA buffer: 0.1% aqueous trifluoroacetic acid (TFA; Sigma).
4. Formic acid buffer: 0.1% aqueous formic acid.
5. TFA/MeCN buffer: 0.1% TFA in 9:1 MeCN:H_2O (MeCN from Sigma).
6. Formic acid/MeCN buffer: 0.1% formic acid in 4:1 MeCN: H_2O.
7. Pierce C18 Peptide Desalting Spin Column (Thermo Fisher Scientific).
8. Aluminum foil (Reynolds).
9. Water bath at 56 °C.
10. EASY-nLC 1000 or similar HPLC with autosampler connected to a Thermo Fisher Q Exactive Hybrid Quadrupole-Orbitrap Mass Spectrometer or any similar high-resolution, accurate-mass mass spectrometer.
11. Proteome Discoverer 2.2 with Mascot search engine.

3 Methods

Stable cell systems are valuable to enable robust and reproducible determination of collagen-I interactomes via an IP-/MS-based proteomics approach. In the absence of MS-grade collagen-I

3.1 Creating Cellular Platforms for Biochemical Studies of Collagen

antibodies, to permit the necessary IPs, we use cloning strategies to introduce short, well-defined HA or FLAG antibody epitopes between an ER-targeting signal sequence and collagen-I's N-propeptide. More recently, Cas9-based approaches may make it possible to introduce such epitopes directly in endogenous gene loci [18, 19]. With necessary genes encoding antibody epitope-tagged collagens in hand, we next engineer cell lines that stably and inducibly express the tagged collagen proteins. As described below, in HT-1080 cells, we used a transfection-based strategy to deliver genes [15]. In Saos-2 cells, we used a lentivirus-based strategy [15, 20]. Work in both cell types is described below. Either may be used to introduce genes for other collagens or collagen disease-causing variants into essentially any cell system of interest. An advantage of HT-1080 cells for collagen-I studies is that, although they are capable of synthesizing and secreting various collagen types, they do not express collagen-I, and therefore the collagen-I interactome can be readily enriched. On the other hand, Saos-2 cells do endogenously express collagen-I. In such a system, it is more straightforward to mimic autosomal dominant collagen-I pathologies by simply introducing the disease-causing collagen-I variant in a background of endogenous wild-type collagen-I expression. Note that we have found that adenoviruses may also be used for robust transient expression of collagen (not described below, as the focus is on stable cell line development). An adenovirus-based strategy can be especially valuable for transient collagen variant expression in primary cells.

3.1.1 Transfection Approach to Prepare Stable HT-1080 Cells Inducibly Expressing Collagen Genes

Col1A1 and *Col1A2* genes were obtained prior to transfer into an appropriate expression vector (Fig. 2a), as described below (*see* **Note 1**).

1. Using appropriate restriction sites (e.g., BamHI and EcoRV), insert a DNA sequence (IDT) encoding the preprotrypsin signal sequence (PPT; to target collagen strands to the secretory pathway), the desired epitope tag (e.g., *HA* or *FLAG*), and a NotI restriction digestion site (i.e., PPT.HA.NotI or PPT.FLAG.NotI) into a pTRE-Tight vector (*see* **Notes 2** and **3**).
2. PCR-amplify (using the primers shown below which remove the native signal sequence) collagen-I genes over 35–40 PCR cycles. For amplification of collagen-I genes, we recommend the use of Q5 Polymerase with the addition of the High GC Enhancer (protocol from NEB) and a 2 min extension cycle (*see* **Note 4**).

   Col1A1: For. 5′-ACATCAGCGGCCGCACAAGAGGAAGG CCAAGTCGAG-3′.

   Rev. 5′- AAAAAAGTCGACTTACAGGAAGCAGACAGGG-3′.

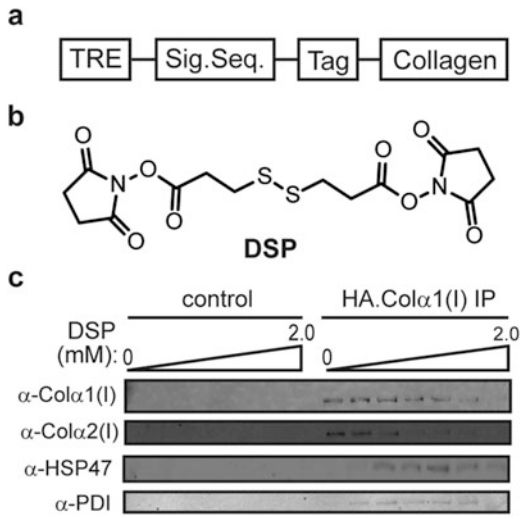

Fig. 2 (**a**) Generalized schematic for collagen-I expression constructs. Either the endogenous collagen signal sequence or the preprotrypsin signal sequence can be employed. The tag can be HA, FLAG, c-MYC, or any of a number of other short antibody epitope tags. (**b**) Structure of dithiobis(succinimidyl propionate) (DSP). (**c**) Optimizing DSP cross-linker concentration by evaluating the co-immunoprecipitation of known collagen-I interactors in the HT-1080 cell system. The control sample represents HT-1080 cells that do not express HA-tagged collagen-I upon induction. This figure was adapted from DiChiara et al. [15]

Col1A2: For. 5′-AAAAAAGCGGCCGCAACATGCCAATC TTTACAAGAGGAAAC-3′.

Rev. 5′-AAAAAAGATATCTTATTTGAAACAGACTGGGCC AATG-3′

3. Restriction digest amplicons using the NotI and EcoRV restriction enzymes (protocol from NEB).
4. Gel purify samples using Gel Purification Kits.
5. Ligate into digested pTRE-Tight vectors prepared in Subheading 3.1.1, **step 1,** using T4 ligase (protocol from NEB) followed by transformation into competent *E. coli* (*see* **Note 5**).
6. Transfect antibody epitope-tagged, tet-regulated collagen-I expression vectors using XFect into HT-1080 Tet-Off cells that constitutively express the tetracycline transactivator along with either a puromycin or hygromycin linear selection marker (protocol from Clontech). Co-transfection with a linear selection marker at a fixed ratio of 25:1 (5 μg: 0.2 μg) reduces the probability of a cell being transfected with the linear selection marker alone, potentially conferring resistance without integration of the collagen gene.

7. Change the media 18–24 h post-transfection.
8. 48 h post-transfection, treat cells with antibiotic (experimentally optimized to be 0.25 μg/mL puromycin or 150 μg/mL hygromycin) for 10–12 days (changing the media every 2 days) for stable selection.
9. Amplify heterostable cell lines, and then split to establish genetically homogenous single colonies to analyze for collagen-I expression and secretion (Fig. 2a). Repeat above process to create cell lines that express both *Col1A1* and *Col1A2* or other collagen variants, as desired (*see* **Note 6**).

3.1.2 Lentiviral Approach to Prepare Stable Saos-2 Cells Inducibly Expressing Collagen Genes

1. Construct pENTR1A vectors encoding the *Col1A1* and *Col1A2* genes by ligating *Col1A1* or *Col1A2* extracted from pTRE.Tight vectors (described above) using the NotI and EcoRV restriction enzymes into a pENTR1A vector already encoding an ER-targeting PPT signal sequence and an HA antibody epitope tag (or other desired tag; *see* **Note 7**). All pENTR1A vectors must be sequence-confirmed before proceeding.
2. Introduce the resulting construct into the appropriate pLenti. CMV/TO.DEST Gateway destination vector via LR clonase-mediated recombination (protocol from Thermo Fisher Scientific). The resulting pLenti vectors must be sequence-confirmed before proceeding to lentiviral production.
3. Produce lentivirus using the third-generation system by co-transfecting HEK293FT cells with the lentiviral plasmids and packaging vectors encoding RRE, REV, and VSVG using Lipofectamine 2000. Briefly, (1) incubate the plasmid mixture (pLenti vector, 15 μg; RRE, 15 μg; REV, 6 μg; and VSVG, 3 μg) with 60 μL of Lipofectamine 2000 in 3 mL of Opti-MEM media for 45 min at room temperature (RT); (2) add the resulting mixture dropwise to a 10 cm dish of HEK293FT cells (~8×10^6 cells plated on poly-D-lysine-coated plates ~12 h pre-transfection) and incubate at 37 °C for 12 h; (3) remove and replace media with DMEM (6 mL) and incubate the plates for another 36 h, monitoring for successful production of lentivirus using Lenti-X GoStix (protocol from Takara); (4) collect viral supernatant 48 h post-transfection; and (5) use supernatant immediately for transductions of Saos-2-TREx cells.
4. Transduce Saos-2TREx (*see* **Note 8**) cells with a range of titers of crude viral supernatants of Tet-responsive HA-collagen-α1 (I). Add polybrene to the viral supernatant (final concentration of 4 μg/mL during transductions) to increase transduction efficiency.

5. Select heterostable cell lines using 250 μg/mL hygromycin or other appropriate selection agent and isolate single colonies (Fig. 2a; *see* **Note 9**).
6. Assay for HA-collagen-α1(I) expression in isolated single colonies using immunoblotting.

3.2 Immunoisolation of the Collagen-I Interactome for Proteomic Analysis

The protocol below uses Saos-2TREx cells inducibly expressing PPT.HA.Colα1(I) (Saos-$2^{Col\alpha1(I)}$ cells) as an example but can be adapted for essentially any cell type of interest. Note that a control IP should also always be performed on cells not expressing the antibody epitope-tagged collagen.

1. Plate Saos-$2^{Col\alpha1(I)}$ cells (~6×10^6) in 10 cm dishes with 10 mL of DMEM supplemented with 15% heat-inactivated FBS, 100 IU/mL penicillin, 100 μg/mL streptomycin, 150 μg/mL hygromycin, and 2 mM L-glutamine. Maintain cells as a monolayer overnight at 37 °C in a humidified atmosphere of 5% CO_2(g).
2. Induce HA-tagged wild-type collagen-I expression by overnight incubation with media containing 4 μg/mL doxycycline (*see* **Note 10**) in the presence of 50 μM ascorbate, a required cofactor for proper collagen hydroxylation and for induction of synthesis and secretion of the endogenous, untagged collagen-I (*see* **Note 11**).
3. After 48 h, remove media, wash with PBS, and add 1 mL of trypsin-EDTA for 5 min. Neutralize trypsin by adding 7 mL of complete DMEM. Pellet cells by spinning at 1000 × *g* for 5 min.
4. Remove media and wash cells twice with PBS at (RT).
5. Resuspend cell pellet in a 15 mL Falcon tube containing 10 mL of PBS and an experimentally optimized concentration of DSP (75 μM for Saos-$2^{Col\alpha1(I)}$ cells; Fig. 2b). Rotate tubes for 30 min at RT to allow the cross-linking to proceed (*see* **Note 12**).
6. Quench excess DSP by adding 1 mL of 1 M aqueous Tris, pH 8, and rotating for 10–15 min at RT.
7. Pellet cells by centrifuging at 1000 × *g* for 5 min at 4 °C, followed by removal of the supernatant.
8. Lyse cells by resuspending them in 1 mL of RIPA buffer at 4 °C. Vortex vigorously for 30 s, and then immediately sonicate (130 Watt, 20 kHz, 70% amplitude) for 6 cycles of one 15 s pulse each, returning tube to ice for 15 s between pulse cycles. Lysates should be clear and fluid after sonication (*see* **Note 13**).
9. Post-sonicating, place the lysate solution on ice for 30 min to ensure complete lysis.

10. Transfer cell lysates to 1.7 mL microcentrifuge tubes, and spin for 15 min (21,100 × *g*) at 4 °C.
11. Transfer to new 1.7 mL tubes. Lysates may be stored at −80 °C at this stage, if desired.
12. Add 50 μL of HA bead slurry (25 μL of dried beads) to 1 mL of lysate solution (*see* **Note 14**), and incubate the sample overnight on a tube roller at 4 °C (*see* **Note 15**).
13. Pellet the beads at 2000 × *g* for 5 min at 4 °C.
14. Wash beads 4× with 1 mL RIPA buffer to remove non-specific binders, rotating 5 min at 4 °C during each wash.
15. Pellet beads at 2000 × *g* for 5 min at 4 °C after the last wash, and remove the supernatant (*see* **Note 16**).

3.3 Collagen Interactome Elution and Precipitation

To enhance the sensitivity of proteomic detection by minimizing the presence of any eluted IgG, we elute the proteins from beads using a nonreducing, denaturing buffer.

1. Elute pelleted beads using 50 μL of elution buffer by heating to 100 °C for 15 min (mix by shaking every 5 min during heating). Do not include a reducing agent during the elution, to minimize release of any antibody fragments via disulfide reduction (*see* **Note 17**).
2. Spin down at 2000 × *g* for 5 min, carefully collecting the supernatant and avoiding uptake of any beads.
3. Repeat **steps 1** and **2** above to elute a second time. Combine all supernatants.
4. Add 450 μL MeOH to microcentrifuge tubes containing 90% of the supernatant (*see* **Note 18**). Vortex vigorously for 30 s.
5. Add 150 μL $CHCl_3$. Vortex vigorously for 30 s.
6. Add 450 μL H_2O. Vortex vigorously 3 × 30 s. Spin down at 10,000 × *g* for 2 min, rotate the tube 180°, and spin down again at 10,000 × *g* for 2 min (*see* **Note 19**).
7. Discard all but ~100 μL of the upper layer of supernatant, being careful not to disturb the thin, white, protein-containing film at the interface between the H_2O/MeOH upper layer and the $CHCl_3$ lower layer.
8. Add 500 μL MeOH. Vortex vigorously for 30 s. White protein particles should be observable. Spin down at 16,300 × *g* for 2 min, followed by rotating the tube 180°, and spin down again at 16,300 × *g* for 2 min.
9. Repeat Subheading 3.3, **step 8**, 3× to remove all residual SDS, which would otherwise interfere with MS analysis.
10. Use a speed vacuum to dry the pellet. Samples can then be maintained at −20 °C until use.

3.4 Protein Digestion and Mass Spectrometry-Based Proteomic Studies

3.4.1 Trypsin Digestion of Protein Pellets and Preparation of Desalted Peptides for Mass Spectrometry Analysis

All procedures should be carried out at RT unless otherwise specified.

1. Add 22.5 μL of 8 M aqueous urea to the precipitated protein pellet from Subheading 3.3, **step 10**. Vortex vigorously 3 × 30 s. Centrifuge at 3000 × *g* for 1 min.
2. Add 2.5 μL of 100 mM DTT dissolved in NH_4HCO_3 buffer to yield a final concentration of 10 mM DTT.
3. Incubate at 56 °C for 1 h.
4. Cool samples to RT, and centrifuge at 3000 × *g* for 1 min to collect any H_2O condensed on the internal surface of the tube.
5. Add 2.75 μL of 550 mM iodoacetamide to yield a final concentration of 55 mM iodoacetamide. Wrap tubes in foil to protect from light, and mix end-over-end for 45 min (*see* **Note 20**).
6. Add 169.75 μL of NH_4HCO_3 buffer. Vortex briefly, and then add 2.5 μL of sequencing grade modified trypsin (0.4 μg/μL) to yield a final volume of 200 μL (*see* **Note 21**).
7. Mix end-over-end at RT for 12 h or for 3 h at 37 °C with agitation on a thermomixer with hot plate.
8. Acidify the sample by adding 11 μL of 98% formic acid to achieve a final concentration of 5% formic acid.
9. Remove white tip from the bottom of the peptide desalting spin column. Place column into a 2 mL microcentrifuge tube. Centrifuge at 3000 × *g* for 1 min and discard flow through.
10. Wash the column with 300 μL of TFA/MeCN buffer, centrifuge at 3000 × *g* for 1 min, and discard flow through (*see* **Note 22**). Repeat once.
11. Wash the column with 300 μL TFA buffer, centrifuge at 3000 × *g* for 1 min, and discard flow through. Repeat once.
12. Add sample to the column, centrifuge at 3000 × *g* for 3 min, and discard flow through. Repeat centrifugation if not all of the sample passed through the column (*see* **Note 23**).
13. Wash the sample on the column by adding 50 μL of formic acid buffer. Centrifuge at 500 × *g* for 3 min. Repeat twice.
14. Place column into a fresh microcentrifuge tube, and elute the peptides from the column by adding 50 μL of formic acid/MeCN buffer. Centrifuge at 3000 × *g* for 3 min. Repeat this elution step once.
15. Evaporate solvent in a vacuum centrifuge until near dryness. Store at −20 °C until mass spectrometry analysis.

3.4.2 Mass Spectrometry and Data Analysis

1. Solubilize digested peptide mixture into a working volume (we typically use 30 μL) of HPLC-grade 0.1% aqueous formic acid by vortexing 3× for 30 s each.
2. Inject samples (typically 1–5 μL volumes are reasonable) into a C_{18} reversed-phase resin (3 μM resin; 120 Å pore size) column (15 cm in length; 50 μM in diameter) on HPLC with autosampler connected to high-resolution, accurate mass/mass spectrometer. Elute peptides into the mass spectrometer for analysis over a 140-min gradient of formic acid buffer ranging to a 95:5 MeCN:H_2O in 0.1% formic acid solution (*see* **Notes 24** and **25**).
3. Operate the mass spectrometer in data-dependent mode with a full scan MS spectrum followed by MS/MS for the top ten precursor ions in each cycle. Depending on instrumentation, the number of precursor ions selected in each cycle may be increased.
4. Analyze raw data using Proteome Discoverer 2.2, performing a database search using Mascot for protein identification [21]. Depending on instrumentation and study objectives, search parameters and data analysis used may vary. For qualitative mapping of the collagen-I interactome in these example cellular systems, Mascot search parameters typically used were as follows: mass tolerance for precursor ions, 10 ppm; fragment ion mass tolerance, 15 mmu; missed cleavages of trypsin, 2; fixed modifications were carbamidomethylation of cysteine; and variable modifications were methionine oxidation and hydroxylation of proline, lysine, aspartate, and/or asparagine. Peptides with unambiguous peptide spectrum match, Mascot scores ≥25, and isolation inference ≤30 were considered identified, resulting in an average false discovery rate of 0.0077 (*see* **Notes 26** and **27**).

4 Notes

1. Sequencing of numerous collagen genes received from commercial sources and other investigators revealed a number of missense mutations as well as, in some cases, large or small deletions of gene segments. We strongly recommend full sequencing of any collagen vector obtained from any source and correction of defects using site-directed mutagenesis or other approaches. We also recommend complete sequencing of collagen genes after any manipulation, including even simple cut-and-paste reactions, not just PCR amplifications.
2. We incorporated an HA- or FLAG-epitope tag downstream of PPT but otherwise at the N-terminus of collagen strands to

enable straightforward, orthogonal immunoblotting and IPs of collagen-I polypeptides. Other antibody epitopes such as cMyc, 3 × FLAG, cleavable tags, etc. can also be used depending on the purpose of the study. The proteomic studies presented here use the HA epitope as an example. We note that, because collagen folding begins at the C-terminus, placement of these small tags at the N-terminus is unlikely to disrupt folding and assembly, which we confirmed for collagen-I via a variety of biochemical assays [15]. Note also that the N-propeptide and thus the epitope-tag will be cleaved extracellularly by N-propeptidases, depending on the cell system used.

3. Tet-inducible vectors were chosen to inducibly control the expression of collagen in engineered stable cell lines. Inducible expression minimizes potential negative selection pressure placed on cells forced to continuously express ectopic collagen that might render continuous propagation of stable cell lines challenging.
4. Each collagen-I gene is highly repetitive in the triple-helical domain and has about 65% GC-content overall, with local regions containing up to 85% GC content in a 50 base-pair span. These factors render PCR amplification of collagen genes problematic, resulting in low yields and many small PCR fragments, likely owing to incomplete gene synthesis. We found that the yield of full-length collagen-I genes was slightly boosted by increasing the recommended final extension time by about 1.25-fold.
5. Note that because each collagen-I gene is over 4000 base pairs in length, more than double the size of the pTRE-Tight expression vector, an inverted molar ratio is required when ligating the two linear pieces of DNA (with the insert more abundant than the vector). Even with inverted ratios, the most common ligation product observed was the pTRE-Tight vector ends being ligated together, despite the use of incompatible NotI and EcoRV restriction enzymes to digest the vector. Sequencing confirmed that, in a rare event, the sticky end of the NotI site was destroyed, leaving a blunt end of DNA that ligated to the EcoRV blunt end. This rare intramolecular ligation was more favorable and occurred more frequently than insertion of the collagen-I genes. To avoid this problem, dephosphorylation of the vector backbone with Antarctic phosphatase prior to ligating the two pieces of DNA proved useful in some cases for successful insertion of collagen genes. We ultimately succeeded in ligating pTRE-Tight and the collagen-I PCR amplicons, confirmed by sequencing the resulting clones with a primer that binds to the vector, providing evidence for the presence of both the 5′- and the 3′-ends of the collagen-I genes. However, sequencing of the full gene revealed that an

apparent recombination event had removed >1000 base pairs of the gene. Thereafter, we transformed collagen gene-containing vectors into recombination-deficient Sure2 *E. coli* cells. When grown at 30 °C, recombination is effectively shut down in these cells, allowing for the synthesis and propagation of intact collagen-I genes. We recommend the use of these recombination-deficient cells at 30 °C for work with collagen genes whenever possible.

6. Expression of the tetracycline transactivator allows doxycycline (dox)-inducible expression of the collagen-I genes of interest. We optimized HT-1080 culture conditions by varying the concentration of dox for 48 h and then split each concentration into two conditions: continued culture in the same concentration of dox or no dox in Tet-free FBS containing media. We found that continuous culture in 1 ng/mL dox, 1000-fold lower than the manufacturer's recommended concentration, efficiently suppresses both collagen-I genes. Removal of the dox-containing media and replacement with dox-free media induces both genes and the collagen proteins can be detected by immunoblotting in both cell lysates and media. Continuous culture in higher dox concentrations made it difficult to induce collagen-I expression via a media change, and so we recommend the use of 1 ng/mL dox during continuous culture.
7. Because we found the ligation of collagen genes into pENTR1A vectors to be extremely slow and inefficient, we used electroporation instead of heat shock to enhance transformation efficiency of the ligated vectors.
8. Expression of the tetracycline repressor in Saos-2-TREx cells allows doxycycline (dox)-inducible expression of the collagen-I gene under control of the tet operon (in contrast to dox-repressed expression in Tet-Off cells like the HT-1080s employed above). To create Saos-2TREx cells, Saos-2 cells were stably transduced with a lentivirus encoding a constitutively expressed tetracycline repressor protein and a blasticidin resistance cassette. Stable cells were selected using 2 μg/mL blasticidin, and single colonies were isolated and assayed for the colony most responsive to dox treatment (using Tet-responsive CFP to visualize inducible control of the tetracycline repressor protein).
9. The production of single colony cell lines from stably transduced Saos-2 cells is challenging. Heterogeneous cells must be plated at a very low density (~1:10,000) in 10 cm dishes for 2–3 weeks prior to picking and expanding colonies.
10. The dox concentration for collagen induction should be separately optimized for each cell system. Note that high concentrations (≥ 10 μg/mL) can be toxic.

11. Depending on the time course used for collagen induction, ascorbate should be refreshed every 24 h owing to its poor stability.
12. Transiently interacting chaperones, collagen-modifying enzymes, and related biogenesis factors are often not observable via traditional IP workflows. Indeed, we find that covalent cross-linking is essential to co-immunoprecipitate even most of the well-established collagen-I interactors, such as protein disulfide isomerase and HSP47. DSP has dual NHS esters (*see* DSP structure in Fig. 2b), thus targeting nearby primary amines from lysine residues in protein complexes and forming a conjugated network of closely interacting proteins [22, 23]. DSP also has a disulfide bond that can be reduced to release cross-linked proteins. Generally, the choice and length of chemical cross-linkers used will impact the quality and the relevance of data produced. The optimal choice of reactive functional groups and the length of cross-linkers vary based on the objectives of a given study [24, 25]. The optimal DSP concentration is cell line- and collagen expression-level dependent and therefore must be experimentally optimized to maximally immunoprecipitate genuine interactors while minimizing non-specific interactions. For HT-1080 cells, we used 150 μM DSP. For Saos-2 cells, we used 75 μM DSP. To optimize the cross-linker concentration for immunoprecipitations (Fig. 2c), we recommend using different concentrations ranging from 0 to 2 mM and then choosing the lowest DSP concentration that yields excellent signal for HA-collagen and also allows detection of known, well-established collagen-I proteostasis network components such as PDI and HSP47. The optimal concentration is typically also the lowest DSP concentration at which the cell pellet becomes slightly viscous in the Falcon tube, providing a rough visual parameter to assess cross-linking success. If co-immunoprecipitations without covalent cross-linking are performed, a different protocol from that described in this protocol is required, employing much milder, non-denaturing buffers and gentler treatments of cell lysates—both of which can lead to high background owing to non-specific protein binding.
13. Likely owing to a small amount of residual DSP activity even after Tris quenching, the cell pellet must be lysed immediately with RIPA buffer to avoid the formation of large cell aggregates. Another option to avoid formation of large cell aggregates is to wash the cells repeatedly with PBS post-cross-linking.
14. Because RIPA buffer contains SDS, which interferes with standard protein concentration assays, we typically do not measure the protein concentration and instead assume that the protein

concentration in the same volume of lysate from the same number of cells is the same.

15. Optional: Lysates can be precleared using 50 μL of packed sepharose or agarose beads for 1 h at 4 °C. The preclear step can help to minimize non-specific binding of proteins to beads.
16. If the immunoprecipitated samples will not be used immediately, we have found that dried beads can be stored at −20 °C for at least a few weeks without compromising sample integrity. However, we find that it is essential to first fully remove any residual RIPA buffer, which can be achieved using an additional wash step with a standard lysis buffer (e.g., 50 mM Tris, 1% Triton, 1 mM PMSF, and protease inhibitor mixture at pH 7.4).
17. Instead of SDS elution, which is our recommended approach, proteins can alternatively be directly digested on the beads after the immunoprecipitation to prepare for proteomic analysis. This approach is less time-consuming, and, in addition, because it skips elution and protein precipitation steps, the results can be somewhat less variable. However, a significant issue is that the HA antibody, which is chemically conjugated to the bead, will also be digested to some extent and the resulting abundant IgG tryptic peptides in the final peptide mixture will substantially reduce sensitivity of the MS-based proteomics. Therefore, we recommend the described SDS elution procedure.
18. To verify successful co-immunoprecipitation of collagen-I and known components of the collagen-I interactome, at this stage and prior to proceeding with any proteomic studies, we typically use 10% of the supernatant volume to run a 10% SDS-PAGE gel, followed by transfer to a nitrocellulose membrane and probing with anti-HA, anti-PDI, and anti-HSP47 (*see* Fig. 2c).
19. Small white droplet inclusions should form and be clearly observed by eye. After spinning and re-equilibration, two layers of solvent should be observed in the tube. Precipitated proteins will form a thin white layer on the surface between the two solvent layers. The thin white layer may stick to the wall of the tube, in which case the spinning should be repeated.
20. Iodoacetamide is unstable and light-sensitive.
21. Sequencing grade modified trypsin has methylated lysine residues to minimize autoproteolysis during the digestion step.
22. We recommend switching to a fresh microcentrifuge tube after every wash.
23. Optional: Reload flow through onto the column, and centrifuge again to maximize the binding of peptides to the column.

24. Other instruments may be used depending on availability. Note that the solvent gradient and method setup were optimized for the instrument listed.
25. We have observed that in a typical experiment, the proportion of tryptic peptides derived from collagen is >50% of the total detected peptides. In some cases, to ensure deeper coverage of the interactome, we remove high levels of collagen-I proteins after elution from the beads via the following protocol: Treat eluted samples with 100 μM DTT to reduce the DSP cross-linker, and release the interactome from the collagen-I bait protein. Pass each sample over a 100 kDa molecular weight cutoff filter (Millipore) to remove collagen-I (and other large proteins). Precipitate the filtrates as in Subheading 3.3, **steps 4–9**, and proceed. Another approach to ensure deeper coverage of the interactome is to (1) run the protein mixture that was eluted from bead on an SDS-PAGE gel, (2) silver stain the gel, (3) cut out the collagen band in the gel, and (4) digest the other bands using trypsin. A disadvantage of both these approaches is that some high molecular weight protein interactors will also be eliminated.
26. To exclude false positives and non-specific proteins binding to antibody-conjugated beads, cells expressing HA-tagged CFP in the cytoplasm (or other appropriate control cells) should be used as a control. Proteins identified with high abundance in the control sample should be excluded from the list of collagen interactors. Proteins with only one unique peptide identified should also be excluded.
27. Tryptic peptides can be labelled with iTRAQ or TMT tags [26, 27] before mixing together and injecting into the mass spectrometer if quantitative comparisons of collagen interactomes are desired (e.g., between wild-type and disease-causing collagen variants). SILAC proteomics [28] can alternatively be performed using cells incubated with media containing stable isotope labeling amino acids. See our recent paper for details on using the quantitative SILAC technique in our collagen system [15].

Acknowledgments

We thank Prof. Joseph Genereux (University of California—Riverside) for technical advice. This work was supported by NIH/-NIAMS Grants R03AR067503 and R01AR071443 (to M.D.S.). N.-D.D. was supported by Fonds de Recherche du Québec – Santé (FRQS) and Canadian Institutes of Health Research postdoctoral fellowships. A.S.D. was supported by a NIH Ruth L. Kirschstein predoctoral fellowship (F31AR067615). This work was also

supported in part by the NIH/NIEHS under award P30-ES002109 and by a Cancer Center Support (core) Grant P30-CA14051 from the NIH/NCI.

References

1. Eyre DR (1980) Collagen: molecular diversity in the body's protein scaffold. Science 207:1315–1322. https://doi.org/10.1126/science.7355290
2. Brinckmann J (2005) Collagens at a glance. Top Curr Chem 247:1–6. https://doi.org/10.1007/b103817
3. Ricard-Blum S (2011) The collagen family. CSHL Perspect Biol 3:a004978. https://doi.org/10.1101/cshperspect.a004978
4. Shoulders MD, Raines RT (2009) Collagen structure and stability. Annu Rev Biochem 78:929–958. https://doi.org/10.1146/annurev.biochem.77.032207.120833
5. Ishikawa Y, Bachinger HP (2013) A molecular ensemble in the rER for procollagen maturation. Biochim Biophys Acta 1833:2479–2491. https://doi.org/10.1016/j.bbamcr.2013.04.008
6. Morello R, Bertin TK, Chen YQ, Hicks J, Tonachini L, Monticone M, Castagnola P, Rauch F, Glorieux FH, Vranka J, Bachinger HP, Pace JM, Schwarze U, Byers PH, Weis M, Fernandes RJ, Eyre DR, Yao ZQ, Boyce BF, Lee B (2006) CRTAP is required for prolyl 3-hydroxylation and mutations cause recessive osteogenesis imperfecta. Cell 127:291–304. https://doi.org/10.1016/j.cell.2006.08.039
7. Myllyharju J, Kivirikko KI (2001) Collagens and collagen-related diseases. Ann Med 33:7–21. https://doi.org/10.3109/07853890109002055
8. Barnes AM, Cabral WA, Weis M, Makareeva E, Mertz EL, Leikin S, Eyre D, Trujillo C, Marini JC (2012) Absence of FKBP10 in recessive type XI osteogenesis imperfecta leads to diminished collagen cross-linking and reduced collagen deposition in extracellular matrix. Hum Mutat 33:1589–1598. https://doi.org/10.1002/Humu.22139
9. Marini JC, Reich A, Smith SM (2014) Osteogenesis imperfecta due to mutations in non-collagenous genes: lessons in the biology of bone formation. Curr Opin Pediatr 26:500–507. https://doi.org/10.1097/Mop.0000000000000117
10. Labbadia J, Morimoto RI (2015) The biology of proteostasis in aging and disease. Annu Rev Biochem 84:435–464. https://doi.org/10.1146/annurev-biochem-060614-033955
11. Hartl FU, Bracher A, Hayer-Hartl M (2011) Molecular chaperones in protein folding and proteostasis. Nature 475:324–332. https://doi.org/10.1038/nature10317
12. Ottani V, Martini D, Franchi M, Ruggeri A, Raspanti M (2002) Hierarchical structures in fibrillar collagens. Micron 33:587–596. https://doi.org/10.1016/S0968-4328(02)00033-1
13. Han L, Grodzinsky AJ, Ortiz C (2011) Nanomechanics of the cartilage extracellular matrix. Annu Rev Mater Res 41:133–168. https://doi.org/10.1146/annurev-matsci-062910-100431
14. Jobling R, D'Souza R, Baker N, Lara-Corrales-I, Mendoza-Londono R, Dupuis L, Savarirayan R, Ala-Kokko L, Kannu P (2014) The collagenopathies: review of clinical phenotypes and molecular correlations. Curr Rheumatol Rep 16:394. https://doi.org/10.1007/S11926-013-0394-3
15. DiChiara AS, Taylor RJ, Wong MY, Doan N-D, Del Rosario AM, Shoulders MD (2016) Mapping and exploring the collagen-I proteostasis network. ACS Chem Biol 11:1408–1421. https://doi.org/10.1021/acschembio.5b01083
16. Kuttner V, Mack C, Gretzmeier C, Bruckner-Tuderman L, Dengjel J (2014) Loss of collagen VII is associated with reduced transglutaminase 2 abundance and activity. J Invest Dermatol 134:2381–2389. https://doi.org/10.1038/jid.2014.185
17. Campeau E, Ruhl VE, Rodier F, Smith CL, Rahmberg BL, Fuss JO, Campisi J, Yaswen P, Cooper PK, Kaufmann PD (2009) A versatile viral system for expression and depletion of proteins in mammalian cells. PLoS One 4:e0006529. https://doi.org/10.1371/journal.pone.0006529
18. Bressan RB, Dewari PS, Kalantzaki M, Gangoso E, Matjusaitis M, Garcia-Diaz C, Blin C, Grant V, Bulstrode H, Gogolok S, Skarnes WC, Pollard SM (2017) Efficient CRISPR/Cas9-assisted gene targeting enables rapid and precise genetic manipulation of mammalian neural stem cells. Development

144:635–648. https://doi.org/10.1242/dev.140855

19. Savic D, Partridge EC, Newberry KM, Smith SB, Meadows SK, Roberts BS, Mackiewicz M, Mendenhall EM, Myers RM (2015) CETChseq: CRISPR epitope tagging ChIP-seq of DNA-binding proteins. Genome Res 25:1581–1589. https://doi.org/10.1101/gr.193540.115
20. Wong MY, Doan N-D, DiChiara AS, Papa LJ 3rd, Cheah JH, Soule CK, Watson N, Hulleman JD, Shoulders MD (2018) A high-throughput assay for collagen secretion suggests an unanticipated role for Hsp90 in collagen production. Biochemistry 57:2814–2827. https://doi.org/10.1021/acs.biochem.8b00378
21. Perkins DN, Pappin DJC, Creasy DM, Cottrell JS (1999) Probability-based protein identification by searching sequence databases using mass spectrometry data. Electrophoresis 20:3551–3567. https://doi.org/10.1002/(Sici)1522-2683(19991201)20:18<3551::Aid-Elps3551>3.0.Co;2-2
22. Kim KM, Yi EC, Kim Y (2012) Mapping protein receptor-ligand interactions via in vivo chemical crosslinking, affinity purification, and differential mass spectrometry. Methods 56:161–165. https://doi.org/10.1016/j.ymeth.2011.10.013
23. Corgiat BA, Nordman JC, Kabbani N (2014) Chemical crosslinkers enhance detection of receptor interactomes. Front Pharmacol 4:171. https://doi.org/10.3389/fphar.2013.00171
24. Leitner A (2016) Cross-linking and other structural proteomics techniques: how chemistry is enabling mass spectrometry applications in structural biology. Chem Sci 7:4792–4803. https://doi.org/10.1039/c5sc04196a
25. Holding AN (2015) XL-MS: protein cross-linking coupled with mass spectrometry. Methods 89:54–63. https://doi.org/10.1016/j.ymeth.2015.06.010
26. Thompson A, Schafer J, Kuhn K, Kienle S, Schwarz J, Schmidt G, Neumann T, Hamon C (2003) Tandem mass tags: a novel quantification strategy for comparative analysis of complex protein mixtures by MS/MS. Anal Chem 75:1895–1904. https://doi.org/10.1021/ac0262560
27. Unwin RD, Pierce A, Watson RB, Sternberg DW, Whetton AD (2005) Quantitative proteomic analysis using isobaric protein tags enables rapid comparison of changes in transcript and protein levels in transformed cells. Mol Cell Proteomics 4:924–935. https://doi.org/10.1074/mcp.M400193-MCP200
28. Ong SE, Blagoev B, Kratchmarova I, Kristensen DB, Steen H, Pandey A, Mann M (2002) Stable isotope labeling by amino acids in cell culture, SILAC, as a simple and accurate approach to expression proteomics. Mol Cell Proteomics 1:376–386. https://doi.org/10.1074/mcp.M200025-MCP200

Chapter 8

Exploring Extracellular Matrix Degradomes by TMT-TAILS N-Terminomics

Elizabeta Madzharova, Fabio Sabino, and Ulrich auf dem Keller

Abstract

Global characterization of protein N termini provides valuable information on proteome dynamics and diversity in health and disease. Driven by the progress in mass spectrometry-based proteomics, novel approaches for the dedicated investigation of protein N termini and protease substrates have been recently developed. Terminal amine isotopic labeling of substrates (TAILS) is a quantitative proteomics approach suitable for high-throughput and system-wide profiling of protein N termini in complex biological matrices. TAILS employs isotopic labeling of primary amines of intact proteins in combination with an amine-reactive high molecular weight polymer (HPG-ALD) for depletion of internal tryptic peptides and high enrichment of protein N termini by negative selection. Thereby, TAILS allows simultaneous identification of the natural N termini, protease-generated neo-N termini, and endogenously modified (e.g., acetylated) N termini. In this chapter, we provide a protocol for tandem mass tag (TMT)-TAILS analysis and further discuss specific considerations regarding N-terminome data interpretation using Proteome Discoverer™ software.

Key words N-terminome, Proteome Discoverer™, Proteolysis, TMT, TAILS

1 Introduction

The protein N terminus has a significant influence on a protein's biological functions [1]. Its sequence and posttranslational modifications (PTMs) often affect protein stability, regulate signal transduction, and determine the protein's final destiny, thereby affecting cellular localization and function and being crucial for regulation of cellular homeostasis [2–4]. Thus, comprehensive analysis of protein N termini can define critical functions of proteins, provide in-depth knowledge on their multifunctional roles in diverse biological processes, and thereby reveal valuable information on the highly dynamic nature of proteomes [1, 2]. Yet, common bottom-up mass spectrometry-based techniques often provide limited information about N termini, mostly due to the high abundance of internal tryptic peptides after trypsin digestion of complex protein

Irit Sagi and Nikolaos A. Afratis (eds.), *Collagen: Methods and Protocols*, Methods in Molecular Biology, vol. 1944, https://doi.org/10.1007/978-1-4939-9095-5_8, © Springer Science+Business Media, LLC, part of Springer Nature 2019

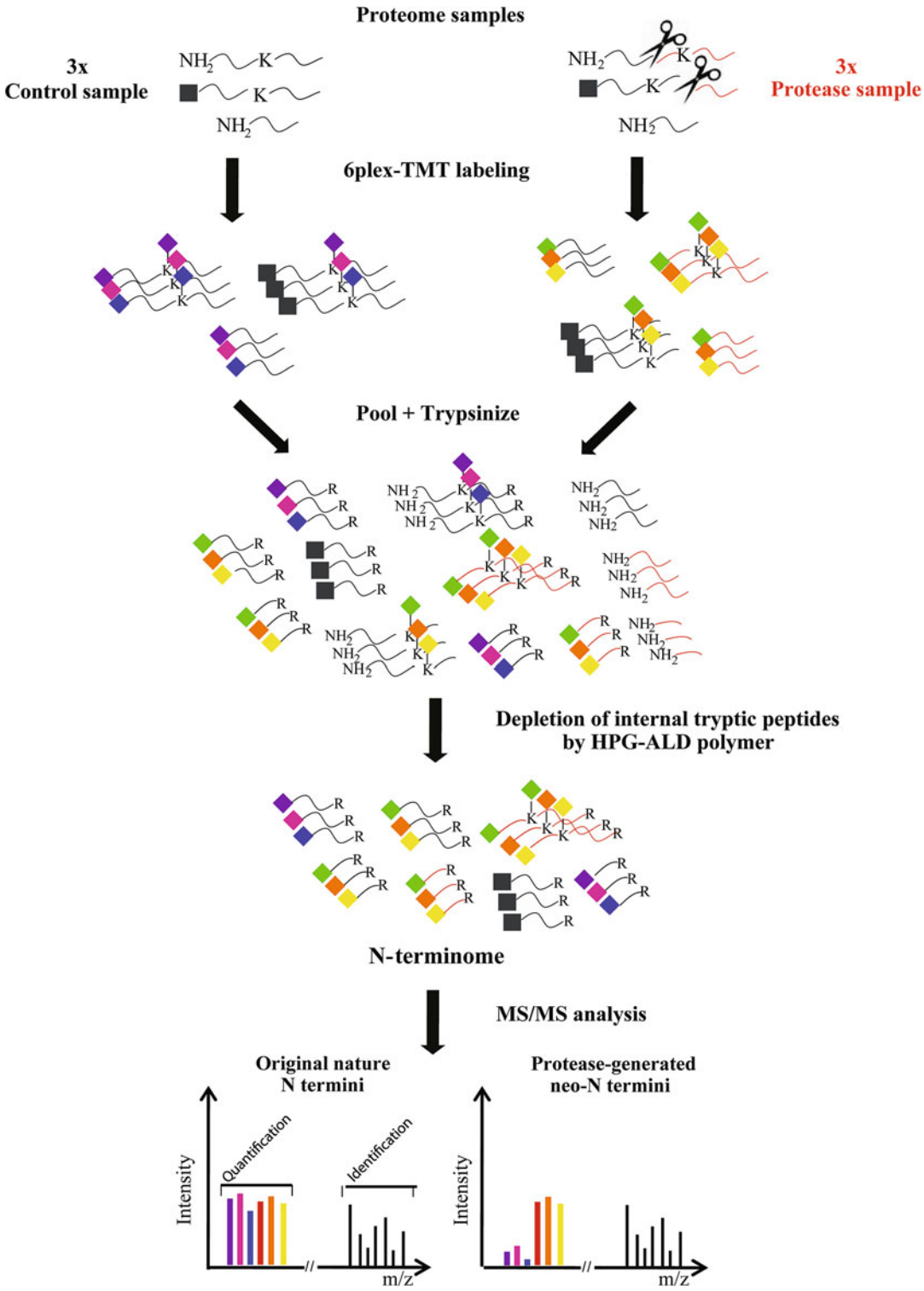

Fig. 1 Standard TAILS workflow. The TAILS experiment starts with the exposure of a complex proteome to a specific test protease. Next, all primary amines (α-amines on the N-terminal and ε-amines of lysine side chains) are labeled with isobaric tags (TMT or iTRAQ, indicated by multicolored diamonds), and samples are

samples. This hinders identification of the small fraction of N-terminal peptides present in the mixture and imposes the use of enrichment strategies [4, 5].

To specifically identify N termini, various approaches have been developed to isolate and characterize N-terminal peptides from highly complex peptide mixtures. These enrichment methods are divided into positive selection methods, enriching N-terminal peptides by affinity interaction, and negative selection methods, where the N-terminome is enriched by selectively removing internal peptides. Positive selection methods have the disadvantage of detecting only endogenously free N termini, since naturally blocked N-terminal peptides do not react with the affinity tags and therefore are excluded from the analysis. By contrast, the negative selection procedures gather information on both endogenously modified natural N termini and unmodified natural and neo-N termini, thereby offering a comprehensive analysis and annotation of the N-terminome [2, 3, 5–7].

Among the N-terminomics strategies, terminal amine isotopic labeling of substrates (TAILS) has gained its popularity due to the highly successful negative selection strategy applied to profile the N-terminome in complex proteome samples (Fig. 1) [8, 9]. To identify substrates of a protease of interest using TAILS, a native proteome is exposed to the protease to generate cleavage events potentially relevant in physiological contexts. Next, the primary amines present in the proteome (i.e., α-amines of protein N termini and ε-amines of lysine side chains) are labeled at the protein level using tags for isotopic labeling such as iTRAQ (isobaric tag for relative and absolute quantitation) or TMT (tandem mass tags). Thereby, the terminal information resulting from proteolytic processing by the protease of interest is unambiguously preserved, since the peptide fragments located downstream of the cleavage site are covalently labeled at the N terminus and can be posteriorly identified and assigned to a specific amino acid sequence of the substrate [1, 3]. The labeled proteomes are digested with trypsin, which generates internal tryptic and C-terminal peptides carrying a free amino group at their N terminus. These tryptic peptides are then depleted by covalently binding to an amine-reactive high

Fig. 1 (continued) pooled and trypsinized. The newly generated internal tryptic and C-terminal peptides are depleted using a high-molecular aldehyde-derivatized polymer (HPG-ALD) that binds to the newly generated free amino group at the N terminus. The labeled N termini and neo-N termini, as well as naturally blocked N termini (acetylation, cyclization, and methylation, indicated by black square), do not react with the polymer and are recovered by ultrafiltration. The enriched N-terminome is analyzed by tandem mass spectrometry, which discriminates between protease-generated neo–N termini and mature protein N termini with help of quantitative information from TMT/iTRAQ reporter ions

molecular weight, aldehyde-derivatized, polyglycerol polymer (HPG-ALD). Peptides naturally N-terminally blocked (e.g., by acetylation, cyclization, or methylation) and neo-N termini carrying an isobaric tag at the N terminus have unreactive N termini and thus remain unbound and can be recovered by ultrafiltration. The N-terminome is collected in the flow-through fraction and analyzed by LC-MS/MS.

By enriching the N-terminome by negative selection, TAILS provides both high coverage of N-terminal peptides present in the proteome and allows reliable isotopic quantification of multiple samples or conditions simultaneously in a single experiment. Hence, TAILS is ideally suited to profile protein N termini and their modifications on a proteome-wide scale [4, 10].

Here, we present a detailed TMT-TAILS workflow for analysis of protein N termini from up to six different conditions using isobaric 6plex-TMT tags. We provide a TMT-TAILS protocol for analyzing the substrate repertoire of glutamyl endoproteinase (GluC) as test protease with canonical specificity and secretomes from mouse fibroblasts as sample proteome. We also discuss specific considerations regarding the analysis of N-terminomics data using Proteome Discoverer™ software and offer a possibility to obtain our MS raw files and Proteome Discoverer™ workflow files to perform a test run before proceeding with the analysis of your samples.

2 Materials

2.1 Digestion with Test Protease (Optional)

1. Proteins or proteome of interest.
2. 1 M HEPES, pH 7.8.
3. 1 M sodium chloride.
4. GluC endoproteinase (test protease).
5. Digestion buffer: 50 mM HEPES, 100 mM NaCl, pH 7.8.

2.2 Identification of Protease Substrates by 6plex-TMT-TAILS

1. 8 M guanidine hydrochloride (GuHCl).
2. 1 M HEPES pH 7.8.
3. 350 mM Tris (2-carboxyethyl) phosphine hydrochloride (TCEP).
4. 250 mM chloroacetamide.
5. TMT 6plex™ reagents.
6. Dimethyl sulfoxide (DMSO).
7. 1 M ammonium bicarbonate (NH_4HCO_3).
8. Acetone (−20 °C).
9. Methanol (MeOH; −20 °C).

10. 100 mM sodium hydroxide (NaOH).
11. 1 M hydrochloric acid (HCl).
12. Hyperbranched polyglycerol-aldehydes (HPG-ALD) polymer (available without commercial or company restriction from Flintbox innovation network, the global intellectual exchange and innovation network (http://www.flintbox.com/public/project/1948)).
13. 5 M sodium cyanoborohydride ($NaBH_3CN$).
14. Trypsin.
15. Amicon® Ultra-0.5 Centrifugal Filter Units (30 kDa cutoff).

2.3 Sample Desalting (StageTip)

1. C18 reverse-phase extraction disk.
2. A blunt-ended syringe needle.
3. 200 μL pipette tips.
4. A 20 mL disposable syringe.
5. Activation buffer: MeOH, 80% ACN, 0.1% acetic acid.
6. Elution buffer: 80% ACN, 0.1% acetic acid.
7. Equilibrium buffer: 3% ACN, 1% trifluoroacetic acid (TFA).
8. Washing buffer: 0.1% formic acid (FA).
9. Resuspension buffer: 3% ACN, 0.1% formic acid.
10. Speed vacuum.

2.4 LC-MS/MS Analysis

1. Thermo Scientific Q Exactive Mass Spectrometer.
2. Thermo Scientific™ EASY-nLC™ 1000 Liquid Chromatography system.
3. Thermo Scientific PepMap™ RSLC C18 column (2 μm, 100 Å, 75 μm × 50 cm).
4. Buffer A: 0.1% formic acid, 99.9% water.
5. Buffer B: 80% ACN, 0.1% formic acid, 19.9% water.
6. Xcalibur software v2.0.

2.5 Data Analysis

1. Thermo Scientific™ Proteome Discoverer software v2.2 available at https://www.thermofisher.com/order/catalog/product/OPTON-30795.
2. SEQUEST database search engine.

3 Methods

3.1 Proteolysis by Test Protease (Optional)

The following steps are only required if the proteome is to be exposed to a protease of interest in vitro. For other studies, which focus only on the nature of the N-terminome or using samples that

have already undergone proteolysis in cell culture or in vivo samples, proceed directly with the 6plex-TMT-TAILS protocol.

1. Start with two samples of 160 μg total protein (concentration ≥ 1 μg/μL) under native conditions in digestion buffer (*see* **Note 1**).
2. Add GluC endoproteinase (or the test protease of interest) at 1:100 (enzyme/proteome) ratio to the test sample and an equivalent volume of digestion buffer to the control sample. **Important**: Different proteases have different buffer requirements; hence adjust buffer composition accordingly.
3. Incubate for 16 h at 37 °C (*see* **Note 2**).
4. Stop reaction by adjusting with 8 M GuHCl and 1 M HEPES, pH 7.8 to a final concentration of 2.5 M GuHCl, 200 mM HEPES, pH 7.8 to denature GluC. **Important**: The protein concentration should not be lower than ~0.4–0.5 μg/μL.
5. Store the sample at −20 °C until further processing.

3.2 6plex-TMT-TAILS

1. To assure total protein denaturation, incubate samples at 65 °C for 15 min.
2. Reduce cysteine residues by adding 1 mM TCEP.
3. Incubate samples at 65 °C for 45 min.
4. Alkylate cysteine residues by adding 5 mM chloroacetamide and mix thoroughly.
5. Incubate samples at 65 °C for 30 min.
6. Divide samples (control and protease-treated) into three aliquots (technical replicates) containing 50 μg total protein each.
7. Resuspend each aliquot containing 200 μg of TMT reagent in DMSO with a volume equivalent to the total volume of sample from **step 6**. **Important:** *see* **Note 3** for preparation of aliquots of TMT reagent.
8. Add TMT reagents to control and protease-treated samples to achieve 1:4 protein/TMT (w/w) ratio and 50% final DMSO concentration.
9. Mix gently and incubate for 1 h at room temperature. **Important:** The incubation time for each channel should be measured as precisely as possible to reduce quantification errors derived from differing labeling times.
10. To quench the labeling reaction, add 100 mM NH_4HCO_4 and incubate for 30 min at room temperature.
11. Combine TMT-labeled samples in a 15 mL tube.
12. Add seven sample volumes of ice-cold acetone and one sample volume of ice-cold MeOH to the labeled proteins.
13. Incubate samples at −80 °C for at least 2 h.

14. Centrifuge samples at 4500 × *g* at 4 °C for 20 min.
15. Carefully discard the supernatant and wash with 5 mL of ice-cold MeOH.
16. Centrifuge at 4500 × *g* at 4 °C for 10 min, and discard the supernatant.
17. Air-dry the pellet. **Important**: Overdrying the sample may impede protein solubilization.
18. Resuspend sample in 30 μL of 100 mM NaOH.
19. Add 100 mM HEPES, pH 7.8 and adjust the volume to a final protein concentration of 1 μg/μL.
20. Take an aliquot of 5 μg of protein as quality control of trypsin digestion.
21. Add trypsin at a ratio of 1:100 trypsin/protein ratio (w/w).
22. Incubate overnight at 37 °C.
23. Remove 5 μg of the digested proteome. Separate digested and non-digested samples by SDS-PAGE and stain with Coomassie Blue or silver to assess digestion efficiency.
24. Remove ~10% of the digested proteome (**preTAILS sample**), and store it at −20 °C.
25. Adjust the pH of the remaining solution to pH 6–7 with 1 M HCl.
26. Add a threefold excess (w/w) of HPG-ALD polymer and 50 mM $NaBH_3CN$ reagent to deplete peptides with free N-terminal amines (fully tryptic peptides) (*see* **Note 4**).
27. Incubate overnight at 37 °C.
28. Pre-wash a 30 kDa Amicon Ultra-0.5 mL centrifugal filter unit with water according to the manufacturer's instructions. Remove the water from the clean Amicon.
29. Transfer the sample to the Amicon previously washed and filter by centrifugation at 10,000 × *g* for 10 min at room temperature. The high molecular weight HPG-ALD polymer bound to the fully tryptic peptides will remain in the filter. Recover unbound peptides in the flow-through.
30. Repeat **step 29** until the entire sample volume is filtered.
31. Wash the polymer with 30 μL of 100 mM NH_4HCO_3 and centrifuge again.
32. Collect the flow-through and combine with the flow-through from **step 29** (**TAILS sample**).

3.3 StageTip Desalting

1. Stamp out two pieces of a C18 Empore disk using a blunt-ended syringe needle, and press the cored pieces close to the end of a P200 pipette tip.

2. Activate the disks by subsequently washing with 40 μL MeOH and 40 μL of 80% ACN and 0.1% acetic acid solution through the StageTip using a 20 mL syringe.
3. Equilibrate the disks by passing through 2× 60 μL of equilibrium buffer. Avoid the tip drying completely.
4. Discard the flow-through.
5. Load 15 μL preTAILS and 150 μL TAILS samples, separately.
6. Wash by adding 2 × 40 μL of washing buffer, and discard the flow-through.
7. Elute samples with 2 × 40 μL of elution buffer.
8. Speed vacuum desalted peptide mixture to dryness.
9. Resuspend samples in resuspension buffer.
10. Determine protein concentration using a NanoDrop spectrophotometer.

3.4 LC-MS/MS Analysis

Analyze preTAILS and TAILS samples with a tandem mass spectrometer coupled to a C18 chromatography system. Due to the large variation of instrumental setups, details of the mass spectrometry analysis are specific to the instrument used. As an example, peptides from our dataset were analyzed on a Thermo Scientific Q Exactive Mass Spectrometer coupled to a Thermo Scientific EASY-nLC™ 1000 Liquid Chromatography system and a Thermo Scientific PepMap™ RSLC C18 column (2 μm, 100 Å, 75 μm × 50 cm). For each analysis, 2 μg of peptide mixture was loaded at a constant flow rate of 250 nL/min in Buffer A and eluted using a 2-h gradient from 6% to 95% Buffer B. A data-dependent acquisition (DDA) mode was applied to record the spectra with the following MS1 parameters, scan range 300–1750 m/z, resolution of 70,000, AGC target 3e6; MS2 parameters, resolution of 17,500, AGC target 1e6; and higher energy collision dissociation (HCD), normalized collision energy of 32%.

3.5 N-Terminome Data Analysis

A variety of tools are available for proteomic assessment of TAILS N-terminomics data with specific search settings, which vary depending on the algorithm and the instrument used for data acquisition [11–15]. Here we describe in detail a workflow for the analysis of a TMT-TAILS dataset collected after treatment of secretomes from murine embryonic fibroblasts with GluC endopeptidase (test protease) using Proteome Discoverer™ 2.2 software.

1. Open Proteome Discoverer™ 2.2 application and select **New Study/Analysis** on the start page.
2. Choose a name for the study and a root directory. Click **OK**.
3. Select the TMTe 6plex as a quantification method to be used in the study.

4. Click **Add Files** and select the mass spectrometry raw file. **Important**: Proteome Discoverer accepts .raw, .mgf, .mzData, .mzXML, and .mzML file formats as an input. **Optional**: As a test run, use our MS raw file (available upon request from the corresponding author).
5. Specify the quantification method used in the input file on the **Input Files** page.
6. On the **Samples** tab, specify samples as "control" and/or "sample" type.
7. Open **New Analysis**, select and drag the input file from the input file page to the Analysis window.
8. Select **Workflows** tab to create workflows to use for the processing and consensus step. **Optional**: Use our processing and consensus workflow files (available upon request from the corresponding author).
9. **Create Processing Step Workflow** by dragging and connecting the following nodes into the Workflow tree window (Fig. 2a):
   - Spectrum File.
   - Spectrum Selector.
   - Sequest HT.
   - Percolator.
   - Reporter Ions Quantifier.
10. For N termini profiling, set the parameters for Sequest HT node (*see* **Note 5**) (Fig. 2b):
    - Upload an appropriate database.
    - Choose enzyme semi-specific ArgC with one missed cleavage (*see* **Note 6**).
    - Set minimum peptide length of 6 amino acids and maximum peptide length of 30 amino acids.
    - Set precursor mass tolerance at 10 ppm and fragment mass tolerance at 0.02 Da.
    - Set TMT6plex lysine (+229.163 Da) and carboxymethyl of cysteine (+58.005 Da) as static modifications.
    - Set TMT-labeled N-termini (+229.163 Da), oxidation of methionine (+15.995 Da), N-terminal acetylation (+42.010565 Da), N-terminal pyro-Glu (−17.026549 Da), or asparagine deamidation (+ 0.984 Da) as dynamic modifications.
11. Create **Consensus Step Workflow** by dragging and connecting the following nodes into the Workflow tree window (Fig. 2c):

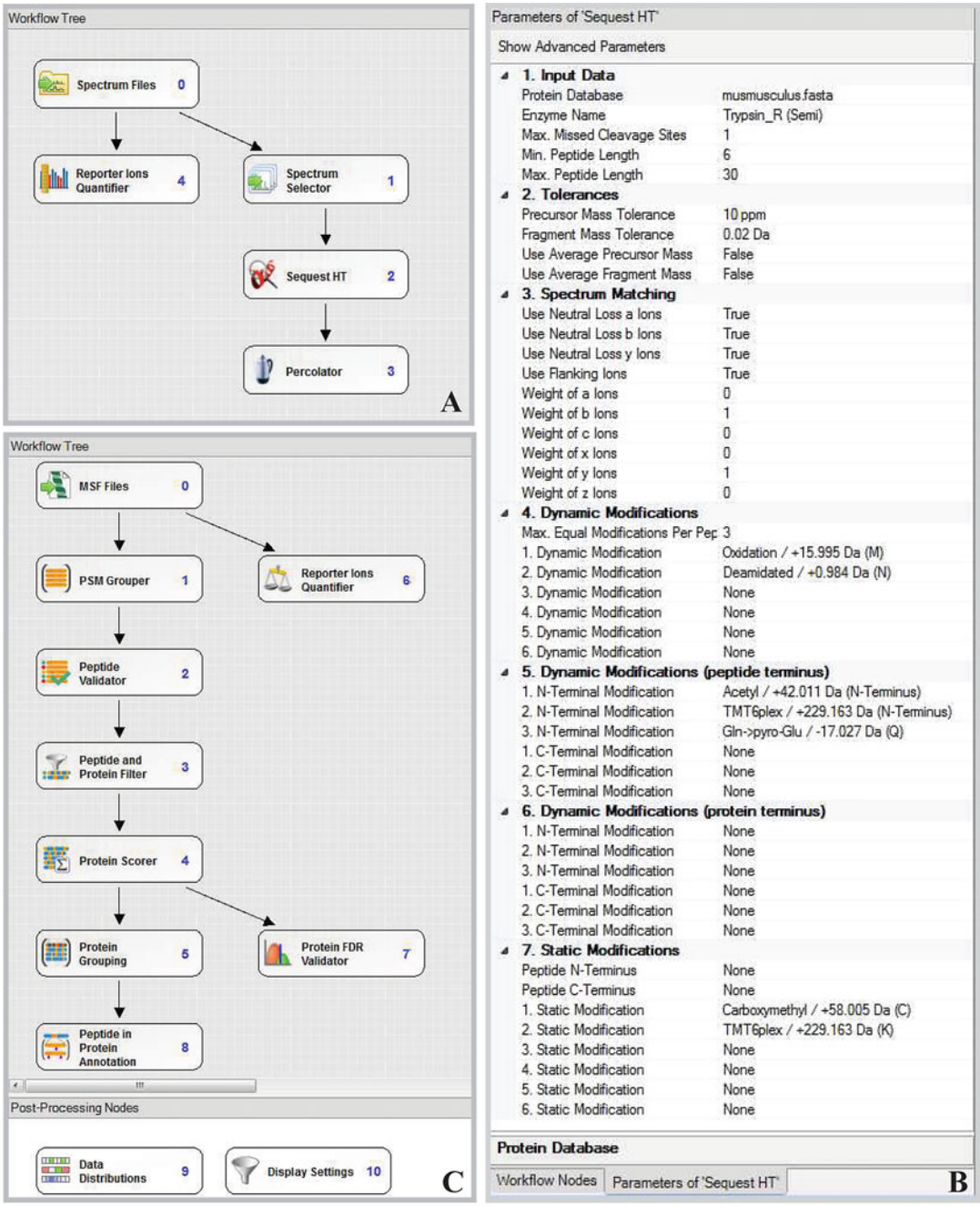

Fig. 2 Proteome Discoverer settings. (**A**) Processing Step Workflow nodes. (**B**) Sequest HT parameters for TAILS analysis of mouse secretome. (**C**) Consensus Step Workflow nodes

- MSF Files.
- PSM Grouper.
- Peptide Validator.
- Peptide and Protein Filter.
- Protein Scorer.
- Protein Grouping.
- Peptide in Protein Annotation.
- Reporter Ions Quantifier.
- Protein FDR Validator.
- As for post-processing nodes, Data Distributions, and Display Settings.

12. In **Grouping and Quantification** tab, specify the ratios to report for quantification and how to group the samples with respect to the specified factor values.
13. Select Sample type as study variable.
14. Choose Sample type: Control denominators to be used for bulk ratio generator and press **Add Ratio**.
15. Press **Run** in the Analysis window to start the search.

Output of analysis results should be inspected on the "Peptide Group" level for interpretation of N-terminal peptides and can be exported to appropriate formats for further analysis, e.g., using spreadsheet applications. To annotate protein N termini for their position in the mature protein, several tools are available including ImproViser [16] and TAILS-ANNOTATOR [4].

4 Notes

1. Avoid using buffers containing primary amines (e.g., Tris, ammonium bicarbonate) since they could interfere with the labeling and enrichment step.
2. The incubation times and enzyme/proteome ratio are based on previously established data for the specific test protease. If not available, monitor digestion of proteins at increasing time points by SDS-PAGE to determine the optimal conditions.
3. The TMT reagent tubes as supplied by the manufacturer contain 0.8 mg total reagent. Resuspend the content of each tube in 400 μL ACN, divide into four tubes containing 100 μL each, and dry using a SpeedVac instrument, thereby obtaining 200 μg TMT reagent per vial. These vials should be stored at −20 °C. Since TMT reagents rapidly hydrolyze in aqueous solutions, they should be resuspended in 100% DMSO immediately before use. Each aliquot containing 200 μg of TMT is sufficient for labeling 50 μg of protein.

4. The actual amount of the HPG-ALD used in the experiment depends on concentration and binding capacity specified by the manufacturer.
5. Parameters for all other nodes work well with default settings but might be adjusted to fine-tune analysis according to the Proteome Discoverer™ 2.2 manual.
6. Lysine labeling by isobaric tags precludes trypsin cleavage; therefore trypsin adopts ArgC specificity. By setting the digestion enzyme as trypsin and by setting lysine labeling as variable modification (variable TMT6plex lysine (+229.163 Da), it is possible to evaluate the efficiency of labeling with TMT.

References

1. Hartmann EM, Armengaud J (2014) N-terminomics and proteogenomics, getting off to a good start. Proteomics 14:2637–2646
2. Lai ZW, Petrera A, Schilling O (2015) Protein amino-terminal modifications and proteomic approaches for N-terminal profiling. Curr Opin Chem Biol 24:71–79
3. Yeom J, Ju S, Choi Y, Paek E, Lee C (2017) Comprehensive analysis of human protein N-termini enables assessment of various protein forms. Sci Rep 7:6599
4. Kleifeld O, Doucet A, Prudova A, auf dem Keller U, Gioia M, Kizhakkedathu JN, Overall CM (2011) Identifying and quantifying proteolytic events and the natural N terminome by terminal amine isotopic labeling of substrates. Nat Protoc 6:1578–1611
5. Marino G, Eckhard U, Overall CM (2015) Protein termini and their modifications revealed by positional proteomics. ACS Chem Biol 10:1754–1764
6. van den Berg BHJ, Tholey A (2012) Mass spectrometry-based proteomics strategies for protease cleavage site identification. Proteomics 12:516–529
7. Rogers LD, Overall CM (2013) Proteolytic post-translational modification of proteins: proteomic tools and methodology. Mol Cell Proteomics 12:3532–3542
8. Schlage P, Egli FE, Nanni P, Wang LW, Kizhakkedathu JN, Apte SS, auf dem Keller U (2014) Time-resolved analysis of the matrix metalloproteinase 10 substrate degradome. Mol Cell Proteomics 13:580–593
9. Prudova A, auf dem Keller U, Butler GS, Overall CM (2010) Multiplex N-terminome analysis of MMP-2 and MMP-9 substrate degradomes by iTRAQ-TAILS quantitative proteomics. Mol Cell Proteomics 9:894–911
10. Kleifeld O, Doucet A, auf dem Keller U, Prudova A, Schilling O, Kainthan RK et al (2010) Isotopic labeling of terminal amines in complex samples identifies protein N-termini and protease cleavage products. Nat Biotechnol 28:281–288
11. Cox J, Mann M (2008) MaxQuant enables high peptide identification rates, individualized p.p.b.-range mass accuracies and proteome-wide protein quantification. Nat Biotechnol 26:1367–1372
12. Deutsch EW, Mendoza L, Shteynberg D, Farrah T, Lam H, Tasman N et al (2010) A guided tour of the trans-proteomic pipeline. Proteomics 10:1150–1159
13. Craig R, Beavis RC (2004) TANDEM: matching proteins with tandem mass spectra. Bioinformatics 20:1466–1467
14. auf dem Keller U, Prudova A, Gioia M, Butler GS, Overall CM (2010) A statistics-based platform for quantitative N-terminome analysis and identification of protease cleavage products. Mol Cell Proteomics 9:912–927
15. auf dem Keller U, Overall CM (2012) CLIPPER: an add-on to the trans-proteomic pipeline for the automated analysis of TAILS N-terminomics data. Biol Chem 393:1477–1483
16. Videm P, Gunasekaran D, Schröder B, Mayer B, Biniossek ML, Schilling O (2014) Automated peptide mapping and protein-topographical annotation of proteomics data. BMC Bioinformatics 15:207

Part III

Imaging Approaches for Collagen

Chapter 9

Sample Preparation of Extracellular Matrix of Murine Colons for Scanning Electron Microscopy

Elee Shimshoni and Irit Sagi

Abstract

Scanning electron microscopy is a useful tool for high-resolution morphological characterization of the extracellular matrix. In certain tissues and surfaces, imaging of the extracellular matrix requires cell removal before sample preparation. In this protocol, we will describe a method for preparing extracellular matrices derived from murine colon for imaging under a scanning electron microscope.

Key words Tissue, Colon, Scanning electron microscope, Extracellular matrix, Decellularization

1 Introduction

Scanning electron microscopy (SEM) is a tool commonly used for obtaining nanometer spatial resolution images of the topography of a wide range of biological specimens, including microorganisms, cells, and tissues. It is a useful tool for studying how morphology and topography of a tissue changes due to disease. Samples imaged under SEM are subjected to high vacuum conditions and must be fixed, completely dry, conductive, and electrically grounded [1, 2]. The structure and organization of collagen and the other extracellular matrix (ECM) proteins in a tissue can be visualized at high resolution using SEM [3, 4]. In certain tissue surfaces, such as the gut mucosa, imaging the ECM is difficult since it is not visible beyond the cells and therefore would require further slicing of the sample. For this reason, in order to image the colonic ECM using SEM, we need to first remove the cells from the tissue via decellularization. Figure 1 demonstrates how the colon tissue looks with and without decellularization. There are various decellularization methods [5], and we chose the method described herein, which includes freeze-thaw cycles followed by ammonium hydroxide treatment, to be the best for structure preservation. In this protocol, we will describe a method for preparing extracellular matrices

Irit Sagi and Nikolaos A. Afratis (eds.), *Collagen: Methods and Protocols*, Methods in Molecular Biology, vol. 1944, https://doi.org/10.1007/978-1-4939-9095-5_9, © Springer Science+Business Media, LLC, part of Springer Nature 2019

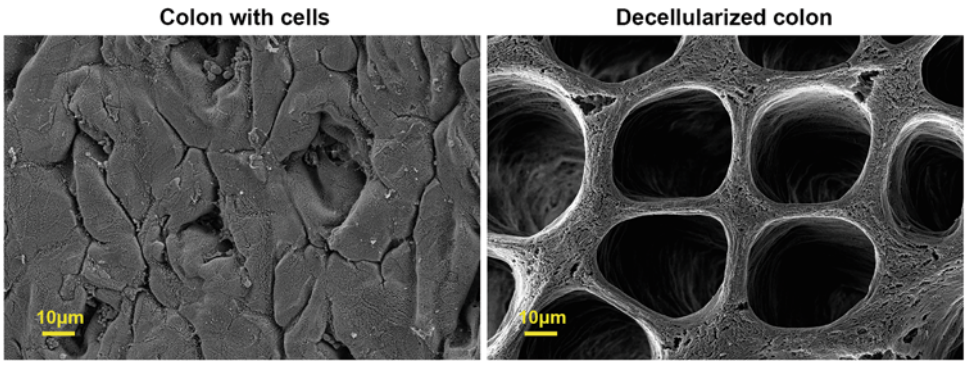

Fig. 1 Scanning electron micrographs of a murine colon with or without cells colon samples were either prepared as described in this protocol (image on the right), or were immediately fixed after harvest and stained with an additional dye that binds to cell membranes (OsO_4). Both images were taken in a 2500× magnification. Images demonstrate the mucosal surface with and without cells, displaying the colonic crypts. As evident by the images, the extracellular matrix scaffold underlying the gut epithelium that can be observed in the decellularized sample is covered by cells in the sample presented on the left

derived from murine colon for imaging of the under SEM using the following processes – decellularization, fixation, staining, dehydration, and mounting.

2 Materials

Use double-distilled water for all solutions.

2.1 Decellularization

1. Tools: scalpel and forceps.
2. Phosphate buffered saline (PBS).
3. Double-distilled water (ddH_2O).
4. 25 mM ammonium hydroxide (NH_4OH) in water. Store in 4 °C.

2.2 Fixation and Staining

1. Fixation solution: 4% paraformaldehyde and 2% glutaraldehyde in water. Make fresh or store in −20 °C until use.
2. ddH_2O.
3. Staining solution: 4% sodium silicotungstate (SST).
4. Dehydration solutions: increasing concentrations of EtOH in water: 30%, 50%, 70%, 96%, and 100% EtOH.

2.3 Sample Mounting

1. Aluminum mounts.
2. Carbon stickers and tape.
3. Tools: high-precision tweezers, scissors, and curved forceps.

3 Methods

3.1 Decellularization

1. Cut 5–10 mm pieces (in length) of fresh or snap-frozen colon.
2. Wash samples twice with PBS, clearing out any residual feces.
3. Wash samples twice with ddH_2O.
4. Place samples in an Eppendorf tube with ddH_2O.
5. Freeze samples on dry ice (*see* **Note 1**) in ddH_2O.
6. Thaw at room temperature and replace ddH_2O.
7. Repeat **steps 4** and **5** five more times (six times in total).
8. Immerse samples in the ammonium hydroxide solution for 20 min in a rotator.
9. Wash six times in ddH_2O (*see* **Note 2**).

3.2 Fixation Staining and Dehydration

1. Immerse in fixation solution and incubate overnight at 4 °C.
2. Wash twice in ddH_2O.
3. Replace water with SST staining solution and incubate for 30 min in motion (*see* **Note 3**).
4. Dehydrate samples by immersing them in increasing concentrations of EtOH (30%, 50%, and then 70%) and incubate twice in each solution for 5 min in motion.
5. Keep samples in 70% EtOH at 4 °C until the day of critical point drying (CPD).
6. Continue dehydration in 96% and 100% EtOH as described in **step 4**.
7. Subject samples to CPD using the appropriate device.

3.3 Sample Mounting

Figure 2 illustrates **steps 1–5**:

1. Take aluminum mounts (one for each sample) and stick a carbon sticker on each one.
2. Gently take each sample out of the CPD gasket using forceps and place on the sticker on the mount.
3. Cut the colon piece open so that the lumen faces up.
4. Gently press on the edges of the sample to allow them to stick to the sticker (*see* **Note 4**).
5. Carefully stick 2–3 small pieces of carbon tape on the edges, leaving as much visible sample surface as possible (*see* **Note 5**).
6. Coat samples with either gold/palladium alloy or another metal in a sputtering machine.
7. Always store samples in a desiccator to keep them dry.

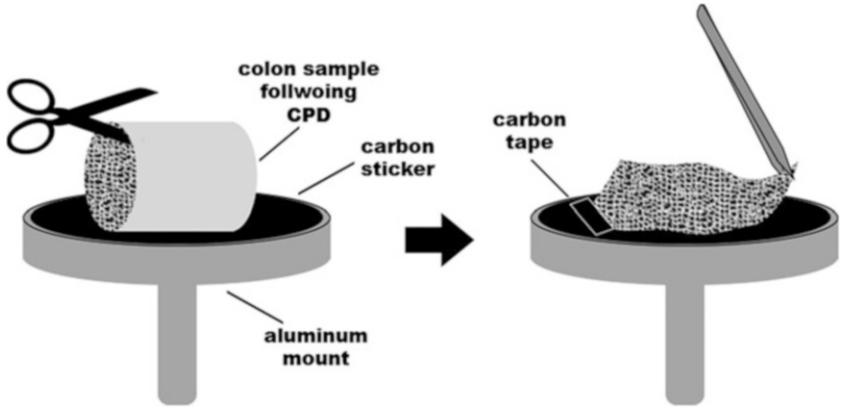

Fig. 2 Sample mounting after critical point drying Dehydrated colon samples should be mounted as illustrated. First the colon tube is placed gently on the carbon sticker stuck to the mount and allowed to adhere. Then the colon is cut open using scissors while trying not to touch the bottom of the sample to not create dents in the sample. Following, take forceps and gently pull the edges, and stick them to the sticker as well. Finally, stick small pieces of carbon tape on the edges of the sample to ground the charges that will be interacting with sample in the microscope

4 Notes

1. For Subheading 3.1, samples can be frozen in the freezer in −80 °C. This is useful for continuing the protocol on a different day, if desired. Dry ice is more rapid, of course. Avoid using liquid nitrogen so freezing occurs more gradually.
2. At the final washes of the decellularization process, make sure the water in the tube is clear, with no remaining debris or feces. Wash the inside of the colon if necessary using a 200 μl pipette.
3. **Steps 3** and **4** of Subheading 3.2 should be done on a shaker, if transferred to a 24-well plate or on a rotator if samples remain in Eppendorf tubes.
4. Make sure not to dent the sample too much during mounting, and leave as much exposed and untouched surface as possible.
5. It is important to secure the edges of the sample with the tape, both to prevent it from detaching and most importantly to improve the conductivity of the sample, so the edge on each side must have a piece of carbon tape on it.

References

1. Hayat MA (2000) Principles and techniques of electron microscopy: biological applications. Cambridge University Press, Cambridge, UK
2. Fischer ER, Hansen BT, Nair V et al (2012) Scanning electron microscopy. In: Current protocols in microbiology p. Unit 2B.2. John Wiley & Sons, Hoboken, NJ
3. Brown BN, Barnes CA, Kasick RT et al (2010) Surface characterization of extracellular matrix scaffolds. Biomaterials 31:428–437

4. Lin CP, Douglas WH, Erlandsen SL (1993) Scanning electron microscopy of type I collagen at the dentin-enamel junction of human teeth. J Histochem Cytochem 41:381–388

5. Lu H, Hoshiba T, Kawazoe N et al (2012) Comparison of decellularization techniques for preparation of extracellular matrix scaffolds derived from three-dimensional cell culture. J Biomed Mater Res A 100:2507–2516

Chapter 10

In Situ Detection of Degraded and Denatured Collagen via Triple Helical Hybridization: New Tool in Histopathology

Yang Li and S. Michael Yu

Abstract

Degraded and denatured collagens are useful markers for physiological events (e.g., bone formation and aging) and pathologic conditions (e.g., cancer, arthritis, and fibrosis). Here we describe histological staining of such collagens using fluorescent collagen hybridizing peptide that can specifically bind to collagen strands by folding into triple helix. The method can report the amount of denatured collagen and/or collagen remodeling activity in tissues via localized fluorescence intensity and can be used in conjunction with conventional staining agents. The collagen hybridizing peptide probes can be used across species and collagen types, providing a versatile tool not only for pathology and developmental biology but also histology-based disease diagnosis, staging, and therapeutic screening.

Key words Matrix metalloproteinase, Collagenase, Collagen fiber, Collagen remodeling, Bone resorption, Immunostaining

1 Introduction

Collagen is the major structural component of the extracellular matrix (ECM) in virtually all mammalian tissue and organs, with an essential role in supporting cell growth and tissue formation. While collagen synthesis and degradation are delicately coordinated during tissue homeostasis, collagen undergoes extensive proteolytic remodeling during development and as a result of a variety of life-threatening conditions such as cancer, myocardial infarction, and fibrosis [1–3]. Although the degraded collagens could be an important marker of tissue damage and remodeling, it is difficult to detect such collagens, particularly in histopathology, using conventional tools, such as collagen stains (e.g., Masson's trichrome), antibodies, and second-harmonic generation microscopy. To address this problem, we developed the collagen hybridizing peptide (CHP) which can specifically bind to enzymatically degraded collagen molecules in tissues [4–6]. The peptide was designed based on the triple helical structure of collagen, which is nearly exclusively found in

Irit Sagi and Nikolaos A. Afratis (eds.), *Collagen: Methods and Protocols*, Methods in Molecular Biology, vol. 1944, https://doi.org/10.1007/978-1-4939-9095-5_10, © Springer Science+Business Media, LLC, part of Springer Nature 2019

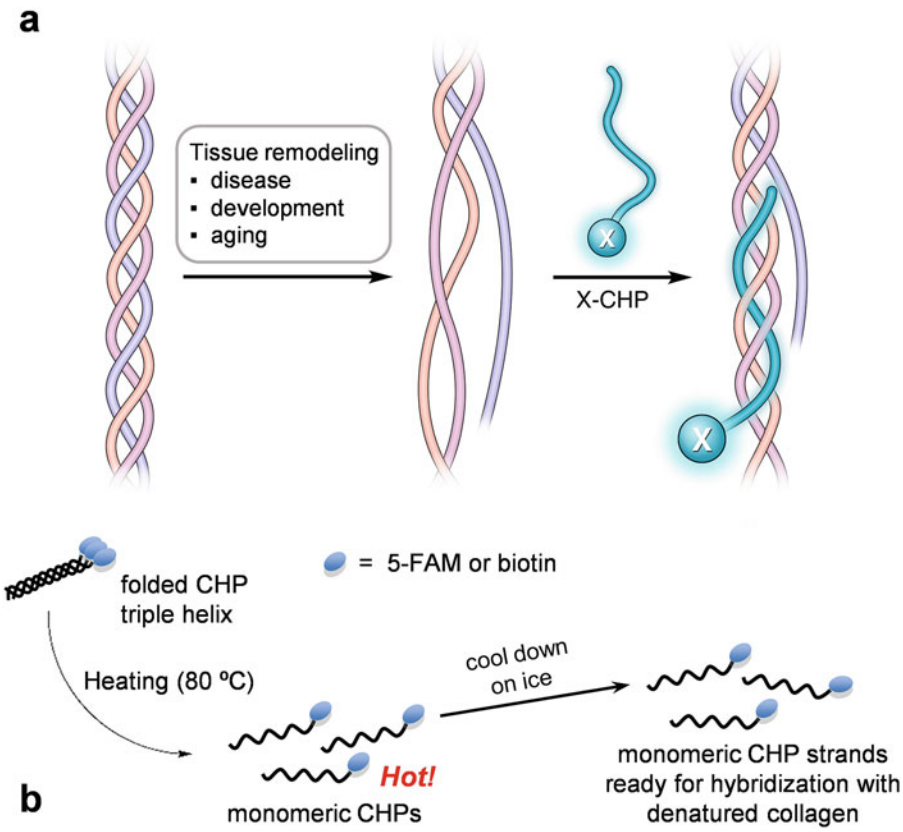

Fig. 1 (**a**) Schematic of a CHP strand (labeled with X) hybridizing to denatured collagen chains and forming a collagen triple helix. During disease progression, tissue development, or aging, collagen can be extensively degraded by collagen-cleaving proteases, causing its triple helix to unfold at the physiological temperature due to thermal instability. X represents the biotin or fluorescent tag. (**b**) The thermal activation step used to generate monomeric CHP strands for collagen hybridization. A dilute CHP solution (15–30 μM) was heated in a water bath at 80 °C for 5 min to dissociate the folded CHP homotrimers. The hot solution was then quenched in an ice-water bath to room temperature. The solution of monomeric CHP was then ready for immediate use to hybridize with denatured collagen in tissue samples. The self-trimerizing of CHP takes several hours to complete in this concentration range, and the effect of the dead time due to quenching (< 3 min) is negligible. The figure is reproduced from ref. 4 with permission from American Chemical Society

the collagen family (Fig. 1a). Following degradation by collagen-cleaving proteases (e.g., MMP), the collagen triple helices become thermally unstable at body temperature and spontaneously unfold, leaving the denatured collagen fragments covalently cross-linked within the matrix (Fig. 1a) [5, 7–9]. The CHP peptide has a collagen-mimetic repeating sequence of glycine(G)–proline (P)–hydroxyproline(O) with a strong propensity to fold into the triple helix. Therefore, it can bind specifically to unfolded collagen chains by forming a new, hybridized triple helical complex, in a fashion that is similar to a primer binding to a melted DNA strand

during a polymerase chain reaction (Fig. 1a) [4–6]. Due to the lack of hybridization sites, the CHP has no affinity toward native, fully folded collagen molecules [5]. Furthermore, the neutral and hydrophilic amino acid composition of CHP makes it virtually nonadherent to other biomolecules [10].

In this chapter, we present detailed procedures for detecting degraded and denatured collagen in histology slides using biotin-labeled CHP. The key difference between this method and a standard immunostaining protocol is that the CHP probe requires a special heating-and-quenching step before application to samples (*see* Fig. 1b). Because of the high triple helix propensity, the CHP peptides tend to self-assemble into homotrimers in solution over time (e.g., during storage at 4 °C) and lose the driving force for collagen hybridization. Therefore, the trimeric CHP needs to be thermally dissociated to single strands by heating briefly at 80 °C before it can be used to bind to unfolded collagen [4]. The hot CHP solution is quenched quickly to room temperature immediately prior to addition to tissue samples to prevent undesired thermal denaturation of the tissue. Since the CHP trimerization has a third-order folding rate with a halftime on the order of hours at low μM concentrations [11, 12], the heating-and-quenching method (Fig. 1b) described in this protocol ensures that the active monomeric form of CHP is delivered to the denatured collagen allowing efficient hybridization.

2 Materials

2.1 Equipment and Tools

1. Unstained animal or human tissue slides (typically 2–20 μm in thickness) which are either fixed and embedded in paraffin or frozen in OCT compound.
2. A humidity chamber for slide staining.
3. Thirteen tissue-slide-staining jars and a vertical slide-staining rack.
4. Pipettors (1000 μL and 200 μL) and tips.
5. A benchtop timer.
6. 15 mL and 50 mL centrifuge tubes and several 1.5 mL microtubes.
7. A hydrophobic barrier pen (PAP pen).
8. A temperature-controlled water bath, or heating block, and a thermometer.
9. An ice bucket or a glass beaker.
10. A floating microtube rack.
11. A benchtop mini-centrifuge for 1.5 mL microtubes.

12. Standard glass coverslips.
13. The fluoroshield mounting medium.
14. A pair of extra-fine point tweezers.
15. A standard fluorescence microscope with common fluorescence channels, such as DAPI, GFP, RFP, Cy5, etc.

2.2 Solvents for Prestaining Steps

1. Xylene, 200 mL.
2. Ethanol, 200 proof, 200 mL.
3. Ethanol, 190 proof, 200 mL.
4. Ethanol, 50%, 200 mL. Add 100 mL of deionized water and 100 mL of 200 proof ethanol to a glass beaker and mix.
5. Phosphate-buffered saline (1× PBS), 2–2.5 L, pH 7.4.
6. Blocking solution: 5 (v/v) % goat serum in 1× PBS, pH 7.4. Thaw the pre-aliquoted and frozen goat serum. Add 0.5 mL of 10× PBS, 0.5 mL of goat serum, and 9 mL of deionized water to a 15 mL centrifuge tube. Mix well and store at 4 °C (*see* **Note 1**).
7. Biotin-blocking solution kit (optional, *see* **Note 2**), containing a streptavidin reagent (Component A) and a biotin reagent (Component B), which is usually purchased from major vendors.

2.3 Staining

1. CHP staining solution. Biotin- or fluorescein-labeled collagen hybridizing peptide (B-CHP or F-CHP) conjugates can be purchased from 3Helix, Utah, USA or other vendors. Dissolve the CHP powder with calculated amount of 1× PBS buffer to prepare a stock solution of 100 μM concentration. Aliquot a desired volume of the B-CHP stock solution (*see* **Note 3**), and dilute it to 20 μM (*see* **Note 4**) with 1× PBS. Store at 4 °C.
2. Diluent solution: 1% bovine serum albumin (BSA) in 1× PBS, pH 7.4. Weigh 0.1 g of BSA and transfer to a 15 mL centrifuge tube containing 10 mL of 1× PBS. Mix well and store at 4 °C.
3. Streptavidin solution: aliquot a desired volume of the stock solution of a streptavidin conjugate, and dilute it to 5 μg/mL concentration with the diluent solution. A variety of commercial avidin or streptavidin conjugates can be used for signal detection. Here, AlexaFluor647-labeled streptavidin is used as an example in this protocol. Store the diluted streptavidin solution at 4 °C.

3 Methods

Carry out all procedures at room temperature unless otherwise specified.

3.1 Slide Preparation and Prestaining Steps

1. Fill two tissue-slide-staining jars with each of the following solvents: xylene, 200 proof ethanol, 190 proof ethanol, 50% ethanol, and deionized water. One hundred milliliter of a solvent is added to each jar. Label the jars with their contents.
2. Place the paraffin-embedded slides onto a staining rack, and immerse the rack in a xylene-containing jar.
3. Incubate the slides for two 5 min cycles in each solvent, following a consecutive order of xylene, 200 proof ethanol, 190 proof ethanol, 50% ethanol, and deionized water. After the final cycle of washing in water, these deparaffinized slides can be directly stained by CHP without any antigen-retrieval process. For OCT-embedded frozen slides (*see* **Note 5**).
4. Fill the bottom of the tissue-staining chamber with water.
5. Using the PAP pen, draw a circle around the specimen(s) on each slide as a hydrophobic barrier to keep staining reagents localized on the tissue sections. Align the slides on the rack inside the staining chamber.
6. Add an enough volume of blocking solution to each tissue sections to fill the space within the barrier circle. To estimate the volume of solution needed to cover all slides (*see* **Note 4**). Incubate the slides with the blocking solution in the staining chamber for 20 min to block the non-specific binding sites.
7. Remove the blocking solution by blotting the slides on a paper towel.
8. Rinse the slides in 100 mL of 1× PBS in a slide-staining jar for 5 min. Rinse three times. (*See* **Note 6**, for the optional biotin-blocking steps.)
9. Blot the slides on a paper towel, and align the slides on the rack inside the staining chamber. The slides are now ready to be stained by CHP.

3.2 Collagen Hybridizing Peptide Staining

1. Turn on the temperature-controlled water bath, and set the temperature to 80 °C (*see* **Note 7**).
2. Fill the ice bucket or a glass beaker with ice and water to make an ice-water bath.
3. Ensure the microtube containing the diluted B-CHP staining solution is capped tightly. Add the tube onto a floating rack, and place the rack into the 80 °C water bath.
4. Allow the B-CHP staining solution to be heated for 5 min (*see* **Note 8**) to dissociate the trimeric peptides into single strands (*see* Fig. 1b).
5. Following heating, immediately vortex and centrifuge the tube for 10 s to collect the condensation inside the tube.

6. Quickly immerse the B-CHP microtube in the ice-water bath and wait for 30 s (*see* **Note 9**) to quench the solution to room temperature (*see* **Note 10**).
7. Quickly add desired amounts of the heated-and-quenched B-CHP solutions onto the slides to fill the space inside the barrier circles (*see* **Note 11**).
8. Close the lid of the staining chamber, and carefully move the chamber into a refrigerator. Incubate the tissue slides in the chamber at 4 °C overnight (*see* **Note 12**).
9. After staining, remove the B-CHP solutions by blotting the slides on a paper towel.
10. Rinse the slides in 100 mL of 1× PBS in a slide-staining jar for 5 min. Rinse three times.
11. Align the slides on the rack inside the staining chamber. Add solutions of AlexaFluor647-conjugated streptavidin onto the slides to fill the space inside the barrier circles (*see* **Note 13**).
12. Incubate the slides with the streptavidin solutions in the staining chamber for 1 h.
13. Remove the streptavidin solutions by blotting the slides on a paper towel. Rinse the slides as in **step 10** three times (*see* **Note 14**).
14. Add a drop of the fluoroshield mounting medium onto the center of each tissue specimen. Use a pair of extra-fine point tweezers to slowly and carefully place a glass coverslip onto each slide. Ensure that the mounting medium fill the space between the slide and the coverslip with no air bubbles trapped. The slides are now ready to be imaged using a standard fluorescence microscope.

4 Notes

1. We recommend preparing the protein solutions, such as the blocking, CHP staining, and streptavidin solutions, within 24 h before usage to ensure freshness.
2. Biotin occurs naturally, functioning as an enzyme cofactor in the cytosol and mitochondria of a wide variety of cell types. Kidney, liver, and spleen tissues may contain a high level of endogenous biotin. Occasionally, when the slides are analyzed with B-CHP and avidin/streptavidin detection, blocking the endogenous biotin in the tissue can significantly reduce the non-specific background signals. This can be done by using a commercial biotin-blocking kit that is available from most reagent vendors. A typical biotin-blocking procedure is described in **Note 6**.

3. Two CHP conjugate reagents are available for histology studies: the fluorescein-labeled F-CHP for fluorescence detection and the biotin-labeled B-CHP for non-green fluorescence and HRP-based colorimetric detection. B-CHP may sometimes be advantageous when the tissue auto-fluoresces in green or when there is a need to enhance signal using enzymatic methods. This protocol focuses on B-CHP and streptavidin detection. To perform F-CHP staining, use F-CHP instead of B-CHP wherever CHP or B-CHP is mentioned in the protocol, and skip **steps 11–13** in Subheading 3.2.
4. Although the optimal concentrations for tissue staining may be sample dependent, a concentration of 20 μM is recommended for initial trials, based on our optimization test (*see* Fig. 2a). In addition, the total volume of CHP staining solution needed for each experiment depends on the number of slides and the area of each tissue section: approximately, it takes 50 μL of solution to cover an area of 1 cm^2 on a slide. A typical tissue slide requires 50–250 μL of staining solution to cover. The volume of the CHP stock solution needed in each experiment can be calculated:

$$V_{\text{CHP stock}} = (V_{\text{total volume to cover all slides}} \times 20\ \mu M)/100\ \mu M$$

5. For OCT-embedded frozen slides, skip **steps 1–3** in Subheading 3.1. Instead, take out the slides from the freezer, and let them warm up to room temperature. Fill two staining jars with 1× PBS. Rinse away the OCT compound by incubating the slides for 5 min in each staining jar.
6. To block endogenous biotin, following **step 8** in Subheading 3.1, apply one or two drops of the streptavidin reagent (Component A, streptavidin) of a biotin-blocking kit to each tissue sample, and incubate for 20 min at room temperature in the humidity chamber. Rinse the slides thoroughly with PBS for 5 min twice in the staining jars. Add one or two drops of the biotin reagent (Component B, biotin), and incubate 20 min at room temperature in the humidity chamber. Rinse thoroughly with PBS twice.
7. To save time, **steps 1–3** in Subheading 3.2 can be performed in parallel of **steps 6–8** in Subheading 3.1, while the slides are being blocked or washed.
8. It is not a problem to heat the CHP solution for over 5 min, since the CHP peptide is chemically stable at hot temperature. It is important to ensure that the slides, the centrifuge, and the ice-water bath are ready before removing the CHP solution from heating. Turn off the heater after the heating is finished.

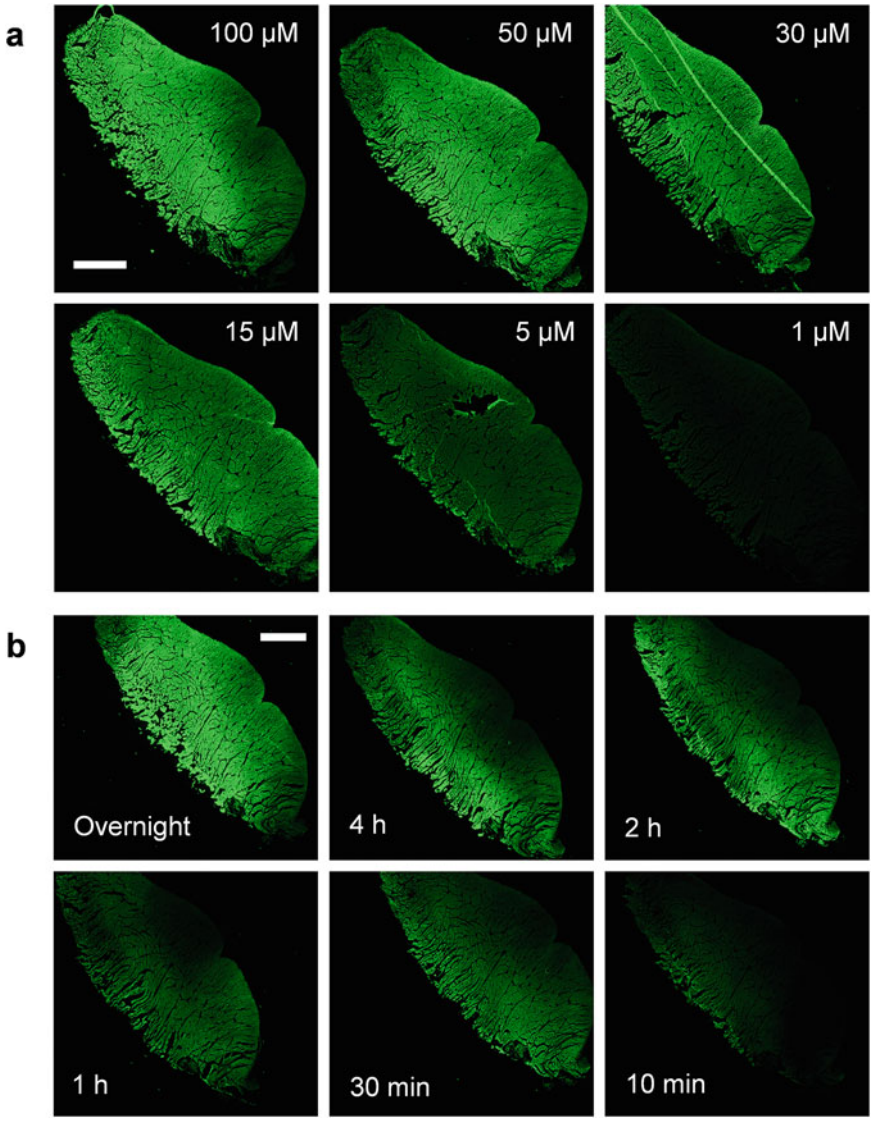

Fig. 2 The optimization tests for CHP staining. (**a**) Fluorescence images of neighboring cryosections of a porcine ligament stained with 100 μL of F-CHP solutions at varying concentrations. Before staining, all slides were denatured in 80 °C water to purposefully denature the collagen molecules for CHP hybridization. The staining time was set at 2 h for all samples. (**b**) Fluorescence images of a set of heated ligament tissue slides stained with F-CHP (100 μL, 15 μM) for different incubation time periods. Scale bars: 2 mm. The figure is reproduced from ref. 4 with permission from American Chemical Society

9. The heated CHP solution must be cooled down to room temperature to avoid thermal damage to the tissue samples. Depending on the solution volume (e.g., 200–3000 μL), the quenching time required varies from 15 s to 90 s.
10. When needed, other staining agents, such as a collagen antibody, can be diluted into the quenched CHP solution for

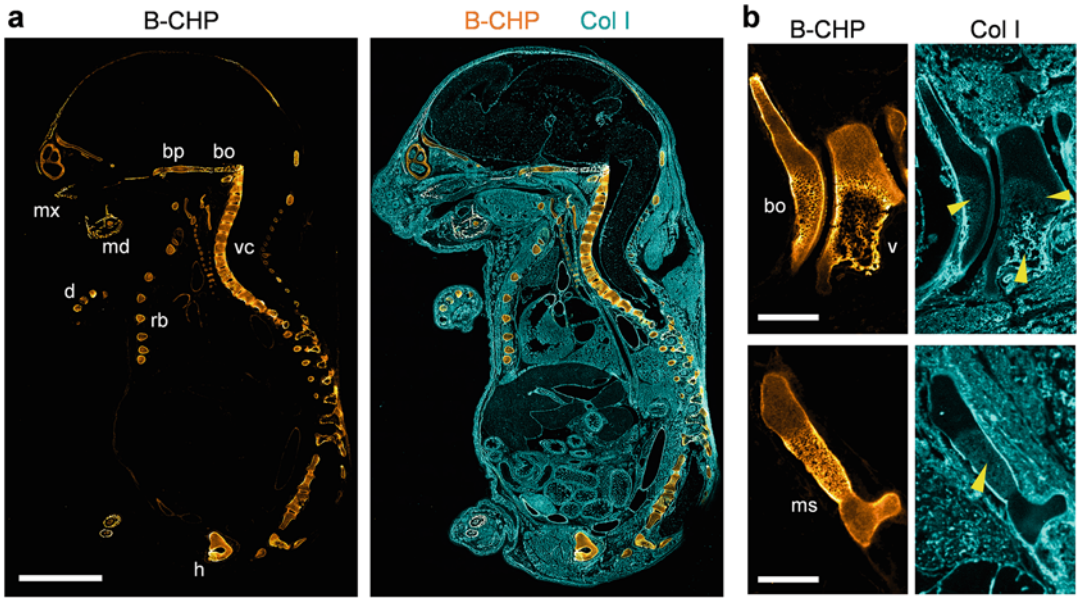

Fig. 3 Histological visualization of collagen degradation during endochondral ossification using CHP. (**a**) Localization of CHP binding in a sagittal section of an 18 d.p.c. mouse embryo double stained with B-CHP (detected by AlexaFluor647-streptavidin, orange) and an anti-collagen I antibody (detected by AlexaFluor555-labeled donkey anti-rabbit IgG H&L, cyan). *mx* maxilla, *md* mandibular bone, *bp* basisphenoid bone, *bo* basioccipital bone, *vc* vertebral column, *rb* rib, *h* hipbone, *d* digital bones. (**b**) Magnified views of the basioccipital bone (*bo*) beside the C1 vertebra (*v*) (top images) and the manubrium sterni (*ms*, bottom images) in the sagittal section of a 17 d.p.c. mouse embryo stained in the same fashion. High level of CHP binding is found in the hypertrophic zone surrounding the newly deposited collagen I bone matrix (yellow arrow heads), which is visualized by the anti-collagen I antibody. Scale bars: 3 mm (**a**), 0.5 mm (**b**). The figure is reproduced from ref. 4 with permission from American Chemical Society

co-staining (*see* Fig. 3, e.g.). Following **step 6** in Subheading 3.2, quickly pipette the desired volume of the antibody stock solution into the quenched CHP staining solution according to the predetermined dilution factor. Mix well, and this solution is ready for double staining.

11. The CHP trimerization has a third-order folding rate with a halftime on the order of hours at low μM concentrations. Therefore, the heating-and-quenching protocol used here ensures that the CHP strands are in the active monomer form until exposed to denatured collagen. However, it is highly recommended to spend minimal time on **steps 5–7** ($\leq$ 3 min) to limit the CHP trimerization during such dead time and to ensure consistent results.
12. We suggest staining the slides at 4 °C, because the CHP hybridizes with collagen chains more strongly at low temperature. Based on our optimization test (*see* Fig. 2b), we

recommend incubating the slides in the CHP solution for at least 2 h. For optimal results, overnight staining is recommended.

13. To detect the primary antibody added during the B-CHP staining step (see **Note 10**), dilute the labeled secondary antibody (e.g., AlexaFluor555 donkey anti-rabbit) into the AlexaFluor647-streptavidin solution according to the predetermined dilution factor (e.g., 1:200), and incubate the slides with the two probes for 1 h at room temperature.
14. When needed, the slides can be further stained with other common staining agents (e.g., Hoechst 33342) following the CHP staining.

Acknowledgments

This work was supported by the National Institutes of Health grant (ORIP, R43OD021986) awarded to Y.L. We also thank the National Institutes of Health and the Department of Defense (NIH, R01AR060484, R21AR065124, and DOD W81XWH-12-1-0555 awarded to S.M.Y.) for supporting the research of the CHP technology.

References

1. Bonnans C, Chou J, Werb Z (2014) Remodelling the extracellular matrix in development and disease. Nat Rev Mol Cell Biol 15:786–801
2. Page-McCaw A, Ewald AJ, Werb Z (2007) Matrix metalloproteinases and the regulation of tissue remodelling. Nat Rev Mol Cell Biol 8:221–233
3. Wahyudi H, Reynolds AA, Li Y et al (2016) Targeting collagen for diagnostic imaging and therapeutic delivery. J Control Release 240:323–331
4. Hwang J, Huang Y, Burwell TJ et al (2017) *In situ* imaging of tissue remodeling with collagen hybridizing peptides. ACS Nano 11:9825–9835
5. Li Y, Foss CA, Summerfield DD et al (2012) Targeting collagen strands by photo-triggered triple-helix hybridization. Proc Natl Acad Sci U S A 109:14767–14772
6. Li Y, Yu SM (2013) Targeting and mimicking collagens *via* triple helical peptide assembly. Curr Opin Chem Biol 17:968–975
7. Chung L, Dinakarpandian D, Yoshida N et al (2004) Collagenase unwinds triple-helical collagen prior to peptide bond hydrolysis. EMBO J 23:3020–3030
8. Danielsen CC (1987) Thermal stability of human-fibroblast-collagenase-cleavage products of type-I and type-III collagens. Biochem J 247:725–729
9. Fisher GJ, Kang S, Varani J et al (2002) Mechanisms of photoaging and chronological skin aging. Arch Dermatol 138:1462–1470
10. Li Y, Ho D, Meng H et al (2013) Direct detection of collagenous proteins by fluorescently labeled collagen mimetic peptides. Bioconjug Chem 24:9–16
11. Ackerman MS, Bhate M, Shenoy N et al (1999) Sequence dependence of the folding of collagen-like peptides. Single amino acids affect the rate of triple-helix nucleation. J Biol Chem 274:7668–7673
12. Boudko S, Frank S, Kammerer RA et al (2002) Nucleation and propagation of the collagen triple helix in single-chain and trimerized peptides: transition from third to first order kinetics. J Mol Biol 317:459–470

Chapter 11

Combination of Traction Assays and Multiphoton Imaging to Quantify Skin Biomechanics

Stéphane Bancelin, Barbara Lynch, Christelle Bonod-Bidaud, Petr Dokládal, Florence Ruggiero, Jean-Marc Allain, and Marie-Claire Schanne-Klein

Abstract

An important issue in tissue biomechanics is to decipher the relationship between the mechanical behavior at macroscopic scale and the organization of the collagen fiber network at microscopic scale. Here, we present a protocol to combine traction assays with multiphoton microscopy in ex vivo murine skin. This multiscale approach provides simultaneously the stress/stretch response of a skin biopsy and the collagen reorganization in the dermis by use of second harmonic generation (SHG) signals and appropriate image processing.

Key words Biomechanics, Collagen, Skin, Multiphoton microscopy

1 Introduction

The mechanical behavior of skin at macroscopic scale is strongly related to its microstructure and mainly to the organization of the collagen fiber network in the dermis. While many microstructural models have been investigated theoretically, only few experimental studies have been reported up to now due to technical limitations. Indeed, it is necessary to monitor the collagen network at a micrometer scale during mechanical assays in a centimeter-sized skin biopsy.

To address this issue, we recently combined traction assays with multiphoton microscopy [1, 2]. This multiscale device measures simultaneously the stress/stretch response of a skin biopsy and the collagen reorganization in the dermis by use of second harmonic generation (SHG) signals. SHG signals correspond to a multiphoton mode of contrast that is specific to collagen fibers and efficiently reveals the micrometer-scale organization of collagen in unstained thick tissues [3–5]. Accordingly, we obtained new quantitative

Irit Sagi and Nikolaos A. Afratis (eds.), *Collagen: Methods and Protocols*, Methods in Molecular Biology, vol. 1944, https://doi.org/10.1007/978-1-4939-9095-5_11, © Springer Science+Business Media, LLC, part of Springer Nature 2019

information about skin biomechanics that evidenced a non-affine reorganization of the collagen network and challenged usual microstructural models [6, 7]. This new technique also allowed characterizing the impact of microstructural changes in the dermis due to genetic modifications, aging, or any other processes [2, 8]. Note that a similar approach has been applied successfully to other tissues (*see*, for instance, [9–18]).

In this chapter, we describe the implementation of incremental uniaxial traction assays with semicontinuous SHG visualization in ex vivo murine skin. We also explain how to analyze the mechanical data and process the SHG images to obtain quantitative parameters. Specifically, we describe how to use the network of hair follicles as endogenous tags to quantify the local deformation and how to extract the fiber orientation to quantify the collagen reorganization in the field of view.

2 Materials

The traction and imaging devices may be either custom-build devices or commercial ones. They need to have dimensions and shapes that enable their combination in the same setup. In concrete terms, the traction device has to be put horizontally in place of the microscope stage (Fig. 1). The specific features of these devices are listed below.

2.1 Traction Device

1. Symmetrical uniaxial traction machine using two identical motors and sensors, one of each side of the skin sample.
2. Motors: Linear actuators. Resolution below 5 μm, accuracy below 5 μm, strokes above 40 mm, maximal holding force above 10 N. Speed between 1 and 100 μm/s (or above).
3. Sensors: Capacity at least 8 N. Resolution below 0.01 N. Overload should be important (more than 80 N) so as to avoid breaking the sensors when screwing the sample in the grips.

2.2 Multiphoton Setup

1. Geometry: laser-scanning upright microscope, with two epi-detection channels, one for SHG and another one for two-photon excited fluorescence (2PEF).
2. Objective lens: high Numerical Aperture (0.9–1.1 NA) moderate magnification (20× or 25×) water-immersion objective lens (*see* **Note 1**).
3. Excitation wavelength: any wavelength in the Ti-Sa range for SHG signal (*see* **Note 2**).
4. Excitation polarization: circular or quasi-circular (*see* **Note 3**).

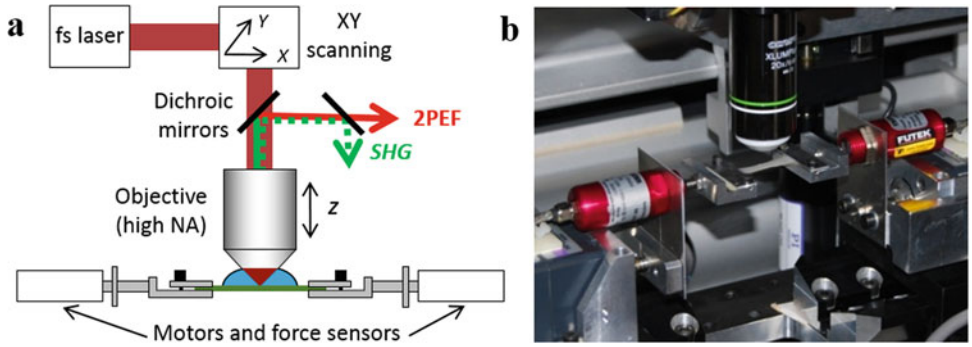

Fig. 1 Experimental setup combining multiphoton microscopy and uniaxial traction assay. (**a**) Schematic representation and (**b**) picture. Adapted from Bancelin et al., Sci Rep 2015, doi:https:/doi.org/10.1038/srep17635, published under license **CC BY 4.0**

5. Excitation power: typically 20–30 mW. Power is adjusted to obtain a good signal-to-noise ratio in the SHG images and avoid both saturation and damage to the skin sample.

3 Methods

3.1 Preparation of Murine Skin Biopsy

1. Sacrifice of mice by cervical dislocation at a specific age.
2. Depilation of the back skin: first, the back of the mouse is shaved using an electric trimmer, then depilatory cream (Nair™) is applied for 15 min, and hairs are removed with a scraper. This last step is repeated two or three times if needed.
3. Tagging of the right foreleg with a dot of black ink to identify the anterior-posterior axis before cutting the skin with scalpels or dissecting scissors. Skin is then gently peeled off and placed in a Petri dish.
4. Removal of the epidermis by incubating the skin 30 min at room temperature with 3.8% ammonium thiocyanate and scraping the epidermis under a binocular magnifier (*see* **Note 4**).
5. Storage in culture medium (Dulbecco's Modified Eagle's Medium) without phenol red (*see* **Note 5**), supplemented with 50 μg/mL penicillin/streptomycin at 6 °C. Medium is changed every 2 days. Skin biopsies should be used for experiments within 5 days.

3.2 Skin Cutting and Fastening for Traction Assays

1. The skin sample is cut into a dog-bone shape using curved dissection scissors, taking care to hold the sample on the outskirt part (not used in mechanical test) so as to damage the sample as little as possible (Fig. 2) (*see* **Note 6**).

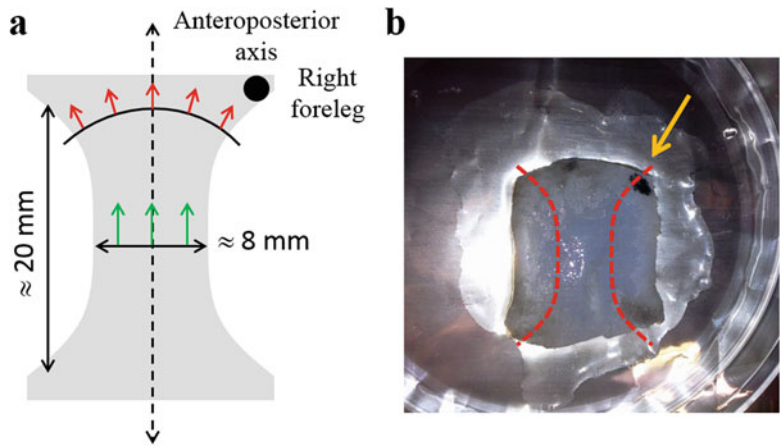

Fig. 2 Preparation of the depilated and de-epidermized skin sample for mechanical test. (**a**) Schematic representation and dimensions of the dog-bone-shaped skin sample. (**b**) Picture before cutting. The orange arrow shows the black spot indicating the right foreleg. The red dots show the dog-bone shape the skin will be cut into. Typical size is 30 × 20 mm^2. Adapted from Bancelin et al., Sci Rep 2015, doi:https:/doi.org/10.1038/srep17635, published under license **CC BY 4.0**

2. The dog-shaped skin sample is attached to the traction device by means of mechanical jaws with rubber joints that pinch the sample on both sides (*see* **Note 7**).
3. The skin dimensions are measured with a digital caliper: thickness (around 1 mm), width at the center (around 8 mm), and length between the jaws (around 20 mm).
4. The hydration of the skin sample is maintained during cutting and fastening with drops of culture medium.
5. The traction device with the attached skin sample is installed in place of the microscope stage, with the papillary dermis facing the objective lens (Fig. 1). Immersion gel is used to ensure optical contact with the objective lens and to prevent dehydration of the skin sample during the experiment. If needed, this immersion gel is first centrifuged to remove small air bubbles that could deteriorate image quality. New drops are added during the experiment if required.

3.3 Traction Assays Under the Multiphoton Microscope

1. The motor displacement and the force are measured continuously (every second) during the whole traction assay (Fig. 3).
2. SHG imaging is performed continuously while adjusting the axial position of the objective lens to find the surface of the skin sample and focus a few μm below.
3. The jaws are moved apart slowly (usually around 0.01 mm s^{-1}) while continuously recording low-resolution SHG images until

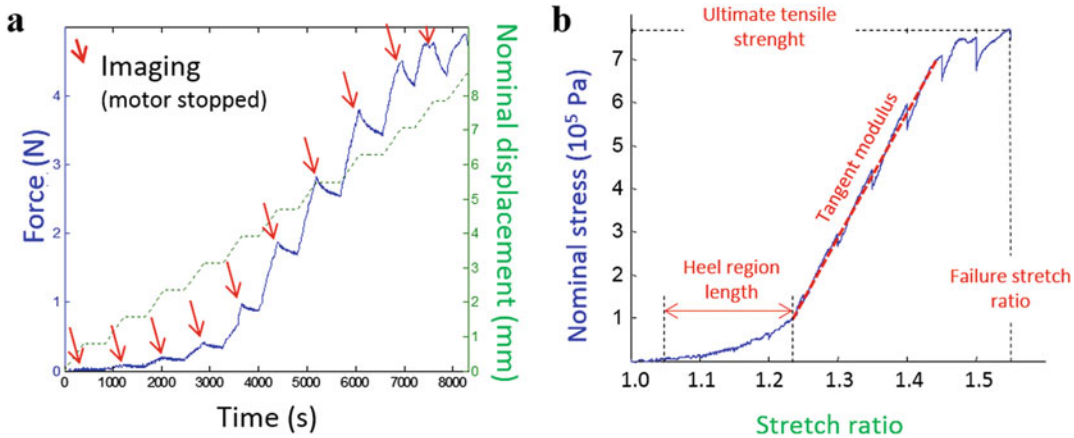

Fig. 3 Mechanical data from wild-type skin sample. (**a**) Experimental timetable showing stepwise stretching of the skin sample (green dotted line) with continuous force measurement (blue continuous line) and time-lapse imaging of immobile sample after each displacement step (red arrows). (**b**) Nominal stress/stretch curve for the same sample, showing the processed mechanical parameters. Adapted from Bancelin et al., Sci Rep 2015, doi:https:/doi.org/10.1038/srep17635, published under license **CC BY 4.0**

no more vertical displacement is observed (*see* **Note 8**). This position will be referred to as the reference position.

4. The motors are stopped and a first SHG image stack is recorded using the following typical parameters: 100 kHz pixel rate, 0.5 μm pixel size, 2 μm axial step, and 480 × 480 × 50 μm^3 stacks, resulting in 5 min acquisition time (*see* **Note 9**). 2PEF signals are acquired simultaneously in a second channel to visualize remains of hairs or other fluorescent structures. Typical SHG images are displayed in Fig. 4.
5. The skin sample is stretched by 5% at a stretch rate of 10^{-4} s^{-1}. Given the length of the skin sample (20 mm between the jaws), it corresponds to a typical speed of 0.002 mm s^{-1}. SHG imaging at low resolution is performed continuously during stretching to follow the region of interest (ROI) imaged in the previous step. If needed, the axial position of the objective lens and the lateral position of the traction device are adjusted with micrometer screws to make sure the same ROI is imaged (*see* **Note 10**).
6. Motors are stopped and a second SHG stack is recorded in the same ROI as previously and using the same parameters (*see* **Note 11**).
7. **Steps 4** and **5** are performed sequentially until the skin sample breaks, usually around a stretch ratio of 1.5. The total duration of this incremental traction assay is 3–4 h (15–20 min per step).

3.4 Mechanical Data Processing

1. The global stretch ratio is obtained as the ratio of the length between the rubber joints of the jaws to the reference length that is the one measured at the reference position (*see* **Note 12**).

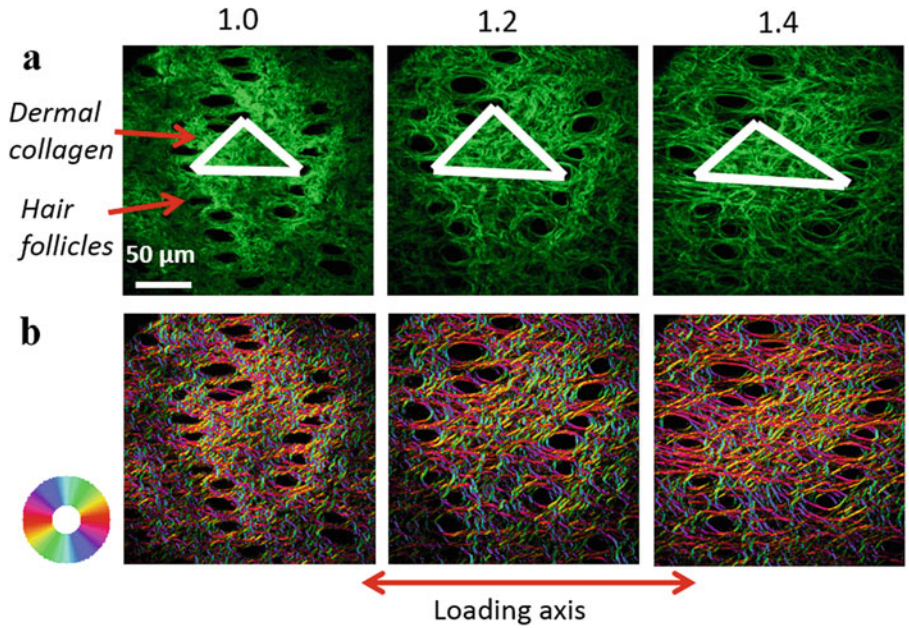

Fig. 4 SHG imaging and image processing of ex vivo stretched skin sample. (**a**) Raw SHG images at 1.0, 1.2, and 1.4 stretch ratio. The deformation of the hair follicle network reveals the local skin deformation. (**b**) Processed SHG images at the same stretch ratios highlighting fiber orientation for each pixel with a color code. Adapted from Bancelin et al., Sci Rep 2015, doi:https:/doi.org/10.1038/srep17635, published under license **CC BY 4.0**

2. The nominal stress is obtained as the measured force divided by the initial skin section (thickness × width) (*see* **Note 12**).
3. The nominal stress is plotted as a function of the stretch ratio, and four quantitative parameters are extracted (*see* Fig. 3b): (1) the tangent modulus, which is the slope of the linear part; (2) the length of the heel region; (3) the ultimate tensile stretch, which is the maximum stress before rupture; and (4) the failure stretch ratio, which is the stretch corresponding to the ultimate tensile strength (*see* **Note 13**).

3.5 Image Processing for Local Deformation Analysis

1. SHG images at approximately the same depth are cropped to obtain a ROI common to all stretching steps showing the same hair follicles (round or elliptical regions with no SHG, interrupting the collagen fiber network, Fig. 4). The size of this ROI increases in the loading direction at increasing stretch ratio.
2. The hair follicles are segmented using the following steps (Fig. 5): application of a median filter to reduce noise (2 pixel radius), inversion of contrast, application of circular opening (8 pixel radius) [19] to smooth the image while preserving follicle edges, thresholding resulting in a binary image, and shape detection to identify and label every follicle. If needed,

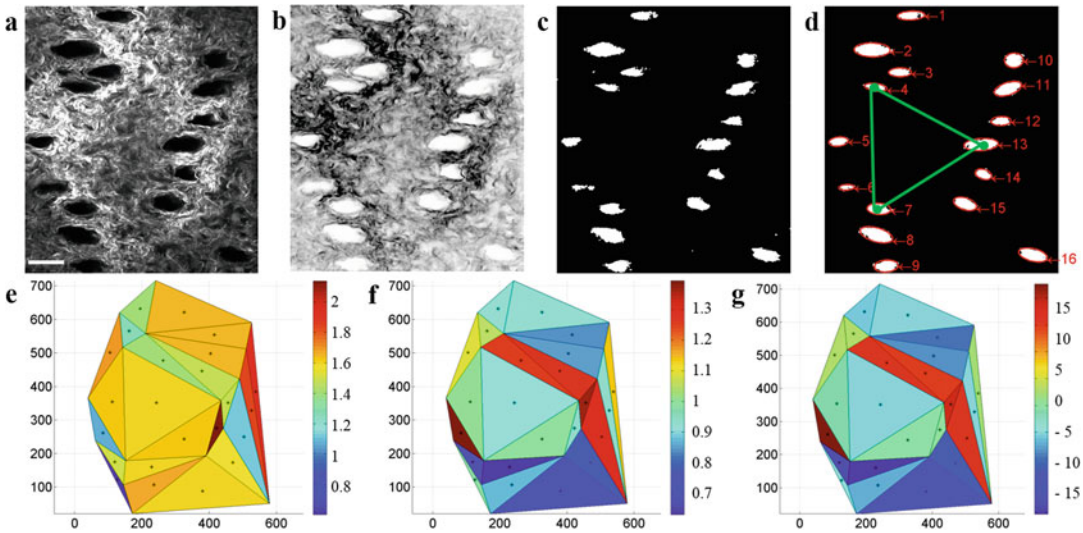

Fig. 5 Hair follicle segmentation in the SHG image for local deformation measurement. (**a**) Raw and (**b**) enhanced SHG image of mice skin papillary dermis; (**c**) binary SHG image after thresholding; (**d**) position detection and numbering of hair follicles; mapping of (**e**) λ_{xx}, (**f**) λ_{yy}, and (**g**) ω tensorial components calculated from the deformation of the hair follicle network—see green triangle in (d)—compared to the initial network before stretching. Scale bar: 50 μm. Reproduced from Bancelin et al., Sci Rep 2015, doi:https:/doi.org/10.1038/srep17635, published under license **CC BY 4.0**

the follicles are renumbered to obtain the same order in all images.

3. The network formed by the follicles is used to calculate the local deformation by performing a Delaunay triangulation and calculating for each triangle the deformation tensor relative to the same triangle in the non-stretched state (Fig. 5).
4. This local deformation tensor map is averaged over the cropped SHG image to obtain three parameters: the local deformations in the directions parallel and perpendicular to the traction and the sliding angle that represents the shear in the ROI (Fig. 5).
5. The local deformation in the traction direction is compared to the global one applied to the tissue: the local and global stretch ratios have to be equal to validate the mechanical assay (no slipping within the jaws, homogeneous tissue response) (*see* **Note 14**).

3.6 Image Processing for Collagen Reorganization

1. A fixed number of SHG images (for instance, 6) with maximum average intensity are selected in every SHG stack for all stretching ratios.
2. Morphological filtering is applied to extract the fiber orientation in every pixel by means of a mean filter (3 pixel diameter) and of a morphological opening [19] using a linear structuring element (Strel; *see* **Note 15**). A stack of images is obtained by

rotating the Strel where the pixelwise maximum provides an enhanced image of the collagen fibers. The position of the maximum provides their local orientation (Fig. 4).

3. A normalized histogram of fiber orientation is calculated for every stretch ratio. The evolution of these histograms with increasing stretch ratio can be quantified using different methods. Our choice is to calculate [20] (1) the maximum of this histogram (i.e., the main orientation), (2) the orientation index, defined as the percentage of fibers oriented along the main orientation:

$$\mathrm{OI} = 100 \times \left[2 \frac{\int_{-90^\circ}^{90^\circ} I(\theta) \cos^2(\theta - \theta_{\max}) \mathrm{d}\theta}{\int_{-90^\circ}^{90^\circ} I(\theta) \mathrm{d}\theta} - 1 \right]$$

and (3) the entropy, defined as the usual statistical entropy, which measures the degree of organization in the skin sample independently of any main orientation:

$$S = -\sum_{\theta=-90^\circ}^{90^\circ} p(\theta) \ln [p(\theta)]$$

where $p(\theta) = \dfrac{I(\theta)}{\sum_{\theta=-90^\circ}^{90^\circ} I(\theta)}$.

4 Notes

1. We need a good resolution, in order to visualize small features, and a large field of view, in order to detect more signal and to visualize a significant region of the tissue. The microscope resolution depends on the NA and on the excitation wavelength, while the field of view depends on the magnification [21]. Consequently, we have to use an objective lens with large NA and moderate magnification.
2. The SHG signal is a non-resonant signal whose intensity does not vary with the excitation wavelength. Nevertheless, it is necessary to choose a specific excitation wavelength in the case of simultaneous detection of specific fluorescent signals.
3. The SHG signal is sensitive to the orientation of the excitation electric field compared to the orientation of the collagen fibers: The SHG signal is smaller when exciting with a linear polarization perpendicular to the fiber. Circular polarization must be used to mitigate this effect and visualize all the fibers in the imaging plane with similar efficiency. It is usually obtained by use of a quarter-wave plate. The resulting polarization is often only quasi-circular, which is sufficient, because of the ellipticity introduced by the various optical components in the microscope.

4. The epidermis is removed because of the presence of pigmented cells. These cells exhibit strong absorption and may therefore induce thermal photodamage during multiphoton imaging. Moreover, the epidermis is a little damaged by the depilation process, so that there is no reason to keep it for imaging.
5. It is highly preferable to use culture medium without phenol red because this dye penetrates into the tissue and exhibits two-photon absorption of the laser excitation during multiphoton imaging. This absorption process may result in tissue heating and eventually damaging.
6. The dog-bone shape is the usual shape for tensile tests because it ensures homogeneous repartition of the strain in the central region of the skin sample and avoids rupture near the jaws (Fig. 2).
7. The skin is pressed on a rubber joint to limit damage and slippage. Accordingly, when removed after the experiment, it is thinned down on the joint line but not broken.
8. This step aims to unfold the skin sample, which results in vertical movements. We make sure that the force does not exceed the sensor noise in this step.
9. The acquisition parameters are a compromise between acquisition time, field of view, stack depth, and voxel size. We need a reasonable acquisition time to be able to perform all the steps of the traction assay within a few hours and ensure that the skin biopsy is still in good conditions at the end of the assay. We need a wide field of view to visualize a representative part of the tissue. We need a small pixel size appropriate to visualize collagen fibers. Finally, the imaging depth is usually limited to 50–100 μm because the imaging quality is deteriorated by scattering and optical aberrations due to undulations at the surface of the sample (which get worse at higher stretch ratios).
10. It is possible to recognize the ROI by looking at the characteristic patterns in hair follicles on the SHG image (Fig. 3). The position of this ROI moves slightly under the objective lens during stretching, and manual readjustment is necessary to follow the same ROI. Axial movements are compensated by adjusting the axial position of the objective lens. Lateral movements are compensated by manually adjusting the position of the traction device with micrometer screws (the traction device is placed on a breadboard fixed on micrometric stages). This manual adjustment is possible only for slow and small displacements, which is the reason why we deliberately choose a slow strain rate.
11. It is necessary to stop the motors when recording the SHG image stack because the skin must be immobile during the

image acquisition (which is quite slow as multiphoton microscopy is a pixel-based imaging technique). As a consequence, the skin relaxes every time the motors are stopped (Fig. 3). This relaxation may be analyzed to extract relaxation mechanical data [6].

12. The absolute stretch ratio is not determined accurately because of the uncertainty in the reference length measurement. Nevertheless, the variations of this parameter are accurately determined. The same comment applies to the nominal stress because of the uncertainty in the skin thickness measurement.
13. The heel region is considered to start when the stress stays over twice the noise for at least 10 s (the noise is measured at very small strains, in the so-called toe region). The end of the heel region is defined as the point at which the stress gets close enough to the linear fit (the difference is smaller than twice the noise).
14. Other parameters can be processed from the segmented image of follicles: The deformation of the follicles shape from round to circular and the variation of the skin porosity (% of skin surface occupied by follicles) [2].
15. The length of the linear structuring element (Strel) is typically 10 μm. A long Strel enables fine angular steps, but is not able to fit curved fibers.

Acknowledgments

This work was supported by grants from Ecole Polytechnique (interdisciplinary project) and from Agence Nationale de la Recherche (contracts ANR-10-INBS-04 France BioImaging, ANR-11-EQPX-0029 Morphoscope2, and ANR-13-BS09-0004-02 Metis). The authors thank Vincent de Greef for his help in the technical implantation of the mechanical setup.

References

1. Goulam Houssen Y, Gusachenko I, Schanne-Klein M-C, Allain J-M (2011) Monitoring micrometer-scale collagen organization in rat-tail tendon upon mechanical strain using second harmonic generation microscopy. J Biomech 44:2047–2052
2. Bancelin S, Lynch B, Bonod-Bidaud C, Ducourthial G, Psilodimitrakopoulos S, Dokladal P, Allain J-M, Schanne-Klein M-C, Ruggiero F (2015) Ex vivo multiscale quantitation of skin biomechanics in wild-type and genetically-modified mice using multiphoton microscopy. Sci Rep 5:17635
3. Zipfel WR, Williams RM, Christie R, Nikitin AY, Hyman BT, Webb WW (2003) Live tissue intrinsic emission microscopy using multiphoton-excited native fluorescence and second harmonic generation. Proc Natl Acad Sci U S A 100:7075–7080
4. Strupler M, Pena A-M, Hernest M, Tharaux P-L, Martin J-L, Beaurepaire E, Schanne-Klein M-C (2007) Second harmonic imaging and scoring of collagen in fibrotic tissues. Opt Express 15(7):4054–4065

5. Chen XY, Nadiarynkh O, Plotnikov S, Campagnola PJ (2012) Second harmonic generation microscopy for quantitative analysis of collagen fibrillar structure. Nat Protoc 7 (4):654–669
6. Lynch B, Bancelin S, Bonod-Bidaud C, Guesquin J-B, Ruggiero F, Schanne-Klein M-C, Allain J-M (2017) A novel microstructural interpretation for the biomechanics of mouse skin derived from multiscale characterization. Acta Biomater 50:302–311
7. Jayyosi C, Affagard J-S, Ducourthial G, Bonod-Bidaud C, Lynch B, Bancelin S, Ruggiero F, Schanne-Klein M-C, Allain J-M, Bruyère-Garnier K, Coret M (2017) Affine kinematics in planar fibrous connective tissues: an experimental investigation. Biomech Model Mechanobiol 16(4):1459–1473
8. Lynch B, Bonod-Bidaud C, Ducourthial G, Affagard J-S, Bancelin S, Psilodimitrakopoulos S, Ruggiero F, Allain J-M, Schanne-Klein M-C (2017) How aging impacts skin biomechanics: a multiscale study in mice. Sci Rep 7:13750
9. Sinclair EB, Andarawis-Puri N, Ros SJ, Laudier DM, Jepsen KJ, Hausman MR (2012) Relating applied strain to the type and severity of structural damage in the rat median nerve using second harmonic generation microscopy. Muscle Nerve 46(6):899–907
10. Wentzell S, Nesbitt RS, Macione J, Kotha S (2013) Measuring strain using digital image correlation of second harmonic generation images. J Biomech 46(12):2032–2038
11. Chow MJ, Turcotte R, Lin CP, Zhang YH (2014) Arterial extracellular matrix: a Mechanobiological study of the contributions and interactions of elastin and collagen. Biophys J 106(12):2684–2692
12. Sigal IA, Grimm JL, Jan NJ, Reid K, Minckler DS, Brown DJ (2014) Eye-specific IOP-induced displacements and deformations of human Lamina Cribrosa. Invest Ophth Vis Sci 55(1):1–15
13. Mauri A, Ehret AE, Perrini M, Maake C, Ochsenbein-Kolble N, Ehrbar M, Oyen ML, Mazza E (2015) Deformation mechanisms of human amnion: quantitative studies based on second harmonic generation microscopy. J Biomech 48(9):1606–1613
14. Alavi SH, Sinha A, Steward E, Milliken JC, Kheradvar A (2015) Load-dependent extracellular matrix organization in atrioventricular heart valves: differences and similarities. Am J Physiol Heart Circ Physiol 309(2): H276–H284
15. Nesbitt S, Scott W, Macione J, Kotha S (2015) Collagen fibrils in skin orient in the direction of applied uniaxial load in proportion to stress while exhibiting differential strains around hair follicles. Materials 8(4):1841–1857
16. Caulk AW, Nepiyushchikh ZV, Shaw R, Dixon JB, Gleason RL (2015) Quantification of the passive and active biaxial mechanical behaviour and microstructural organization of rat thoracic ducts. J R Soc Interface 12(108). ARTN 20150280
17. Benoit A, Latour G, Schanne-Klein M-C, Allain J-M (2016) Simultaneous microstructural and mechanical characterization of human corneas at increasing pressure. J Mech Behav Biomed Mater 60:93–105
18. Krasny W, Morin C, Magoariec H, Avril S (2017) A comprehensive study of layer-specific morphological changes in the microstructure of carotid arteries under uniaxial load. Acta Biomater 57:342–351
19. Serra J (1982) Analysis and mathematical morphology. Academic Press
20. Bayan C, Levitt JM, Miller E, Kaplan D, Georgakoudi I (2009) Fully automated, quantitative, noninvasive assessment of collagen fiber content and organization in thick collagen gels. J Appl Phys 105(10):102042
21. Zipfel WR, Williams RM, Webb WW (2003) Nonlinear magic: multiphoton microscopy in the biosciences. Nat Biotech 21 (11):1369–1377

Chapter 12

Analysis of Collagen-Binding Integrin Interactions with Supramolecular Aggregates of the Extracellular Matrix

Uwe Hansen

Abstract

Integrin-mediated interactions of cells with the extracellular matrix (ECM) are important for their activities. The ECM itself is a complex network of macromolecules forming aggregates or suprastructures. Moreover, the molecular composition is important for the macromolecular organization and, thereby, the functional properties of the ECM. In addition, collagen molecules lose their integrin-binding capabilities after incorporation into fibrils. Therefore, we have established detailed protocols for the analysis of integrin-matrix interactions at the supramolecular level.

Key words Cell adhesion assay, Integrins, Matrix superstructures, Collagens, Chondrocytes, Transmission electron microscopy

1 Introduction

Integrin-mediated interactions of cells with the extracellular matrix (ECM) are vitally important in the control and modulation of their activities, e.g., division, differentiation, survival, metabolism, and programmed cell death [1, 2]. However, the ECM is a complex network of macromolecules forming aggregates or suprastructures. In vivo, ECM suprastructures are always heterotypically assembled as they predominantly consist of several molecular components combined in various quantities. The molecular composition is important for their macromolecular organization and, thereby, their functional properties within the ECM. During collagen fibril formation, minor ECM components are crucial for the overall aggregation of collagen monomers [3]. Consequently, native collagen fibrils are known as macromolecular alloys. Their function in the ECM depends strongly on the composition of both collagen and non-collagenous components, and notably, the recognition of

Irit Sagi and Nikolaos A. Afratis (eds.), *Collagen: Methods and Protocols*, Methods in Molecular Biology, vol. 1944, https://doi.org/10.1007/978-1-4939-9095-5_12, © Springer Science+Business Media, LLC, part of Springer Nature 2019

collagens by integrins is strongly influenced by the suprastructural organization of the ECM [4, 5]. In most studies of integrin-matrix interactions, monomolecular ligands have been employed; however, integrins in situ encounter extracellular matrix aggregates in which integrin-binding epitopes can be newly created as well as obliterated. We have demonstrated the discrepancy between integrin sensing of molecular collagens and aggregated collagens by showing that collagen molecules lose their integrin-binding capabilities after incorporation into fibrils. Nevertheless, these collagen-binding integrins interact with non-collagenous macromolecules of the fibril periphery [5], and so it is therefore crucial to define integrin-matrix interactions at the supramolecular level. Here we present established detailed protocols for the analysis of interactions between collagen-binding integrins and ECM components at different stages of aggregation and for the interaction of collagen-binding integrins of chondrocytes with collagens in their monomeric and fibrillar states of aggregation.

2 Materials

1. Chondrocytes: Primary chondrocytes were obtained from sternal cartilage of 17-day-old chicken embryos.
2. Collagenase B: 1 mg/ml collagenase B.
3. Collagenase buffer: 1 mM cysteine, 100 U/ml penicillin, 100 μg/ml streptomycin (sterile filtered) in DMEM.
4. Integrins: 25 μg/ml soluble recombinant human integrins α1β1, α2β1, and α10β1, in which transmembrane and intracellular domains were replaced by a Jun-/fos-zipper motif or the pUC-HMT-β1jun-construct, respectively, were prepared as described previously [6, 7].
5. Anti-integrin-β1-antibodies (9EG7): 30 μg/ml of the activating 9EG7 antibody.
6. I-domains: Both human and chicken GST-α1I and GST-α2I were produced and purified using glutathione affinity chromatography as described previously [8, 9].
7. Discoidin domain receptor (DDR): Recombinant soluble protein comprising the entire DDR2 ectodomain fused to the Fc-sequence of human IgG2 was produced in episomally transfected HEK293-EBNA cells and was purified by affinity chromatography as previously described [10, 11].
8. Penicillin: 100 U/ml penicillin.
9. Streptomycin: 100 μg/ml streptomycin.

10. Collagens:

    Collagens II, IX, and XI in their native molar proportions of $f_{II,IX,XI} = 8:1:1$.

    Purified monomeric cartilage collagens II, IX, or XI.

    Authentic fibrils fragments from cartilage of 17-day-old chicken embryos or adult chicken, juvenile or adult bovine knee joint cartilage or human osteoarthritic hip cartilage.
11. Tris buffer:

    50 mM Tris–HCl, 150 mM NaCl, pH 7.4 (for collagen purification).

    50 mM Tris–HCl, 400 mM NaCl, pH 7.4 (for in-vitro fibrillogenesis).
12. HEPES buffer: 0.1 M HEPES, 0.4 M NaCl, pH 7.4.
13. Staining wash buffer: 150 mM NaCl, 2 mM sodium phosphate, pH 7.4.
14. Adhesion blocking buffer: 2 mM Tris–HCl buffer, 150 mM NaCl, pH 7.4.
15. Collagen reconstitute buffer: 50 mM HEPES, 200 mM NaCl, pH 7.4.

3 Methods

3.1 Primary Chondrocyte Isolation (See Note 1)

1. Primary chondrocytes were obtained from sternal cartilage of 17-day-old chicken embryos [12].
2. After removal of the perichondria, the dissected sterna were washed three times in Krebs-Ringer buffer.
3. Chondrocytes were released from their extracellular matrix by overnight treatment with 1 mg/ml collagenase B in collagenase buffer at 37 °C and 5% CO_2.
4. Sedimented cells were resuspended and separated from undigested matrix by filtration through a triple layer of 100 μm pore size nylon membranes in a Swinnex filter.
5. Residual collagenase was removed by two gentle centrifugation steps at $600 \times g$ for 7 min with substitution of the supernatant with fresh Krebs-Ringer buffer.
6. After a further centrifugation step, the cell pellet was resuspended in DMEM with 100 U/ml penicillin and 100 μg/ml streptomycin (sterile filtered) and quantified using a Neubauer counting chamber.

3.2 Collagen Purification

Mixtures of cartilage collagens II, IX, and XI in their native molar proportions $f_{II,IX,XI} = 8:1:1$ were isolated from chicken embryo chondrocytes cultured in suspension of agarose as described in

[13]. The separation of the three collagen types occurred by ion-exchange chromatography as described in [3].

Authentic fibril fragments were obtained from sternal cartilage of 17-day-old chicken embryos or adult chicken, juvenile and adult bovine knee joint cartilage, and human osteoarthritic hip cartilage [14] as follows:

1. Homogenize small cartilage samples for 20 s on ice in 500 μl of Tris buffer (three times).
2. Short centrifugation step at 2500 × *g* for 3 min.
3. Collect the supernatant and homogenize the pellet again.
4. Repeat this procedure three times.
5. Combine all supernatants for use in experiments.

3.3 Cell Adhesion Assay

1. Use non-tissue grade, 96-well microtiter plates.
2. Before coating, mark the bottom of each well using a pen as a point of reference for microscopic images before and after the mechanical removal of non-adherent cells.
3. *Experiments with monomeric collagens:* Coat cell culture dishes with 100 μl/well of solutions of collagens II, IX, and XI at molar fractions $f_{II,IX,XI} = 8:1:1$ (total collagen concentration: 150 μg/ml) in HEPES buffer overnight at 4 °C (*see* **Notes 2** and **3**).
4. *Experiments with collagen fibrils:* Induce collagen fibril formation in the wells by diluting 50 μl of 300 μg/ml total concentration of monomeric collagens II, IX, and XI dissolved in HEPES buffer with 50 μl of distilled water and incubate for 3 h at 37 °C (*see* **Notes 2** and **4**).
5. Fibronectin coating as positive control: Add 100 μl of HEPES buffer, containing 20 μg/ml of fibronectin to the wells.
6. Complete all coatings overnight at 4 °C.
7. Remove unbound substrate proteins by washing twice with 0.1% BSA in DMEM.
8. Block unspecific binding sites with 0.5% BSA in DMEM for 60 min.
9. Further washing step with 0.1% BSA in DMEM.
10. Optional second blocking step with 10 μg/ml recombinant DDR2-receptors in adhesion blocking buffer (in control experiments without DDR2) for 1 h (blocking of potential binding sides for DDR2-receptors of chondrocytes on collagens).
11. Washing of the wells twice with 0.1% BSA in DMEM.

12. Add 7.5×10^4 cells/100 μl freshly isolated cranial chondrocytes diluted in DMEM supplemented with penicillin/streptavidin.
13. Attachment of the cells to the substrates for 45 min (short-term adhesion assay) (*see* **Note 5**).
14. Take photographs of each well with an inverse microscope (phase-contrast (pH 1), ten-fold magnification, point of reference should be visible).
15. Remove unbound cells by gentle agitation on a Vortex shaker at 800 rpm for 15 s.
16. Wash two times with DMEM.
17. Add 100 μl DMEM to the wells and take photographs of the previously selected areas.
18. For analysis, merge the corresponding microscopic photographs in silico and count the cells in the overlapping areas.
19. Quantify bound cells by direct counting in at least five randomly selected representative fields.
20. Pool the results from three independent experiments.
21. Determine means and standard deviations with standard algorithms.

3.4 Immunoelectron Microscopy

1. Spot 15 μl aliquots of authentic fibril fragments, reconstituted fibrils, or monomeric collagens onto sheets of Parafilm.
2. Absorption of aggregates on 200 square mesh nickel grids coated with formvar/carbon by floating on the drops for 15 min.
3. Wash grids with staining wash buffer.
4. Block for 60 min with 2% dried skimmed milk in PBS.
5. Treatment of the grids with PBS, containing 2 mM $MgCl_2$ and 375 ng of soluble recombinant human integrins α1β1, α2β1, and α10β1 and 450 ng of the activating antibody 9EG7 [15] for 60 min. In controls: replace $MgCl_2$ by 10 mM EDTA.
6. Washing of grids with PBS.
7. Incubate the grids with a suspension of 18 nm colloidal gold particles coated with goat antibodies against rat immunoglobulins in PBS, containing 0.2% dried skimmed milk for 60 min.
8. Wash grids five times with distilled water (removal of all remaining phosphate buffer contaminants).
9. Negative staining of the grids with 2% uranyl acetate in distilled water for 15 min.
10. Dip grids briefly into a drop of distilled water.
11. Dry grids with filter paper.
12. Analysis by transmission electron microscopy (Fig. 1).

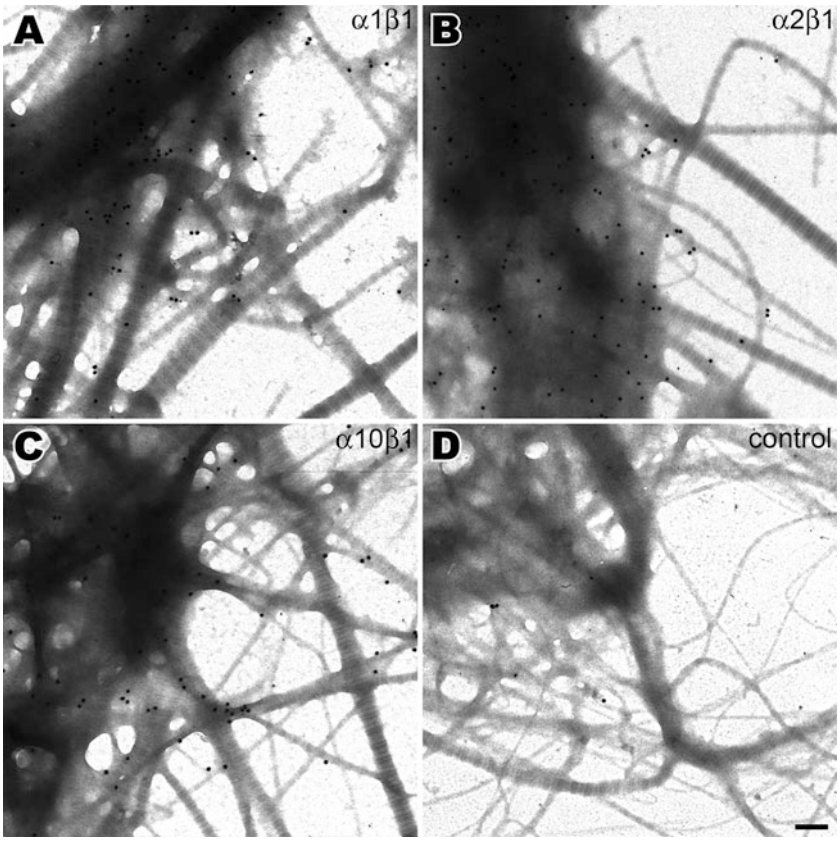

Fig. 1 Electron micrographs of ultrastructural immuno-localization of the binding of soluble integrins to isolated authentic cartilage matrices. After blocking of unspecific binding sites, recombinant integrins were added and detected by anti-integrin-β1-antibodies (9EG7). The binding of integrins to cartilage fibrils with peripheral components is visualized by immuno-gold transmission electron microscopy. Scale bar = 200 nm

3.5 Binding Experiments on Grids for Transmission Electron Microscopy

3.5.1 Purified Monomeric Cartilage Collagens II, IX, or XI

1. Coat grids at room temperature for 15 min with purified monomeric cartilage collagens II, IX, or XI in HEPES buffer in order to prevent fibril formation.
2. Wash grids with PBS.
3. Block for 60 min with 2% dried skimmed milk in PBS.
4. Incubate with 375 μg/ml of soluble recombinant α1β1-, α2β1-, α10β1-integrins in the presence of the integrin-activating antibody 9EG7 and 2 mM $MgCl_2$ or 10 mM EDTA (negative control).
5. Wash with PBS.
6. Expose the grids to immuno-gold particles coated with anti-IgG antibodies.
7. Stain samples with 2% uranyl acetate for 15 min.
8. Take electron micrographs from five randomly selected fields.
9. Count gold particles/field.

3.5.2 Reconstituted Collagen Fibrils Containing Collagen Types II, IX, and XI

1. Reconstitute collagen fibrils from monomeric collagens II, IX, and XI (300 μg/ml total concentration) as adhesion substrates by adjusting the buffer salinity to collagen reconstitute buffer and warm to 37 °C as described above (*see* **Note 6**).
2. Apply 10 μl of 150 μg/ml total concentration of reconstituted collagen fibril suspension onto the surface of 400 square mesh uncoated nickel grids.
3. Wash the attached collagen fibrils five times with PBS in order to remove remaining collagen monomers (*see* **Note 7**).
4. Block unspecific binding sites with 2% dried skimmed milk in PBS.
5. Incubate the reconstituted collagen fibrils with integrins and primary and secondary antibodies as described under 3.4.
6. Coat the grids with a thin layer of carbon generated on mica plates and float on distilled water. Put the grid under the carbon layer floating on water surface and take out both the grid and the carbon layer.
7. Dry the grid carefully on filter paper.
8. Stain the samples with 2% (v/w) uranyl acetate.
9. Analyze samples by transmission electron microscopy.

3.5.3 Binding Experiments with Solutions of 25 μg/ml Recombinant, GST-Tagged Chicken α1I- and α2I-Domains

1. Coat grids with 10 μl purified monomeric cartilage collagens II, IX, or XI in HEPES buffer or 10 μl reconstituted collagen fibril suspension from monomeric collagens II, IX, and XI at room temperature for 15 min.
2. Wash grids with PBS.
3. Block for 60 min with 2% dried skimmed milk in PBS.
4. Add solutions of 25 μg/ml recombinant, GST-tagged chicken α1I- or α2I-domains to the grids.
5. Wash grids with PBS in order to remove unbound material.
6. Incubate grids with a murine monoclonal anti-GST antibody for the detection of bound I-domains.
7. Wash with PBS.
8. Expose the grids to immuno-gold particles coated with anti-IgG antibodies.
9. Stain samples with 2% uranyl acetate for 15 min.
10. Analysis by transmission electron microscopy.
11. Quantification of gold particles per unit area (150 μm^2) by counting on several randomly selected EM-observation fields. Determine means and standard deviations by standard procedures.

Double-labelling experiments for peripheral non-collagenous macromolecules and for integrins were carried out in a two-step

procedure, firstly with specific antibodies to components of the fibril periphery, e.g., aggrecan, fibronectin, decorin, COMP, matrilin-1, or collagen VI, and with 12 nm gold particles coated with specific anti-immunoglobulins, followed by washing, and secondly with soluble integrins, the antibody 9EG7 (*see* Subheading 3.4), and with 18 nm gold particles coated with goat antibodies against rat immunoglobulins.

All incubation and washing steps with buffers and reagents as described before (*see* Subheading 3.4).

4 Notes

1. The described protocol for the analysis of integrin-mediated interactions was established by using chondrocytes and cartilage-specific ECM components; however, the underlying mechanisms are probably true for many other cell types, and therefore, the protocol is easy to adapt for use with other cells.
2. The state of aggregation should be controlled in preparation for transmission electron microscopy. Therefore, after coating overnight, attached collagens should be scratched off from the cell culture dishes. 10 μl drops of this material should be placed on formvar-carbon-coated grids, stained with 2% uranyl acetate for 15 min, and analyzed by transmission electron microscopy.
3. Collagens will remain in their molecular form, and fibril formation is prevented under these buffer and temperature conditions.
4. Quantitative conversion of the monomeric collagens into fibril suspensions by changing the buffer and temperature conditions.
5. We have used a short-term adhesion assay as cells produce rapidly their own ECM after seeding to the cell culture dishes. Therefore, we ensure that we analyze the interaction of cells with the different coatings, rather than with a mixture of coating and ECM components produced by the cells.
6. We have changed our previously published method for the reconstitution of collagen fibril from monomeric collagen types II, IX, and XI as the efficiency of fibril formation is more efficient using HEPES buffer instead of Tris buffer (Fig. 2).
7. Although fibril formation is essentially complete under these conditions, traces of collagen monomers should be removed by percolating the above buffer solution through the uncoated grids into filter paper. This procedure should be repeated several times with PBS.

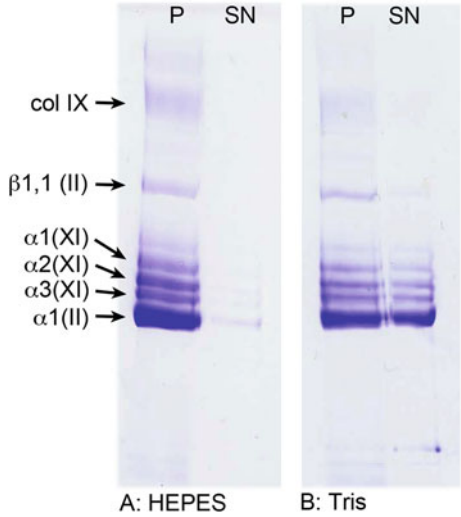

Fig. 2 Characterization of the efficiency of the in vitro fibrillogenesis of ternary mixtures of cartilage collagens: SDS-PAGE of collagen samples after completion of in vitro fibrillogenesis on 4.5–15% polyacrylamide gels without prior reduction with β-mercaptoethanol. The collagens were dissolved in (**a**) HEPES buffer or (**b**) Tris buffer, and fibril formation was initiated by adding an equal volume of distilled water and by heating up to 37 °C. After completion of fibril formation, collagens were centrifuged, and the formed collagen fibrils were collected as a pellet (P), whereas still remaining monomeric collagens were found in the supernatant (SN). In comparison to collagen mixtures dissolved in Tris buffer, collagen mixtures dissolved in HEPES buffer were nearly completely formed into collagen fibrils (compare SN in A with SN in B). *P* pellet, *SN* supernatant

Acknowledgments

This work was supported by Deutsche Forschungsgemeinschaft grants BR1497/4-1 and EB177/9-1 to PB and JAE and a grant from BBSRC UK (BB/I011226/1) to BL.

References

1. Lu P, Weaver VM, Werb Z (2012) The extracellular matrix: a dynamic niche in cancer progression. J Cell Biol 196:395–406
2. Nelson CM, Bissell MJ (2006) Of extracellular matrix, scaffolds, and signaling: tissue architecture regulates development, homeostasis, and cancer. Annu Rev Cell Dev Biol 22:287–309
3. Blaschke UK, Eikenberry EF, Hulmes DJS, Galla HJ, Bruckner P (2000) Collagen XI nucleates assembly and limit lateral growth of cartilage fibrils. J Biol Chem 275:10370–10378
4. Mercier I, Lechaire JP, Desmouliere A, Gaill F, Aumailley M (1996) Interactions of human skin fibroblasts with monomeric or fibrillar collagens induce different organization of the cytoskeleton. Exp Cell Res 225:245–256
5. Woltersdorf C, Bonk M, Leitinger B, Huhtala M, Käpylä J, Heino J et al (2017) The binding capacity of α1β1-, α2β1- and α10β1-integrins depends on noncollagenous surface macromolecules rather than the collagens in cartilage fibrils. Matrix Biol 63:91–105

6. Eble JA, Beermann B, Hinz HJ, Schmidt-Hederich A (2001) α2β1 integrin is not recognized by rhodocytin but is the specific, high affinity target of rhodocetin, an RGD-independent disintegrin and potent inhibitor of cell adhesion to collagen. J Biol Chem 276:12274–12284
7. de Santana Evangelista K, Andrich F, Figueiredo de Rezende F, Niland S, Cordeiro MN, Horlacher T et al (2009) Plumieribetin, a fish lectin homologous to mannose-binding B-type lectins, inhibits the collagen-binding α1β1 integrin. J Biol Chem 284:34747–34759
8. Tulla M, Pentikäinen OT, Viitasalo T, Käpylä J, Impola U, Nykvist P et al (2001) Selective binding of collagen subtypes by integrin α1I, α2I, and α10I domains. J Biol Chem 276:48206–48212
9. Käpylä J, Ivaska J, Riikonen R, Nykvist P, Pentikainen O, Johnson M, Heino J (2000) Integrin alpha2 I-domain recognizes type I and type IV collagens by different mechanisms. J Biol Chem 275:3348–3354
10. Leitinger B (2003) Molecular analysis of collagen binding by the human discoidin domain receptors, DDR1 and DDR2: identification of collagen binding sites in DDR2. J Biol Chem 278:16761–16769
11. Xu H, Raynal N, Stathopoulos S, Myllyharju J, Farndale RW, Leitinger B (2011) Collagen binding specificity of the discoidin domain receptors: binding sites on collagens II and III and molecular determinants for collagen IV recognition by DDR1. Matrix Biol 30:16–26
12. Böhme K, Winterhalter KH, Bruckner P (1995) Terminal differentiation of chondrocytes in culture is a spontaneous process and is arrested by transforming growth factor-beta2 and basic fibroblast growth factor in synergy. Exp Cell Res 216:191–198
13. Bruckner P, Hörler I, Mendler M, Houze Y, Winterhalter KH, Eich-Bender SG, Spycher MA (1989) Induction and prevention of chondrocyte hypertrophy in culture. J Cell Biol 109:2537–2545
14. Mendler M, Eich-Bender SG, Vaughan L, Winterhalter KH, Bruckner P (1989) Cartilage contains mixed fibrils of collagen types II, IX, and XI. J Cell Biol 108:191–197
15. Lenter M, Uhlig H, Hamann A, Jenö P, Imhof B, Vestweber D (1993) A monoclonal antibody against an activation epitope on mouse integrin chain β1 blocks adhesion of lymphocytes to the endothelial integrin α6β1. Proc Natl Acad Sci U S A 90:9051–9055

Part IV

Collagen in Health and Disease

Chapter 13

Assessing Collagen Deposition During Aging in Mammalian Tissue and in *Caenorhabditis elegans*

Alina C. Teuscher, Cyril Statzer, Sophia Pantasis, Mattia R. Bordoli, and Collin Y. Ewald

Abstract

Proper collagen homeostasis is essential for development and aging of any multicellular organism. During aging, two extreme scenarios are commonly occurring: a local excess in collagen deposition, for instance during fibrosis, or a gradual overall reduction of collagen mass. Here, we describe a histological and a colorimetric method to assess collagen levels in mammalian tissues and in the nematode *Caenorhabditis elegans*. The first method is the polychrome Herovici staining to distinguish between young and mature collagen ratios. The second method is based on hydroxyproline measurements to estimate collagen protein levels. In addition, we show how to decellularize the multicellular organism *C. elegans* in order to harvest its cuticle, one of the two major extracellular matrices, mainly composed of collagen. These methods allow assessing collagen deposition during aging either in tissues or in whole organisms.

Key words Collagen, Aging, Tissue, Herovici staining, Hydroxyproline, Cuticle, Isolation, Freeze-cracking, Age-synchronizing, Extracellular matrix, *C. elegans*

1 Introduction

Cells and tissues are embedded within extracellular matrices (ECM), which are important for tissue geometry, integrity, and function [1]. In mammals, collagens constitute about 30% of the total protein mass in the body and are the major component of the ECM [2]. In humans, collagen turnover can be extremely slow as observed in the lens of the eye and in cartilage structures (with a half-life time of 114 years [3–5]) or extremely fast, within 72 h after physical exercise, in Achilles tendons [6]. Hence, depending on the tissue or organ, some collagens are synthesized, secreted, and integrated in the ECM once early in life and are not replaced over

Alina C. Teuscher and Cyril Statzer contributed equally to this chapter.

Irit Sagi and Nikolaos A. Afratis (eds.), *Collagen: Methods and Protocols*, Methods in Molecular Biology, vol. 1944, https://doi.org/10.1007/978-1-4939-9095-5_13, © Springer Science+Business Media, LLC, part of Springer Nature 2019

the entire lifetime, whereas other collagens have a higher turnover rate.

During aging, the connective tissue or ECM integrity declines due to accumulation of damage from collagen fragmentation, oxidation, and glycation [2, 7–12] leading to a continuous reduction of collagen mass, as best illustrated by wrinkles and sagging skin [13, 14], but also observed in other connective tissues that support organ function. This deterioration in ECM integrity has been implicated in many age-dependent diseases, such as diabetes, cancer, chronic liver diseases, and cardiovascular diseases [2, 7–12]. In parallel, the accumulation of molecular damage [15], chronic inflammation (inflammaging) [16], or injury during aging might locally drive abnormal collagen deposition resulting in fibrosis [17]. These observations suggest that in general the overall collagen mass tends to decline as a function of age, but due to the increasing incidence of damage or injury, atypical collagen accumulation might occur more locally in certain parts of the body. Therefore, proper assessment of the extent of collagen deposition might reveal novel insights in maintenance and remodelling of the ECM during aging.

A direct role for proper collagen deposition and remodelling during aging has become evident by studying model organisms, such as mice and *C. elegans*. For instance, deficits in the ECM remodelling enzyme (MMP14) lead to premature aging, short lifespan, and cell senescence in mice [18]. Interestingly, long-lived mice preserve connective tissue elasticity and integrity during aging [19, 20]. Consistent with these findings, in the nematode *C. elegans*, collagen synthesis declines during aging. Moreover, most if not all long-lived *C. elegans* mutants delay this progressive decrease in collagen mass [21]. Delaying this progressive reduction in collagen mass by actively prolonging the biosynthesis of collagens during lifetime is required and sufficient for healthy aging and longevity in *C. elegans* [21].

In addition to studying the progressive age-dependent decrease in ECM integrity in mice, *C. elegans* provides additional unique opportunities to explore this phenomenon during aging, since (1) *C. elegans* is transparent, thereby allowing ECM components to be tagged by fluorescent proteins to directly monitor ECM homeostasis and integrity noninvasively in vivo [21], and (2) *C. elegans* is a well-established aging model because of its short lifespan (about 3 weeks) and powerful established genetics. However, histological methods are not as commonly used or even developed in *C. elegans* compared to mice. Below, we describe a histological method (Herovici staining) to be used for both *C. elegans* and mammalian tissue, a colorimetric method (measurement of hydroxyproline levels) to estimate collagen levels in both *C. elegans* and mammalian tissue, and a technique to isolate the

C. elegans cuticle (extracellular matrix) to be used for further assessment of collagen deposition or other analysis.

The Herovici staining protocol [22] is one of the several histological methods used to assess the extent of collagen deposition in a tissue. Compared to other widely used collagen staining techniques (e.g., picrosirius red staining or Masson's trichrome staining), the Herovici protocol allows to distinguish between young (e.g., collagen III) and mature collagen (e.g., collagen I) without cross-polarized filters, providing an obvious advantage in the visualization and analysis of processes, where changes in collagen ratios are expected or known to occur. The sequential use of several dyes results in a polychromatic staining, with young collagen appearing blue, mature collagen colored pink to red, and cytoplasm counterstained in yellow (Fig. 1). Moreover, cell nuclei are stained dark blue to black by hematoxylin. The Herovici method is mostly used for histological studies in skin; however, the staining protocol works well in other tissues or organs too (e.g., liver or lung).

Collagen levels can also be determined by using hydroxyproline measurements. Collagens have characteristic [Gly-X-Y] repeats, whereby glycine is at every third position, X is frequently proline, and Y is frequently 4-hydroxyproline. These prolonged stretches of [Gly-X-Y] repeats in the collagen protein are important to form a stable triple helix from the three constitutive collagen chains [2]. Since collagens are enriched in hydroxyproline and this post-translational modification is not as common as in other proteins, measuring hydroxyproline abundancy results in an estimate of total collagen levels [23, 24]. For a more accurate estimation of collagen amounts by hydroxyproline measurements, one could decellularize tissue samples of interest [25] in order to decrease the levels of other hydroxyproline-containing proteins found in the cytoplasm.

Here we show techniques to isolate the *C. elegans* cuticle, a procedure to further enrich for collagen content during sample harvesting for instance for hydroxyproline measurements. The cuticle and basement membranes are the two major extracellular matrices of *C. elegans* [26]. The *C. elegans* cuticle is mainly composed of collagens [27]. Two methods are described to isolate this cuticle. The first and simpler method was modified from Leushner et al. [28], and the second method was adapted from Cox et al. [29]. The advantages and differences of each method are explained in Subheading 3 below.

In summary, collagen deposition and remodelling become faulty during aging resulting either in a generalized decline in collagen biosynthesis or, locally, in excessive and amorphous collagen deposition (fibrosis). The methods described here are tailored for mammalian tissue samples and the organism *C. elegans* to enable the quantification of total collagen protein levels (hydroxyproline measurement), to distinguish between young and mature collagen ratios, and to enrich for collagen-containing extracellular

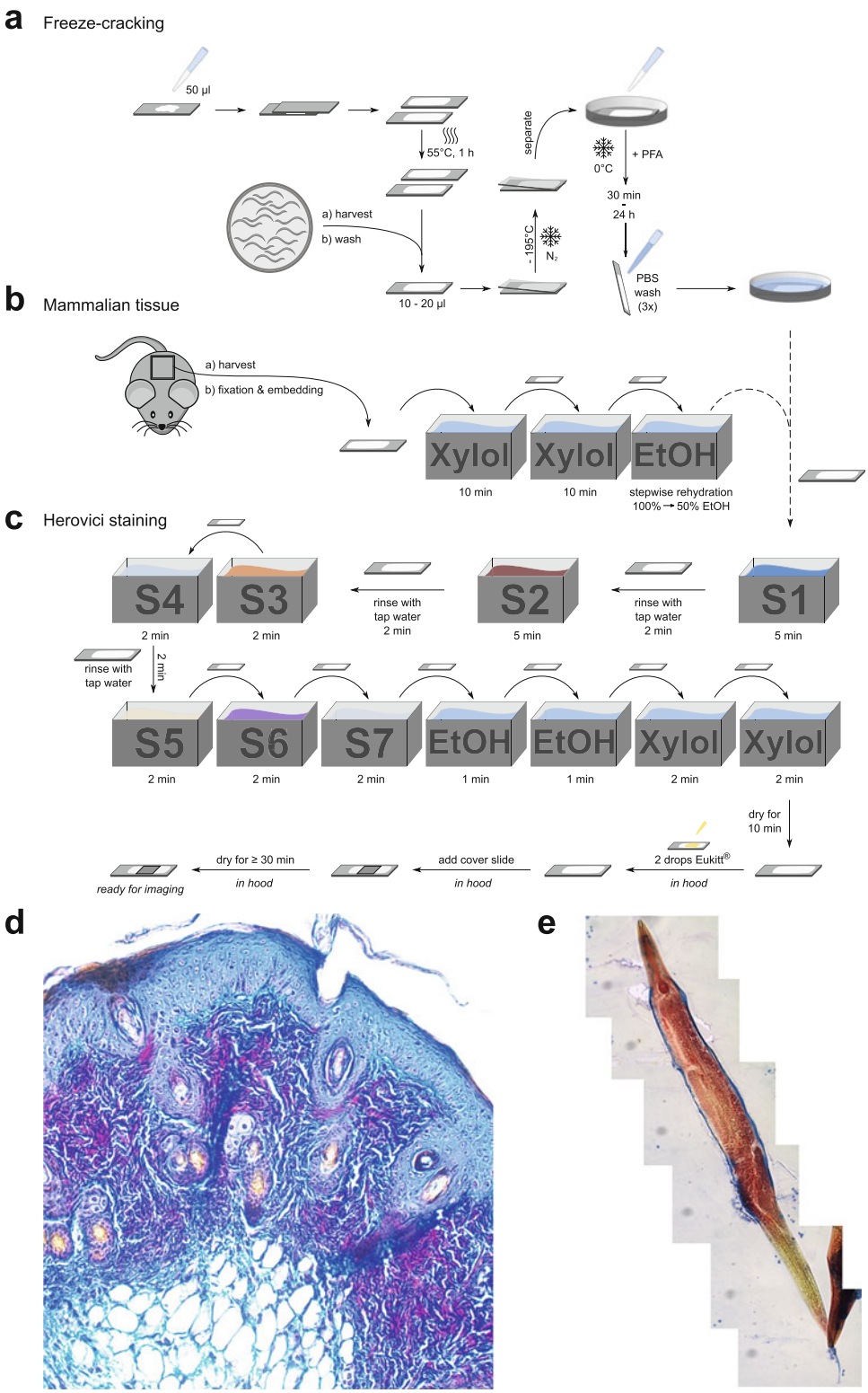

Fig. 1 Herovici staining for mammalian tissue and *C. elegans*. (**a**–**c**) A schematic of the individual steps of the Herovici staining described in Subheading 3 (*see* Subheading 3.1). (**a**) Freeze-cracking of *C. elegans*

matrices in *C. elegans*. In addition, we describe in detail how to synchronize *C. elegans* in order to start a time course for aging studies. With these methods in hand, the investigator should be able to assess collagen deposition during aging and in age-related pathologies.

2 Materials

General mouse necropsy and mammalian tissue harvesting or *C. elegans* maintenance are described elsewhere [30, 31]. *C. elegans* strains can be acquired from the *Caenorhabditis* Genetics Center (CGC, https://cgc.umn.edu, [31]). For the preparation of all solution, distilled water and analytical grade reagents are recommended. All Herovici staining solutions are stored in glass bottles at room temperature protected from light. Disposal of waste materials should be carried out according to specific local regulations. Suitable protection (lab coat, safety glasses, and gloves) and the use of a fume hood are recommended for the handling of acids and other hazardous substances.

2.1 Herovici Staining for Mammalian Tissue and C. elegans

1. 70–100% EtOH.
2. Microscope slides with cut edges and frosted end, 1 mm thick, 76 × 26 mm.
3. Poly-L-Solution: 400 mg Sigma P1524 poly-L-Lysine; 0.2 g sodium azide (0.1%) in 200 ml ddH_2O. Can be reused and stored at 4 °C.
4. PBS: 8 g NaCl, 0.2 g KCl, 1.42 g Na_2HPO_4, 0.24 g KH_2PO_4, pH adjusted with HCl to pH 7.4.
5. PFA: 4% paraformaldehyde solution in PBS.
6. Herovici's Solution 1: Add 270 ml of deionized water to a glass beaker. Weigh 1.25 g celestine blue powder, and transfer it to the glass beaker. Weigh 15 g of aluminum potassium sulfate dodecahydrate (CAS: 7784-24-9; 31242, Merck) and add it to the glass beaker. Heat and boil the solution until the powders are dissolved (approximately 3–5 min). Let the solution cool down to room temperature, and transfer to a 500 ml graduated cylinder, and add distilled water to a final volume of 300 ml.

Fig. 1 (continued) (*see* Subheading 3.1.1). (**b**) Mammalian tissue harvesting and deparaffinization (*see* Subheading 3.1.2). (**c**) Shared part of the Herovici staining protocol for both *C. elegans* and mammalian tissue (*see* Subheading 3.1.3). (**d**) Herovici-stained mouse skin specimen. The young collagen (collagen type III) is stained in blue, whereas the mature collagen (collagen type I) is stained in red. Cytoplasm is counterstained in yellow and cell nuclei dark blue to black. Three layers forming the skin (epidermis, dermis, hypodermis) can be identified. (**e**) Herovici-stained *C. elegans* at day 1 of adulthood

Add 60 ml of glycerol once the solution has cooled down to room temperature (*see* **Note 1**).

7. Herovici's Solution 2: Weigh 1 g of hematoxylin powder, transfer it to a glass beaker, and dissolve it in 100 ml of 95% ethanol in distilled water (alcoholic hematoxylin). Weigh 4.5 g of ferrous II sulfate ($FeSO_4$) powder and 2.5 g ferric III chloride ($FeCl_3$) powder, and transfer them to a separate glass beaker containing 298 ml distilled water. Add 2 ml of 36% (concentrated) hydrochloric acid (toxic, *see* **Note 2**). Stir the solution on a magnetic stirrer till powders dissolve (*see* **Note 3**). Mix this solution with the alcoholic hematoxylin from **step 1** (*see* **Notes 4–6**).
8. Herovici's Solution 3: Add 300 ml of distilled water to a glass beaker. Weigh 1.25 g of metanil yellow, and transfer it to the glass beaker. Add 25 drops (use a 1 ml pipette tip) of glacial acetic acid (*see* **Notes 7** and **8**).
9. Herovici's Solution 4: Add 1800 ml of distilled water to a glass beaker. Add 9 ml of glacial acetic acid (toxic, *see* **Notes 7** and **9**).
10. Herovici's Solution 5: Weigh >1 g of lithium carbonate (Li_2CO_3) powder, and dissolve it in 78 ml distilled water (aqueous Li_2CO_3). The solution will be saturated (*see* **Note 10**). Add 1 ml of saturated aqueous Li_2CO_3 to 500 ml distilled water to a glass beaker (*see* **Notes 11** and **12**).
11. Herovici's Solution 6: Weigh 0.15 g of methyl blue powder, and dissolve it in 150 ml distilled water in a glass beaker. Weigh 0.2 g of acid fuchsin powder, and dissolve it in 150 ml of saturated aqueous picric acid in a separate glass beaker. Mix the two solutions together. Add 30 ml of glycerol and 0.15 ml of saturated aqueous Li_2CO_3 (*see* **Notes 11** and **13**).
12. Herovici's Solution 7: Add 10 ml of glacial acetic acid to 1 L of distilled water (*see* **Notes 7** and **14**).

2.2 Total Collagen Quantification for Mammalian Tissue and C. elegans

1. 5 N NaOH.
2. 5% sodium hypochlorite solution (or household bleach).
3. Sterile ddH_2O.
4. M9 buffer: 3 g KH_2PO_4, 7.52 g Na_2HPO_4, 5 g NaCl, and 0.05 g $MgSO_4$ in 1 L ddH_2O, autoclaved [31].

2.2.1 Age Synchronization of C. elegans

2.2.2 Total Protein Quantification

1. QuickZyme Protein Assay Kit (QuickZyme Biosciences) or equivalent kit from other manufactures suitable for protein quantification of acid hydrolyzed samples.
2. Pierce™ BCA Protein Assay Kit (Thermo Fisher) or equivalent kit from other manufactures.

2.2.3 Total Collagen Quantification

1. QuickZyme Total Collagen Kit (QuickZyme Biosciences) or equivalent kit from other manufactures.
2. Aqueous hydrogen chloride solution: 4 M, 6 M, and 12 M.

2.3 Materials for Cuticle (Extracellular Matrix) Isolation in C. elegans

1. Sodium dodecyl sulfate (SDS) buffer: 1% SDS in ddH_2O.
2. Triton X-100 buffer: 0.5% Triton X-100 in ddH_2O.
3. 15 ml glass conical centrifuge tubes with screw gaps.

2.3.1 Cuticle Isolation (Freeze-Thaw Protocol)

2.3.2 Cuticle Isolation (ST Buffer Protocol)

1. M9 buffer: 3 g KH_2PO_4, 7.52 g Na_2HPO_4, 5 g NaCl, 0.0493 g $MgSO_4$ in 1 L ddH_2O, autoclaved.
2. Sonication buffer: 10 mM Tris–HCl, pH 7.4; 1 mM EDTA; in ddH_2O.
3. 0.1 M PMSF buffer: 1 mM phenylmethanesulfonylfluoride in isopropanol.
4. ST buffer: 1% SDS; 0.125 M Tris–HCl, pH 6.8; in ddH_2O.

3 Methods

3.1 Herovici Staining for Mammalian Tissue and C. elegans

All procedures are carried out at room temperature, if not indicated otherwise. Glass slides with tissue sections fixed in 4% paraformaldehyde (PFA in PBS) are used for the Herovici staining protocol. Reusable Herovici solutions can be poured back in their original container. At the end of this procedure, tissue sections will be ready to be imaged under the microscope. In this section, we first describe the harvesting and preparation for mammalian tissue (*see* Subheading 3.1.1) and then for *C. elegans* (*see* Subheading 3.1.2) followed by the shared methodical part (*see* Subheading 3.1.4).

3.1.1 Harvesting and Preparing Mammalian Tissue Sections (Fig. 1a)

1. Organs or tissues of interest are harvested as described elsewhere [30], fixed in 4% paraformaldehyde for 24 h at 4 °C, submersed in increasing concentrations of ethanol, embedded into paraffin [32], and sectioned with a microtome (3.5 μm sections).
2. Deparaffinize tissue sections by immerging the glass slides in xylol for 10 min. Repeat this step once for a total of two.
3. Rehydrate the tissue sections stepwise from 100% to 50% (100%, 96%, 90%, 80%, 70%, 50%) ethanol by immerging the glass slides for 1 min in each solution.
4. Continue the protocol; *see* Subheading 3.1.4.

3.1.2 Preparation of Poly-L-Slides for Freeze-Cracking of C. elegans

1. Clean microscope slides with Kimwipes and 70%–100% EtOH.
2. Pipette 50 μl Poly-L-Solution on the non-frosted part of the microscope slide. Place another microscope slide on top, so that the transparent parts completely overlay and the frosted parts are hanging over on the opposite sides.
3. Slide the two slides apart: one side per slide should now be covered with a thin layer of Poly-L-Solution.
4. Turn the slides around, so that the Poly-L-Solution sides are facing upward, and place the slides in a 55 °C incubator for 1 h to dry. Slides can now be used directly or stored for several months in a clean slide box at 4 °C.

3.1.3 Harvesting and Preparing C. elegans Samples Using a Freeze-Cracking Method (Fig. 1b)

The described *C. elegans* freeze-cracking method was adopted from Duerr 2006 [33]. For freeze-cracking use a minimum of 4000 *C. elegans* or better about 8000–12,000 *C. elegans* (*see* **Note 15**). For a protocol to age-synchronize and culture *C. elegans* (*see* Subheading 3.2.2):

1. Place the fixation solution (4% paraformaldehyde (PFA in PBS)) and several empty 10 cm petri dishes on ice in order to pre-chill for later use.
2. Wash *C. elegans* off culturing plates using M9 buffer, and collect them in a 15 ml conical centrifuge tube.
3. Centrifuge for 1 min at 1000 rpm (standard table centrifuge is ca. 200 × *g*; *see* **Note 16**), and remove supernatant. Wash the *C. elegans* until the supernatant is clean and no bacteria are visible (*see* **Note 17**).
4. Rinse *C. elegans* by filling up the 15 ml conical centrifuge tube with 14 ml ddH_2O, centrifuge for 1 min at 1000 rpm (200 × *g*), remove supernatant, and add ddH_2O to the pelleted *C. elegans* to a total volume of 100 μl.
5. Using a glass Pasteur pipette, place a small drop of animals (ca.10–20 μl) on a Poly-L-Solution covered slide. Wait shortly to let the *C. elegans* settle on the slide. Use the pipette to spread the *C. elegans* out so that they do not overlap.
6. Carefully place another Poly-L-Solution covered slide on top of the slide with the *C. elegans* so that the Poly-L-covered sides face each other, while the frosted parts are not overlapping.
7. Put on safety goggles and gloves. Hold the two slides slightly pressed together into liquid nitrogen until the bubbling stops. Take the slides out. Wait for ca. 20 s. Then start to snip with your finger carefully against one of the slides until they rip apart.

8. Check which slide has most of the *C. elegans* attached to it, and place either only this slide or both slides separately into individual empty 10 cm petri dishes, which are standing on ice.
9. Pipette 100–200 μl 4% PFA pre-chilled onto the *C. elegans* covered part of the slides. Fix the *C. elegans* by incubating the slides at 4 °C for at least 30 min or up to 24 h.
10. After fixation, rinse the slides gently at least three times with PBS. Proceed immediately with staining, or store the slides in a Coplin jar or petri dish containing PBS at 4 °C for several days.

3.1.4 The Herovici Staining for Both Mammalian Tissue and C. elegans (Fig. 1c)

1. Immerse slides in Solution 1 for 5 min (*see* **Note 1**).
2. Rinse slides under running tap water for 2 min (*see* **Note 18**).
3. Immerse slides in Solution 2 for 5–6 min (*see* **Notes 5**, **6**, and **19**).
4. Rinse slides under running tap water for 2 min (*see* **Note 18**).
5. Immerse slides in Solution 3 for 2 min (*see* **Note 8**).
6. Transfer slides directly to Solution 4 for 2 min (*see* **Note 9**).
7. Rinse slides under running tap water for 2 min (*see* **Note 18**).
8. Immerse slides in Solution 5 for 2 min (*see* **Note 12**).
9. Transfer slides directly to Solution 6 for 2 min (*see* **Note 13**).
10. Transfer slides directly to Solution 7 for 2 min (*see* **Note 14**).
11. Immerse the slides in 100% ethanol for 1 min. Repeat this dehydration step once for a total of two.
12. Immerse the slides in xylol for 2 min. Repeat this step once for a total of two.
13. Let the slides dry for a minimum of 10 min (*see* **Note 20**).
14. Mount the slides with a mounting media (e.g., Eukitt®), and let them dry under a fume hood (*see* **Note 21**).
15. After adding the cover slip, the specimen is ready for imaging. Examples of a Herovici-stained mammalian tissue section and a *C. elegans* are shown in Fig. 1d, e, respectively.

3.2 Total Collagen Quantification for Mammalian Tissue and C. elegans

The collagen content in a tissue or whole-organism sample can be determined in multiple ways (Fig. 2). It is generally advised to select the normalization entity to be as conclusive as possible. Here, total collagen quantification is combined with either absolute animal number (*C. elegans*) or with total protein determination for both mammalian tissue and *C. elegans*. Here, we focus mainly on how to establish aged *C. elegans* cultures and on the assessment of collagen levels in *C. elegans*, since the use of hydroxyproline measurement in mammalian tissue is well-established.

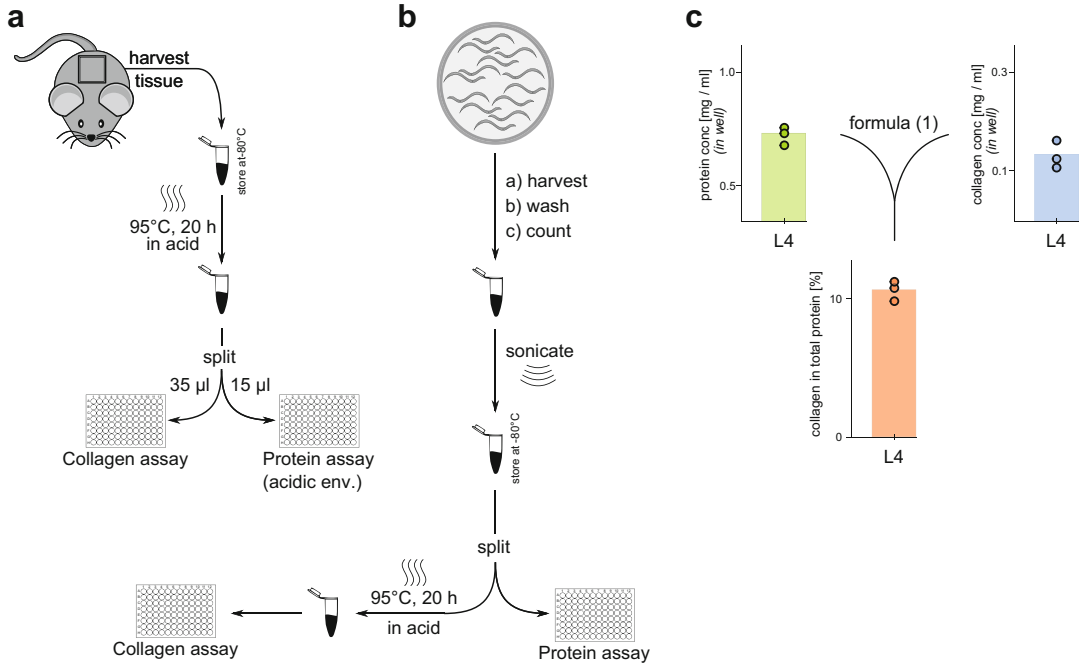

d

$$\frac{collagen}{protein} = \frac{[Coll_{Well}] \cdot dil_{assay}^{coll} \cdot dil_{digestion}}{[Protein_{Well}] \cdot dil_{assay}^{prot}} \quad (1)$$

$$\frac{collagen}{individual} = \frac{[Coll_{Well}] \cdot dil_{assay}^{coll} \cdot dil_{digestion}}{\frac{\overline{animals}_{counted}}{Vol_{counted}}} \quad (2)$$

$[Coll_{Well}]$ = collagen concentration per well as obtained by the assay.

dil_{assay} = dilution in assay well (e.g. to avoid signal saturation).

$dil_{digestion}$ = dilution through HCl and then water addition.

$\frac{\overline{animals}_{counted}}{Vol_{counted}}$ = average of counted animals divided by the volume used for counting (e.g. 20 µl).

$\frac{collagen}{protein}$ = ratio of collagen to total protein, can be expressed as collagen in total protein [%]

Fig. 2 Total collagen quantification using hydroxyproline assay for mammalian tissue and *C. elegans*. (**a**, **b**) Schematic of the collagen assay that can be performed using mammalian tissue (**a**) as well as *C. elegans* samples (**b**). Please *see* Subheading 3 (*see* Subheading 3.2) for detailed protocol steps. (**c**) An example of how to quantify the collagen-to-protein ratio for larval L4 stage *spe-9(hc88) C. elegans* samples is shown. (**d**) Formula (1) shows how to calculate the ratio of collagen content to total protein levels. The dilution term referring to the digestion is omitted when the total protein content is determined using the hydrolyzed sample. Formula (2) shows how to normalize collagen content per individual *C. elegans*

3.2.1 Mammalian Tissue (Fig. 2a)

There are several ways to assess hydroxyproline levels in mammalian tissues. Here, we briefly outline the use of a colorimetric method using the QuickZyme Kit for both hydroxyproline and total protein measurements. The advantage of this protocol is that each HCl hydrolyzed tissue sample can be split to measure (1) hydroxyproline levels to estimate collagen protein content and (2) to measure total protein levels from the same sample in order to normalize the collagen content to total protein levels. Equivalent kits or protocols

from other manufacturers can be used. For more details, please follow the manufacturer's instruction.

1. Organs or tissues of interest are harvested as described elsewhere [30]. Frozen organs/tissues and formalin-fixed or paraffin-embedded tissues can also be used.
2. Hydrolyze the tissue in 6 M HCl in a safety centrifuge tube for 16 h at 95 °C in a one 1:10 ratio of wet tissue weight to acid volume (*see* **Note 22**). Split the hydrolysate: 35 μl is used for collagen quantification and 15 μl to assess the total protein content (*see* **Note 23**).
3. To generate the standard curve for the colorimetric quantification of collagen and total protein levels, please follow the manufacturer's instructions.

3.2.2 Synchronizing *C. elegans* for an Age-Dependent Time Course Analysis (Fig. 2b)

C. elegans samples are prepared in one batch and harvested in user-defined intervals over the animal's lifespan. To age-synchronize the *C. elegans* population, we describe a bleach preparation protocol to harvest eggs from gravid *C. elegans* adults. For each time point and condition, 2000–5000 animals are required; therefore ca. 10,000–100,000 eggs should be harvested in the initial lysis step.

1. Use multiple culturing plates containing a large amount of gravid *C. elegans* adults to perform a population lysis. Wash the culturing plates with sterile H_2O. Pipette the H_2O across the plate several times to loosen *C. elegans* that are stuck onto the bacterial lawn.
2. Collect the liquid containing the *C. elegans* in a sterile 15 ml conical centrifuge tube. Centrifuge for 1 min at 1000 rpm (standard table centrifuge is ca. 200 × *g*; *see* **Note 24**). Discard supernatant. Wash residual bacteria away from *C. elegans* by filling up the 15 ml conical centrifuge tube with sterile H_2O, spin down, and discard the supernatant. Repeat this step until the supernatant is clear. Spin down to pellet gravid *C. elegans*, and add H_2O to a total volume of 3.5 ml.
3. Put on gloves and eye protection. Add 1 ml of 5% sodium hypochlorite solution (or household bleach), and add 0.5 ml of 5 N NaOH. Close 15 ml conical centrifuge tube, and shake well. In 1-min intervals, hold the 15 ml conical centrifuge tube under a dissecting scope to observe lysis of gravid *C. elegans*, and shake well after observation to optimize lysis. Once almost all *C. elegans* are lysed, add M9 buffer to a total volume of 15 ml, and centrifuge at 3000 rpm (ca. 1800 × *g*) for 1 min to pellet the eggs (*see* **Note 25**). Discard supernatant, and wash the eggs at least three times by filling up to 15 ml with M9 buffer and re-pelleting the eggs by centrifugation at 3000 rpm (ca. 1800 × *g*) for 1 min. Discard the supernatant (*see* **Note 26**).

4. After lysis and subsequent washing steps, the samples are incubated while rotating for 12 h in M9 buffer supplemented with 5 μg/ml cholesterol.
5. 500–1000 larval L1 *C. elegans* larvae are placed on each 10 cm culturing plate. If a temperature-sensitive sterile strain is used, the sterility mechanism has to be activated at the needed time point (*see* **Note 27**). If floxuridine (FUDR) is used to avoid offsprings, the animals are transferred at the larval L4 stage to 50 μg/ml FUDR culturing plates (*see* **Notes 28** and **29**).
6. 2000–5000 *C. elegans* (2–10 plates) are harvested for each condition and time point. Transfer all animals from the plates to a 15 ml conical centrifuge tube. The animals are centrifuged briefly at low speed (200 rpm, ca. 8 × *g*) to pellet aged *C. elegans* adults. The suspension containing unhatched eggs or larvae (if FUDR is used) is aspirated and discarded. Repeat this washing step three times or until only the desired *C. elegans* adults are present and supernatant is clear (*see* **Note 30**).
7. From the last wash that was filled up with M9 buffer to a total volume of 14 ml, take five times 20 μl aliquots, and place these aliquots on a petri dish lid to count the number of animals in each 20 μl drop using a dissecting scope (*see* **Notes 31** and **32**). To estimate total number of *C. elegans*, average the number of *C. elegans* from each 20 μl drop and multiply by 700 to get an estimate of the total number of *C. elegans* present in 14 ml sample.
8. Centrifuge for 1 min at 1000 rpm (ca. 200 × *g*) to softly pellet *C. elegans*. Discard supernatant. Use a glass Pasteur pipette to transfer the *C. elegans* pellet to a labelled 1.5 ml Eppendorf collection tube, fill up with sterile H_2O to a total volume of 200 μl, and store at −80 °C (*see* **Notes 16**, **33**, and **34**).
9. At the end of the time course, once all samples have been collected, proceed by thawing all tubes. At least 3–5 freeze-thaw cycles should be performed by thawing at room temperature and freezing in liquid nitrogen (or dry ice with EtOH or by placing back into the −80 °C).
10. Then sonicate all samples on ice until all animals are disrupted. The *C. elegans* cuticle is the hardest to break. With a standard sonication device, it will take several repeats to break down all *C. elegans* (*see* **Note 35**).

3.2.3 Total Protein Quantification for C. elegans (Fig. 2)

To determine the total collagen content as a fraction of total protein abundance, the total protein content has to be determined separately.

1. Pipette 25 μl of each sonicated sample as well as of the provided standard solutions into a 96-well plate, and quantify the total protein content following the manufacturer's instructions (Pierce™ BCA Protein Assay Kit, Thermo Fisher, or equivalent kit from other manufacturers). If needed, dilute the sample with M9.
2. Use a plate reader to quantify the color change at the specified wavelength.

3.2.4 Total Collagen Quantification for *C. elegans* (Fig. 2)

Here, we determine the total collagen abundance by digesting the sample and directly measuring the concentration of the amino acid hydroxyproline in each sample.

1. The sonicated samples are transferred into heat-stable tubes provided by the kit manufacturer (QuickZyme Total Collagen Kit, QuickZyme Biosciences, or equivalent kit from other manufacturers). The provided collagen standard does not require to be sonicated but is otherwise treated identically as the samples.
2. According to the manufacturer's instructions, the sample and standard are mixed with 12 M HCl solution and incubated for 20 h at 95 °C.
3. In brief, after the digestion the supernatant is isolated, the acid content lowered, assay buffer added, and the plate incubated at room temperature for 20 min followed by the addition of the detection reagent and subsequent incubation at 60 °C for 1 h. The color change is quantified using a plate reader (*see* **Note 36**).
4. The total collagen content per sample in a well can be directly determined through the measured color change. In a first step, the collagen reference sample (1.2 mg/ml of rat tail collagen) is used to generate a standard curve relating the magnitude of the color change to the collagen content of the well. Over the used concentration range, this relationship is approximately linear. With the standard curve available, the collagen content of the samples can be quantified. It must be noted that the collagen standard supplied in the QuickZyme Biosciences Kit contains rat tail collagen. To validate the use of rat tail collagen as a reference for hydroxyproline levels for *C. elegans* collagens, the potential hydroxyproline occurrences on the Y position in the *C. elegans* [Gly-X-Y] triple repeats in collagens were estimated in silico. The relative proline abundance on the Y position is similar between *C. elegans* and rat tail collagens (personal communication Jan M. Gebauer). Example results for *C. elegans* protein and collagen concentration are shown in Fig. 2b.
5. The total collagen-to-total protein ratio can be determined by combining the measured collagen and protein concentrations according to formula (1). In the case of *C. elegans*, the total collagen abundance per animal can be calculated by subjecting

the measured collagen concentration to formula (2). All formulas to determine the relative collagen contents are depicted in Fig. 2c.

3.3 Methods for Cuticle (Extracellular Matrix) Isolation in *C. elegans*

3.3.1 Cuticle Isolation (Freeze-Thaw Protocol)

This method was modified from Leushner et al. [28], for the use in *C. elegans*. The two advantages of using this protocol compared to the ST protocol is (1) its simplicity and (2) the SDS-cleaned cuticles might still contain Schiff base products or other adducts that might be of importance of the desired analysis [34]. The major problem with this protocol is that the *C. elegans* cuticle tends to stick on plastic; this can be avoided by using glass materials instead. All steps after the freeze-thawing should be carried out on ice, except steps involving SDS. We recommend to use about 12,000 *C. elegans* per sample to isolate a sufficient number of cuticles. Please *see* Subheading 3.2.2 for a protocol to age-synchronize the *C. elegans* samples. An example of an aged *C. elegans* (7-day adult) is shown in Fig. 3a for comparison with the isolated cuticles Fig. 3b, c.

1. Use 12,000 adult *C. elegans* (about 8–12 full culturing plates). Pipette around 3 ml M9 buffer on each plate. Gently tilt plates to collect the liquid on one side, and carefully pipette the M9 buffer several times across the plate to loosen up the *C. elegans* stuck on the bacterial food lawn. Transfer the animals from the plates into a 15 ml conical centrifuge tube.
2. Wash the *C. elegans* three times with 15 ml ddH_2O by centrifugation at around 1000 rpm (ca. 200 × *g*) for 1 min, and discard the supernatant (*see* **Note 33**).
3. After the last washing step, discard the supernatant again, and use a glass Pasteur pipette to transfer the *C. elegans* pellet into a 1.5 ml Eppendorf microfuge tube (*see* **Note 37**). Centrifuge 1.5 ml tube at around 100 × *g* for 30 s, discard supernatant, and fill up with ddH_2O to 100 μl.
4. Freeze the tubes in liquid nitrogen for 1 min (or until frozen), followed by a thawing step at room temperature. Repeat this freeze-thaw cycle at least three times.
5. Sonicate the samples five times in intervals of 20 s each at an amplitude of 80% with 20 s breaks on ice in between (Sonoplus mini20 from Bandelin) (*see* **Note 38**).
6. Use a glass Pasteur pipette to transfer the ruptured *C. elegans* to 15 ml glass tubes (with screw gaps) (*see* **Note 39**), and suspend them in 10 ml 1% SDS solution, followed by overnight incubation onto a rotor at 37 °C. The 1% SDS should wash out all the internal cells and organs from the disrupted cuticles (Fig. 3b).

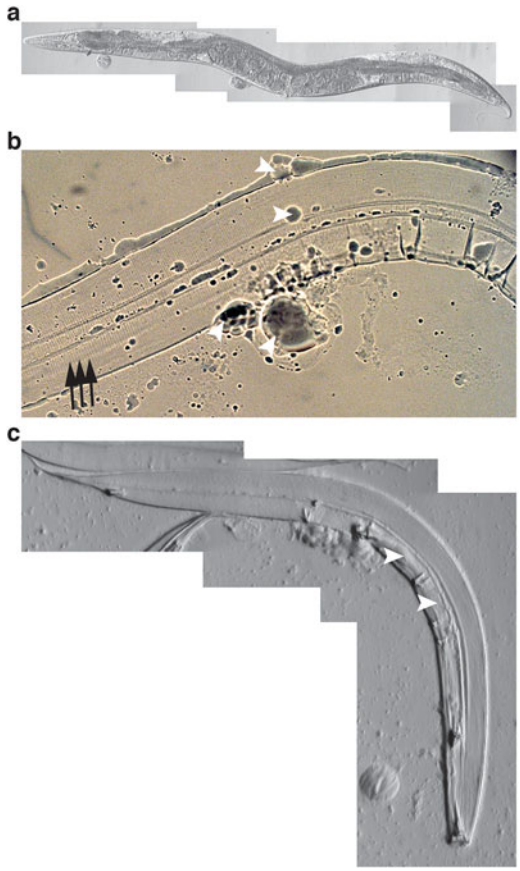

Fig. 3 Isolated *C. elegans* cuticles. (**a**) Differential contrast image of a day 7 adult *C. elegans*. Anterior to the left and ventral side down. (**b**) Intact *C. elegans* cuticle after 1% SDS before washing step. Black arrows point to the annuli structure of the cuticle. White arrowheads point to debris. (**c**) Intact *C. elegans* cuticle after washing. Sometimes other extracellular matrices, such as the basement membranes of the gonad (white arrowheads), are still attached

7. On the following day, wash the cuticles with sterile ddH_2O containing 0.5% Triton-X by centrifuging at 3000 rpm (ca. 1800 × *g*) for 1 min; discard supernatant (*see* **Note 40**).
8. The cleaned cuticles (Fig. 3c) can now be further processed, analyzed, or stored at −20 °C.

3.3.2 Cuticle Isolation (ST Buffer Protocol)

This method was adapted from Cox et al. [29]. Please *see* Subheading 3.3.1 for the comparison with the other cuticle isolation freeze-thaw method, and *see* Subheading 3.2.2 for a protocol to age-synchronize the *C. elegans* samples. All steps after the sonication should be carried out on ice, except steps involving SDS.

1. Collect 12,000 (adult) *C. elegans* with M9 buffer in a 15 ml tube as described in the first step of Subheading 3.3.1.

2. Wash the *C. elegans* pellet three times by centrifugation at around 1000 rpm (ca. 200 × *g*) for 1 min, and discard the supernatant (*see* **Note 33**).
3. After the last washing step, discard the supernatant, and resuspend the *C. elegans* pellet in 5 ml sonication buffer. Incubate on ice for 10 min.
4. Add 30 μl 0.1 M PMSF to the solution, and sonicate five times for 20 s with an amplitude of 80% with 20 s breaks on ice in between (Sonoplus mini20 from Bandelin).
5. Wash the ruptured *C. elegans* cuticles three times with the sonication buffer by centrifugation at 1500 rpm (around 450 × *g*) for 1 min, and discard the supernatant.
6. Discard the supernatant, and transfer the cuticles with a glass Pasteur pipette to a 1.5 ml microfuge tube (*see* **Note 37**). Centrifuge the 1.5 ml tube at around 100 × *g* for 30 s, discard supernatant, and fill up with sonication buffer to 100 μl.
7. Add 1 ml ST buffer, and heat the tube for 2.5 min at 95 °C.
8. Incubate the tubes on a rotator overnight at room temperature.
9. Wash cuticles three times with 0.5% Triton-X in sterile ddH_2O by centrifuging at 3000 rpm (ca. 1800 × *g*) for 1 min; discard supernatant.
10. The cleaned cuticles can now be further processed, analyzed, or stored at −20 °C.

4 Notes

4.1 Herovici Staining for Mammalian Tissue and C. elegans

1. Solution 1 can be reused.
2. Caution. Hydrochloric acid should be handled with care and added to the solution under a fume hood.
3. If required filter the solution to eliminate visible impurities.
4. Alcoholic hematoxylin and the ferrous solution are prepared separately and mixed at the end.
5. Solution 2 has a shelf life of approximately 2–3 months due to oxidation.
6. Solution 2 can be reused.
7. Caution. Glacial acetic acid should be handled with care and added to the solution under a fume hood.
8. Solution 3 can be reused.
9. Do not reuse Solution 4.

10. By adding more than 1 g of Li_2CO_3 to 78 ml distilled water, the solution will be saturated. Do not shake to try to dissolve the precipitate. Let the solution stand.
11. Pipette the aqueous Li_2CO_3 from the top without disturbing the precipitate accumulated on the bottom of the container.
12. Solution 5 can be reused.
13. Solution 6 can be reused.
14. Do not reuse Solution 7.
15. Per plate you can make 2–3 freeze-cracked *C. elegans* slides.
16. To prevent adhesion of animals to plastic pipette tips, one can either add 0.5% Triton-X as a detergent or switch to glass pipettes.
17. Bacteria prevent the animals to properly stick to the slides.
18. Regular water. This step can be performed directly in the sink.
19. A longer incubation may be needed if the solution has not been freshly prepared.
20. A longer drying time (30 min–1 h) is perfectly fine.
21. Eukitt® will need approximately 30 min to dry.

4.2 Total Collagen Quantification for Mammalian Tissue and C. elegans

22. Ideally, a 1:10 ratio of wet tissue weight to acid volume is recommended, with a minimal volume of 200 μl 6 M HCl per tube. For example, 50 mg of tissue mixed with 500 μl of 6 M HCl can be used.
23. To be able to relate the total collagen content of the sample as robustly as possible to the total protein abundance, we recommend to measure the later directly in the hydrolyzed sample. To be able to quantify the free amino acid level present in the acidic hydrolyzed sample, a suitable kit has to be chosen. We recommend the Total Protein Assay, QuickZyme Biosciences.
24. When centrifuging *C. elegans*, either turn off the breaks or turn down the deceleration to a minimum.
25. In general, complete lysis can take about 4–8 min. Hence, it is important to regularly check if all *C. elegans* are lysed. If lysis is performed for too long, the eggs will suffer from increasing damage.
26. Sometimes three washes are not enough to wash out all bleach solution. Hence, check by smelling the 15 ml conical centrifuge tube if bleach odor is still present.
27. We recommend the *C. elegans* mutant *spe-9(hc88)*. Due to a temperature-sensitive defect in spermatogenesis, the animals are not able to lay fertilized eggs when shifted to 25 °C during development. To ensure all animals are sterile, L1 animals can be cultured at 25 °C until day 1 or 2 of adulthood.

28. To avoid food scarcity, check the grow-up plates often, and if needed, transfer to fresh plates.
29. To check the effectiveness of the intervention, a selected number of plates can be used for validation by, for example, placing a fluorescent reporter strain on them.
30. Since the collagen content is changing over the lifespan of *C. elegans*, it is crucial to work with age-synchronous populations. Thus, all eggs and larvae must be removed as best as possible. This can be achieved by transferring animals often to new plates and rigorous washing or through filtration.
31. Because adult *C. elegans* will sink to bottom of the conical centrifuge tube, shake the 15 ml conical centrifuge tube well between taking the aliquots for counting. Try to pipette from the middle of the 15 ml conical centrifuge tube for consistency.
32. Use a pipette with a large orifice to sample *C. elegans* during the counting procedure. Since adults grow in size, a too small pipette tip can lead to an underestimation of older populations.
33. At this step of the protocol is a good time point for a break or to wait until all time points from before are collected, for instance, if you collect daily samples over the 2–3 weeks lifespan of *C. elegans*.
34. It is recommended to fill up all sample *C. elegans* pellets to 200 μl to simplify the downstream steps.
35. Example sonication configuration using a Bandelin Sonoplus, UW mini20 device: Amplitude 80%, 30s intervals, pulse 1.0 s on, 1.0 s off. However, using a more powerful sonicator is recommended to accelerate *C. elegans* fragmentation.
36. It is advised to perform a few test reactions prior to processing the entire batch for both quantification methods to be able to adjust sample dilution should it be too concentrated.

4.3 Cuticle (Extracellular Matrix) Isolation in C. elegans

37. *C. elegans* tend to stick on the plastic tip or on the plastic tubes. Hence, make sure to use a glass Pasteur pipette and pipette the *C. elegans* on the bottom of the plastic tube to avoid sticking on the side of the tube.
38. If the cuticles in the freezing protocol are ruptured too much, you can consider performing only the freezing and thawing cycles or only sonication.
39. One of the major problems is losing too many cuticles or *C. elegans*. Therefore, use always glass pipettes to transfer worms and cuticles.
40. Triton-X prevents the cuticles from sticking to the tubes during the washing steps.

Acknowledgments

We thank Marjolein Wildwater for sharing her improved freeze-cracking protocol, Eline Jongsma for her assistance in adapting the freeze-cracking protocol, Salome Brütsch and Hayley Hiebert for their help to develop the *C. elegans* Herovici staining protocol, Anna Bircher for contributing to the early stages of the cuticle isolation protocols and imaging cuticles, Max Hess for providing the *C. elegans* example image, and Jan M. Gebauer for bioinformatic prediction of potential prolines in collagens that might become hydroxylated in *C. elegans*. Some *C. elegans* strains were provided by the CGC, which is funded by NIH Office of Research Infrastructure Programs (P40 OD010440). This work was supported by the Swiss National Science Foundation [PZ00P3 161512] to S.P. and M.R.B. and [PP00P3 163898] to A.C.T., C. S., and C.Y.E. Alina C. Teuscher and Cyril Statzer contributed equally to this work.

References

1. Hynes RO (2009) The extracellular matrix: not just pretty fibrils. Science 326:1216–1219
2. Ricard-Blum S (2011) The collagen family. Cold Spring Harb Perspect Biol 3: a004978–a004978
3. Sivan S-S, Wachtel E, Tsitron E et al (2008) Collagen turnover in normal and degenerate human intervertebral discs as determined by the racemization of aspartic acid. J Biol Chem 283:8796–8801
4. Heinemeier KM, Schjerling P, Heinemeier J et al (2016) Radiocarbon dating reveals minimal collagen turnover in both healthy and osteoarthritic human cartilage. Sci Transl Med 8:346ra90–346ra90
5. Toyama BH, Hetzer MW (2013) Protein homeostasis: live long, won't prosper. Nat Rev Mol Cell Biol 14:55–61
6. Kjaer M, Langberg H, Miller BF et al (2005) Metabolic activity and collagen turnover in human tendon in response to physical activity. J Musculoskelet Neuronal Interact 5:41–52
7. Myllyharju J, Kivirikko KI (2001) Collagens and collagen-related diseases. Ann Med 33:7–21
8. Fisher GJ, Quan T, Purohit T et al (2009) Collagen fragmentation promotes oxidative stress and elevates matrix metalloproteinase-1 in fibroblasts in aged human skin. Am J Pathol 174:101–114
9. Shoulders MD, Raines RT (2009) Collagen structure and stability. Annu Rev Biochem 78:929–958
10. Sell DR, Monnier VM (2012) Molecular basis of arterial stiffening: role of glycation–a mini-review. Gerontology 58:227–237
11. Snedeker JG, Snedeker JG, Gautieri A et al (2014) The role of collagen crosslinks in ageing and diabetes–the good, the bad, and the ugly. Muscles Ligaments Tendons J 4:303–308
12. Myllyharju J (2004) Collagens, modifying enzymes and their mutations in humans, flies and worms. Trends Genet 20:33–43
13. Fenske NA, Lober CW (1986) Structural and functional changes of normal aging skin. J Am Acad Dermatol 15:571–585
14. Shuster S, Black MM, McVitie E (1975) The influence of age and sex on skin thickness, skin collagen and density. Br J Dermatol 93:639–643
15. López-Otín C, Blasco MA, Partridge L et al (2013) The hallmarks of aging. Cell 153:1194–1217
16. Franceschi C, Campisi J (2014) Chronic inflammation (inflammaging) and its potential contribution to age-associated diseases. J Gerontol A Biol Sci Med Sci 69(Suppl 1):S4–S9
17. Wynn TA (2007) Common and unique mechanisms regulate fibrosis in various fibroproliferative diseases. J Clin Investig 117:524–529
18. Gutiérrez-Fernández A, Soria-Valles C, Osorio FG et al (2015) Loss of MT1-MMP causes cell senescence and nuclear defects which can be reversed by retinoic acid. EMBO J 34:1875–1888

19. Flurkey K, Papaconstantinou J, Miller RA et al (2001) Lifespan extension and delayed immune and collagen aging in mutant mice with defects in growth hormone production. Proc Natl Acad Sci U S A 98:6736–6741
20. Wilkinson JE, Burmeister L, Brooks SV et al (2012) Rapamycin slows aging in mice. Aging Cell 11:675–682
21. Ewald CY, Landis JN, Porter Abate J et al (2015) Dauer-independent insulin/IGF-1-signalling implicates collagen remodelling in longevity. Nature 519:97–101
22. Herovici C (1963) A polychrome stain for differentiating precollagen from collagen. Stain Technol 38:204–205
23. McAnulty RJ (2005) Methods for measuring hydroxyproline and estimating in vivo rates of collagen synthesis and degradation. Methods Mol Med 117:189–207
24. Qiu B, Wei F, Sun X et al (2014) Measurement of hydroxyproline in collagen with three different methods. Mol Med Rep 10:1157–1163
25. Naba A, Clauser KR, Hynes RO (2015) Enrichment of extracellular matrix proteins from tissues and digestion into peptides for mass spectrometry analysis. J Vis Exp 101: e53057
26. Kramer JM (2005) Basement membranes, WormBook : the online review of C elegans biology. pp 1–15
27. Page AP and Johnstone IL (2007) The cuticle, WormBook : the online review of C elegans biology. pp 1–15
28. Leushner JR, Semple NL, Pasternak J (1979) Isolation and characterization of the cuticle from the free-living nematode *Panagrellus silusiae*. Biochim Biophys Acta 580:166–174
29. Cox GN, Kusch M, Edgar RS (1981) Cuticle of *Caenorhabditis elegans*: its isolation and partial characterization. J Cell Biol 90:7–17
30. Treuting PM, Snyder JM (2015) Mouse necropsy. Curr Protoc Mouse Biol 5:223–233
31. Stiernagle T (2006) Maintenance of *C. elegans*, WormBook : the online review of C elegans biology. pp 1–11
32. Fischer AH, Jacobson KA, Rose J et al (2008) Paraffin embedding tissue samples for sectioning. CSH Protoc 2008:pdb.prot4989
33. Duerr JS (2006) Immunohistochemistry, WormBook : the online review of C elegans biology. pp 1–61
34. Davis BO, Anderson GL, Dusenbery DB (1982) Total luminescence spectroscopy of fluorescence changes during aging in *Caenorhabditis elegans*. Biochemistry 21:4089–4095

Chapter 14

Procollagen C-Proteinase Enhancer 1 (PCPE-1) in Liver Fibrosis

Efrat Kessler and Eyal Hassoun

Abstract

Fibrosis is characterized by excessive deposition of collagen and additional extracellular matrix (ECM) components in response to chronic injuries. Liver fibrosis often results from chronic hepatitis C virus infection and alcohol abuse that can deteriorate to cirrhosis and liver failure. Current noninvasive diagnostic methods of liver fibrosis are limited in their ability to detect and differentiate between early and intermediate stages of fibrosis. New biomarkers of fibrosis that reflect ECM turnover are therefore badly needed. Procollagen C-proteinase enhancer 1 (PCPE-1), a connective tissue glycoprotein that functions as a positive regulator of C-terminal procollagen processing and subsequent collagen fibril assembly, is a promising candidate. Its tissue distribution and expression profile overlap those of collagen, and its expression in fibrosis is upregulated in parallel to the increase in collagen expression. The potential of PCPE-1 as a biomarker of liver fibrosis was recently established using a CCl_4 mouse model of liver fibrosis by showing that the increase in collagen and PCPE-1 content in the fibrotic mouse liver was reflected by elevated plasma levels of PCPE-1. This was achieved using a newly developed highly sensitive, specific, accurate, and reproducible ELISA for mouse PCPE-1, which is based on commercially available antibodies and is offered as a new research tool in the field. A similar ELISA test was developed for human PCPE-1, and preliminary results with plasma from liver fibrosis patients revealed increased plasma concentrations of PCPE-1 in some patients. The protocols of both ELISA tests are outlined herein in great detail to permit their application by any laboratory with similar interests.

Key words Collagen, Procollagen C-proteinase enhancer 1, PCPE-1, ELISA, Liver fibrosis, Biomarkers

1 Introduction

Fibrosis is defined by excessive accumulation of collagen and other extracellular matrix (ECM) components in response to chronic injuries, leading to impairment of organ function. It can affect many organs and tissues, including the liver [1–3]. In the Western Hemisphere, the main causes of liver fibrosis are chronic hepatitis C virus infection and chronic alcohol abuse that in the absence of effective therapy can deteriorate to cirrhosis with its serious

Irit Sagi and Nikolaos A. Afratis (eds.), *Collagen: Methods and Protocols*, Methods in Molecular Biology, vol. 1944, https://doi.org/10.1007/978-1-4939-9095-5_14, © Springer Science+Business Media, LLC, part of Springer Nature 2019

consequences, hepatocellular dysfunction, hepatocellular carcinoma, and liver failure [4].

Diagnosis and quantitation of liver fibrosis require accurate, reproducible, and easily applied methods and are important to make therapeutic decisions, determine prognosis, monitor disease progression, and evaluate new anti-fibrotic drugs [3–5]. Current approaches to evaluate liver fibrosis include invasive and noninvasive methods. Despite the availability of many noninvasive diagnostic methods for liver fibrosis, liver biopsy, an invasive technique, is still considered the best (gold standard) method for assessment of liver fibrosis [5, 6]. Because of its invasiveness, liver biopsy suffers several limitations, in particular risk of injury, sampling errors, high cost, and inaccurate interpretation by the observer [6, 7]. The available noninvasive methods comprise imaging techniques such as FibroScan and MRI that assess liver stiffness and immunoassays of blood markers [5, 8–11]. The blood markers are classified into direct and indirect. Direct markers are ECM components (e.g., the carboxyl propeptide of type I procollagen (PICP), the amino propeptide of type III procollagen (PIIINP), matrix metalloproteinases (MMPs), etc.) that reflect ECM turnover. The indirect markers comprise molecules released by the malfunctioning liver, including (but not limited to) α2-macroglobulin, apolipoprotein A1, haptoglobin, γ-glutamyl transferase (GGT), and bilirubin, which are components of an algorithm-based test known as FibroTest [5, 10, 11].

Noninvasive methods applied clinically rely on indirect markers. Such markers however are suitable mainly for detection of advanced disease. Their ability to detect early stages of liver fibrosis or monitor progression of fibrosis is limited [4, 12]. New direct markers are therefore badly needed [12].

Procollagen C-proteinase enhancer 1 (PCPE-1) is a 50–55 kDa extracellular matrix glycoprotein that binds to the procollagen C-propeptide and stimulates its removal by BMP-1/tolloid-like proteinases (BTPs; also known as procollagen C-proteinases or PCPs), a reaction essential for collagen fibril assembly [13, 14]. The tissue distribution of PCPE-1 overlaps that of collagen [15, 16], and its expression is upregulated in liver [17–19] and cardiac fibrosis [20–22], hypertrophic/keloid scars [23], and scarring cornea [24]. Furthermore, PCPE-1 does not affect proteolytic processing of other BTPs' substrates in the ECM [25, 26], meaning that its enhancing activity is specific to procollagen substrates. PCPE-1 has been identified in human sera [27–29] and plasma [30] and rat plasma [18]. Together these properties of PCPE-1 suggested it could be useful as a new direct marker of liver fibrosis, a possibility supported by our recent studies on a mouse CCl_4 model of liver fibrosis [19]. Using histochemical, immunofluorescence, and immunoblotting analyses, we confirmed that after 4 to 6 weeks of repeated CCl_4 administration, the treated mice developed liver

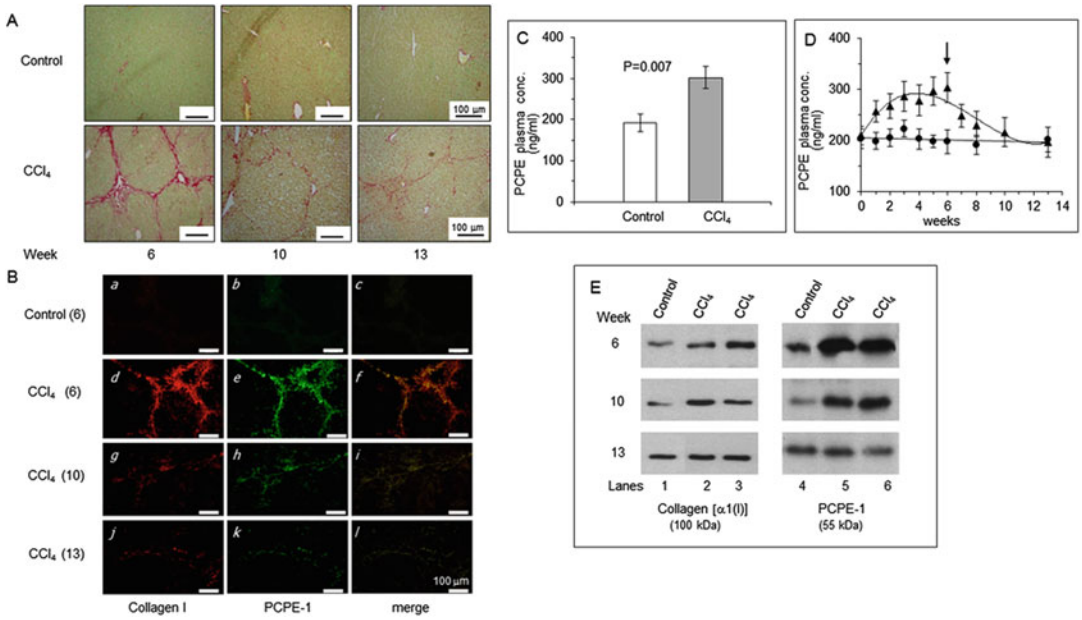

Fig. 1 Plasma concentrations of mPCPE-1 reflect the progression of liver fibrosis in CCl_4-treated mice. Mice were treated biweekly with CCl_4 for 6 weeks at which time, treatment was terminated, and the mice were followed for 7 additional weeks. Liver fibrosis was assessed at the indicated times by Sirius red collagen staining (**a**), immunofluorescence (**b**), and immunoblotting (**e**). Each panel in **a** and **b** displays results for a single randomly selected mouse from the indicated group. Numbers in brackets in **b** represent time expressed in weeks. (**c**) Plasma concentrations of PCPE-1 after 6 weeks of CCl_4 treatment are significantly higher than those of control mice ($n = 12$). (**d**) Plasma concentrations of PCPE-1 in CCl_4-treated (▲) and control (●) mice as a function of time. *Arrow*, termination of CCl_4 treatment. Results are presented as mean ± SD. (n at weeks 0 to 6 = 12; n at weeks 7–10 = 9; n at week 13 = 6). Plasma concentrations of mPCPE-1 were determined by the sandwich ELISA described herein at the indicated time points. (**e**) Immunoblot evaluating collagen I and PCPE-1 content in liver extracts from CCl_4-treated and control mice at weeks 6, 10, and 13. Samples from a single control mouse and two CCl_4-treated mice (all randomly selected) are shown. The amounts of protein applied on each lane were 4 and 36 μg for collagen and PCPE-1 detection, respectively (Reproduced from ref. 19, Open Access)

fibrosis (increased collagen and PCPE-1 content; Fig. 1a, b, e, 6 weeks). The increase in liver collagen and PCPE-1 expression was accompanied by elevated plasma levels of PCPE-1 (Fig. 1c), determined using a sandwich ELISA we developed for mPCPE-1 [19]. Furthermore, a gradual increase in the plasma levels of PCPE-1 during a 6-week CCl_4 treatment was evident (Fig. 1d). Regression of fibrosis after termination of CCl_4 treatment (i.e., a gradual decrease in liver collagen and PCPE-1 expression) was reflected by a gradual decrease in the plasma levels of PCPE-1, reaching basal levels 6–7 weeks after terminating CCl_4 administration (Figs. 1a, b, d, e and 2). Surprisingly, in another recent study by other investigators [31], in which PCPE-1 was evaluated as a biomarker of liver fibrosis in patients with chronic hepatitis B, the serum levels of PCPE-1 (determined using a commercial ELISA kit for hPCPE-1)

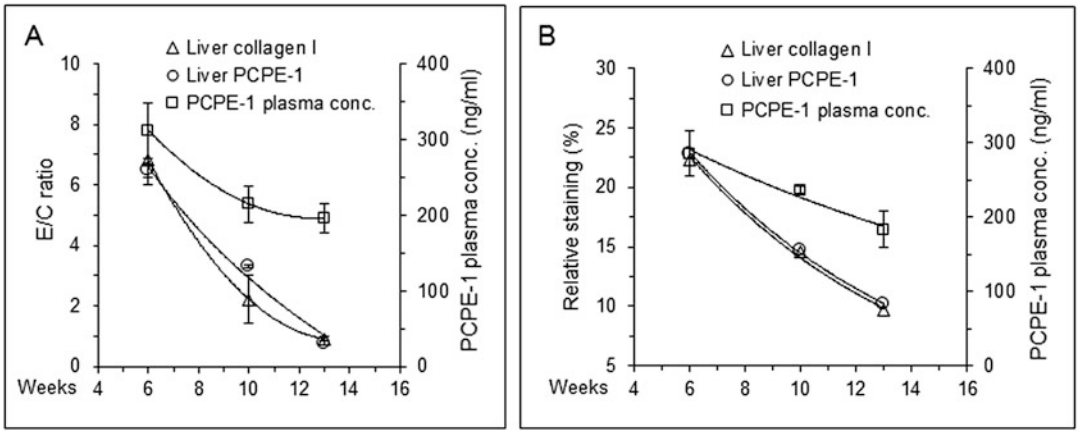

Fig. 2 Plasma concentrations of mPCPE-1 decline during liver recovery in parallel to the decline of type I collagen and PCPE-1 liver content. (**a**) The relative amounts of collagen type I and PCPE-1 were determined by densitometry of the respective protein bands in the immunoblot shown in Fig. 1e. E/C, ratio of absorbance units obtained for CCl_4-treated (E) and control (C) mice, respectively. The values are mean ± SD ($n = 2$). Values of PCPE-1 plasma concentrations represent the mean ± SD obtained at weeks 6, 10, and 13; $n = 12$, 9, and 6, respectively. (**b**) The relative amounts of PCPE-1 and collagen type I in the liver were derived from the immunofluorescence analysis shown in Fig. 1b. Values represent relative staining, expressed as the percentage of stained area out of the total area in each panel. Values correspond to data derived for a single representative mouse per group at the specified time point. Plasma concentrations of PCPE-1 are those obtained for the respective mice. Each value is the mean ± SD; $n = 4$ (Reproduced from ref. 19, Open Access)

were found to be lower than those of healthy (control) individuals. While the reason for this difference is not clear, the authors concluded that PCPE-1 might be used as a noninvasive marker of liver fibrosis.

The ELISA we developed for measuring mPCPE-1 concentrations is specific, accurate, sensitive, and reproducible (inter- and intra-assay CV <10%) [19], thus meeting the criteria mandatory for immunoassays of blood markers. Furthermore, the assay, which permits measurements of PCPE-1 in mice plasma, employs commercially available antibodies and is simple and inexpensive, so it is offered as a new research tool in the field. To permit its application in other laboratories, the ELISA procedure is described below in detail, along with a similar assay for determination of human (h) PCPE-1 [32], that permits measurements of hPCPE-1 in human plasma/serum and can be applied in studies on liver fibrosis patients.

2 Materials

2.1 Proteins and Antibodies

1. Mouse (m) PCPE-1: Purified from the culture medium of 3T6 mouse fibroblasts [13]. The concentration of the stock solution we used [19] was 250 μg/ml in 50 mM Tris–HCl,

150 mM NaCl, 5 mM $CaCl_2$, 0.1% Brij 35, pH 7.5 (*see* **Note 1**). Purified recombinant mPCPE-1 is available commercially (R&D 2239-PE) and can be used instead.

2. Human (h) recombinant PCPE-1: Purified from the culture media of 293-EBNA cells expressing the recombinant protein [25, 33]. The concentration of the stock solution used by us [32] was 0.5 mg/ml in 50 mM HEPES, 150 mM NaCl, 5 mM $CaCl_2$, and pH 7.5. Purified recombinant hPCPE-1 is also available commercially (R&D 2627-PE).
3. Bovine serum albumin (Sigma A7906).
4. Rat monoclonal antibody against mPCPE-1: The antibody (R&D MAB2239) is supplied as lyophilized powder and is stored at −20 °C. Before the first use, the content (500 μg) is dissolved in 1.0 ml of sterile PBS (final concentration 500 μg/ml) and is stored in aliquots at −80 °C.
5. Goat polyclonal rabbit antibody to mPCPE-1: The antibody (R&D AF2239) is supplied as lyophilized powder and is stored at −20 °C. Before the first use, the content (100 μg) is dissolved in 0.5 ml sterile PBS (final concentration 200 μg/ml) and is stored in aliquots at −80 °C.
6. Alkaline phosphatase (APA) conjugated rabbit antibody to goat IgG (Sigma A4187).
7. Mouse monoclonal antibody 7A1/11 against hPCPE-1: This antibody was developed in our laboratory and purified by protein G-Sepharose chromatography followed by affinity chromatography, i.e., adsorption to and elution from hPCPE-1-Sepharose beads. The hPCPE-1-specific IgG fraction obtained by affinity chromatography was stored in aliquots at −80 °C at concentrations ranging from 0.15 to 0.4 mg/ml (depending on the preparation) in 0.05 M HEPES, 0.15 M NaCl, 5 mM $CaCl_2$, and pH 7.5. Monoclonal antibody 7A1/11 is available commercially (Santa Cruz sc-73001; Sigma C2122) (*see* **Note 2**).
8. Rabbit polyclonal antibody (IgG fraction) against hPCPE-1: IgG fraction, 16 mg/ml in PBS. Stored in aliquots at −20 °C. Produced and purified in our laboratory using standard protocols. Similar antibodies are available commercially (Protein Tech 14993-1-AP; Sigma P 6243).
9. APA-conjugated goat antibody against rabbit IgG (Sigma SAB3700950).

2.2 Reagents/Buffers

1. Alkaline phosphatase substrate: para-Nitrophenylphosphate (pNPP) 5 mg tablets (Sigma S-0942).
2. Magnesium chloride ($MgCl_2$): 2 M solution in H_2O. Diluted to the desired concentration before use (*see* **Note 3**).

3. Phosphate-buffered saline (PBS): 137 mM NaCl, 2.7 mM KCl, 6.5 mM $Na_2HPO_4 \cdot 2H_2O$, 1.5 mM KH_2PO_4, pH 7.3.
4. PBST buffer (PBST): PBS + 0.05% Tween-20.
5. Blocking buffer (BSA/PBS): 5% BSA in PBS. As a routine 100 ml solution is prepared. Pipet 20 ml of 5× PBS into a 100 ml beaker. Add 80 ml of water. Add 5 g BSA. Leave for about 30 min with gentle stirring until the BSA powder is solubilized. Adjust to 100 ml with water. Store at −20 °C until use.
6. Carbonate buffer: 0.1 M sodium bicarbonate ($NaHCO_3$)/sodium carbonate (Na_2CO_3), pH 9.2. Titrate a 0.1 M $NaHCO_3$ solution with a 0.1 M solution of Na_2CO_3 to pH 9.2.
7. APA assay buffer: 1 mg/ml pNPP in 0.9 M diethanolamine-HCl, 0.5 mM $MgCl_2$, pH 9.8. Diethanolamine (DEA) buffer is prepared by adding 9.7 ml of a 99% DEA solution (Sigma D8885) to 80 ml of water and titrating to pH 9.8 using 6 N HCl. The volume is then adjusted with water to 100 ml, and the buffer is stored at 4 °C. Before the reaction (*see* Subheadings 3.1.6 and 3.2, **step 6**), pNPP is dissolved in 10 ml DEA buffer, and $MgCl_2$ (5 μl of a 1 M solution) is added to the DEA buffer solution.

2.3 Supplies and Equipment

1. Ninety-six wells plates.
2. Multichannel pipettor: For simultaneous pipetting and removal of solutions to and from eight wells.
3. Stepper: For stepwise pipetting of a constant volume from a single tip into individual wells.
4. Orbital shaker.
5. Cold room/refrigerator.
6. Incubator set to 30 °C.
7. Microplate reader capable of measuring absorbance at 405 nm, with shaking at constant temperature.

3 Methods

3.1 Sandwich ELISA for mPCPE-1

1. Adsorption of the first Ab (MAB2239): Dilute the stock solution 1:100 in carbonate buffer (final concentration 5 μg/ml; prepare just enough for the number of wells to be used; discard remaining solution). Pipet 50 μl of the Ab solution into each well in a 96 well plate using a stepper (*see* **Note 4**). Incubate over night at 4 °C.
2. Blocking: On the following day, remove and discard the first antibody solution and wash the wells twice with PBST. Add to

each well 200 μl of blocking buffer, and incubate for 2 h at 30 °C.

3. Addition of mPCPE-1 samples: Remove and discard the blocking buffer. Wash the wells four times with PBST. Tap the plate gently on the bench to fully remove residual amounts of PBST. Pipet 50 μl/well of an mPCPE-1 sample diluted in blocking buffer, in duplicates for the standard curve and in triplicates for samples with unknown mPCPE-1 concentrations (e.g., diluted plasma). Assign three wells for determination of basal OD levels (blanks; all of the reagents except PCPE-1). To these wells, pipet 50 μl of blocking buffer instead of a PCPE-1 sample. Incubate for 2 h at 30 °C (*see* **Note 5**).
4. Addition of the second Ab (goat polyclonal antibody to mPCPE-1). Prepare a 0.1 μg/ml solution of the antibody in blocking buffer. Remove and discard the PCPE-1 samples, and wash the wells four times with PBST. Pipet 50 μl of the second Ab solution into each well using a stepper, and incubate for 1 h at 30 °C.
5. Addition of APA-conjugated rabbit anti goat IgG antibody: Dilute the antibody 1:2000 in blocking buffer. Remove and discard the second Ab solution, and wash the wells four times with PBST, drying the wells by tapping gently on the bench. Pipet into each well 50 μl of the diluted APA-conjugated antibody. Incubate for 45 min at 30 °C.
6. Addition of APA substrate solution: Remove and discard the APA-conjugated antibody solution, and wash the wells four times with PBST. Add to each well 100 μl of a freshly prepared alkaline phosphatase substrate solution using a stepper. Place the plate in an ELISA plate reader pre-equilibrated to 30 °C with shaking. Follow the rate of increase in absorbance at 405 nm (due to release of the chromophore para-nitro-phenol) with constant shaking and recording absorbance at 5 min intervals for about 30 min. Altogether, up to and including this step, the procedure is accomplished in 2 days.
7. Calculation of mPCPE-1 concentrations: Absorbance values are converted to mPCPE-1 concentrations expressed as ng/ml based on the standard curve (Fig. 3a) and corrected for the dilutions as follows: (1) calculate the average OD/min value obtained for the blanks and for each PCPE-1 sample; (2) calculate the net OD/min values for each PCPE-1 concentration by subtracting the average blank value; (3) from the calibration curve (created using the net average values derived for known mPCPE-1 concentrations), calculate the mOD/min value corresponding to 1 ng mPCPE (per well; 50 μl), and use this value to derive the amount of mPCPE-1 in 50 μl of the unknown PCPE-1 sample; and (4) calculate concentration first

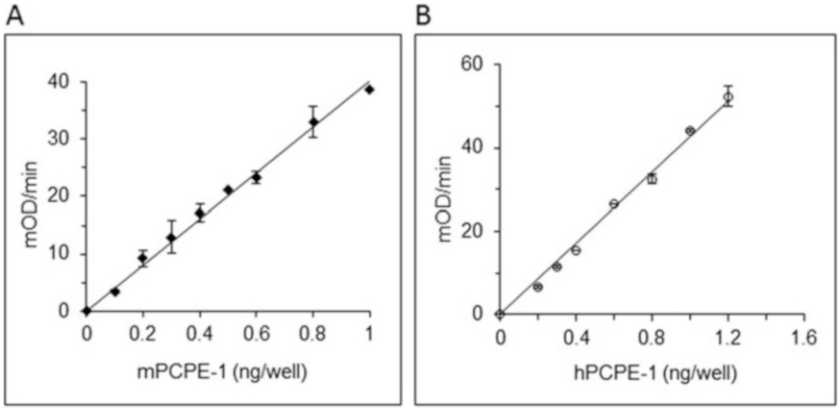

Fig. 3 Standard curves for determination of mouse and human PCPE-1. (**a**) Sandwich ELISA for mPCPE-1. Increasing amounts of purified mPCPE-1 were adsorbed to wells pre-coated with a rat monoclonal antibody to mPCPE-1. Bound mPCPE-1 was detected using a goat antibody to mPCPE-1 and quantified using an APA-conjugated rabbit anti goat IgG antibody. (**b**) Sandwich ELISA for hPCPE-1. Increasing amounts of purified hPCPE-1 were adsorbed to wells pre-coated with mouse mAb 7A11/1 to hPCPE-1. Bound hPCPE-1 was detected using a rabbit polyclonal Ab to hPCPE-1 and quantified using an APA-conjugated goat anti rabbit IgG antibody. Each value in **a** and **b** represents mean ± SD; $n = 2$. mOD, optical density expressed in milli units (Adapted from refs. 19 (**a**) and 32 (**b**), both Open Access)

in ng/ml (multiply by 20), and then correct for the sample dilution.

For instance, for a mouse plasma sample diluted 20-fold:

$$X = \frac{B}{A} \times 20 \times D$$

A = mOD/min/1 ng mPCPE-1 (derived from the calibration curve).

B = mOD/min for the diluted plasma sample.

D = Plasma dilution.

X = PCPE concentration (ng/ml) of the unknown sample.

The average normal concentration of mouse plasma PCPE-1 is ~200 ng/ml. In CCl_4-induced liver fibrosis, it can increase up to ~300 ng/ml, about 50% higher than the control (untreated mice) [19].

3.2 Sandwich ELISA for hPCPE-1

1. Adsorption of the first antibody (mAb 7A11/1): Dilute the antibody solution in carbonate buffer to a final concentration of 5 μg/ml (*see* **Note 2**). Pipet 50 μl of the Ab solution into each well in a 96 well plate. Incubate over night at 4 °C.
2. Blocking: On the following day, remove and discard the first antibody solution. Wash the wells twice with PBST. Add to each well 200 μl of blocking buffer, and incubate for 2 h at 30 °C.

3. Addition of hPCPE-1 samples: Remove and discard the blocking buffer. Wash the wells four times with PBST. Add 50 μl/well of a hPCPE-1 sample diluted in blocking buffer, in duplicates for the standard curve and in triplicates for samples with unknown hPCPE-1 concentrations (e.g., diluted human plasma/serum). Assign three wells for determination of basal OD levels (blanks; all reagents except for hPCPE-1). To these wells, pipet 50 μl of blocking buffer instead of a hPCPE-1 sample. Incubate for 2 h at 30 °C (*see* **Note 6** for hPCPE-1 sample preparation).
4. Addition of the second Ab (rabbit polyclonal IgG to hPCPE-1). Prepare a 0.1 μg/ml solution of the antibody in blocking buffer (*see* **Note 7**). Remove and discard the PCPE-1 samples. Wash the wells four times with PBST. Pipet 50 μl of the second Ab solution into each well, and incubate for 1 h at 30 °C.
5. Addition of APA-conjugated goat anti rabbit IgG: Dilute the antibody 1:2000 in blocking buffer. Remove and discard the second Ab solution from the wells. Wash the wells four times with PBST. Pipet into each well 50 μl of the diluted APA-conjugated antibody. Incubate for 45 min at 30 °C.
6. Addition of APA substrate solution: Remove and discard the APA-conjugated antibody solution. Wash four times with PBST. Add to each well 100 μl of a freshly prepared alkaline phosphatase substrate solution. Place the plate in an ELISA plate reader pre-equilibrated to 30 °C. Follow the rate of increase in absorbance at 405 nm (due to release of the chromophore para-nitro-phenol) with constant shaking and recording absorbance at 5 min intervals for about 30 min. Altogether, up to and including this step, the procedure is accomplished in 2 days.
7. Calculate PCPE-1 concentrations based on the standard curve (Fig. 3b). Absorbance values are converted to hPCPE-1 concentrations expressed as ng/ml based on the standard curve and correcting for the dilutions as follows: (1) calculate the average OD/min value obtained for the blanks and for each PCPE-1 sample; (2) calculate the net OD/min values for each PCPE-1 concentration by subtracting the average blank value; (3) from the calibration curve (created using the net average values derived for the known hPCPE-1 concentrations), calculate the mOD/min value corresponding to 1 ng hPCPE/well (50 μl), and use this value to derive the amount of hPCPE-1 in 50 μl of the unknown PCPE-1 sample; and (4) calculate concentration first in ng/ml (multiply by 20), and then correct for the dilution of the unknown sample.

For instance, for a human plasma sample diluted 20-fold when:

$$X = \frac{B}{A} \times 20 \times D$$

A = mOD/min/1 ng hPCPE-1.

B = mOD/min for the unknown sample.

D = Dilution of the unknown sample.

X = hPCPE-1 concentration (in ng/ml) of the unknown sample.

The average plasma concentration of hPCPE-1 in healthy adults is ~300 ng/ml [28, 32]. In liver fibrosis patients, it may increase to 450–600 ng/ml (50–100% higher than normal) [32].

4 Notes

1. Purified PCPE-1 is required to create a calibration curve in the ELISA test. PCPE-1 is a sticky protein. Brij 35 is added to PCPE-1 solutions of concentrations lower than 0.5 mg/ml to minimize loss due to PCPE-1 adsorption to the test tube. The stock solution is stored at −80 °C in small aliquots to minimize repeated thawing and freezing. This is true for both mouse and human PCPE-1.
2. The commercial 7A1/11 mAb antibody is supplied as the total IgG fraction, while we used an immuno-affinity-purified IgG fraction, enriched for hPCPE-1-specific antibodies. When using a commercial preparation, the amount needed for the first step in the ELISA should be determined empirically.
3. We used a 4.9 M stock solution of $MgCl_2$ $6H_2O$ (Sigma 104-20). This product is discontinued. A 2 M solution is available (Sigma 68475) and can be used instead. The use of ready to use $MgCl_2$ solution is recommended because of the hygroscopic nature of $MgCl_2$.
4. In all of the steps except for the addition of PCPE-1 samples (**step 3**), we recommend using automatic pipetting to speed up the procedure. Blocking (**step 2**) and washing (after each incubation step) buffers are added to and removed from the wells using a multichannel pipettor. The first antibody (**step 1**), the second antibody (**step 4**), the APA-conjugated third antibody (**step 5**) and the APA substrate (**step 6**) are all added using a stepper. The PCPE-1 samples are each pipetted manually, replacing the tip for each PCPE-1 concentration (**step 3**).
5. Dilutions of mPCPE-1 samples: Each experiment should include a standard curve with known mPCPE-1 concentrations between 0 and 1 ng/well to permit calculation of unknown mPCPE-1 concentrations. For this purpose, dilute the

Table 1
Preparation of mPCPE-1 solutions with recommended concentrations (2–20 ng/ml; 0.1–1 ng/50 μl) for a calibration curve[a]

Tube	mPCPE-1 0.5 ng/μl in blocking buffer (μl)	Blocking buffer (μl)	mPCPE-1 ng/50 μl (well)
1	2	498	0.1
2	4	496	0.2
3	6	494	0.3
4	8	492	0.4
5	10	490	0.5
6	12	488	0.6
7	16	484	0.8
8	20	480	1.0

[a]Total volume for each concentration is 500 μl

mPCPE-1 stock solution of 250 μg/ml 1:500 in blocking buffer to obtain a diluted stock solution of 0.5 ng/μl. This solution should be used on the same day. The rest should be discarded. A detailed description on how the 0.5 ng/μl mPCPE-1 solution is diluted for preparation of mPCPE-1 solutions with known concentrations (0.1–1.0 ng/well) for the calibration curve is presented in Table 1. Plasma samples are diluted 1:20 and 1:40 in blocking buffer. PCPE-1 concentrations of the diluted plasma samples should be determined in at least duplicates, preferably, in triplicates. Most importantly, fresh plasma samples should each be divided into small aliquots and stored at −80 °C until use. Repeated thawing and freezing should be avoided to prevent loss of the PCPE protein from the plasma, apparently due to degradation. Thus, once thawed, the plasma sample should be used only once. The remaining plasma should be discarded.

6. Dilutions of recombinant hPCPE-1 samples: As in the case of the ELISA for mPCPE-1, each experiment should include a calibration curve with known hPCPE-1 concentrations (0.2–1.2 ng/well). The stock solution of 0.5 mg/ml is diluted 1:1000 in blocking buffer to a final concentration of 0.5 ng/μl. This solution should be used on the same day. The rest should be discarded. A detailed description on how the 0.5 ng/μl hPCPE-1 solution is diluted for preparation of samples with known hPCPE-1 concentrations required for the calibration curve is presented in Table 2.
7. Dilutions of the rabbit polyclonal antibody against hPCPE-1: Dilute the stock antibody solution to a concentration of 1 mg/

Table 2
Preparation of hPCPE-1 solutions with recommended concentrations (4–24 ng/ml; 0.2–1.2 ng/50 μl) for a calibration curve[a]

Tube	hPCPE-1 0.5 ng/μl in blocking buffer (μl)	Blocking buffer (μl)	hPCPE-1 ng/50 μl (well)
1	4	496	0.2
2	6	494	0.3
3	8	492	0.4
4	12	488	0.6
5	16	484	0.8
6	20	480	1.0
7	24	476	1.2

[a]Total volume for each concentration is 500 μl

ml in PBS. This solution can be stored in aliquots at −20 or −80 °C. Further dilutions are prepared in blocking buffer on the day of the assay, and the remaining diluted solution should be discarded after use.

References

1. Zeisberg M, Kalluri R (2013) Cellular mechanisms of tissue fibrosis. 1. Common and organ-specific mechanisms associate with tissue fibrosis. Am J Physiol Cell Physiol 304:C216–C225
2. Wynn TA, Ramalingam TR (2012) Mechanisms of fibrosis: therapeutic translation for fibrotic disease. Nat Med 18:1028–1040
3. Lotersztajn S, Julien B, Teixeira-Clerc F et al (2005) Hepatic fibrosis: molecular mechanisms and drug targets. Annu Rev Pharmacol Toxicol 45:605–628
4. Manning DS, Afdhal NH (2008) Diagnosis and quantitation of fibrosis. Gastroenterology 134:1670–1681
5. Papastergiou V, Tsochatzis E, Burroughs AK (2012) Non-invasive assessment of liver fibrosis. Ann Gastroenterol 25:218–231
6. Bedossa P, Carrat F (2009) Liver biopsy: the best, not the gold standard. J Hepatol 50:1–3
7. Rockey DC, Caldwell SH, Goodman ZD et al (2009) American association for the study of liver diseases. Liver biopsy. Hepatology 49:1017–1044
8. Duarte-Rojo A, Altamirano JT, Feld JJ (2012) Noninvasive markers of fibrosis: key concepts for improving accuracy in daily clinical practice. Ann Hepatol 11:426–439
9. Patel K, Shackel NA (2014) Current status of fibrosis markers. Curr Opin Gastroenterol 30:253–259
10. Gressner OA, Weiskirchen R, Gressner AM (2007) Biomarkers of liver fibrosis: clinical translation of molecular pathogenesis or based on liver-dependent malfunction tests. Clin Chim Acta 381:107–113
11. Nallagangula KS, Nagaraj SK, Venkataswamy L et al (2018) Liver fibrosis: a compilation on the biomarkers status and their significance during disease progression. Future Sci OA 4(1): FSO250
12. Karsdal MA, Krarup H, Sand JMB et al (2014) Review article: the efficacy of biomarkers in chronic fibroproliferative diseases-early diagnosis and prognosis, with liver fibrosis as an exemplar. Aliment Pharmacol Ther 40:233–249
13. Kessler E, Adar R (1989) Type I procollagen C-proteinase from mouse fibroblasts: purification and demonstration of a 55 kDa enhancer glycoprotein. Eur J Biochem 186:115–121
14. Kessler E, Takahara K, Biniaminov L et al (1996) Bone morphogenetic protein-1: The

type I procollagen C-proteinase. Science 271:360–362

15. Kessler E, Mould PA, Hulmes DJS (1990) Procollagen type I C-proteinase enhancer is a naturally occurring connective tissue glycoprotein. Biochem Biophys Res Commun 173:81–86
16. Takahara K, Kessler E, Biniaminov L et al (1994) Type I procollagen C-proteinase enhancer protein: Identification, primary structure, and chromosomal localization of the cognate human gene (PCOLCE). J Biol Chem 269:26280–26285
17. Ogata I, Auster AS, Matsui A et al (1997) Type I procollagen C-proteinase enhancer protein (PCPE) is expressed in cirrhotic but not in normal rat liver. Hepatology 26:611–617
18. Ippolito DL, AbdulHameed MDM, Tawa GJ et al (2016) Gene expression patterns associated with histopathology in toxic liver fibrosis. Toxicol Sci 149:67–88
19. Hassoun E, Safrin M, Ziv H et al (2016) Procollagen C-proteinase enhancer 1 (PCPE-1) as a plasma marker of muscle and liver fibrosis in mice. PLoS One 11(7):e0159606
20. Shalitin N, Schlesinger H, Levy MJ et al (2003) Expression of procollagen C-proteinase enhancer in cultured rat heart fibroblasts: Evidence for co-regulation with type I collagen. J Cell Biochem 90:397–407
21. Kessler-Icekson G, Schlesinger H, Freimann S et al (2006) Expression of procollagen C-proteinase enhancer-1 in the remodeling rat heart is stimulated by aldosterone. Int J Biochem Cell Biol 38:358–365
22. Yu L, Ruifrok WPT, Meissner M et al (2013) Genetic and pharmacological inhibition of galectin-3 prevents cardiac remodeling by interfering with myocardial fibrogenesis. Circ Heart Fail 6:107–117
23. Wong VW, You F, Januszyk M et al (2014) Transcriptional profiling of rapamycin treated fibroblasts from hypertrophic and keloid scars. Ann Plast Surg 72:711–719
24. Malecaze F, Massoudi D, Fournié P et al (2014) Upregulation of bone morphogenetic protein-1/mammalian tolloid and procollagen C-proteinase enhancer-1 in corneal scarring. Invest Ophthalmol Vis Sci 55:6712–6721
25. Moali C, Font B, Ruggiero F et al (2005) Substrate-specific modulation of a multisubstrate proteinase. C-terminal processing of fibrillar procollagens is the only BMP-1-dependent activity enhanced by PCPE-1. J Biol Chem 280:24188–24194
26. von Marschall Z, Fisher LW (2010) Dentin sialophosphoprotein (DSPP) is cleaved into its two natural dentin matrix products by three isoforms of bone morphogenetic protein-1 (BMP-1). Matrix Biol 29:295–303
27. Pieper R, Gatin CL, Makusky AJ et al (2003) The human serum proteome: display of nearly 3700 chromatographically separated protein spots on two-dimensional electrophoresis gels and identification of 325 distinct proteins. Proteomics 3:1345–1364
28. Mesilaty-Gross S, Anikster Y, Vilensky B et al (2009) Different patterns of human serum procollagen C-proteinase enhancer-1 (PCPE-1). Clin Chim Acta 403:76–80
29. Olswang-Kuz Y, Liberman B, Weiss I et al (2011) Quantification of human serum procollagen C-proteinase enhancer (hsPCPE) glycopattern. Clin Chim Acta 412:1762–1766
30. Grgurevic L, Macek B, Durdevic D et al (2007) Detection of bone and cartilage-related proteins in plasma of patients with bone fracture using liquid chromatography-mass spectrometry. Int Orthop 31:743–751
31. Gokce O, Ozenirler S, Yucel AA et al (2018) Evaluation of serum procollagen C-proteinase enhancer 1 level as a fibrosis marker in patients with chronic hepatitis B. Eur J Gastroenterol Hepatol 30(8):918–924. https://doi.org/10.1097/MEG.0000000000001123
32. Hassoun E, Safrin M, Wineman E et al (2017) Data comparing the plasma levels of procollagen C-proteinase enhancer 1 (PCPE-1) in healthy individuals and liver fibrosis patients. Data Brief 14:777–781
33. Moschcovich L, Bernocco S, Font B et al (2001) Folding and activity of recombinant human procollagen C-proteinase enhancer. EurJ Biochem 268:2991–2996

Chapter 15

Tumorigenic Interplay Between Macrophages and Collagenous Matrix in the Tumor Microenvironment

Chen Varol

Abstract

The tumor microenvironment is a heterogeneous tissue that in addition to tumor cells, contain tumor-associated cell types such as immune cells, fibroblasts, and endothelial cells. Considerably important in the tumor microenvironment is its noncellular component, namely, the extracellular matrix (ECM). In particular, the collagenous matrix is subjected to significant alterations in its composition and structure that create a permissive environment for tumor growth, invasion, and dissemination. Among tumor-infiltrating immune cells, tumor-associated macrophages (TAMs) are numerous in the tumor stroma and are locally educated to mediate important biological functions that profoundly affect tumor initiation, growth, and dissemination. While the influence of TAMs and mechanical properties of the collagenous matrix on tumor invasion and progression have been comprehensively investigated individually, their interaction within the complex tumor microenvironment was overlooked. This review summarizes accumulating evidence that indicate the existence of an intricate tumorigenic crosstalk between TAMs and collagenous matrix. A better mechanistic comprehension of this reciprocal interplay may open a novel arena for cancer therapeutics.

Key words Tumor-associated macrophages, Tumor microenvironment, Collagenous matrix

1 Introduction

Cancer is not merely a disease of tumor cells, but a multifaceted show, in which stromal cells and tumor microenvironment play crucial roles. Imbalance in the noncellular component of the tumor microenvironment, the ECM, is a characteristic marker of various solid tumors and is actively involved in their progression and dissemination [1, 2]. Collagen constitutes the most abundant scaffold in the tumor microenvironment. During cancer invasion, the tumor stroma undergoes constant architectural changes, characterized by collagen degradation, redeposition, cross-linking, and stiffening. These structural transitions yield novel biomechanical and biophysical cues, which can both inhibit and promote tumor progression, depending on the stage of cancer development [3]. Coevolving with the tumor ECM are immune cells that constitute

Irit Sagi and Nikolaos A. Afratis (eds.), *Collagen: Methods and Protocols*, Methods in Molecular Biology, vol. 1944, https://doi.org/10.1007/978-1-4939-9095-5_15, © Springer Science+Business Media, LLC, part of Springer Nature 2019

the predominant cellular component of the tumor stroma. In particular, TAMs are abundant in the stroma of experimental and human tumors and are locally programmed to perform key tumorigenic functions [4, 5]. Emerging evidence unravel a pivotal role for TAMs in the shaping of the dynamically evolving collagenous ECM within the tumor microenvironment [6]. Reciprocally, alterations within the tumor collagenous matrix regulate the migration and function of these phagocytic cells [6]. This overview summarizes the recent progress in our comprehension of the tumorigenic interplay between collagenous matrix and macrophages.

2 Collagen Buildup and Remodeling Promote Tumor Progression, Invasion, and Metastasis

The tumor cellular ecosystem is nourished by its ECM, comprising a 3D supramolecular network of proteins, glycoproteins, proteoglycans, and polysaccharides. Traditionally, ECM has been regarded primarily as a physical scaffold that plays a supportive role in maintaining tissue morphology. However, the tumor ECM differs considerably from its normal tissue counterpart [7], a product of aberrantly expressed or modified structural proteins and deregulated remodeling events choreographed by specific proteolytic and protein cross-linking enzymes [8]. The ensuing abnormal ECM actively promotes cancer by providing critical biomechanical and biochemical cues that drive tumor cell growth, survival, invasion, and metastasis [1, 2, 9].

Force modulates cell fate, directs tissue development, and facilitates tumor invasion [10]. Aggressive tumors frequently display desmoplasia, resulting from enhanced deposition, cross-linking, and geometrical organization (e.g., linearization) especially of interstitial collagen fibers that are often positioned perpendicular to the tumor boundary [10–13]. The resultant increased stiffness correlates with tumor aggression and an increased propensity toward metastasis [12, 14, 15]. Cancer and immune cells can exploit these wrapped stiff collagen bundles as invasion "highways" [16]. Collagenous ECM stiffening can be enzyme-dependent. In this case, it is predominantly catalyzed by lysyl oxidases (LOX), which are capable of cross-linking collagens and elastin, thereby increasing insoluble matrix deposition and tissue stiffness [17]. Matrix stiffening can also be accomplished by nonenzymatic collagen cross-linking, such as glycation and transglutamination or increased biglycan and fibromodulin proteoglycan deposition [3]. Specifically, fibronectin polymerization is essential for collagen network formation [18]. The dynamic and reciprocal interactions between collagen and fibronectin may induce tumor progression and metastasis. In lung metastases, for example, increased

fibronectin expression is essential for the recruitment and adherence of pro-metastatic myeloid cells, which express the fibronectin receptor integrin α4β1 [19]. The secreted protein acidic and rich in cysteine (SPARC) glycoprotein is an additional example for nonenzymatic collagen cross-linking and can either suppress or promote progression of different cancers [20]. In this respect, orthotopic pancreatic tumors grown in SPARC-deficient mice display reduced deposition of fibrillar collagens I and III, basement membrane collagen IV, and the collagen-associated proteoglycan decorin [21]. SPARC is expressed by various types of malignant cells and associated stromal cells and modulates tumor development, invasion, and metastasis [20].

Collagenous matrix buildup has a significant impact on many hallmarks of cancer [2]. To grow beyond a certain size and metastasize, tumors require angiogenesis, a specialized form of branching morphogenesis whereby new blood vessels develop from a pre-existing vascular network [22]. A stiffened collagenous ECM fosters angiogenesis by providing mechanical signals that facilitate endothelial cell migration, growth, survival, branching morphology, and vessel lumen formation [23–27]. Hypoxia is a key driver of tumor angiogenesis and can lead to overproduction of LOX-like protein-2 (LOXL2), which promotes collagen type IV scaffolding in the endothelial basal lamina, resulting in sprouting angiogenesis [28]. Interactions between endothelial cells and collagen IV in the vascular basement membrane play key roles in modulating angiogenesis [29]. Collagen type IV can directly promote angiogenesis and neovessel survival in a dose-dependent manner [30]. It is the triple-helical fragments of intact type IV collagen that stimulate endothelial cell adhesion and migration [31]. Importantly however, proteolytic exposure of cryptic sites within specific collagen subtypes can also release fragments associated with anti-angiogenic activity. Well-known examples are the non-collagenous domain 1 (NC1 domain) of type IV collagen [32, 33] and the endostatin fragment of type XVIII collagen [34]. Collagen-rich, stiffened ECM can also advance cancer growth by impeding anti-tumorigenic T-cell function. Accordingly, collagen is a ligand for the inhibitory leukocyte-associated Ig-like receptor (LAIR-1), which is expressed on various immune cells [35] and has been linked with suppression of cytotoxic T-cell activity [36]. In another aspect, cellular quiescence must be overcome to establish a neoplastic lesion. Indeed, mechanical-sensing of stiffer ECM initiates intracellular signaling cascades that promote cell proliferation and override tumor suppressor activity [12, 37–40]. In addition, the rigid tumoral ECM also enhances tumor cell invasion and metastasis by inducing focal adhesion assemblies and favoring epithelial-mesenchymal transition (EMT) [11, 15, 41] and by facilitating the formation of "premetastatic niches" in destination organs [42, 43].

Collagen proteolysis is a prerequisite for the invasion of tumor cells through physical barriers that resist tumor expansion into the surrounding tissue. It is also a rate-limiting step for traversing metastatic tumor cells trying to exit the blood or lymphatic vessel across a continuous basement membrane [44]. Several classes of proteases contribute to ECM breakdown and remodeling, most of which are upregulated in the course of metastasis in different types of cancers. Proteolytic enzymes including matrix metalloproteinases (MMPs 1, 2, 13, 14) and cathepsins (B, K, and L) show activity against fibrillar and non-fibrillar collagens [45–47]. MMPs represent the most prominent family of zinc-dependent endopeptidases associated with tumorigenesis [46]. Liottta and colleagues were the first to define tumor cell-derived MMP (now known as MMP2) that degrades non-fibrillar type IV collagen, the main constitute of basement membranes [48]. Indeed, higher levels of basement membrane-degrading MMP activity correlate with a higher number of metastases in animal models [49]. Mounting evidence supports a dominant role of MMP14 in the migration and invasion of metastatic tumor cells [50]. Cysteine cathepsins are another major class of proteolytic enzymes in the tumor microenvironment [45] that influence collagenous matrix. Indeed, intracellular lysosomal cathepsin-governed collagen degradation serves as a major pathway of ECM turnover during malignancy [51]. In particular, cathepsin B extracted from tumor tissues is capable of degrading type IV collagen [52]. Imaging has further revealed that it participates in intracellular digestion of type IV collagen in human breast cancer and glioma cells [53, 54]. Moreover, degradation of type I collagen by cathepsin B [55] or K [56] facilitates breast cancer bone metastasis. Secreted cathepsin L can also promote tumor metastasis through degradation of ECM components such as laminin, type I and IV collagen, fibronectin, and elastin [57]. Collectively, these studies highlight that the induction of collagen deposition and remodeling processes directly facilitate cancer growth and dissemination by various mechanisms.

3 TAMs Support Cancer Growth and Dissemination

Epidemiological meta-analyses indicate a clear correlation between the density of TAMs and poor prognosis in many, but not all, human cancers [58, 59]. TAMs represent a major component of the lymphoreticular infiltrates in solid tumors and prominently arise from classical Ly6C^{hi} monocytes [60, 61], which arrive in response to tumor cell-derived growth factors and chemoattractants, especially colony-stimulating factor 1 (CSF-1) (*reviewed in* [62]) and CCL2 [60, 61, 63], respectively. They respond to local cues within the tumor microenvironment that usually bias away their functional polarization from the classically activated (M1) macrophage

phenotype to the alternatively activated type termed "M2" [64]. Yet, TAMs are considered a heterogeneous cell population with multidimensional functional plasticity and often exhibit markers that are characteristic of both types. They perform various pro-tumoral functions that effect every hallmark of cancer progression [65]. For example, TAMs acquire M2-like properties that qualify them to subvert adaptive immunity [66]. This is typically manifested by production of the anti-inflammatory cytokines IL-10 and TGFβ [67] and the release of chemokines that preferentially attract T lymphocytes devoid of cytotoxic functions [68]. Moreover, TAMs orchestrate the so-called angiogenic switch required for malignant transition by producing neoangiogenic molecules that increase vascular density [69]. They are inclined to cluster in "hot spots" in hypoxic avascular areas with a high level of angiogenesis [70], where their pro-angiogenic activity is further augmented [71, 72]. TAMs also play pivotal roles in the metastatic process. Specifically, a CSF1-epidermal growth factor (EGF) paracrine loop between TAMs and tumor cells has been implicated in the promotion of breast cancer invasion and dissemination [73, 74]. In addition, monocytes recruited via the CCR2-CCL2 axis to the premetastatic niche create an environment optimized for rapid development of metastases [19, 75–78].

4 TAMs Are Builders of the Tumorigenic Collagenous Matrix

The role of TAMs or collagenous matrix remodeling in tumor development and dissemination has each been the subject in a plethora of studies. Nevertheless, studies on how these pathways are intertwined to advance tumorigenesis are only now emerging. Early reports have demonstrated the accumulation of macrophages and their association with a fibrous cellular capsule formed around s.c. implanted mammary carcinoma tumors [79]. A follow-up study has further provided initial evidence for their capacity to function as collagen-producing cells during tumor encapsulation [80]. Intravital imaging of mammary tumors has also demonstrated the accumulation of TAMs at the tumor's collagen-rich border, where they support the intravasation of cancer cells [16]. These observations were the first to introduce the idea that TAMs may be involved with tumorigenic collagen remodeling, an idea that has been affirmed by a group of recent studies discussed below.

Utilizing an orthotopic colorectal cancer (CRC) mouse model, we have found that Ly6C^{hi} monocyte-derived TAMs play a key role in the buildup of the tumorigenic collagenous niche by directly contributing to the deposition, cross-linking, and linearization of fibrillar collagens [60]. Complementary transcriptomic and proteomic analyses revealed that Ly6C^{hi} monocytes directly produce type I and VI collagen in the tumor milieu, and upon their maturation

into TAMs, they further upregulate the expression of type XIV collagen. The latter belongs to a family of fibril-associated collagens and interacts predominantly with type I collagen to promote fibrillogenesis [81, 82]. It appears that TAMs in this CRC model play a dominant role in the deposition of these collagen subtypes given their reduced representation in TAM-deficient vs. TAM-sufficient tumors [60]. Remarkably, CRC TAMs also express various molecules that participate in posttranslational modifications of intracellular collagen and its assembly, such as the glycoprotein procollagen C-endopeptidase enhancer (PCOLCE), the enzyme prolyl 4-hydroxylase α polypeptide I (P4HA1), the collagen cross-linkers procollagen-lysine 2-oxoglutarate 5-dioxygenase-1 and procollagen-lysine 2-oxoglutarate 5-dioxygenase-3 (PLOD-1, PLOD-3), the proteoglycan biglycan, and the glycoprotein SPARC [60]. The expression of the latter has also been detected in TAMs sorted from human ovarian carcinoma [83] as well as from experimental and human pancreatic ductal adenocarcinoma (PDAC) [84]. Other studies have highlighted a key involvement for immune cell-derived SPARC in the assembly and organization of collagenous matrix in pancreatic [85] and mammary tumors [86]. Moreover, macrophage-derived SPARC promotes cancer cell migration and metastasis by modulating integrin-ECM interactions [87].

While our study reports a pro-fibrotic role for CCR2^{+}Ly6C^{hi} monocyte-derived TAMs in CRC [60], a recent study uncovered that in PDAC this function is in fact associated with tissue-resident embryonic yolk-sac-derived macrophages [84]. Accordingly, in the settings of an orthotopic KPC model of PDAC, the embryonic-derived TAMs, rather than the monocyte-derived TAMs, exhibit a pro-fibrotic profile as manifested by their increased transcription of collagen types Ia2, IIIa1, Va1, VIa1, Xa1, and XVIIIa1, their augmented ex vivo production of type I and IV collagen, and the reduced collagen density in PDAC tumors following their inducible ablation [84]. Notably, their expression of collagen types IVa4, Xa1, XVIIa1, and XVIIIa1 was even higher than cancer-associated fibroblasts (CAFs). A similar pro-fibrotic phenotype was also found in human embryonic-derived CXCR4^{+} macrophages isolated from PDAC samples, suggesting conservation of function across species [84]. These two studies [60, 84] underscore the importance of understanding the task division between TAMs of different ontogenies in different tumor types.

An association between TAM presence and tumorigenic collagen remodeling is also supported by other studies. In a model of breast cancer, depletion of TAMs alters tumor collagen fibrillar microstructures that are important for tumor metastasis [88]. Moreover, TAMs extracted from human ovarian carcinoma express genes encoding for types I, V, and VI collagen [83]. The synthesis of the latter has also been demonstrated in monocytes associated

with triple-negative breast cancer xenografts [89] and TGFβ1-stimulated human macrophages [90]. The ability of macrophages to acquire a fibroblast-like function and directly synthesize specific collagen subtypes is further supported by studies in other pathological settings, such as renal fibrosis [91–93], atherosclerotic plaques [94, 95], fibrosis and diastolic dysfunction in the aging heart [96], and helminth infection [97], and very recently also in ERK-activated brain microglia in the context of neurodegenerative disease [98] and during wound granulation in a process mediated by miR-21 [99]. Macrophages (hemocytes) also emerge as a major source of basement membrane collagen IV in the developing *Drosophila* embryo [100].

CAFs are considered to be the key producers of collagenous matrix in developing tumors [101]. Accumulating evidence indicates that TAMs can also elicit the pro-fibrotic activity of CAFs. In support of this, we have observed reduced gene expression of collagen type I in CAFs sorted from TAM-deficient colorectal tumors [60]. In another example, the addition of monocytes to triple-negative breast cancer xenografts facilitated collagen deposition by stromal CAFs [89]. TAMs can also serve as a reservoir of growth factors and cytokines that foster the pro-fibrotic activity of CAFs, such as the platelet-derived growth factor (PDGF) [102], epidermal growth factor (EGF) [73], and TGFβ [103]. With respect to the latter, Ly6C^{hi} monocyte-derived TGFβ1 has been shown to facilitate the transition of hepatic stellate cells into collagen-producing myofibroblasts in a model of liver fibrosis [104]. Similarly, M2 macrophage-derived TGFβ1 induces the proliferation of fibroblasts and their differentiation into myofibroblasts during wound healing scar formation [105]. Macrophages may also engage the activity of the LOX collagen cross-linker enzyme in adjacent fibroblasts as has recently been shown in a model of skin injury [106]. Finally, utilizing a computational two-cell system, the Medzhitov and Alon groups have recently discovered that macrophages and fibroblasts form a stable cell circuit, which is robust to perturbations owing to cell-contact-dependent mutual exchange of growth factors (PDGF and CSF-1, respectively) and negative feedback regulation [107]. These types of cell circuits may be important to stabilize fibrogenic interactions between TAMs and CAFs in the tumor microenvironment. Collectively, these reports outline a pivotal role for TAMs in the tumorigenic collagenous matrix buildup through their direct deposition of specific types of collagen or via their governed promotion or stabilization of CAF's pro-fibrotic activity.

5 TAMs Are Remodelers of the Tumorigenic Collagenous Matrix

Collagen remodeling events, including collagen cross-linking and collagenolysis, are typical of various solid tumors and direct tumor development, invasion, and dissemination through physical barriers [1, 2, 44]. MMPs represent the most studied and prominent family of matrix proteinases associated with tumorigenesis [46]. Interstitial collagens are hydrolyzed by the "classic" collagenases MMP1, MMP8, MMP13, and MT1-MMP (MMP14). MMP2 digests solubilized monomers of collagens I, II, and III, and MMP9 cleaves solubilized collagen I and III monomers [108]. The basement membrane is dominated by a scaffolding of cross-linked type IV collagen molecules, and its breaching during malignancy is mediated mainly by MMP2 and MMP9 [109, 110] as well as the membrane-anchored proteases MMP14, MT2-MMP (MMP15), and MT3-MMP (MMP16) [111]. TAMs are considered to be a major source of collagen remodeling enzymes in the tumor microenvironment [6, 112]. With respect to MMP9, Coussens et al. have initially reported that MMP9 expression by tumor-infiltrating BM-derived hematopoietic cells promotes metastatic growth [113]. Further studies have attributed MMP9-governed angiogenesis and tumorigenicity to TAMs [114–117]. Yet, other studies have highlighted tumor-associated neutrophils as the predominant and immediate source of active MMP9, which is uniquely unencumbered by tissue inhibitor of metalloproteinases-1 (TIMP-1) [118]. We have shown that Ly6C^{hi} monocytes recruited to orthotopically implanted colorectal tumors upregulate the expression of MMP12, MMP13, and MMP14 [60]. Recently, Madsen et al. reported that CCR2^{+}Ly6C^{hi} monocytes acquire a collagen catabolic transcriptomic signature during invasive tumor growth and degrade collagen through mannose receptor-dependent cellular uptake [119]. These collagen-endocytosing TAMs expressed genes encoding for MMP8, MMP9, MMP12, and MMP13. CAFs on the other hand expressed higher levels of MMP2 and its activator MMP14, suggesting their possible association with initial collagen fragmentation [119]. Noteworthy, the proteolytic activity of MMPs can be regulated at multiple levels, including transcription, compartmentalization, conversion from zymogen to active enzyme, and restraining by endogenous inhibitors such as TIMPs. Therefore, when judging the pathophysiological relevance of MMP expression in TAMs, their collagenase activity has to be verified.

Another family of matrix proteases with collagen remodeling activity is the cysteine cathepsins, which function in proteolytic pathways that increase neoplastic progression. These enzymes can be secreted, localized at the cell-surface or intracellularly in association with lysosomes [45, 47]. In TAMs, cathepsins may drive lysosomal degradation of internalized collagens [119]. Indeed,

collagen-endocytosing TAMs express a wide panel of cathepsin transcripts including B, while L and K are higher in CAFs [119]. Gene and protein expression of cathepsins B, D, and L has also been noticed in CRC TAMs [60]. Moreover, TAM polarization by tumor-derived IL-4 induced the activity of cathepsins B and S that promote pancreatic tumor growth, angiogenesis, and invasion [120]. TAM-derived cathepsin B has also been implicated in the dissemination of breast cancer metastases to the lung [121]. Further studies are required to determine the functional contribution of specific TAM-derived cathepsins to the remodeling of the collagenous tumorigenic niche. TAMs may also directly promote collagen cross-linking via their provision of cross-linker enzymes. In CRC, we have shown enhanced expression of the ECM covalent cross-linker enzymes transglutaminase-I and transglutaminase-II and coagulation factor XIII subunit a1, which were also reduced in whole tumor tissue of TAM-deficient colorectal tumors [60].

6 Abnormal Tumorigenic Collagenous Matrix May Reciprocally Modulate TAM Recruitment and Function

As summarized above, accumulating evidence indicate that TAMs contribute to the increased matrix rigidity in various solid tumors through their direct and indirect modulation of collagen deposition and its geometrical organization. These kinds of alterations in collagenous matrix may in turn affect the migration behavior and function of TAMs. The ability of macrophages to sense the ECM in their vicinity relies on mechanosensors such as integrins, which transmit force from the extracellular environment via their interaction with numerous cytoskeletal and signaling proteins [122]. Force sensing is transmitted from the extracellular environment via the interaction of integrins with numerous cytoskeletal and signaling proteins that accumulate in a force-dependent manner into focal adhesions and other types of cell-matrix adhesions [122]. A specific example is the integrin αvβ3, which binds various matrix proteins including vitronectin, fibronectin, fibrinogen, as well as denatured or proteolysed collagen and can affect tumor growth by various ways [123]. Collagen and its digestion products can act as chemotactic stimuli for monocytes and macrophages. Accordingly, activation of the collagen tyrosine kinase receptor discoidin domain receptor 1 (DDR1) plays a critical role in macrophage accumulation at early and late stages of atherogenesis [124], and type I collagen degradation products might directly serve as chemotactic stimuli for human peripheral blood monocytes [125]. Moreover, LOX-governed collagen matrix modifications promote the recruitment, invasion, and retention of $CD11b^+$ myeloid cells to

premetastatic sites [42]. Biophysical parameters of the collagenous matrix can also instruct the 3D migration mode of macrophages. Macrophages can apply two main migration modes while moving through 3D matrices: amoeboid or mesenchymal [126]. In fibrillar type I collagen, macrophages tend to use the amoeboid migration mode, while in denser collagen I matrices, they have a preference for the mesenchymal migration mode [127]. In case of the latter, they may form 3D collagenolytic podosome-like structures at the tips of cell protrusions [127]. In addition, a dense collagenous matrix may also dictate their pro-tumoral polarization. Indeed, human monocytes grown on collagen-rich matrix exhibit increased proliferation and a pro-tumorigenic M2 polarization state [128, 129], and increased matrix rigidity promotes M2 polarization of macrophages [130]. Altogether, the altered collagenous matrix deposition and architecture in the tumor microenvironment may be essential for the regulation of TAM recruitment, retention, intra-tumor tissue mobility, and tumorigenic activity. Further studies are required to determine the type of mechanosensors used by TAMs to sense the dynamically changing collagenous matrix during tumor development and their governed molecular programming of TAM migration and behavior.

7 Concluding Remarks

It is becoming conceded that TAMs fundamentally shape the tumorigenic collagenous matrix. They can do so by direct deposition of specific subtypes of collagen and instruction of collagen cross-linking and linearization, as well as by encouraging the pro-fibrotic activity of co-localizing CAFs. TAMs also bring into the tumor microenvironment a unique repertoire of collagen remodeling enzymes that are capable of orchestrating collagenous matrix rearrangement and allow the invasion and dissemination of cancer cells through physical barriers. In turn, TAMs can sense the dynamically evolving abnormal collagenous matrix and respond by changing their migration mode and function. This kind of interplay appears to be indispensable in generating a tumor microenvironment permissive to tumor growth, invasion, and metastatic dissemination. While recent studies have advanced our comprehension of TAM-mediated collagen remodeling, they remain so far largely descriptive. Formidable challenges remain to delineate the mechanistic relevance of TAM-derived collagenous matrix deposition, especially with respect to its biophysical, biochemical, and structural properties. This includes a better definition of the specific subtypes of collagen produced by resident versus Ly6C^{hi} monocyte-derived TAMs in comparison with other collagen-producing cells such as CAFs. In this respect, there is still a great unmet need for understanding how TAM-elicited changes in the

structure and composition of collagenous matrix and the ensuing proteolysis products influence the behavior of different target cells in the tumor microenvironment. Another remaining challenge is to unravel the exact enzymatic and nonenzymatic pathways used by TAMs to instruct collagen assembly, cross-linking, and linearization. Such a functional molecular view of TAM-derived collagen remodeling requires a multidisciplinary integrated research approach that encompasses various methods. For example, the combination of specific macrophage ablation tools with optical imaging and electron microscopy covering wide ranges of spatial and temporal resolutions may allow in-depth characterization of TAM-guided (direct or indirect) structural alterations within the native tumor collagenous scaffolds during distinct developmental phases. Subsequently, image-guided, site-directed proteomics might be utilized to reveal collagen composition in defined niches of the tumor occupied by specific TAM subsets. Another challenge would be to study how abnormal collagenous matrix affect the behavior of TAMs in terms of mobility and function. This calls for studies that would map the expression of specific mechanosensors on TAM subsets with correlation to the spatial availability of specific collagen ligands in distinct tumor niches and during distinct developmental phases. Such studies can benefit from transgenic systems that target deficiency or overexpression of specific mechanosensors to distinct TAM subsets and their complementary molecular profiling using transcriptomic and proteomic approaches. Finally, ex vivo platforms based on decellularized native 3D-ECM tumor scaffolds supplemented with specific TAM subsets will enable coupling of remodeled collagen macromolecule architecture and composition to functional cell-macromolecular interactions. Collectively, mechanistic insights derived from such analyses may be further used to rationalize novel agents targeting TAM-collagen remodeling reactions as diagnostic or therapeutic agents.

References

1. Lu P, Weaver VM, Werb Z (2012) The extracellular matrix: a dynamic niche in cancer progression. J Cell Biol 196(4):395–406. https://doi.org/10.1083/jcb.201102147
2. Pickup MW, Mouw JK, Weaver VM (2014) The extracellular matrix modulates the hallmarks of cancer. EMBO Rep 15 (12):1243–1253. https://doi.org/10.15252/embr.201439246
3. Fang M, Yuan J, Peng C, Li Y (2014) Collagen as a double-edged sword in tumor progression. Tumour Biol 35(4):2871–2882. https://doi.org/10.1007/s13277-013-1511-7
4. Biswas SK, Allavena P, Mantovani A (2013) Tumor-associated macrophages: functional diversity, clinical significance, and open questions. Semin Immunopathol 35(5):585–600. https://doi.org/10.1007/s00281-013-0367-7
5. Noy R, Pollard JW (2014) Tumor-associated macrophages: from mechanisms to therapy. Immunity 41(1):49–61. https://doi.org/10.1016/j.immuni.2014.06.010
6. Varol C, Sagi I (2018) Phagocyte-extracellular matrix crosstalk empowers tumor development and dissemination. FEBS J 285(4):734–751. https://doi.org/10.1111/febs.14317

7. Naba A, Clauser KR, Hoersch S, Liu H, Carr SA, Hynes RO (2012) The matrisome: in silico definition and in vivo characterization by proteomics of normal and tumor extracellular matrices. Mol Cell Proteomics 11(4): M111 014647. https://doi.org/10.1074/mcp.M111.014647
8. Mason SD, Joyce JA (2011) Proteolytic networks in cancer. Trends Cell Biol 21 (4):228–237. https://doi.org/10.1016/j.tcb.2010.12.002
9. Hoye AM, Erler JT (2016) Structural ECM components in the premetastatic and metastatic niche. Am J Physiol Cell Physiol 310 (11):C955–C967. https://doi.org/10.1152/ajpcell.00326.2015
10. Butcher DT, Alliston T, Weaver VM (2009) A tense situation: forcing tumour progression. Nat Rev Cancer 9(2):108–122. https://doi.org/10.1038/nrc2544
11. Levental KR, Yu H, Kass L, Lakins JN, Egeblad M, Erler JT, Fong SF, Csiszar K, Giaccia A, Weninger W, Yamauchi M, Gasser DL, Weaver VM (2009) Matrix crosslinking forces tumor progression by enhancing integrin signaling. Cell 139(5):891–906. https://doi.org/10.1016/j.cell.2009.10.027
12. Provenzano PP, Inman DR, Eliceiri KW, Knittel JG, Yan L, Rueden CT, White JG, Keely PJ (2008) Collagen density promotes mammary tumor initiation and progression. BMC Med 6:11. https://doi.org/10.1186/1741-7015-6-11
13. Paszek MJ, Zahir N, Johnson KR, Lakins JN, Rozenberg GI, Gefen A, Reinhart-King CA, Margulies SS, Dembo M, Boettiger D, Hammer DA, Weaver VM (2005) Tensional homeostasis and the malignant phenotype. Cancer Cell 8(3):241–254. https://doi.org/10.1016/j.ccr.2005.08.010
14. Barcus CE, O'Leary KA, Brockman JL, Rugowski DE, Liu Y, Garcia N, Yu M, Keely PJ, Eliceiri KW, Schuler LA (2017) Elevated collagen-I augments tumor progressive signals, intravasation and metastasis of prolactin-induced estrogen receptor alpha positive mammary tumor cells. Breast Cancer Res 19(1):9. https://doi.org/10.1186/s13058-017-0801-1
15. Pickup MW, Laklai H, Acerbi I, Owens P, Gorska AE, Chytil A, Aakre M, Weaver VM, Moses HL (2013) Stromally derived lysyl oxidase promotes metastasis of transforming growth factor-beta-deficient mouse mammary carcinomas. Cancer Res 73 (17):5336–5346. https://doi.org/10.1158/0008-5472.CAN-13-0012
16. Wyckoff JB, Wang Y, Lin EY, Li JF, Goswami S, Stanley ER, Segall JE, Pollard JW, Condeelis J (2007) Direct visualization of macrophage-assisted tumor cell intravasation in mammary tumors. Cancer Res 67 (6):2649–2656. https://doi.org/10.1158/0008-5472.CAN-06-1823
17. Xiao Q, Ge G (2012) Lysyl oxidase, extracellular matrix remodeling and cancer metastasis. Cancer Microenviron 5(3):261–273. https://doi.org/10.1007/s12307-012-0105-z
18. Velling T, Risteli J, Wennerberg K, Mosher DF, Johansson S (2002) Polymerization of type I and III collagens is dependent on fibronectin and enhanced by integrins alpha 11beta 1 and alpha 2beta 1. J Biol Chem 277(40):37377–37381. https://doi.org/10.1074/jbc.M206286200
19. Kaplan RN, Riba RD, Zacharoulis S, Bramley AH, Vincent L, Costa C, MacDonald DD, Jin DK, Shido K, Kerns SA, Zhu Z, Hicklin D, Wu Y, Port JL, Altorki N, Port ER, Ruggero D, Shmelkov SV, Jensen KK, Rafii S, Lyden D (2005) VEGFR1-positive haematopoietic bone marrow progenitors initiate the pre-metastatic niche. Nature 438 (7069):820–827. https://doi.org/10.1038/nature04186
20. Chlenski A, Cohn SL (2010) Modulation of matrix remodeling by SPARC in neoplastic progression. Semin Cell Dev Biol 21 (1):55–65. https://doi.org/10.1016/j.semcdb.2009.11.018
21. Arnold SA, Rivera LB, Miller AF, Carbon JG, Dineen SP, Xie Y, Castrillon DH, Sage EH, Puolakkainen P, Bradshaw AD, Brekken RA (2010) Lack of host SPARC enhances vascular function and tumor spread in an orthotopic murine model of pancreatic carcinoma. Dis Model Mech 3(1–2):57–72. https://doi.org/10.1242/dmm.003228
22. Carmeliet P, Jain RK (2000) Angiogenesis in cancer and other diseases. Nature 407 (6801):249–257. https://doi.org/10.1038/35025220
23. Liu J, Agarwal S (2010) Mechanical signals activate vascular endothelial growth factor receptor-2 to upregulate endothelial cell proliferation during inflammation. J Immunol 185(2):1215–1221. https://doi.org/10.4049/jimmunol.0903660
24. Montesano R, Orci L, Vassalli P (1983) In vitro rapid organization of endothelial cells into capillary-like networks is promoted by collagen matrices. J Cell Biol 97(5 Pt 1):1648–1652

25. Ingber D, Folkman J (1988) Inhibition of angiogenesis through modulation of collagen metabolism. Lab Investig 59(1):44–51
26. Myers KA, Applegate KT, Danuser G, Fischer RS, Waterman CM (2011) Distinct ECM mechanosensing pathways regulate microtubule dynamics to control endothelial cell branching morphogenesis. J Cell Biol 192 (2):321–334. https://doi.org/10.1083/jcb.201006009
27. Newman AC, Nakatsu MN, Chou W, Gershon PD, Hughes CC (2011) The requirement for fibroblasts in angiogenesis: fibroblast-derived matrix proteins are essential for endothelial cell lumen formation. Mol Biol Cell 22(20):3791–3800. https://doi.org/10.1091/mbc.E11-05-0393
28. Bignon M, Pichol-Thievend C, Hardouin J, Malbouyres M, Brechot N, Nasciutti L, Barret A, Teillon J, Guillon E, Etienne E, Caron M, Joubert-Caron R, Monnot C, Ruggiero F, Muller L, Germain S (2011) Lysyl oxidase-like protein-2 regulates sprouting angiogenesis and type IV collagen assembly in the endothelial basement membrane. Blood 118(14):3979–3989. https://doi.org/10.1182/blood-2010-10-313296
29. Kalluri R (2003) Basement membranes: structure, assembly and role in tumour angiogenesis. Nat Rev Cancer 3(6):422–433. https://doi.org/10.1038/nrc1094
30. Bonanno E, Iurlaro M, Madri JA, Nicosia RF (2000) Type IV collagen modulates angiogenesis and neovessel survival in the rat aorta model. In Vitro Cell Dev Biol Anim 36 (5):336–340. https://doi.org/10.1290/1071-2690(2000)036<0336:TICMAA>2.0.CO;2
31. Herbst TJ, McCarthy JB, Tsilibary EC, Furcht LT (1988) Differential effects of laminin, intact type IV collagen, and specific domains of type IV collagen on endothelial cell adhesion and migration. J Cell Biol 106 (4):1365–1373
32. Sudhakar A, Nyberg P, Keshamouni VG, Mannam AP, Li J, Sugimoto H, Cosgrove D, Kalluri R (2005) Human alpha1 type IV collagen NC1 domain exhibits distinct antiangiogenic activity mediated by alpha1beta1 integrin. J Clin Invest 115(10):2801–2810. https://doi.org/10.1172/JCI24813
33. Petitclerc E, Boutaud A, Prestayko A, Xu J, Sado Y, Ninomiya Y, Sarras MP Jr, Hudson BG, Brooks PC (2000) New functions for non-collagenous domains of human collagen type IV. Novel integrin ligands inhibiting angiogenesis and tumor growth in vivo. J Biol Chem 275(11):8051–8061
34. Kim YM, Jang JW, Lee OH, Yeon J, Choi EY, Kim KW, Lee ST, Kwon YG (2000) Endostatin inhibits endothelial and tumor cellular invasion by blocking the activation and catalytic activity of matrix metalloproteinase. Cancer Res 60(19):5410–5413
35. Meyaard L (2008) The inhibitory collagen receptor LAIR-1 (CD305). J Leukoc Biol 83 (4):799–803. https://doi.org/10.1189/jlb.0907609
36. Meyaard L, Hurenkamp J, Clevers H, Lanier LL, Phillips JH (1999) Leukocyte-associated Ig-like receptor-1 functions as an inhibitory receptor on cytotoxic T cells. J Immunol 162 (10):5800–5804
37. Rosenfeldt H, Grinnell F (2000) Fibroblast quiescence and the disruption of ERK signaling in mechanically unloaded collagen matrices. J Biol Chem 275(5):3088–3092
38. Provenzano PP, Inman DR, Eliceiri KW, Keely PJ (2009) Matrix density-induced mechanoregulation of breast cell phenotype, signaling and gene expression through a FAK-ERK linkage. Oncogene 28 (49):4326–4343. https://doi.org/10.1038/onc.2009.299
39. Tilghman RW, Cowan CR, Mih JD, Koryakina Y, Gioeli D, Slack-Davis JK, Blackman BR, Tschumperlin DJ, Parsons JT (2010) Matrix rigidity regulates cancer cell growth and cellular phenotype. PLoS One 5 (9):e12905. https://doi.org/10.1371/journal.pone.0012905
40. Mouw JK, Yui Y, Damiano L, Bainer RO, Lakins JN, Acerbi I, Ou G, Wijekoon AC, Levental KR, Gilbert PM, Hwang ES, Chen YY, Weaver VM (2014) Tissue mechanics modulate microRNA-dependent PTEN expression to regulate malignant progression. Nat Med 20(4):360–367. https://doi.org/10.1038/nm.3497
41. Leight JL, Wozniak MA, Chen S, Lynch ML, Chen CS (2012) Matrix rigidity regulates a switch between TGF-beta1-induced apoptosis and epithelial-mesenchymal transition. Mol Biol Cell 23(5):781–791. https://doi.org/10.1091/mbc.E11-06-0537
42. Erler JT, Bennewith KL, Cox TR, Lang G, Bird D, Koong A, Le QT, Giaccia AJ (2009) Hypoxia-induced lysyl oxidase is a critical mediator of bone marrow cell recruitment to form the premetastatic niche. Cancer Cell 15 (1):35–44. https://doi.org/10.1016/j.ccr.2008.11.012
43. Bondareva A, Downey CM, Ayres F, Liu W, Boyd SK, Hallgrimsson B, Jirik FR (2009) The lysyl oxidase inhibitor, beta-aminopropionitrile, diminishes the metastatic

colonization potential of circulating breast cancer cells. PLoS One 4(5):e5620. https://doi.org/10.1371/journal.pone.0005620

44. Liotta LA (2016) Adhere, degrade, and move: the three-step model of invasion. Cancer Res 76(11):3115–3117. https://doi.org/10.1158/0008-5472.CAN-16-1297
45. Gocheva V, Joyce JA (2007) Cysteine cathepsins and the cutting edge of cancer invasion. Cell Cycle 6(1):60–64. https://doi.org/10.4161/cc.6.1.3669
46. Kessenbrock K, Plaks V, Werb Z (2010) Matrix metalloproteinases: regulators of the tumor microenvironment. Cell 141(1):52–67. https://doi.org/10.1016/j.cell.2010.03.015
47. Mohamed MM, Sloane BF (2006) Cysteine cathepsins: multifunctional enzymes in cancer. Nat Rev Cancer 6(10):764–775. https://doi.org/10.1038/nrc1949
48. Liotta LA, Abe S, Robey PG, Martin GR (1979) Preferential digestion of basement membrane collagen by an enzyme derived from a metastatic murine tumor. Proc Natl Acad Sci U S A 76(5):2268–2272
49. Liotta LA, Tryggvason K, Garbisa S, Hart I, Foltz CM, Shafie S (1980) Metastatic potential correlates with enzymatic degradation of basement membrane collagen. Nature 284(5751):67–68
50. Sabeh F, Shimizu-Hirota R, Weiss SJ (2009) Protease-dependent versus -independent cancer cell invasion programs: three-dimensional amoeboid movement revisited. J Cell Biol 185(1):11–19. https://doi.org/10.1083/jcb.200807195
51. Curino AC, Engelholm LH, Yamada SS, Holmbeck K, Lund LR, Molinolo AA, Behrendt N, Nielsen BS, Bugge TH (2005) Intracellular collagen degradation mediated by uPARAP/Endo180 is a major pathway of extracellular matrix turnover during malignancy. J Cell Biol 169(6):977–985. https://doi.org/10.1083/jcb.200411153
52. Buck MR, Karustis DG, Day NA, Honn KV, Sloane BF (1992) Degradation of extracellular-matrix proteins by human cathepsin B from normal and tumour tissues. Biochem J 282(Pt 1):273–278
53. Sameni M, Moin K, Sloane BF (2000) Imaging proteolysis by living human breast cancer cells. Neoplasia 2(6):496–504
54. Sameni M, Dosescu J, Sloane BF (2001) Imaging proteolysis by living human glioma cells. Biol Chem 382(5):785–788. https://doi.org/10.1515/BC.2001.094
55. Withana NP, Blum G, Sameni M, Slaney C, Anbalagan A, Olive MB, Bidwell BN, Edgington L, Wang L, Moin K, Sloane BF, Anderson RL, Bogyo MS, Parker BS (2012) Cathepsin B inhibition limits bone metastasis in breast cancer. Cancer Res 72(5):1199–1209. https://doi.org/10.1158/0008-5472.CAN-11-2759
56. Duong LT, Wesolowski GA, Leung P, Oballa R, Pickarski M (2014) Efficacy of a cathepsin K inhibitor in a preclinical model for prevention and treatment of breast cancer bone metastasis. Mol Cancer Ther 13(12):2898–2909. https://doi.org/10.1158/1535-7163.MCT-14-0253
57. Sudhan DR, Siemann DW (2015) Cathepsin L targeting in cancer treatment. Pharmacol Ther 155:105–116. https://doi.org/10.1016/j.pharmthera.2015.08.007
58. Bingle L, Brown NJ, Lewis CE (2002) The role of tumour-associated macrophages in tumour progression: implications for new anticancer therapies. J Pathol 196(3):254–265. https://doi.org/10.1002/path.1027
59. Zhang QW, Liu L, Gong CY, Shi HS, Zeng YH, Wang XZ, Zhao YW, Wei YQ (2012) Prognostic significance of tumor-associated macrophages in solid tumor: a meta-analysis of the literature. PLoS One 7(12):e50946. https://doi.org/10.1371/journal.pone.0050946
60. Afik R, Zigmond E, Vugman M, Klepfish M, Shimshoni E, Pasmanik-Chor M, Shenoy A, Bassat E, Halpern Z, Geiger T, Sagi I, Varol C (2016) Tumor macrophages are pivotal constructors of tumor collagenous matrix. J Exp Med 213(11):2315–2331. https://doi.org/10.1084/jem.20151193
61. Franklin RA, Liao W, Sarkar A, Kim MV, Bivona MR, Liu K, Pamer EG, Li MO (2014) The cellular and molecular origin of tumor-associated macrophages. Science 344(6186):921–925. https://doi.org/10.1126/science.1252510
62. Pollard JW (2004) Tumour-educated macrophages promote tumour progression and metastasis. Nat Rev Cancer 4(1):71–78. https://doi.org/10.1038/nrc1256
63. Mantovani A, Ming WJ, Balotta C, Abdeljalil B, Bottazzi B (1986) Origin and regulation of tumor-associated macrophages: the role of tumor-derived chemotactic factor. Biochim Biophys Acta 865(1):59–67
64. Mantovani A, Sica A (2010) Macrophages, innate immunity and cancer: balance, tolerance, and diversity. Curr Opin Immunol 22

(2):231–237. https://doi.org/10.1016/j.coi.2010.01.009

65. Hanahan D, Coussens LM (2012) Accessories to the crime: functions of cells recruited to the tumor microenvironment. Cancer Cell 21 (3):309–322. https://doi.org/10.1016/j.ccr.2012.02.022
66. Mantovani A, Sozzani S, Locati M, Allavena P, Sica A (2002) Macrophage polarization: tumor-associated macrophages as a paradigm for polarized M2 mononuclear phagocytes. Trends Immunol 23(11):549–555
67. Sica A, Saccani A, Bottazzi B, Polentarutti N, Vecchi A, van Damme J, Mantovani A (2000) Autocrine production of IL-10 mediates defective IL-12 production and NF-kappa B activation in tumor-associated macrophages. J Immunol 164(2):762–767
68. Mantovani A, Savino B, Locati M, Zammataro L, Allavena P, Bonecchi R (2010) The chemokine system in cancer biology and therapy. Cytokine Growth Factor Rev 21(1):27–39. https://doi.org/10.1016/j.cytogfr.2009.11.007
69. Lin EY, Pollard JW (2007) Tumor-associated macrophages press the angiogenic switch in breast cancer. Cancer Res 67 (11):5064–5066. https://doi.org/10.1158/0008-5472.CAN-07-0912
70. Leek RD, Lewis CE, Whitehouse R, Greenall M, Clarke J, Harris AL (1996) Association of macrophage infiltration with angiogenesis and prognosis in invasive breast carcinoma. Cancer Res 56(20):4625–4629
71. Lewis JS, Landers RJ, Underwood JC, Harris AL, Lewis CE (2000) Expression of vascular endothelial growth factor by macrophages is up-regulated in poorly vascularized areas of breast carcinomas. J Pathol 192(2):150–158. https://doi.org/10.1002/1096-9896(2000)9999:9999<::AID-PATH687>3.0.CO;2-G
72. Colegio OR, Chu NQ, Szabo AL, Chu T, Rhebergen AM, Jairam V, Cyrus N, Brokowski CE, Eisenbarth SC, Phillips GM, Cline GW, Phillips AJ, Medzhitov R (2014) Functional polarization of tumour-associated macrophages by tumour-derived lactic acid. Nature 513(7519):559–563. https://doi.org/10.1038/nature13490
73. Wyckoff J, Wang W, Lin EY, Wang Y, Pixley F, Stanley ER, Graf T, Pollard JW, Segall J, Condeelis J (2004) A paracrine loop between tumor cells and macrophages is required for tumor cell migration in mammary tumors. Cancer Res 64(19):7022–7029. https://doi.org/10.1158/0008-5472.CAN-04-1449
74. Lin EY, Nguyen AV, Russell RG, Pollard JW (2001) Colony-stimulating factor 1 promotes progression of mammary tumors to malignancy. J Exp Med 193(6):727–740
75. Zhao L, Lim SY, Gordon-Weeks AN, Tapmeier TT, Im JH, Cao Y, Beech J, Allen D, Smart S, Muschel RJ (2013) Recruitment of a myeloid cell subset (CD11b/Gr1 mid) via CCL2/CCR2 promotes the development of colorectal cancer liver metastasis. Hepatology 57(2):829–839. https://doi.org/10.1002/hep.26094
76. Lu X, Kang Y (2009) Chemokine (C-C motif) ligand 2 engages CCR2+ stromal cells of monocytic origin to promote breast cancer metastasis to lung and bone. J Biol Chem 284(42):29087–29096. https://doi.org/10.1074/jbc.M109.035899
77. Qian BZ, Li J, Zhang H, Kitamura T, Zhang J, Campion LR, Kaiser EA, Snyder LA, Pollard JW (2011) CCL2 recruits inflammatory monocytes to facilitate breast-tumour metastasis. Nature 475(7355):222–225. https://doi.org/10.1038/nature10138
78. Kitamura T, Qian BZ, Soong D, Cassetta L, Noy R, Sugano G, Kato Y, Li J, Pollard JW (2015) CCL2-induced chemokine cascade promotes breast cancer metastasis by enhancing retention of metastasis-associated macrophages. J Exp Med 212(7):1043–1059. https://doi.org/10.1084/jem.20141836
79. Vaage J, Pepin KG (1985) Morphological observations during developing concomitant immunity against a C3H/he mammary tumor. Cancer Res 45(2):659–666
80. Vaage J, Harlos JP (1991) Collagen production by macrophages in tumour encapsulation and dormancy. Br J Cancer 63(5):758–762
81. Ansorge HL, Meng X, Zhang G, Veit G, Sun M, Klement JF, Beason DP, Soslowsky LJ, Koch M, Birk DE (2009) Type XIV collagen regulates fibrillogenesis: premature collagen fibril growth and tissue dysfunction in null mice. J Biol Chem 284(13):8427–8438. https://doi.org/10.1074/jbc.M805582200
82. Gerecke DR, Meng X, Liu B, Birk DE (2003) Complete primary structure and genomic organization of the mouse Col14a1 gene. Matrix Biol 22(3):209–216
83. Liguori M, Solinas G, Germano G, Mantovani A, Allavena P (2011) Tumor-associated macrophages as incessant builders and destroyers of the cancer stroma. Cancer 3 (4):3740–3761. https://doi.org/10.3390/cancers3043740
84. Zhu Y, Herndon JM, Sojka DK, Kim KW, Knolhoff BL, Zuo C, Cullinan DR, Luo J,

Bearden AR, Lavine KJ, Yokoyama WM, Hawkins WG, Fields RC, Randolph GJ, DeNardo DG (2017) Tissue-resident macrophages in pancreatic ductal adenocarcinoma originate from embryonic hematopoiesis and promote tumor progression. Immunity 47 (2):323–338 e326. https://doi.org/10.1016/j.immuni.2017.07.014

85. Puolakkainen PA, Brekken RA, Muneer S, Sage EH (2004) Enhanced growth of pancreatic tumors in SPARC-null mice is associated with decreased deposition of extracellular matrix and reduced tumor cell apoptosis. Mol Cancer Res 2(4):215–224
86. Sangaletti S, Stoppacciaro A, Guiducci C, Torrisi MR, Colombo MP (2003) Leukocyte, rather than tumor-produced SPARC, determines stroma and collagen type IV deposition in mammary carcinoma. J Exp Med 198 (10):1475–1485. https://doi.org/10.1084/jem.20030202
87. Sangaletti S, Di Carlo E, Gariboldi S, Miotti S, Cappetti B, Parenza M, Rumio C, Brekken RA, Chiodoni C, Colombo MP (2008) Macrophage-derived SPARC bridges tumor cell-extracellular matrix interactions toward metastasis. Cancer Res 68 (21):9050–9059. https://doi.org/10.1158/0008-5472.CAN-08-1327
88. Burke RM, Madden KS, Perry SW, Zettel ML, Brown EB 3rd (2013) Tumor-associated macrophages and stromal TNF-alpha regulate collagen structure in a breast tumor model as visualized by second harmonic generation. J Biomed Opt 18(8):86003. https://doi.org/10.1117/1.JBO.18.8.086003
89. Allaoui R, Bergenfelz C, Mohlin S, Hagerling C, Salari K, Werb Z, Anderson RL, Ethier SP, Jirstrom K, Pahlman S, Bexell D, Tahin B, Johansson ME, Larsson C, Leandersson K (2016) Cancer-associated fibroblast-secreted CXCL16 attracts monocytes to promote stroma activation in triple-negative breast cancers. Nat Commun 7:13050. https://doi.org/10.1038/ncomms13050
90. Schnoor M, Cullen P, Lorkowski J, Stolle K, Robenek H, Troyer D, Rauterberg J, Lorkowski S (2008) Production of type VI collagen by human macrophages: a new dimension in macrophage functional heterogeneity. J Immunol 180(8):5707–5719
91. Nikolic-Paterson DJ, Wang S, Lan HY (2014) Macrophages promote renal fibrosis through direct and indirect mechanisms. Kidney Int Suppl 4(1):34–38. https://doi.org/10.1038/kisup.2014.7
92. Meng XM, Wang S, Huang XR, Yang C, Xiao J, Zhang Y, To KF, Nikolic-Paterson DJ, Lan HY (2016) Inflammatory macrophages can transdifferentiate into myofibroblasts during renal fibrosis. Cell Death Dis 7 (12):e2495. https://doi.org/10.1038/cddis.2016.402
93. Yang J, Lin SC, Chen G, He L, Hu Z, Chan L, Trial J, Entman ML, Wang Y (2013) Adiponectin promotes monocyte-to-fibroblast transition in renal fibrosis. J Am Soc Nephrol 24 (10):1644–1659. https://doi.org/10.1681/ASN.2013030217
94. Weitkamp B, Cullen P, Plenz G, Robenek H, Rauterberg J (1999) Human macrophages synthesize type VIII collagen in vitro and in the atherosclerotic plaque. FASEB J 13 (11):1445–1457
95. Medbury HJ, James V, Ngo J, Hitos K, Wang Y, Harris DC, Fletcher JP (2013) Differing association of macrophage subsets with atherosclerotic plaque stability. Int Angiol 32 (1):74–84
96. Cieslik KA, Taffet GE, Carlson S, Hermosillo J, Trial J, Entman ML (2011) Immune-inflammatory dysregulation modulates the incidence of progressive fibrosis and diastolic stiffness in the aging heart. J Mol Cell Cardiol 50(1):248–256. https://doi.org/10.1016/j.yjmcc.2010.10.019
97. Bertrand S, Godoy M, Semal P, Van Gansen P (1992) Transdifferentiation of macrophages into fibroblasts as a result of Schistosoma mansoni infection. Int J Dev Biol 36 (1):179–184
98. Mass E, Jacome-Galarza CE, Blank T, Lazarov T, Durham BH, Ozkaya N, Pastore A, Schwabenland M, Chung YR, Rosenblum MK, Prinz M, Abdel-Wahab O, Geissmann F (2017) A somatic mutation in erythro-myeloid progenitors causes neurodegenerative disease. Nature 549 (7672):389–393. https://doi.org/10.1038/nature23672
99. Sinha M, Sen CK, Singh K, Das A, Ghatak S, Rhea B, Blackstone B, Powell HM, Khanna S, Roy S (2018) Direct conversion of injury-site myeloid cells to fibroblast-like cells of granulation tissue. Nat Commun 9(1):936. https://doi.org/10.1038/s41467-018-03208-w
100. Matsubayashi Y, Louani A, Dragu A, Sanchez-Sanchez BJ, Serna-Morales E, Yolland L, Gyoergy A, Vizcay G, Fleck RA, Heddleston JM, Chew TL, Siekhaus DE, Stramer BM (2017) A moving source of matrix components is essential for de novo basement membrane formation. Curr Biol

27(22):3526–3534 e3524. https://doi.org/10.1016/j.cub.2017.10.001

101. Kalluri R, Zeisberg M (2006) Fibroblasts in cancer. Nat Rev Cancer 6(5):392–401. https://doi.org/10.1038/nrc1877
102. Vignaud JM, Marie B, Klein N, Plenat F, Pech M, Borrelly J, Martinet N, Duprez A, Martinet Y (1994) The role of platelet-derived growth factor production by tumor-associated macrophages in tumor stroma formation in lung cancer. Cancer Res 54 (20):5455–5463
103. Pickup M, Novitskiy S, Moses HL (2013) The roles of TGFbeta in the tumour microenvironment. Nat Rev Cancer 13 (11):788–799. https://doi.org/10.1038/nrc3603
104. Karlmark KR, Weiskirchen R, Zimmermann HW, Gassler N, Ginhoux F, Weber C, Merad M, Luedde T, Trautwein C, Tacke F (2009) Hepatic recruitment of the inflammatory Gr1+ monocyte subset upon liver injury promotes hepatic fibrosis. Hepatology 50 (1):261–274. https://doi.org/10.1002/hep.22950
105. Hesketh M, Sahin KB, West ZE, Murray RZ (2017) Macrophage phenotypes regulate scar formation and chronic wound healing. Int J Mol Sci 18(7):E1545. https://doi.org/10.3390/ijms18071545
106. Knipper JA, Willenborg S, Brinckmann J, Bloch W, Maass T, Wagener R, Krieg T, Sutherland T, Munitz A, Rothenberg ME, Niehoff A, Richardson R, Hammerschmidt M, Allen JE, Eming SA (2015) Interleukin-4 receptor alpha signaling in myeloid cells controls collagen fibril assembly in skin repair. Immunity 43(4):803–816. https://doi.org/10.1016/j.immuni.2015.09.005
107. Zhou X, Franklin RA, Adler M, Jacox JB, Bailis W, Shyer JA, Flavell RA, Mayo A, Alon U, Medzhitov R (2018) Circuit design features of a stable two-cell system. Cell 172 (4):744–757 e717. https://doi.org/10.1016/j.cell.2018.01.015
108. Fields GB (2013) Interstitial collagen catabolism. J Biol Chem 288(13):8785–8793. https://doi.org/10.1074/jbc.R113.451211
109. Collins HM, Morris TM, Watson SA (2001) Spectrum of matrix metalloproteinase expression in primary and metastatic colon cancer: relationship to the tissue inhibitors of metalloproteinases and membrane type-1-matrix metalloproteinase. Br J Cancer 84 (12):1664–1670. https://doi.org/10.1054/bjoc.2001.1831
110. Zeng ZS, Cohen AM, Guillem JG (1999) Loss of basement membrane type IV collagen is associated with increased expression of metalloproteinases 2 and 9 (MMP-2 and MMP-9) during human colorectal tumorigenesis. Carcinogenesis 20(5):749–755
111. Hotary K, Li XY, Allen E, Stevens SL, Weiss SJ (2006) A cancer cell metalloprotease triad regulates the basement membrane transmigration program. Genes Dev 20 (19):2673–2686. https://doi.org/10.1101/gad.1451806
112. Jiang D, Lim SY (2016) Influence of immune myeloid cells on the extracellular matrix during cancer metastasis. Cancer Microenviron 9 (1):45–61. https://doi.org/10.1007/s12307-016-0181-6
113. Coussens LM, Tinkle CL, Hanahan D, Werb Z (2000) MMP-9 supplied by bone marrow-derived cells contributes to skin carcinogenesis. Cell 103(3):481–490
114. Huang S, Van Arsdall M, Tedjarati S, McCarty M, Wu W, Langley R, Fidler IJ (2002) Contributions of stromal metalloproteinase-9 to angiogenesis and growth of human ovarian carcinoma in mice. J Natl Cancer Inst 94(15):1134–1142
115. Hiratsuka S, Nakamura K, Iwai S, Murakami M, Itoh T, Kijima H, Shipley JM, Senior RM, Shibuya M (2002) MMP9 induction by vascular endothelial growth factor receptor-1 is involved in lung-specific metastasis. Cancer Cell 2(4):289–300
116. Giraudo E, Inoue M, Hanahan D (2004) An amino-bisphosphonate targets MMP-9-expressing macrophages and angiogenesis to impair cervical carcinogenesis. J Clin Invest 114(5):623–633. https://doi.org/10.1172/JCI22087
117. Du R, Lu KV, Petritsch C, Liu P, Ganss R, Passegue E, Song H, Vandenberg S, Johnson RS, Werb Z, Bergers G (2008) HIF1alpha induces the recruitment of bone marrow-derived vascular modulatory cells to regulate tumor angiogenesis and invasion. Cancer Cell 13(3):206–220. https://doi.org/10.1016/j.ccr.2008.01.034
118. Deryugina EI, Zajac E, Juncker-Jensen A, Kupriyanova TA, Welter L, Quigley JP (2014) Tissue-infiltrating neutrophils constitute the major in vivo source of angiogenesis-inducing MMP-9 in the tumor microenvironment. Neoplasia 16(10):771–788. https://doi.org/10.1016/j.neo.2014.08.013
119. Madsen DH, Jurgensen HJ, Siersbaek MS, Kuczek DE, Grey Cloud L, Liu S, Behrendt N, Grontved L, Weigert R, Bugge TH (2017) Tumor-associated macrophages

derived from circulating inflammatory monocytes degrade collagen through cellular uptake. Cell Rep 21(13):3662–3671. https://doi.org/10.1016/j.celrep.2017.12.011

120. Gocheva V, Wang HW, Gadea BB, Shree T, Hunter KE, Garfall AL, Berman T, Joyce JA (2010) IL-4 induces cathepsin protease activity in tumor-associated macrophages to promote cancer growth and invasion. Genes Dev 24(3):241–255. https://doi.org/10.1101/gad.1874010
121. Vasiljeva O, Papazoglou A, Kruger A, Brodoefel H, Korovin M, Deussing J, Augustin N, Nielsen BS, Almholt K, Bogyo M, Peters C, Reinheckel T (2006) Tumor cell-derived and macrophage-derived cathepsin B promotes progression and lung metastasis of mammary cancer. Cancer Res 66(10):5242–5250. https://doi.org/10.1158/0008-5472.CAN-05-4463
122. Doyle AD, Yamada KM (2016) Mechanosensing via cell-matrix adhesions in 3D microenvironments. Exp Cell Res 343(1):60–66. https://doi.org/10.1016/j.yexcr.2015.10.033
123. Jin H, Varner J (2004) Integrins: roles in cancer development and as treatment targets. Br J Cancer 90(3):561–565. https://doi.org/10.1038/sj.bjc.6601576
124. Franco C, Britto K, Wong E, Hou G, Zhu SN, Chen M, Cybulsky MI, Bendeck MP (2009) Discoidin domain receptor 1 on bone marrow-derived cells promotes macrophage accumulation during atherogenesis. Circ Res 105(11):1141–1148. https://doi.org/10.1161/CIRCRESAHA.109.207357
125. Postlethwaite AE, Kang AH (1976) Collagen-and collagen peptide-induced chemotaxis of human blood monocytes. J Exp Med 143(6):1299–1307
126. Wiesner C, Le-Cabec V, El Azzouzi K, Maridonneau-Parini I, Linder S (2014) Podosomes in space: macrophage migration and matrix degradation in 2D and 3D settings. Cell Adhes Migr 8(3):179–191
127. Van Goethem E, Poincloux R, Gauffre F, Maridonneau-Parini I, Le Cabec V (2010) Matrix architecture dictates three-dimensional migration modes of human macrophages: differential involvement of proteases and podosome-like structures. J Immunol 184(2):1049–1061. https://doi.org/10.4049/jimmunol.0902223
128. Kaplan G (1983) In vitro differentiation of human monocytes. Monocytes cultured on glass are cytotoxic to tumor cells but monocytes cultured on collagen are not. J Exp Med 157(6):2061–2072
129. Wesley RB 2nd, Meng X, Godin D, Galis ZS (1998) Extracellular matrix modulates macrophage functions characteristic to atheroma: collagen type I enhances acquisition of resident macrophage traits by human peripheral blood monocytes in vitro. Arterioscler Thromb Vasc Biol 18(3):432–440
130. Patel NR, Bole M, Chen C, Hardin CC, Kho AT, Mih J, Deng L, Butler J, Tschumperlin D, Fredberg JJ, Krishnan R, Koziel H (2012) Cell elasticity determines macrophage function. PLoS One 7(9):e41024. https://doi.org/10.1371/journal.pone.0041024

Chapter 16

FACS Analysis of Col1α Protein Levels in Primary Fibroblasts

Noam Cohen and Neta Erez

Abstract

Chronic inflammatory diseases are often associated with organ fibrosis, a progressive condition in which excessive deposition of extracellular matrix (ECM), mainly composed of collagen I (Col I), is deposited by activated fibroblasts and severely impairs tissue architecture and function, eventually resulting in organ failure. Moreover, enhanced collagen deposition by activated fibroblasts and increased stiffness of the extracellular matrix were demonstrated to be associated with tumor progression and metastasis. In order to quantitatively analyze fibrotic activation of fibroblasts and collagen deposition, it is essential to assess collagen content. While various histological methods allow assessment of collagen in tissue sections (e.g., Masson trichrome and Sirius red), reliable measurement and quantification of collagen levels in vitro remain a challenge in the field. In this protocol, we utilize intracellular staining of Col1α and flow cytometry analysis to analyze collagen content in primary fibroblasts isolated from fresh single cell suspensions of metastases-bearing lungs.

Key words Cancer-associated fibroblasts, FACS, Collagen, Lung metastases

1 Introduction

Cancer-associated fibroblasts (CAFs) are a vastly heterogeneous multifunctional population of fibroblastic cells shown to promote tumor growth by directly stimulating tumor cell proliferation, by enhancing angiogenesis, and by modifying the extracellular matrix (ECM), to support tumor cell invasion [1, 2]. CAFs are also key mediators of tumor-promoting inflammation by secreting cytokines and chemokines that recruit and modulate the function of immune cells in the tumor microenvironment [3–8].

In addition, CAFs foster tumor progression by modifying ECM architecture through enhanced deposition of collagen and by mediating increased cross-linking of collagen fibers, thus stiffening the stroma, which was found to correlate with tumor progression [9–11]. In some cancer types, in particular of the breast and pancreas, activation of fibroblasts leads to substantial deposition of

Irit Sagi and Nikolaos A. Afratis (eds.), *Collagen: Methods and Protocols*, Methods in Molecular Biology, vol. 1944, https://doi.org/10.1007/978-1-4939-9095-5_16, © Springer Science+Business Media, LLC, part of Springer Nature 2019

fibrotic ECM. Such aberrant fibrotic responses, termed desmoplasia, correlate with poor prognosis [11].

Moreover, several recent studies demonstrated in lung and liver metastasis that formation of hospitable pre-metastatic niche is associated with enhanced collagen expression and collagen cross-linking, leading to increased tissue stiffness that supports metastatic growth [12–14]. Thus, studying the molecular pathways in fibroblasts that are associated with enhanced collagen deposition is crucial to our understanding of tumor-promoting ECM modifications. Such changes can be quantitatively assessed in vivo by histological analysis of collagen in tissues [15, 16]. However, in order to specifically analyze factors that instigate pro-fibrotic changes in fibroblasts, establishment of in vitro assays is required. Nevertheless, quantitative analysis of collagen in cultured fibroblasts has been challenging, since analysis of modifications in gene expression are not always indicative of protein levels. Analyses at the protein level (e.g., Western blotting) are also challenging and often do not provide robust and consistent results, since collagen is a very big and complex protein, containing several subunits and multiple posttranslational modifications.

Flow cytometry is a well-established method for quantitative analysis of cell surface markers, by labeling with specific fluorophore-conjugated antibodies. In recent years, the applications of FACS-related methods expanded significantly, and they can now be utilized for analyzing multiple characteristic of single cells, including protein levels and phosphorylation levels of intracellular proteins [17]. Analyzing such intracellular characteristics requires additional steps of cell fixation and permeabilization.

In this protocol, we use FACS analysis to quantify collagen-1α levels in primary lung fibroblasts, isolated from fresh lungs of mice and cultured in vitro for several days. This method can be used to analyze the effect of various treatments/triggers on modifications of collagen levels in fibroblasts. In combination with other metrics for pro-fibrogenic activity (expression of pro-fibrotic genes, collagen contraction activity, etc.), this method is useful to study questions regarding fibrosis and fibroblast activation.

2 Materials

2.1 Lung Dissection

1. Surgery tools (washed with detergent and then dipped in 70% ethanol).
2. Styrofoam surface to rest the mice on during dissection.
3. Pins or needles to hold mice during dissection.
4. Plastic jar with lid for digestion.
5. Magnetic stir bar.

6. Incubator at 37 °C.
7. Multipoint magnetic stirrer.
8. PBS.
9. 10 cm plate.

2.2 Single Cell Suspension

1. Centrifuge (fit for spinning of 50 ml conical tubes).
2. Dissociation solution (made freshly before use): 0.02 g dispase II, 0.02 g collagenase IV, 0.01 g deoxyribonuclease, 20 ml serum-free medium (SFM).
3. 10% FCS DMEM.
4. 70 μm cell strainer.
5. Red blood cell lysis buffer: 4 g NH_4Cl, 0.5 g $KHCO_3$, 500 ml DDW.

2.3 Cell Culture

1. Collagen mixture: 0.05 mg rat tail collagen I in 1 ml 0.02 N acetic acid. Adjust volumes as required in specific steps (*see* **Note 1**).
2. 10% FCS DMEM.
3. DMEM.
4. Six-well plate.
5. 10 cm plate.
6. Trypsin-EDTA.
7. PBS.

2.4 Antibody Staining

1. PBS.
2. Trypsin-EDTA.
3. *FACS buffer*: PBS, 1% FCS, 2 mM EDTA.
4. *Staining buffer*: PBS, 1% FCS, 0.09% Na^+-azide. Adjust buffer pH to 7.4–7.6.
5. Anti-mouse Col1α-FITC.
6. Cytofix/Cytoperm Plus kit.
7. FACS tubes with filter.

3 Methods

The protocol described is suitable for six mice, but can be easily adjusted for smaller or lager mouse numbers.

3.1 Lung Dissection

Since isolated fibroblasts are cultured, it is best to perform the dissection in a laminar flow hood, under sterile conditions.

1. Euthanize mice using carbon dioxide (CO_2) inhalation.

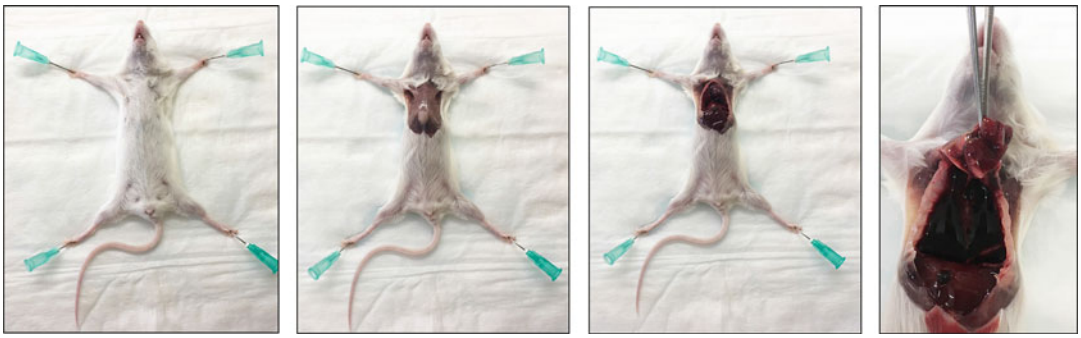

Fig. 1 Lung dissection, sequential steps from left to right: pin mouse to diaper coated Styrofoam surface, dissect out skin, cut through the ribs with scissors and use forceps to disconnect the lungs

Fig. 2 Whole lung in PBS post-dissection

2. On a Styrofoam surface, place the mouse on its back, and pin firmly the upper limbs using 25-gauge needles (Fig. 1).
3. Spray the mouse generously with 70% ethanol.
4. Use scissors to cut the skin. For sterility purposes, it is recommended to use a different set of scissors for skin and for inner cavities. Use scissors to cut through the ribs to expose the thoracic cavity.
5. Remove the lungs gently and transfer into 10 cm dish containing PBS (Fig. 2).

3.2 Single Cell Suspension

1. Place the lungs in digestion jar.
2. Mince thoroughly with curved scissors.

3. Add 20 ml dissociation solution (*see* **Note 2**).
4. Place on multipoint magnetic stirrer in 37 °C incubator, and stir for 30 min.
5. In the meantime, prepare 6 ml of collagen mixture and coat six-well plate (1 ml per well). Incubate the plate at 37 °C incubator for 30 min (*see* **Note 3**).

   *This stage can also be done in advance. Collagen-coated plates can be kept in 4 °C with PBS for 3 days.
6. Take out the digestion jar, and stop the reaction by adding 20 ml of cold 10% FCS DMEM.
7. Strain the tissue/media mixture through a 70 μm cell strainer placed on top of a 50 ml conical tube.
8. Centrifuge the conical tube for 5 min at 300 × *g* at 4 °C.
9. Decant the supernatant using a glass pipette attached to a vacuum, without disturbing the cell pellet.
10. Resuspend cell pellet in 10 ml RBC lysis buffer and incubate for 5 min at RT.
11. Neutralize RBC lysis buffer by adding 10 ml of 10% FCS DMEM.
12. Centrifuge the conical tube with cells for 5 min at 300 × *g* at 4 °C.
13. Decant the supernatant and resuspend in 12 ml 10% FCS DMEM (2 ml per mouse).
14. Wash the six-well plate with PBS twice, and seed the cells in a six-well plate (one well per mouse).
15. Incubate the cells in 5% CO_2, 37 °C incubator.

3.3 Cell Culture

1. On day 2, wash cells with PBS and change to fresh media to dispose of any cell debris.
2. On day 3 (or when cells are ~80% confluent, usually takes 1–2 days after isolation), coat six 10 cm plates with collagen mixture (7 ml per plate), and incubate at 37 °C incubator for 30 min (*see* **Note 4**) (Fig. 3).
3. Detach cells with trypsin-EDTA and split into 10 cm plates (one well into one plate).
4. On day 4, wash cells with PBS and change to fresh media.
5. When cells are 80–90% confluent (usually takes 1–2 days), detach cells, count them, and seed 300,000 cells per well in a six-well plate for desired experiments (*see* **Note 5**).
6. On the next day, wash cell twice with PBS, and incubate with SFM for 6 h (*see* **Note 6**).
7. Wash out the SFM and incubate cells with your treatment media for 24 h.

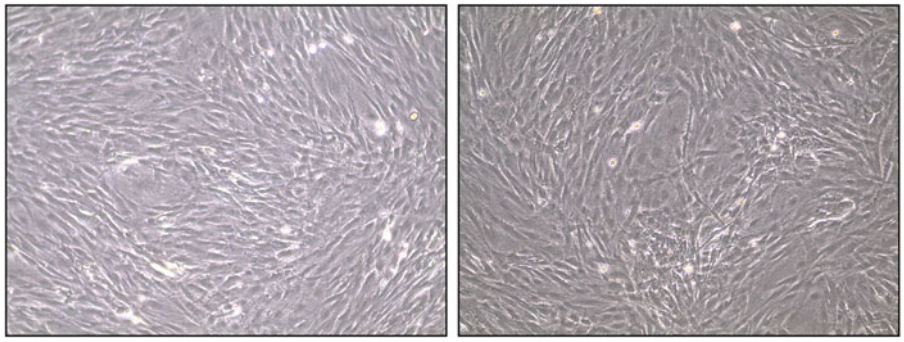

Fig. 3 Bright field image of cultured lung fibroblasts at ~90% confluency. Magnification ×100

3.4 Antibody Staining

1. Following 24 h of incubation with treatment media, wash cells twice with PBS.
2. Add to each well 500 μl trypsin-EDTA to detach cells.
3. Neutralize trypsin by adding 1 ml 10% FCS DMEM.
4. Place cells into Eppendorf tubes (one tube per well) and centrifuge for 5 min at 300 × *g*.
5. Resuspend cell pellet in 1 ml PBS and centrifuge for 5 min at 300 × *g*.
6. Decant supernatant and resuspend cells in 100 μl of fixation/permeabilization buffer.
7. Incubate cells on ice for 20 min.
8. Wash cells with 250 μl 1× BD wash buffer and spin for 5 min at 300 × *g* at 4 °C. Repeat twice.
9. Resuspend cell pellet in each tube in 110 μl 1× BD wash buffer.
10. Remove 10 μl from each tube to a new Eppendorf tube, to be used as unstained control. This control will be composed of a mixture of 10 μl from each sample (total volume: 6 × 10 = 60 μl).
11. Bring volume in unstained tube to 200 μl with FACS buffer.
12. Add to all test tubes 2 μl of anti-mouse Col1α-FITC antibody.
13. Incubate cells on ice for 30 min in the dark.
14. Wash cells with 250 μl 1× BD wash buffer, and spin for 5 min at 300 × *g* at 4 °C. Repeat twice.
15. Decant supernatant and resuspend cells in 200 μl FACS buffer.
16. Filter the cells in all tubes into matching FACS tubes with filter top to avoid cell clumps.
17. Keep samples on ice while analyzing.

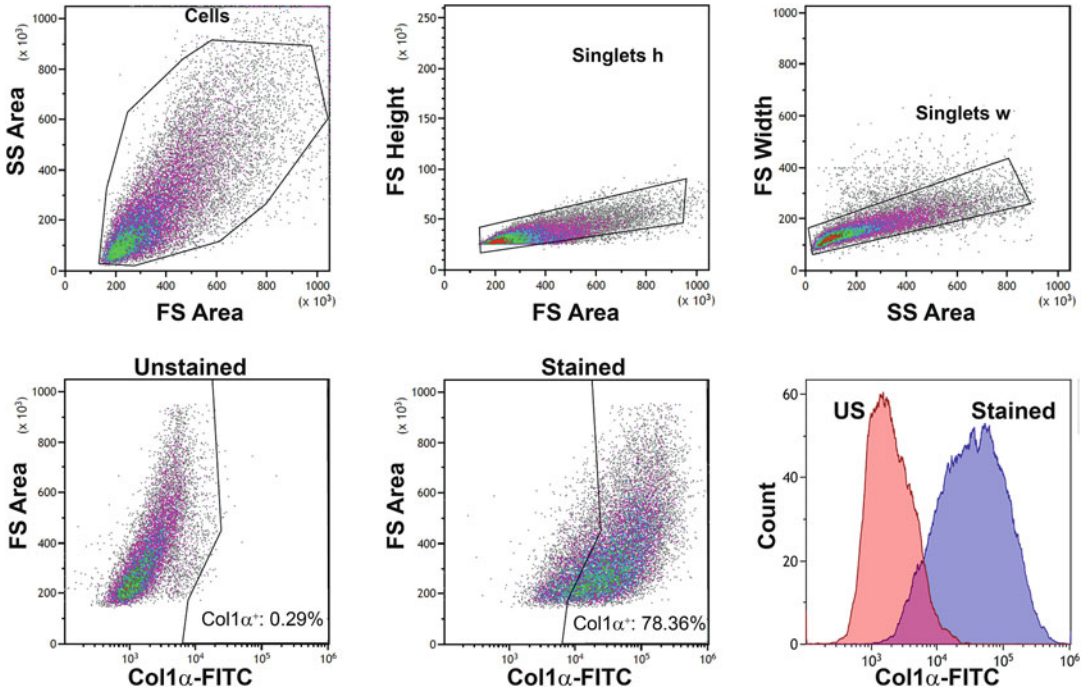

Fig. 4 FACS analysis of Col1α in NLF analyzed by Kaluza® 1.5 Flow Analysis Software (Beckman Coulter, Inc.)

3.5 FACS Analysis

1. Run control unstained tube to determine gates.
2. Acquire test tubes using the same parameters.
3. Analyze results with a suitable flow cytometry analysis software such as Kaluza (Fig. 4).

4 Notes

1. The concentration of rat tail collagen I (BD) varies between batches. Adjust the required volume to the specific concentration you have in order to get 0.05 mg rat tail collagen I in 1 ml of 0.02 N acetic acid.
2. This volume of dissociation solution will efficiently dissociate up to ten lungs.
3. Fibroblast are activated when they are plated directly on the stiff surface of a plastic culture dish; therefore, for optimal culturing of primary fibroblasts, a preliminary step of collagen coating is required, as detailed above.
4. The times in this section may vary between different experiments. Cells should reach 80–90% confluence before splitting them.

5. Pause point: At this point cells can be frozen in freezing media (90% FCS, 10% DMSO) for future analysis.
6. Short starvation is used in order to maintain cells in basal level before incubation with specific treatments.

References

1. Kalluri R, Zeisberg M (2006) Fibroblasts in cancer. Nat Rev Cancer 6:392–401. https://doi.org/10.1038/nrc1877
2. Östman A, Augsten M (2009) Cancer-associated fibroblasts and tumor growth - bystanders turning into key players. Curr Opin Genet Dev 19:67–73. https://doi.org/10.1016/j.gde.2009.01.003
3. Erez N, Glanz S, Raz Y et al (2013) Cancer-associated fibroblasts express pro-inflammatory factors in human breast and ovarian tumors. Biochem Biophys Res Commun 437:397–402. https://doi.org/10.1016/j.bbrc.2013.06.089
4. Erez N, Truitt M, Olson P, Hanahan D (2010) Cancer-associated fibroblasts are activated in incipient Neoplasia to orchestrate tumor-promoting inflammation in an NF-kappaB-dependent manner. Cancer Cell 17:135–147. https://doi.org/10.1016/j.ccr.2009.12.041
5. Feig C, Jones JO, Kraman M et al (2013) Targeting CXCL12 from FAP-expressing carcinoma-associated fibroblasts synergizes with anti—PD-L1 immunotherapy in pancreatic cancer. Proc Natl Acad Sci U S A 110:20212–20217. https://doi.org/10.1073/pnas.1320318110 http://www.pnas.org/cgi/doi/10.1073/pnas.1320318110/-/DCSupplemental
6. Martey CA, Pollock SJ, Turner CK et al (2004) Cigarette smoke induces cyclooxygenase-2 and microsomal prostaglandin E 2 synthase in human lung fibroblasts: implications for lung inflammation and cancer. Am J Physiol Lung Cell Mol Physiol 14642:981–991. https://doi.org/10.1152/ajplung.00239.2003
7. Sharon Y, Raz Y, Cohen N et al (2015) Tumor-derived Osteopontin reprograms normal mammary fibroblasts to promote inflammation and tumor growth in breast cancer. Cancer Res 75 (6):963–974. https://doi.org/10.1158/0008-5472.CAN-14-1990
8. Lotti F, Jarrar AM, Pai RK et al (2013) Chemotherapy activates cancer-associated fibroblasts to maintain colorectal cancer-initiating cells by IL-17A. J Exp Med 210:2851–2872. https://doi.org/10.1084/jem.20131195
9. Goetz JG, Minguet S, Navarro-lérida I et al (2011) Biomechanical remodeling of the microenvironment by stromal caveolin-1 favors tumor invasion and metastasis. Cell 146:148–163. https://doi.org/10.1016/j.cell.2011.05.040.Biomechanical
10. Levental KR, Yu H, Kass L et al (2009) Matrix crosslinking forces tumor progression by enhancing integrin signaling. Cell 139:891–906. https://doi.org/10.1016/j.cell.2009.10.027.Matrix
11. Erler JT, Weaver VM (2009) Three-dimensional context regulation of metastasis. Clin Exp Metastasis 26:35–49. https://doi.org/10.1007/s10585-008-9209-8
12. Cox TR, Bird D, Baker A et al (2013) LOX-mediated collagen crosslinking is responsible for fibrosis-enhanced metastasis. Cancer Res 73:1721–1732. https://doi.org/10.1158/0008-5472.CAN-12-2233.LOX-mediated
13. Erler JT, Bennewith KL, Nicolau M et al (2006) Lysyl oxidase is essential for hypoxia-induced metastasis. Nature 440:1222–1226. https://doi.org/10.1038/nature04695
14. Nielsen SR, Quaranta V, Linford A et al (2016) Macrophage-secreted granulin supports pancreatic cancer metastasis by inducing liver fibrosis. Nat Cell Biol 18:549–560. https://doi.org/10.1038/ncb3340
15. Bauman TM, Nicholson TM, Abler LL et al (2014) Characterization of fibrillar collagens and extracellular matrix of glandular benign prostatic hyperplasia nodules. PLoS One 9:1–9. https://doi.org/10.1371/journal.pone.0109102
16. Street JM, Souza ACP, Alvarez-Prats A et al (2014) Automated quantification of renal fibrosis with Sirius red and polarization contrast microscopy. Physiol Rep 2:1–9. https://doi.org/10.14814/phy2.12088
17. Adan A, Alizada G, Kiraz Y et al (2017) Flow cytometry: basic principles and applications. Crit Rev Biotechnol 37:163–176. https://doi.org/10.3109/07388551.2015.1128876

Chapter 17

Methods for the Construction of Collagen-Based Triple-Helical Peptides Designed as Matrix Metalloproteinase Inhibitors

Gregg B. Fields

Abstract

The triple-helical structure of collagen has been accurately reproduced in numerous chemical and recombinant model systems. Triple-helical peptides have found application for dissecting collagen-stabilizing forces, isolating receptor and protein binding sites in collagen, evaluating collagen-mediated cell signaling activities, mechanistic examination of collagenolytic proteases, and developing novel biomaterials and drug delivery vehicles. Due to their inherent stability to general proteolysis, triple-helical peptides present an opportunity as in vivo inhibitory agents. The present chapter provides methods for the construction of collagen-based triple-helical peptides designed as matrix metalloproteinase inhibitors.

Key words Collagen, Matrix metalloproteinases, Triple-helical peptides, Triple-helical inhibitor, Peptide-based drugs, Transition state analog

1 Introduction

1.1 Collagen

Collagen is the most abundant protein in animals and is the major structural protein found in the connective tissues such as basement membranes, tendons, ligaments, cartilage, bone, and skin. The defining feature of collagen is the supersecondary structure, composed of three parallel extended left-handed polyproline type II alpha chains of primarily repeating Gly-Xxx-Yyy triplets. Three left-handed strands intertwine in a right-handed fashioned around a common axis to form a triple helix. The packing of the triple-helical coiled-coil structure favors Gly in every third position. In the collagen Gly-Xxx-Yyy triplet, the residue in the Xxx position is often L-proline (Pro), and the residue in the Yyy position is often 4(R)-hydroxy-L-proline (Hyp), accounting for 20% of the total amino acid composition in collagen [1].

Depending on the primary structure of the alpha chains [2], collagens have been classified into two main categories,

Irit Sagi and Nikolaos A. Afratis (eds.), *Collagen: Methods and Protocols*, Methods in Molecular Biology, vol. 1944, https://doi.org/10.1007/978-1-4939-9095-5_17, © Springer Science+Business Media, LLC, part of Springer Nature 2019

homotrimeric and heterotrimeric. Homotrimeric collagens have three identical alpha chain sequences (designated α1). Examples of such type of collagens are types II and III. Alternatively, heterotrimeric collagens have either three alpha chain of different sequences, designated as α1, α2, and α3 (i.e., type V), or two alpha chains of identical sequence (α1) and a third alpha chain of different sequences (α2), such as types I and VI [3]. Furthermore, based on their quaternary structure, collagens are grouped into subfamilies such as fibrillar, collagen associated with banded fibrils [i.e., fibril-associated collagens with interrupted triple helices (FACITs)], network-forming (i.e., basement membrane and short chain), transmembranous, and membrane associated with interrupted triple helices (MACITs) [3]. The collagen triple helix is essential for the integrity of multiple connective tissues. Most collagens assist in anchoring cells to the extracellular matrix and some function in cellular regulation.

1.2 Collagen-Model Triple-Helical Peptides

For several decades triple-helical peptides (THPs) or "mini-collagens" consisting of collagen-model sequences and their three-dimensional folds have been constructed and studied to fully investigate the structural and biological roles of collagenous proteins [4–11]. In order to properly study the biological roles of collagen, THPs need to form triple-helical structures that are thermally stable to in vitro and in vivo conditions. Several factors influence the stability of THPs. The chains are held together by hydrogen bonds that form between the peptide amine of Gly residues and peptide carbonyl groups in an adjacent polypeptide chain [7, 12]. These interstrand hydrogen bonds formed between the GlyN–H and XxxC=O are critical for triple-helix stability, as replacement of a central amide bond of $(\text{Pro-Pro-Gly})_{10}$ with either an ester or (*E*)-alkene, or replacement of the central Pro-Pro with a Pro-*trans*-Pro isostere, substantially destabilizes the THP [13–15]. It has long been noted that the thermal stability of the collagen triple helix is enhanced by Hyp residues. The stability arising from Hyp is based on stereoelectronic effects preorganizing the main chain in the proper conformation for triple-helix formation [16]. Collagen-model sequences have often been "sandwiched" between repeats of Gly-Pro-Hyp to obtain THPs of reasonable stability.

Incorporation of several non-native amino acids in the proper position within the peptide sequence can further enhance triple-helix stability. The first Pro in the Pro-Pro-Gly triplet prefers an endo ring pucker conformation, while the second Pro prefers the exo ring pucker conformation [17]. This observation suggested that Pro derivatives preferring the C^{γ}-endo ring pucker could preorganize triple-helix formation when in the Xaa position, whereas those that prefer the C^{γ}-exo ring pucker could preorganize triple-helix formation when in the Yaa position [18]. One such example of

a stabilizing non-native amino acid is 4*R*-fluoroproline (4*R*-Flp). Incorporation of 4*R*-fluoroproline has been shown to induce hyperstability in the triple helix of (Pro-4*R*Flp-Gly)$_{10}$ compared to (Pro-4*R*Hyp-Gly)$_{10}$ [19, 20]. The 4*R*-fluoro group in 4*R*-fluoroproline stabilizes the C^{γ}-exo pucker conformation. Similar to 4*R*-Flp, incorporation of 4*R*-methylproline (4*R*-mep) in the Xaa position significantly increases triple-helix stability [18].

1.3 THPs Designed as Inhibitors

THPs represent small, well-folded peptidic structures. There has been a recent surge in the advancement of peptide drugs, as they tend to have lower toxicities and greater efficacies than existing drugs [21–24]. The size of THPs makes immunogenicity unlikely; in fact, with the exclusion of specific glycosylated sequences, collagen peptides are non-immunogenic. The triple-helical nature of the inhibitor renders it reasonably stable to proteolysis, as observed in vitro in mouse, rat, and human serum and/or plasma and in vivo in rats [25–29]. The stability of THPs has allowed for their administration orally [30].

Application of THPs as biomaterials and drug delivery vehicles has been described recently [27, 31–33]. The use of THPs as inhibitors has been explored to a considerably lesser extent. When identifying integrin binding sites, THPs have been shown to inhibit integrin binding to native collagens [34–36]. THPs that bind to leukocyte-associated Ig-like receptor-1 (LAIR-1) induce inhibition of T-cell activation [37], while THPs that bind to human osteoclast-associated receptor (OSCAR) inhibit osteoclastogenesis [38].

1.4 Triple-Helical Matrix Metalloproteinase Inhibitors

A well-established strategy to develop protease inhibitors is modification of a bioactive peptide such that the hydrolytically susceptible peptide bond is replaced. Metallo(zinc)-proteases use the nucleophilic attack of a water molecule as one of the steps of amide bond hydrolysis [39]. The tetrahedral intermediate that results from water addition to the amide carbonyl has given rise to phosphorus-based amide bond replacements (Fig. 1, lower right). The use of phosphinic pseudo-dipeptides can be a very effective approach to develop highly selective and potent inhibitors of a variety of Zn^{2+} metalloproteases [40, 41]. Phosphinic peptides [$\Psi\{PO_2H–CH_2\}$; Y = CH_2 in Fig. 1] have been shown to behave as transition state analog inhibitors of matrix metalloproteinases (MMPs) [42]. Phosphinate *triple-helical* MMP inhibitors allow for interaction with both the enzyme active site and secondary binding sites (exosites) (Fig. 2) [43, 44].

We have developed selective, high-affinity inhibitors for MMPs based on triple-helical structure and phosphinate analogs of Gly-Leu, Gly-Val, and Gly-Ile (Tables 1 and 2) [40, 43, 45–49]. Two homotrimeric triple-helical peptide inhibitors (THPIs), C_6-(Gly-Pro-Hyp)$_4$-Gly-Pro-Pro-Gly$\Psi\{PO_2H–CH_2\}$ Val-Val-Gly-Glu-Gln-Gly-Glu-Gln-Gly-Pro-Pro-(Gly-Pro-Hyp)$_4$-

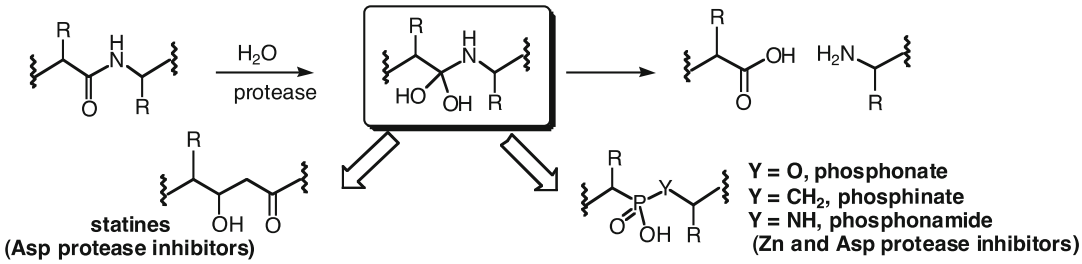

Fig. 1 Tetrahedral intermediate (boxed) and statin and phosphorus-based transition state analog inhibitors. Used with permission from [40]

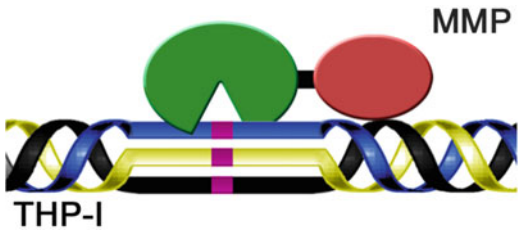

Fig. 2 Model structure of a triple-helical peptide inhibitor (THPI) of MMPs. The non-hydrolyzable $PO_2H–CH_2$ bond, which functions as a transition state analog, is indicated in purple. Used with permission from [40]

Table 1
Inhibition of MMP-2 and MMP-9 by THPIs

Enzyme	Inhibitor	Temperature[a] (°C)	$K_i^{(app)}$ (nM)
MMP-2	C_6-α1(V)GlyΨ{$PO_2H–CH_2$}Val THPI	10	4.14 ± 0.47
		37	19.23 ± 0.64
	α1(V)GlyΨ{$PO_2H–CH_2$}Val [$mep_{14,32}$,$Flp_{15,33}$] THPI	25	189.1 ± 26.54
		37	2.24 ± 0.11
MMP-9	C_6-α1(V)GlyΨ{$PO_2H–CH_2$}Val THPI	10	1.76 ± 0.05
		37	1.29 ± 0.00
	α1(V)GlyΨ{$PO_2H–CH_2$}Val [$mep_{14,32}$,$Flp_{15,33}$] THPI	25	90.6 ± 6.67
		37	0.98 ± 0.092

[a]Assay temperature

NH_2 [designated C_6-α1(V)GlyΨ{$PO_2H–CH_2$}Val THPI] and (Gly-Pro-Hyp)$_4$-Gly-mep-Flp-Gly-Pro-Gln-GlyΨ{$PO_2H–CH_2$}Leu-Ala-Gly-Gln-Arg-Gly-Ile-Arg-Gly-mep-Flp-(Gly-Pro-Hyp)$_4$-Tyr-NH_2 [designated α1(I–III)GlyΨ{$PO_2H–CH_2$}Leu THPI], were shown to inhibit MMPs in the low nanomolar range [40, 45]. The THPI sequences were based on either the α1(V) 436–450 collagen region, which is hydrolyzed at the Gly-Val bond by MMP-2 and MMP-9, or the interstitial collagen consensus sequence α1(I–III)769–783, which is hydrolyzed by MMP-1, MMP-2, MMP-8, MMP-9, MMP-13, membrane-type 1 MMP (MT1-MMP), and MT2-MMP [50, 51].

Table 2
Inhibition of MMPs by GlyΨ{PO_2H–CH_2}Xxx THPIs

Enzyme	Inhibitor	Inhibitor T_m (°C)	$K_i^{(app)a}$ (nM)
MMP-1	GlyΨ{PO_2H–CH_2}Leu	30	7.83 ± 1.03
MT1-MMP	GlyΨ{PO_2H–CH_2}Leu	30	111.68 ± 28.7
MMP-1	GlyΨ{PO_2H–CH_2}Ile-His-Lys-Gln	26	169.2 ± 28.4
MMP-3	GlyΨ{PO_2H–CH_2}Ile-His-Lys-Gln	26	No inhibition at 1 μM
MMP-8	GlyΨ{PO_2H–CH_2}Ile-His-Lys-Gln	26	124.6 ± 6.9
MT1-MMP	GlyΨ{PO_2H–CH_2}Ile-His-Lys-Gln	26	4704 ± 708.4
MMP-1	GlyΨ{PO_2H–CH_2}Ile-Tyr-Phe-Gln	25	110.59 ± 29.8
MMP-2	GlyΨ{PO_2H–CH_2}Ile-Tyr-Phe-Gln	25	17.82 ± 1.9
MMP-3	GlyΨ{PO_2H–CH_2}Ile-Tyr-Phe-Gln	25	13600.33 ± 5160.7
MMP-8	GlyΨ{PO_2H–CH_2}Ile-Tyr-Phe-Gln	25	62.1 ± 2.5
MMP-9	GlyΨ{PO_2H–CH_2}Ile-Tyr-Phe-Gln	25	0.03 ± 0.02
MMP-13	GlyΨ{PO_2H–CH_2}Ile-Tyr-Phe-Gln	25	77.13 ± 14.4
MT1-MMP	GlyΨ{PO_2H–CH_2}Ile-Tyr-Phe-Gln	25	46.15 ± 4.7

[a]Assay performed at room temperature (~25 °C)

The first-generation THPIs were limited for potential in vivo applications, due to (a) thermal instability or (b) lack of selectivity. The melting temperature (T_m) of C_6-α1(V)GlyΨ{PO_2H–CH_2}Val THPI was 25 °C, below that desired for a stable triple helix under physiological conditions [40]. The α1(I-III)GlyΨ{PO_2H–CH_2}Leu THPI was selective toward collagenolytic MMPs, but that group included seven enzymes. The non-native amino acids (*2S,4R*)-4-fluoroproline (Flp) and (*2S,4R*)-4-methylproline (mep) were utilized to create a more thermally stable α1(V)GlyΨ{PO_2H–CH_2}Val THPI (Table 1). The resulting THPI, α1(V)GlyΨ{PO_2H–CH_2}Val [$mep_{14,32}$,$Flp_{15,33}$], exhibited an increase of 18 °C in thermal stability over the initial THPI [49]. This THPI was effective in vivo in a mouse model of multiple sclerosis, reducing clinical severity and weight loss [49].

Two different approaches were applied to obtain selective THPIs for MT1-MMP, utilizing data obtained from phage display generation of MT1-MMP selective substrates and combinatorial chemistry generation of MT1-MMP selective inhibitors [49]. Two THPIs were developed to be more selective within the collagenolytic members of the MMP family (Table 2). One of these THPIs, GlyΨ{PO_2H–CH_2}Ile-His-Lys-Gln THPI, was more effective against MMP-8 than MT1-MMP and was utilized in vivo in a mouse model of sepsis [49]. The THPI targeting

Table 3
Inhibition of MMPs by heterotrimeric THPIs

Enzyme	Inhibitor	$K_i^{(app)a,b}$ (nM)
MMP-1	THCP8	NI
MMP-3		18,400 ± 11,600
MMP-13		136 ± 8.7
MT1-MMP		382 ± 111.1
MMP-1	THCP9	NI
MMP-3		12,700 ± 4700
MMP-13		106 ± 71.3
MT1-MMP		210 ± 42.4
MMP-1	THCP12	NI
MMP-3		NI
MMP-13		180 ± 62.4
MT1-MMP		320 ± 56.0

[a]Assay performed at room temperature (~25 °C)
[b]NI = No inhibition

MMP-8 minimized lung damage, increased production of the anti-inflammatory cytokine IL-10, and vastly improved mouse survival [49].

Utilizing the GlyΨ{PO_2H–CH_2}Ile-Tyr-Phe-Gln THPI (Table 2), the intracellular role of MMP-9 on citrate synthase activity post-MI was evaluated in vivo [52]. Citrate synthase activity decreased in the infarcted, left ventricle tissue of WT mice at day 1 post-MI, but this reduction was not observed in MMP-9 null mice or THPI-treated mice, suggesting that MMP-9 deletion or inhibition helps to maintain mitochondrial activity post-MI. MMP-9 cleaved citrate synthase in vitro, generating a ~20 kDa fragment [52].

In a further attempt to obtain an MT1-MMP selective THPI, synthesis of heterotrimeric THPIs has been pursued [48]. Heterotrimeric THPIs effectively inhibited MT1-MMP and MMP-13 (K_i = 100–300 nM) but had little or no activity against MMP-1 and MMP-3 (Table 3). Since the homotrimeric THPI analog of the heterotrimer THPI, α1(I–III)GlyΨ{PO_2H–CH_2}Leu THPI, was an effective MMP-1 inhibitor (Table 2), the presence of the phosphinate in only one strand was responsible for the selectivity for MT1-MMP versus MMP-1 [48].

2 Materials

All commercially available materials and reagents are used as received.

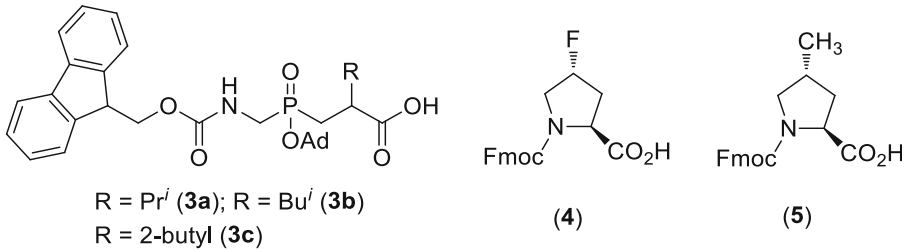

Fig. 3 Structures of Fmoc-phosphinate dipeptide building blocks (**3**), Fmoc-Flp (**4**), and Fmoc-mep (**5**). The phosphinate dipeptides are analogs of Gly-Val (**3a**), Gly-Leu (**3b**), and Gly-Ile (**3c**). Used with permission from [49]

2.1 Peptide Synthesis

1. Knight single-stranded peptide (SSP) [Mca-Lys-Pro-Leu-Gly-Leu-Lys(Dnp)-Ala-Arg-NH_2] [53–56].
2. Synthesis of Fmoc-Gly-Val phosphinate dipeptide [(*R*,*S*)-2-isopropyl-3-((1-(*N*-(Fmoc)amino)-methyl)-adamantyloxy-phosphinyl) propanoic acid] (Fig. 3a) [46].
3. Synthesis of Fmoc-Gly-Leu phosphinate dipeptide [(*R*,*S*)-2-isobutyl-3-((1-(*N*-(Fmoc)amino)-methyl)-adamantyloxyphosphinyl) propanoic acid] (Fig. 3b) [46].
4. Synthesis of Fmoc-Gly-Ile phosphinic dipeptide [(*R*,*S*)-2-(2-butyl)-3-((1-(*N*-(Fmoc)amino)-methyl)-adamantyloxy-phosphinyl) propanoic acid] (Fig. 3c) [47].
5. Fmoc deprotection solution. This solution is prepared by mixing 1,8-diazabicyclo[5.4.0]undec-7-ene (DBU), piperidine, and *N*-methylpyrrolidone (NMP) in a ratio of 1:5:44 (v/v). 1 L of such solution is composed of 20 mL DBU, 100 mL of piperidine, and 880 mL of NMP.
6. Dde deprotection solution. The 1-(4,4-dimethyl-2,6-dioxocyclohexylidene)ethyl (Dde) protecting groups are removed using 2% hydrazine in dimethylformamide (DMF). This solution is prepared by mixing 2 mL hydrazine hydrate and 98 mL DMF.
7. Peptide cleavage cocktail. Under the fume hood, prepare the peptide cleavage solution containing 5% H_2O in trifluoroacetic acid (TFA, peptide synthesis grade). To prepare 5 mL of such a solution, mix 250 μL of H_2O and 4.75 mL of TFA. For every 100 mg of resin, use 1.5 mL cleavage cocktail (*see* **Note 1**).
8. Peptide lyophilization. Synthetic peptides and conjugates are lyophilized.

2.2 HPLC Characterization and Purification

1. All analytical runs are performed using a Vydac C18 column (5 μm, 300 Å, 150 mm × 4.6 mm) or similar.
2. Preparative runs are carried out using a Vydac C18 column (15–20 μm, 300 Å, 250 mm × 22 mm) or similar.

3. Water is of HPLC or Milli-Q quality.
4. The following solvent system is used: solvent A contains 0.1% TFA in H_2O, while solvent B contains 0.1% TFA in acetonitrile. The analytical gradient ranging from 2 to 100% B over 20 min using 1 mL/min flow rate is used. The preparative HPLC elution gradients are 7–30% of B in 40 min [for GlyΨ{PO_2H–CH_2}Ile-His-Lys-Gln THPI], 10–35% of B in 50 min [for GlyΨ{PO_2H–CH_2}Ile-Tyr-Phe-Gln THPI], and 20–50% of B in 30 min [for α1(V)GlyΨ{PO_2H–CH_2}Val [$mep_{14,32}$, $Flp_{15,33}$] THPI] with a flow rate of 10 mL/min. In both cases peptide detection is carried out at $\lambda = 220$ and 280 nm. Homogenous fractions are combined and lyophilized.

2.3 Mass Spectrometry

The molecular weight of peptides and peptide conjugates are determined using matrix-assisted laser desorption/ionization time-of-flight mass spectrometry (MALDI-TOF MS). MALDI-TOF MS analysis is performed using an Applied Biosystems Voyager DE-PRO Biospectrometry workstation or Bruker Microflex LF mass spectrometer using sinapinic acid (SA), α-cyano-4-hydroxycinnamic acid (HCCA), or 2,5-dihydroxybenzoic acid (DHB) as matrix.

2.4 Circular Dichroism (CD) Spectroscopy

Triple-helical peptide structure is evaluated by near-UV CD spectroscopy. Typically, CD spectra of collagen-like peptides are recorded over the range of $\lambda = 190$–250 nm and with a sample concentration of 0.1 mg/mL in 0.5% acetic acid solution (v/v). Thermal transition curves are obtained by recording the molar ellipticity ($[\Theta]$) at $\lambda = 225$ nm with an increase in temperature of 20 °C/h over the range of 5–80 °C. The temperature is controlled by a JASCO PTC-348WI temperature control unit.

2.5 Absorption Spectrophotometry

Peptide concentration is measured by UV-Vis absorption spectrophotometry. Triple-helical peptide concentration is calculated according to the Beer-Lambert law, using the following formula:

$$C = A/(l \times 3 \times \varepsilon)$$

where C = peptide concentration (M), A = measured absorbance, and l = cell path length (cm). Please note that in case of triple-helical peptides, the molar absorption coefficient ε has to be multiplied by a number of chromophoric groups present in a molecule.

2.6 Enzymatic Assay Buffers and Stock Solutions

1. 0.1 M $ZnCl_2$.
2. Knight SSP can be prepared as a 20 mM stock solution in water and stored at −20 °C [55].

3. Enzyme assay buffer (EAB): 50 mM Tris–HCl, pH 7.5, 100 mM NaCl, 10 mM $CaCl_2$, 0.05% Brij 35.
4. TS buffer (TSB): 50 mM Tris–HCl, pH 7.5, 150 mM NaCl, 10 mM $CaCl_2$, 0.01% Brij-35, 1 μM $ZnCl_2$.
5. TSB*Zn: 50 mM Tris–HCl, pH 7.5, 100 mM NaCl, 10 mM $CaCl_2$, 0.05% Brij-35, 0.02% NaN_3, 1 μM $ZnCl_2$.
6. 4-Aminophenylmercuric acetate (APMA) solution:
   (a) Prepare APMA stock of 100 mM in dimethyl sulfoxide (DMSO).
   (b) Store at 4 °C (this stock is stable for several months).

3 Methods

3.1 Peptide Synthesis Protocols

For the incorporation of individual amino acids by Fmoc-solid-phase methodology, O-(6-chlorobenzotriazol-1-yl)-*N*,*N*,*N*′,*N*-tetramethyluronium hexafluorophosphate (HCTU)/1-hydroxybenzotriazole (HOBt) activation is recommended [57]. Reagent amounts including Fmoc-amino acids (Fmoc-AA), HCTU, HOBt, and *N*,*N*-diisopropylethylamine (DIPEA) are calculated in relation to peptide synthesis scale (typically expressed in mmol). Microwave-assisted peptide synthesis is achieved on a Liberty Microwave Peptide Synthesizer (CEM Corporation, Matthews, NC).

3.1.1 General Amino Acid Coupling Cycles

For Fmoc-amino acid couplings, the following molar excess is recommended: Fmoc-AA = 5 equiv., HCTU = 4.9 equiv., HOBt = 4.9 equiv., and N-methylmorpholine (NMM) or DIPEA = 10 equiv. Recommended coupling time using conventional automatic peptide synthesizer is 1 h, while microwave-assisted synthesis proceeds for 5 min at 50 °C and 25 W.

3.1.2 General Fmoc Deprotection Cycle

The Fmoc-protecting group is removed by gentle treatment of peptidyl-resin using standard Fmoc deprotection solution. This step can be performed on an automated peptide synthesizer using the appropriate deprotection program or manually as follows:

1. Place the resin in a peptide synthesis reaction vessel.
2. Add the appropriate amount of Fmoc deprotection solution (3–5 times the resin volume).
3. Agitate the resin for 5 min. Drain the solution.
4. Repeat **step 2**.
5. Agitate the resin for another 15 min. Drain the solution.
6. Wash resin (3 times) using 5 mL of DMF.

3.1.3 General Peptide-Resin Cleavage Protocol

1. Place the peptide-resin in a round bottom flask under inert atmosphere (Ar) in a fume hood.
2. Mix 50 μL of H_2O and 50 μL thioanisole with 900 μL of TFA to create the cleavage cocktail.
3. Cleave the peptide from the resin using 1.5 mL of cleavage cocktail per 100 mg of dry resin.
4. Cleavage and side-chain deprotection of the peptide is accomplished by treating the resin for 3–4 h (*see* **Note 1**).
5. Filter the resin and collect the filtrate.
6. Crude peptides are precipitated from the filtrate with cold MTBE and centrifuged.
7. Dissolve the pellet in H_2O and lyophilize.

3.1.4 Solid-Phase Synthesis of GlyΨ{PO_2H–CH_2}Ile-His-Lys-Gln THPI and GlyΨ{PO_2H–CH_2}Ile-Tyr-Phe-Gln THPIs

General methods Subheadings 3.1.1 and 3.1.2 are followed, with the following modifications.

1. Synthesis is performed on a Liberty automated microwave peptide synthesizer using NovaPEG Rink Amide resin (loading 0.5 mmol/g).
2. The coupling of usual Fmoc-amino acids is achieved with 5 equiv. of each amino acid, 4.9 equiv. of HCTU (0.5 M in DMF), and 8.0 equiv. of NMM (2 M in DMF) using microwave power of 25 W at 50 °C with the reaction time of 300 s (double coupling for all Arg residues first at 0 W, 25 °C for 25 min followed by 25 W, 50 °C for 300 s).
3. The removal of Fmoc-protecting group is accomplished using 10% piperazine in DMF (microwave power of 35 W at 75 °C and the reaction time of 30 s, followed by a second treatment under the same conditions for 180 s).
4. The unusual amino acids Fmoc-4*R*-fluoro-L-proline (Fmoc-Flp-OH) and Fmoc-4*R*-methyl-L-proline (Fmoc-mep-OH) are coupled using 3 equiv. of amino acid, 2.9 equiv. of HCTU, and 6 equiv. of NMM with microwave power of 25 W at 50 °C for 300 s. The coupling of Fmoc-mep-OH is repeated.
5. The Fmoc-protected phosphinic dipeptides are attached using 3 equiv. dipeptide, 3 equiv. DIPCDI, 6 equiv. HOBt, and DIPEA to adjust pH to ~8 at 40 °C for 40 min and room temperature overnight.
6. Following dipeptide addition the peptide-resin is capped using 0.5 M Ac_2O, 0.125 M DIPEA, and 0.015 M HOBt in DMF at room temperature for 1 h.
7. The deprotection of Fmoc group, immediately after incorporation of the phosphinic dipeptide into the sequence, is

performed without microwave power but with increased reaction times of 500 and 800 s.

8. The amino acid immediately after the dipeptide is attached using the same conditions as for the dipeptide; Pro11 is double coupled.
9. The final cleavage of peptide from the resin and side-chain deprotection is carried out using 7 mL of triisopropylsilane-phenol-H_2O-TFA (2:5:5:88) under inert atmosphere (Ar) for 3 h.

3.1.5 Solid-Phase Synthesis of α1(V)GlyΨ{PO_2H–CH_2}Val [$mep_{14,32}$, $Flp_{15,33}$] THPI

General methods Subheadings 3.1.1 and 3.1.2 are followed, with the following modifications.

1. Synthesis is performed on a CEM liberty blue automated microwave peptide synthesizer using NovaPEG Rink Amide resin (loading 0.48 mmol/g).
2. The coupling of usual Fmoc-amino acids is achieved with 5 equiv. of each amino acid (0.2 M), 5 equiv. of DIPCDI (0.5 M in DMF), and 5 equiv. of Oxyma (1 M in DMF). Fmoc-amino acid coupling cycles are carried out for 15 s at 75 °C and 110 s at 90 °C.
3. Fmoc deprotection is achieved with 10% piperazine (w/v) in ethanol: *N*-methyl-2-pyrrolidone (10:90) for 15 s at 75 °C and 50 s at 90 °C.
4. Fmoc-Flp-OH is incorporated using 2.5 equiv. of amino acid for 600 s at 25 °C and 300 s at 75 °C.
5. Fmoc-mep-OH and Fmoc-GlyΨ{PO_2H–CH_2}Val are incorporated using 2.5 equiv. of each compound for 1500 s at 25 °C and 600 s at 75 °C.
6. Coupling of Fmoc-Pro-OH following GlyΨ{PO_2H–CH_2}Val is performed for 1500 s at 25 °C and 600 s at 75 °C for using 5 equiv. of amino acid.
7. The final cleavage of peptide from the resin and side-chain deprotection is carried out using 7 mL of triisopropylsilane-phenol-H_2O-TFA (2:5:5:88) under inert atmosphere (Ar) for 3 h.

3.1.6 Synthesis of Single-Stranded Peptide 1 (SSP1)

General methods Subheadings 3.1.1 and 3.1.2 are followed, with the following modifications.

1. Synthesis of SSP1 (Fig. 4) is performed in 0.1 mmol scale on NovaPEG Rink Amide resin (0.48 mmol/g).
2. The coupling of Fmoc-(2*S*)-propargylglycine (Fmoc-Pra-OH) is carried out at 45 °C for 45 min using 25 W microwave power.
3. The coupling of Pro14 is repeated.

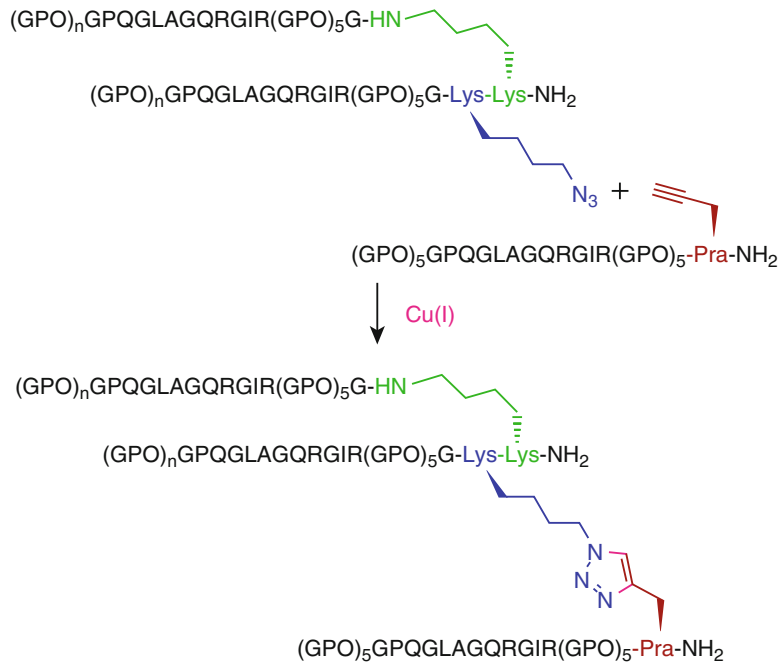

Fig. 4 Schematic of the click-based assembly of THCP6 and THCP7. Assembly was achieved with DSP3 or DSP4 and SSP1, where $n = 5$ (DSP3) or 6 (DSP4). Used with permission from [48]

3.1.7 Synthesis of Single-Stranded Peptide 2 (SSP2)

General methods Subheadings 3.1.1 and 3.1.2 are followed, with the following modifications.

1. Synthesis of SSP2 (Figs. 5 and 6) was performed on TentaGel resin (0.26 mmol/g).
2. The coupling of Fmoc-Pra is as for SSP1. Residues Arg24 and Arg27 are double coupled, where the first coupling is for 25 min at 25 °C using no power followed by 5 min at 25 °C using 25 W power, and the second coupling is for 5 min at 50 °C with microwave power of 25 W.
3. Fmoc removal at Ala21 is achieved by initial treatment for 30 s and final treatment for 3 min at 75 °C with microwave power of 35 W.
4. Coupling of the Fmoc-GlyΨ{P(OAd)(OH)–CH_2}Ile-OH dipeptide (3 equiv.) is performed using *N*,*N*′-diisopropylcarbodiimide (DIC)/HOBt/DIPEA (3 equiv./6 equiv./3 equiv.) for 80 min at 40 °C with microwave power of 25 W and then left overnight at ambient temperature.
5. The removal of the Fmoc group, immediately after incorporation of the dipeptide into the sequence and for the rest of the synthesis, is performed in two stages: Initial and final

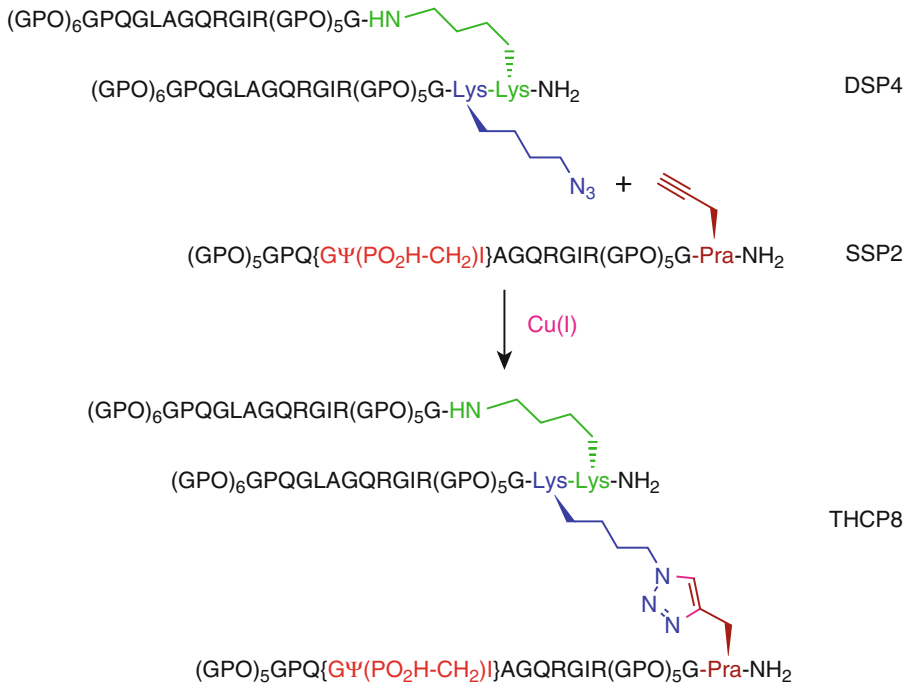

Fig. 5 Schematic of the click-based assembly of THCP8. Assembly was achieved with DSP4 and SSP2. Used with permission from [48]

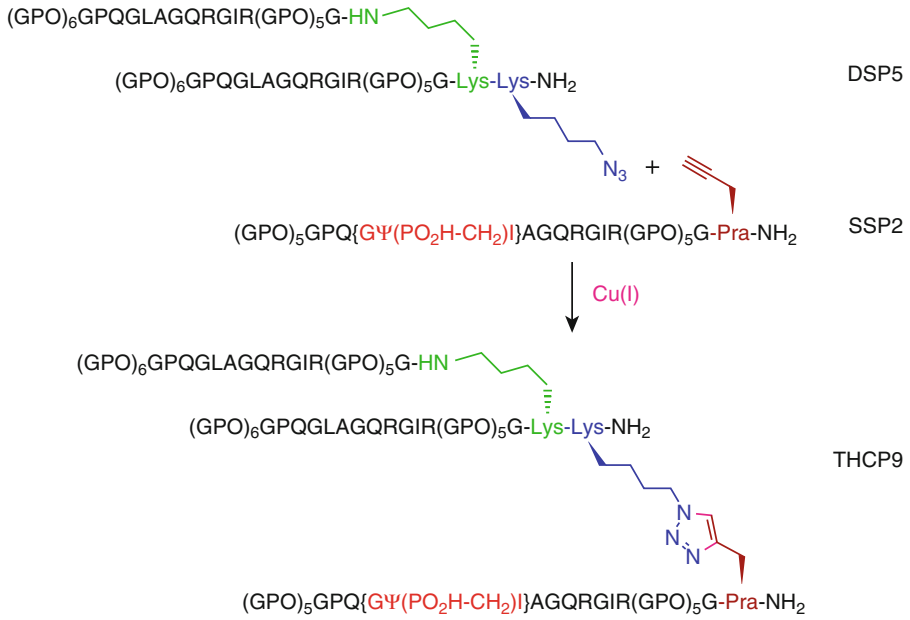

Fig. 6 Schematic of the click-based assembly of THCP9. Assembly was achieved with DSP5 and SSP2. Used with permission from [48]

treatments at 50 °C without microwave power but with increased reaction time of 500 s and 800 s, respectively.

6. The coupling of the rest of the amino acids after dipeptide incorporation is performed with increased reaction time of 20 min, with double coupling of Pro14 and Gln18.
7. Cleavage of the peptide from the resin and side-chain deprotection is carried out using 7 mL of triisopropylsilane-phenol-H_2O-TFA (2:5:5:88) under inert atmosphere (Ar) for approximately 4 h.

3.1.8 Synthesis of Double-Stranded Peptide 3 (DSP3)

General methods Subheadings 3.1.1 and 3.1.2 are followed, with the following modifications.

1. The synthesis of DSP3 (Fig. 4) is performed on NovaPEG Rink Amide resin (0.6 mmol/g).
2. Fmoc-Lys(ivDde)-OH is initially coupled to the resin followed by Fmoc-Lys(N_3)-OH. Both couplings are carried out using 3 equiv. of amino acid, 2.7 equiv. of HCTU, 2.8 equiv. of HOBt, and 6 equiv. of NMM at 50 °C for 20 min with microwave power of 25 W.
3. The resin-bound dipeptide is removed from the synthesizer, treated twice with 4 mL of 2% hydrazine hydrate in DMF for 1 h each time to remove the ivDde group, washed with DMF, and transferred back to the synthesizer reaction vessel.
4. Coupling of the remaining residues is extended to 15 min, and Pro14 was double coupled.

3.1.9 Synthesis of Double-Stranded Peptide 4 (DSP4)

General methods Subheadings 3.1.1 and 3.1.2 are followed, with the following modifications.

1. Synthesis of DSP4 (Figs. 4 and 5) is carried out by adding one more Gly-Pro-Hyp repeat on resin-bound DSP3 applying the standard peptide synthesis protocol.

3.1.10 Synthesis of Double-Stranded Peptide 5 (DSP5)

General methods Subheadings 3.1.1 and 3.1.2 are followed, with the following modifications.

1. Synthesis of DSP5 (Fig. 6) is performed on TentaGel resin (0.26 mmol/g) using the procedure outlined for DSP3 but first coupling Fmoc-Lys(N_3)-OH followed by Fmoc-Lys (ivDde)-OH.

3.1.11 Synthesis of Single-Stranded Peptide 10 (SSP10)

General methods Subheadings 3.1.1 and 3.1.2 are followed, with the following modifications.

1. Synthesis of SSP10 (Fig. 7) is performed on TentaGel S Ram resin (0.26 mmol/g).
2. Two consecutive Fmoc-Lys(N_3) residues are coupled to the resin as described for DSP3.

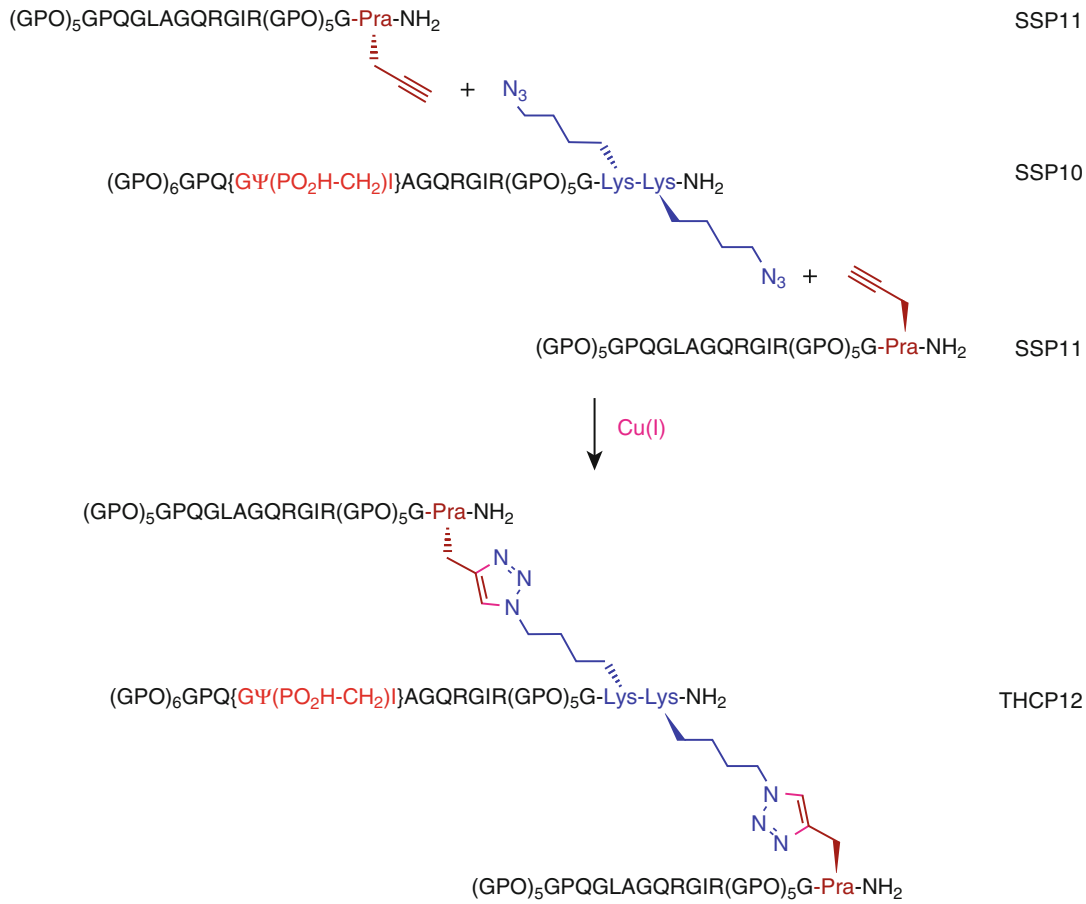

Fig. 7 Schematic of the click-based assembly of THCP12. Assembly was achieved with SSP10 and SSP11. Used with permission from [48]

3. Coupling up to Ala21 is as for SSP2. Arg24 and Arg27 are double coupled, with the coupling time extended to 10 min.
4. Coupling of the Fmoc-GlyΨ{P(OAd)(OH)–CH_2}Ile-OH dipeptide is performed as described for SSP2.
5. The coupling time of the remainder of the amino acids is increased to 20 min and Pro14 is double coupled.
6. The removal of Fmoc groups after incorporation of the phosphinate moiety is carried out as described for SSP2.

3.1.12 Synthesis of Single-Stranded Peptide 11 (SSP11)

General methods Subheadings 3.1.1 and 3.1.2 are followed, with the following modifications.

1. The synthesis of SSP11 (Fig. 7) is performed in 0.1 mmol scale on TentaGel S Ram resin (0.26 mmol/g) by following the procedure described for SSP1, except an extra Gly residue is included after the Pra.

3.1.13 Click Chemistry

A general click reaction procedure is as follows.

1. A solution of $CuSO_4 \cdot 5H_2O$ (5 equiv.) in 5% DMF in H_2O (30 μL/μmol of $CuSO_4 \cdot 5H_2O$) is added to a solution of SSP (1 equiv.) and DSP (1 equiv.) in H_2O (300 μL/μmol of total peptide, SSP + DSP).
2. The reaction mixture is vortexed and sodium ascorbate (20 equiv.) is added.
3. The resulting solution is mixed for 1–2 min and kept at room temperature with occasional mixing.
4. After 12 h, the reaction mixture is diluted with H_2O to 2 mL, filtered through a Titan 2, 30 mm filter green 0.45 μm Nylon membrane, and purified by RP-HPLC (*see* below).
5. The pure fractions are combined and lyophilized to afford a white solid.

3.2 Characterization of THPIs

3.2.1 Mass Spectrometry

The peptide molecular mass is confirmed by MALDI-TOF mass spectrometry using HCCA or SA MALDI matrices following trypsin digestion.

1. 0.5 mg of desired peptide is dissolved in 250 μL of 0.1 M $NaHCO_3$ solution.
2. 85 μL of immobilized, TPCK-treated trypsin resin solution is measured into a 2 mL centrifuge tube and washed with 250 μL of 0.1 M $NaHCO_3$ solution three times.
3. The peptide solution in $NaHCO_3$ is then added to the washed trypsin and incubated at 37–43 °C for 4–12 h.
4. The tube is centrifuged to remove the trypsin.
5. The pH of the solution is adjusted to 4 with 0.1 M HCl.
6. The solution is applied to a pre-moist C18 ZipTip, washed with 0.1% TFA-H_2O to remove salt, and finally washed with 0.1% TFA-acetonitrile to collect peptide fragments.
7. The filtrate is used to record MALDI-TOF mass spectra.

3.2.2 Circular Dichroism (CD) Spectroscopy

Triple helicity is monitored by CD spectroscopy in the far UV wavelengths [53, 58–65]. The general protocol is as follows:

1. Dissolve the peptide in an appropriate buffer to a final concentration of 0.1 mg/mL. Leave the peptide in solution for 24–48 h at 4 °C to allow for triple-helix formation.
2. Record a series of spectra (n = 5–10) over the range of λ = 190–250 nm. A typical spectrum for a triple helix shows a positive molar ellipticity at λ = 225 nm and a negative molar ellipticity at λ = 205 nm.
3. Determine the melting temperature by monitoring the change in molar ellipticity at λ = 225 nm with a constant change in

temperature (20 °C/h) from 5 to 80 °C. For samples exhibiting sigmoidal melting curves, the inflection point in the transition region (first derivative) is defined as T_m. The first derivative from the transition curve can be obtained using JASCO or GraphPad Prism software (GraphPad, USA). Alternatively, T_m is evaluated from the midpoint of the transition.

3.3 Enzyme Activation

Activation of all MMPs takes place in the TS buffer. *See* also **Note 2**.

3.3.1 Activation of ProMMP-1

1. Dilute proMMP-1 to 100 μg/mL in TS buffer.
2. Activate proMMP-1 by adding APMA to a final concentration of 1 mM.
3. Incubate at 37 °C for 2–3 h.
4. Immediately after incubation dilute MMP-1 to 20 μg/mL and store at −37 °C until ready to use.
5. Activity is initially measured with the Knight substrate. MMP-1 has a weak activity toward fTHP-15.

3.3.2 Activation of ProMMP-2

1. Dilute proMMP-2 to 100 μg/mL in TS buffer.
2. Activate proMMP-2 by adding APMA to a final concentration of 1 mM.
3. Incubate at 37 °C for 24 h.
4. Immediately after incubation dilute MMP-2 to 20 μg/mL and store at −37 °C until ready to use.
5. MMP-2 can also be obtained in active form.

3.3.3 Activation of ProMMP-3

1. Chymotrypsin is prepared as a 1 mg/mL stock in 1 mM HCl.
2. PMSF is prepared as a 0.2 M stock in ethanol.
3. Activate proMMP-3 at 20 μg/mL in EAB containing 5 μg/mL chymotrypsin.
4. Incubate at 37 °C for 30 min.
5. Terminate activation with 2 mM PMSF. Pre-warm the PMSF to 37 °C just prior to adding to the sample.
6. Store at −80 °C for future use.
7. Measure activity using the Knight substrate at 10 μM final substrate concentration.

3.3.4 Activation of ProMMP-8

1. Dilute proMMP-8 to 100 μg/mL in TS buffer.
2. Activate proMMP-8 by adding APMA to a final concentration of 1 mM.
3. Incubate at 37 °C for 1 h.

4. Immediately after incubation dilute MMP-8 to 20 μg/mL and store at −37 °C until ready to use.

3.3.5 Activation of ProMMP-9

1. Dilute proMMP-9 to 100 μg/mL in TS buffer.
2. Activate proMMP-9 by adding APMA to a final concentration of 1 mM.
3. Incubate at 37 °C for 24 h.
4. Immediately after incubation dilute MMP-9 to 20 μg/mL and store at −80 °C until ready to use.
5. MMP-9 can also be obtained in active form.

3.3.6 Activation of ProMMP-12

1. Dilute proMMP-12 to 100 μg/mL in TS buffer.
2. Activate proMMP-12 by adding APMA to a final concentration of 1 mM.
3. Incubate at 37 °C for 24 h.
4. Immediately after incubation dilute MMP-12 to 20 μg/mL and store at −80 °C until ready to use.

3.3.7 Activation of ProMMP-13

1. Dilute proMMP-13 to 100 μg/mL in TS buffer.
2. Activate proMMP-13 by adding APMA to a final concentration of 1 mM.
3. Incubate at 37 °C for 2 h.
4. Immediately after incubation dilute MMP-13 to 20 μg/mL and store at −80 °C until ready to use.

3.3.8 Activation of ProMT1-MMP

1. Activation buffer: 50 mM Tris, 1 mM $CaCl_2$, 0.5% (v/v) Brij-35, pH 9.0.

Method 1

2. Activate proMT1-MMP at 40 μg/mL with 0.86 μg/mL recombinant furin in activation buffer.
3. Incubate at 37 °C for 1.5 h.
4. Stop furin activation by adding SSM 3 trifluoroacetate to a final concentration of 1 μM.

Method 2

1. Prepare 4-(2-aminoethyl-benzenesulfonyl fluoride hydrochloride) (AEBSF) 100 mM stock in deionized water (*see* **Note 3**).
2. Activate proMT1-MMP at 100 μg/mL with 5 μg/mL recombinant human active trypsin-3 in TS buffer.
3. Incubate at 37 °C for 2 h.
4. Add AEBSF to a final concentration of 1 mM and incubate at room temperature for 15 min to stop the activation.
5. Store the activated enzyme at −80 °C for future use.

3.3.9 Activation of ProMT2-MMP (MMP-15)

1. Prepare AEBSF 100 mM stock in deionized water.
2. Activate proMT2-MMP at 100 μg/mL with 0.1 μg/mL trypsin-3 in TS buffer.
3. Incubate at 37 °C for 2 h.
4. Add AEBSF to a final concentration of 1 mM and incubate at room temperature for 15 min to stop the reaction.
5. Store the activated enzyme at −80 °C for future use.

3.4 Enzymatic Assays Using Knight SSP

Enzyme kinetics can be determined in a microplate reader such as BioTek Synergy 4 running Gen5 1.11, Gen5 2.00, and Gen5 2.01 software as described previously [45, 66]. Manual assays are performed in black low volume 384 well plates.

1. A 12-point serial dilution of Knight SSP substrate is made starting at 20 mM.
2. 5 μL of each peptide solution is loaded in 12 different wells in a 384 well plate.
3. The plate is read to obtain initial fluorescence in relative fluorescence units (RFUs).
4. 5 μL of 2× enzyme stock solution is added to each well.
5. The fluorescence is monitored continuously for 15 min to determine initial reaction rates. The kinetic protocol at 25 °C has 30 s shaking followed by each well read every 20 s.
6. Plates are stored at ambient temperature for 24 h before a final reading. All measurements are done in triplicate.
7. To determine rates of hydrolysis (Corr V_i; μM/s), fluorescence (RFU) is plotted over time (s), slopes are divided by fluorescence change after 24 h, and then multiplied by the substrate concentration (μM) {Corr V_i = (slope/change in RFU) × [peptide]}.
8. Kinetic parameters are calculated by Lineweaver-Burk, Hanes-Woolf, and Eadie-Hofstee linear plots (substrate concentration versus reaction velocity) as well as nonlinear Michaelis-Menten regression by GraphPad prism.
9. When kinetics parameters from the above four modes correlate well, the experiment is considered a success. However, when linear analysis displays significant exponential character, enzyme concentration is reduced and the experiment repeated until linearity is obtained.

3.5 Inhibitor Assays

1. Peptide substrate and inhibitor solutions are prepared using TSB*Zn and left overnight at 4 °C to allow the proper folding of the peptide triple helix.

2. 1–2.5 nM enzyme is incubated with varying concentration of inhibitor for 2 h at room temperature. A 2 h incubation is utilized based on the generally observed behavior of slow on and off rates for tight-binding inhibitors [67] and studies demonstrating that high-affinity phosphinate inhibitors of Zn^{2+} metalloproteinases are slow binding [68].
3. Residual enzyme activity is monitored by adding Knight substrate solution in TSB*Zn to produce a final concentration of $<0.1K_M$.
4. Initial velocity rates are determined from the first 10 min of hydrolysis when product release is linear with time.
5. Fluorescence is measured on a BioTek synergy H1 reader or H4 hybrid reader using $\lambda_{excitation} = 324$ nm and $\lambda_{emission} = 393$ nm.
6. Apparent K_i values are calculated from the following formulas [40]:

$$v_i/v_o = \left\{ E_t - I_t - K_i^{(app)} + \left(\left(E_t - I_t - K_i^{(app)} \right)^2 + 4E_t K_i^{(app)} \right)^{0.5} \right\} \Big/ 2E_t \quad (1)$$

$$K_i^{(app)} = K_i(\{A_t + K_M\}/K_M) \quad (2)$$

where I_t is the total inhibitor concentration, E_t is the total enzyme concentration, A_t is the total substrate concentration, v_o is the activity in the absence of inhibitor, and K_M is the Michaelis constant.

7. The value of $E_t/K_i^{(app)}$ does not exceed 100 so that the inhibitor is distributed in both free and bound forms, and $K_i^{(app)}$ can be calculated by fitting inhibition data to Eq. 1. Because the substrate concentration is less than $K_M/10$, $K_i^{(app)}$ values are insignificantly different from true K_i values.
8. In cases where weak inhibition occurs, $K_i^{(app)}$ values are calculated using $v_i = v_o/(1 + I_t/K_i^{(app)})$.

4 Notes

1. When crude peptide shows unsatisfactory yield and/or purity, a different cleavage cocktail could be used. Please refer to [69].
2. ProMMP-1, proMMP-3, proMMP-8, and proMMP-12 can be activated at 20 ng/μL concentration with a 5 ng chymotrypsin/5 ng trypsin mixture for 30 min at 37 °C. In our experience, this mode of activation results in greater activity of these enzymes compared with the manufacturer's recommended activation protocols. The reaction is stopped by addition of

2 mM PMSF. Enzyme activity is tested with 5 μM Knight SSP in TS buffer.

3. AEBSF solutions in water are slightly acidic. A stock solution is recommended at a concentration of 20 or 100 mM in water. Stock solutions should be stored at a pH less than 7. If a final pH > 7 is required, the pH adjustment should be done shortly before use. Stock solutions are stable for up to 2 months at −20 °C or 1 week at 4 °C. AEBSF should be added to an assay buffer just before use. AEBSF is inactivated by 50% at 37 °C after 5 h.

Acknowledgments

I gratefully acknowledge the National Institutes of Health (CA098799 and NHLBI Contract 268201000036C-0-0-1), the Multiple Sclerosis National Research Institute, and the Texas Higher Education Star Award Program for the support of my laboratory's research on THPIs.

References

1. Woodhead-Galloway J (1980) Collagen: the anatomy of a protein. Edward Arnold Limited, London, pp 10–19
2. Gordon MK, Hahn RA (2010) Collagens. Cell Tissue Res 339:247–257
3. Cole WG (1994) Collagen genes: mutations affecting collagen structure and expression. Prog Nucleic Acid Res Mol Biol 47:29–80
4. Shoulders MD, Raines RT (2009) Collagen structure and stability. Annu Rev Biochem 78:929–958
5. Brodsky B, Shah NK (1995) The triple-helix motif in proteins. FASEB J 9:1537–1546
6. Fields GB, Prockop DJ (1996) Perspectives on the synthesis and application of triple-helical, collagen-model peptides. Biopolymers (Peptide Sci) 40:345–357
7. Jenkins CL, Raines RT (2002) Insights on the conformational stability of collagen. Nat Prod Rep 19:49–59
8. Koide T (2005) Triple helical collagen-like peptides: engineering and applications in matrix biology. Connect Tissue Res 46:131–141
9. Koide T (2007) Designed triple-helical peptides as tools for collagen biochemistry and matrix engineering. Philos Trans R Soc B 362:1281–1291
10. Brodsky B, Thiagarajan G, Madhan B, Kar K (2008) Triple-helical peptides: an approach to collagen conformation, stability, and self-association. Biopolymers 89:345–353
11. Fields GB (2010) Synthesis and biological applications of collagen-model triple-helical peptides. Org Biomol Chem 8:1237–1258
12. Bella J, Eaton M, Brodsky B, Berman HM (1994) Crystal and molecular structure of a collagen-like peptide at 1.9 Å resolution. Science 266:75–81
13. Jenkins CL, Vasbinder MM, Miller SJ, Raines RT (2005) Peptide bond isosteres: Ester or (E)-alkene in the backbone of the collagen triple helix. Org Lett 7:2619–2622
14. Dai N, Wang XJ, Etzkorn FA (2008) The effect of a trans-locked Gly-pro alkene isostere on collagen triple helix stability. J Am Chem Soc 130:5396–5397
15. Dai N, Etzkorn FA (2009) Cis-trans proline isomerization effects on collagen triple-helix stability are limited. J Am Chem Soc 131:13728–13732
16. Kotch FW, Guzei IA, Raines RT (2008) Stabilization of the collagen triple helix by O-methylation of hydroxyproline residues. J Am Chem Soc 130:2952–2953
17. DeRider ML, Wilkens SJ, Waddell MJ, Bretscher LE, Weinhold F, Raines RT, Markley JL (2002) Collagen stability: insights from NMR spectroscopic and hybrid density functional computational investigations of the

effect of electronegative substituents on prolyl ring conformations. J Am Chem Soc 124 (11):2497–2505
18. Shoulders MD, Satyshur KA, Forest KT, Raines RT (2010) Stereoelectronic and steric effects in side chains preorganize a protein main chain. Proc Natl Acad Sci U S A 107:559–564
19. Holmgren SK, Taylor KM, Bretscher LE, Raines RT (1998) Code for collagen's stability deciphered. Nature 392:666–667
20. Holmgren SK, Bretscher LE, Taylor KM, Raines RT (1999) A hyperstable collagen mimic. Chem Biol 6:63–70
21. Dutton G (2007) Development of peptide drugs advances briskly. Gen Engin Biotechnol News 27(10):18–20
22. Thayer AM (2011) Improving peptides. Chem Eng News May 30:13–20
23. Albericio F, Kruger HG (2012) Therapeutic peptides. Future Med Chem 4:1527–1531
24. DePalma A (2015) Peptides: new processes, lower costs. Gen Eng Biotechnol News 35 (13):24–26
25. Fan C-Y, Huang C-C, Chiu W-C, Lai C-C, Liou G-G, Li H-C, Chou M-Y (2008) Production of multivalent protein binders using a self-trimerizing collagen-like peptide scaffold. FASEB J 22:3795–3804
26. Ndinguri MW, Zheleznyak A, Lauer JL, Anderson CJ, Fields GB (2012) Application of collagen-model triple-helical peptide-amphiphiles for CD44 targeted drug delivery systems. J Drug Delivery 2012:592602 592613 pages
27. Yasui H, Yamazaki CM, Nose H, Awada C, Takao T, Koide T (2013) Potential of collagen-like triple helical peptides as drug carriers: their in vivo distribution, metabolism, and excretion profiles in rodents. Biopolymers (Pept Sci) 100:705–713
28. Yamazaki CM, Nakase I, Endo H, Kishimoto S, Mashiyama Y, Masuda R, Futaki S, Koide T (2013) Collagen-like cell-penetrating peptides. Angew Chem Int Ed Engl 52:5497–5500
29. Shinde A, Feher KM, Hu C, Slowinska K (2015) Peptide internalization enabled by folding: triple-helical cell-penetrating peptides. J Pept Sci 21:77–84
30. Koide T, Yamamoto N, Taira KB, Yasui H (2016) Fecal excretion of orally administered collagen-like peptides in rats: contribution of the triple-helical conformation to their stability. Biol Pharm Bull 39:135–137
31. Fallas JA, O'Leary LE, Hartgerink JD (2010) Synthetic collagen mimics: self-assembly of homotrimers, heterotrimers and higher order structures. Chem Soc Rev 39:3510–3527
32. Chattopadhyay S, Raines RT (2014) Collagen-based biomaterials for wound healing. Biopolymers 101:821–833
33. An B, Lin Y-S, Brodsky B (2016) Collagen interactions: drug design and delivery. Adv Drug Deliv Rev 97:69–84
34. Miles AJ, APN S, Furcht LT, Fields GB (1994) Promotion of cell adhesion by single-stranded and triple-helical peptide models of basement membrane collagen a1(IV)531-543: evidence for conformationally dependent and conformationally independent type IV collagen cell adhesion sites. J Biol Chem 269:30939–30945
35. Knight CG, Morton LF, Peachey AR, Tuckwell DS, Farndale RW, Barnes MJ (2000) The collagen-binding A-domains of integrin a1b1 and a2b1 recognize the same specific amino acid sequence, GFOGER, in native (triple-helical) collagens. J Biol Chem 275:35–40
36. Kim JK, Xu Y, Xu X, Keene DR, Gurusiddappa S, Liang X, Wary KK, Hook M (2005) A novel binding site in collagen type III for integrins a1b1 and a2b1. J Biol Chem 280:32512–32520
37. Lebbink RJ, Raynal N, de Ruiter T, Bihan DG, Farndale RW, Meyaard L (2009) Identification of multiple potent binding sites for human leukocyte associated Ig-like receptor LAIR on collagens II and III. Matrix Biol 28:202–210
38. Haywood J, Qi J, Chen CC, Lu G, Liu Y, Yan J, Shi Y, Gao GF (2016) Structural basis of collagen recognition by human osteoclast-associated receptor and design of osteoclastogenesis inhibitors. Proc Natl Acad Sci U S A 113:1038–1043
39. Babine RE, Bender SL (1997) Molecular recognition of protein-ligand complexes: applications to drug design. Chem Rev 97:1359–1472
40. Lauer-Fields JL, Brew K, Whitehead JK, Li S, Hammer RP, Fields GB (2007) Triple-helical transition-state analogs: a new class of selective matrix metalloproteinase inhibitors. J Am Chem Soc 129:10408–10417
41. Georgiadis D, Dive V (2015) Phosphinic peptides as potent inhibitors of zinc-Metalloproteases. Top Curr Chem 360:1–38
42. Gall AL, Ruff M, Kannan R, Cuniasse P, Yiotakis A, Dive V, Rio MC, Basset P, Moras D (2001) Crystal structure of the stromelysin-3 (MMP-11) catalytic domain complexed with a phosphinic inhibitor mimicking the transition-state. J Mol Biol 307:577–586
43. Lauer-Fields JL, Chalmers MJ, Busby SA, Minond D, Griffin PR, Fields GB (2009) Identification of specific Hemopexin-like domain

residues that facilitate matrix metalloproteinase Collagenolytic activity. J Biol Chem 284:24017–24024

44. Bertini I, Fragai F, Luchinat C, Melikian M, Toccafondi M, Lauer JL, Fields GB (2012) Structural basis for matrix metalloproteinase 1 catalyzed Collagenolysis. J Am Chem Soc 134:2100–2110
45. Lauer-Fields JL, Whitehead JK, Li S, Hammer RP, Brew K, Fields GB (2008) Selective modulation of matrix metalloproteinase 9 (MMP-9) functions via exosite inhibition. J Biol Chem 283:20087–20095
46. Bhowmick M, Sappidi RR, Fields GB, Lepore SD (2011) Efficient synthesis of Fmoc-protected Phosphinic Pseudodipeptides: building blocks for the synthesis of matrix metalloproteinase inhibitors (MMPIs). Biopolymers (Pept Sci) 96:1–3
47. Bhowmick M, Fields GB (2012) Synthesis of Fmoc-Gly-Ile Phosphinic Pseudodipeptide: residue specific conditions for construction of matrix metalloproteinase inhibitor building blocks. Int J Pept Res Ther 18:335–339
48. Bhowmick M, Stawikowska R, Tokmina-Roszyk D, Fields GB (2015) Matrix metalloproteinase inhibition by Heterotrimeric triple-helical peptide transition state analogs. Chembiochem 16:1084–1092
49. Bhowmick M, Tokmina-Roszyk D, Onwuha-Ekpete L, Harmon K, Robichaud T, Fuerst R, Stawikowska R, Steffensen B, Roush WR, Wong H, Fields GB (2017) Second generation triple-helical peptide transition state analog matrix metalloproteinase inhibitors. J Med Chem 60:3814–3827
50. Lauer-Fields JL, Sritharan T, Stack MS, Nagase H, Fields GB (2003) Selective hydrolysis of triple-helical substrates by matrix metalloproteinase-2 and -9. J Biol Chem 278:18140–18145
51. Minond D, Lauer-Fields JL, Cudic M, Overall CM, Pei D, Brew K, Visse R, Nagase H, Fields GB (2006) The roles of substrate thermal stability and P_2 and P'_1 subsite identity on matrix metalloproteinase triple-helical peptidase activity and collagen specificity. J Biol Chem 281:38302–38313
52. de Castro Brás LE, Cates CA, DeLeon-Pennell KY, Ma Y, Iyer RP, Halade GV, Yabluchanskiy A, Fields GB, Weintraub ST, Lindsey ML (2014) Citrate synthase is a novel in vivo matrix Metalloproteinase-9 substrate that regulates mitochondrial function in the post-myocardial infarction left ventricle. Antioxid Redox Signal 21:1974–1985
53. Lauer-Fields JL, Broder T, Sritharan T, Nagase H, Fields GB (2001) Kinetic analysis of matrix metalloproteinase triple-helicase activity using fluorogenic substrates. Biochemistry 40:5795–5803
54. Del Valle JR, Goodman M (2003) Asymmetric hydrogenations for the synthesis of Boc-Protected-4-Alkylprolinols and Prolines. J Org Chem 68:3923–3931
55. Neumann U, Kubota H, Frei K, Ganu V, Leppert D (2004) Characterization of Mca-Lys-pro-Leu-Gly-Leu-Dpa-Ala-Arg-NH_2, a fluorogenic substrate with increased specificity constants for collagenases and tumor necrosis factor converting enzyme. Anal Biochem 328:166–173
56. Bhowmick M, Fields GB (2013) Stabilization of triple-helical peptides for in vivo applications. Methods Mol Biol 1081:167–194
57. Fields GB, Tian Z, Barany G (1993) Principles and practice of solid-phase peptide synthesis. In: Grant GA (ed) synthetic peptides: a User's guide. W.H. Freeman & Co, New York, pp 77–183
58. Fields CG, Lovdahl CM, Miles AJ, Matthias-Hagen VL, Fields GB (1993) Solid-phase synthesis and stability of triple-helical peptides incorporating native collagen sequences. Biopolymers 33:1695–1707
59. Fields CG, Mickelson DJ, Drake SL, McCarthy JB, Fields GB (1993) Melanoma cell adhesion and spreading activities of a synthetic 124-residue triple-helical "mini-collagen". J Biol Chem 268:14153–14160
60. Grab B, Miles AJ, Furcht LT, Fields GB (1996) Promotion of fibroblast adhesion by triple-helical peptide models of type I collagen-derived sequences. J Biol Chem 271:12234–12240
61. Lauer-Fields JL, Tuzinski KA, Shimokawa K, Nagase H, Fields GB (2000) Hydrolysis of triple-helical collagen peptide models by matrix metalloproteinases. J Biol Chem 275:13282–13290
62. Lauer-Fields JL, Nagase H, Fields GB (2000) Use of Edman degradation sequence analysis and matrix-assisted laser desorption/ionization mass spectrometry in designing substrates for matrix metalloproteinases. J Chromatogr A 890:117–125
63. Malkar NB, Lauer-Fields JL, Borgia JA, Fields GB (2002) Modulation of triple-helical stability and subsequent melanoma cellular responses by single-site substitution of fluoroproline derivatives. Biochemistry 41:6054–6064
64. Yu Y-C, Tirrell M, Fields GB (1998) Minimal lipidation stabilizes protein-like molecular architecture. J Am Chem Soc 120:9979–9987

65. Yu Y-C, Berndt P, Tirrell M, Fields GB (1996) Self-assembling amphiphiles for construction of protein molecular architecture. J Am Chem Soc 118:12515–12520
66. Palmier MO, Van Doren SR (2007) Rapid determination of enzyme kinetics from fluorescence: overcoming the inner filter effect. Anal Biochem 371:43–51
67. Copeland RA (2005) Tight binding inhibition. In: Copeland RA (ed) Evaluation of enzyme inhibitors in drug discovery. John Wiley & Sons, Inc., Hoboken, NJ, pp 178–213
68. Yiallouros I, Vassiliou S, Yiotakis A, Zwilling R, Stöcker W (1998) Phosphinic peptides, the first potent inhibitors of astacin, behave as extremely slow-binding inhibitors. Biochem J 331:375–379
69. Guy CA, Fields GB (1997) Trifluoroacetic acid cleavage and Deprotection of resin-bound peptides following synthesis by Fmoc chemistry. Methods Enzymol 289:67–83

Index

A

Age-synchronizing 174, 176, 179, 182, 183
Aging ..... v, 136, 146, 169–186, 209
Amino propeptide of type III procollagen (PIIINP) 190

B

Biomarkers 87–90, 93, 191
Biomedical properties 17
Biophysical characterization 23, 203
Biopsy 145, 147, 153, 190
Bone 39, 40, 69, 73, 95, 99, 143, 229
Bone resorption 135

C

Caenorhabditis elegans (*C. elegans*) 169–186
Calcium phosphate 40
Cancer-associated fibroblasts (CAFs) 208–212, 221
Carboxyl propeptide of type I procollagen (PICP) 190
Cell adhesion ..... v, 160–161, 205
Chondrocytes 158–160, 164
Cloning 3, 7, 10, 101
Co-immunoprecipitations 102, 110, 111
Collagenase 80, 83, 158, 159, 210, 223
Collagen fibers 145, 150, 152, 153, 204, 221
Collagen hybridizing peptide (CHP) 135–143
Collagenopathies 3, 96
Collagen proteostasis network 95, 96, 110
Collagen remodeling 207, 208, 210, 212, 213
Collagen VI 164
Collagen type I 18, 23, 24, 173, 192, 209
Colons 129–132
Cross-linking ..... v, 23–26, 29, 31, 33–35, 221
Cryogenic TEM (cryoTEM) 40, 44–48, 50, 52
Cuticles 171, 175, 182–184, 186
Cytotoxicity 24

D

Decellularization 129–132
Dystrophic epidermolysis bullosa (DEB) 4

E

ELISA 191, 192, 194–199
Exon skipping 4
Extracellular matrix (ECM) ..... v, 23, 57, 61, 63, 65, 71, 72, 115–126, 129–132, 135, 157–164, 169–171, 175, 182–184, 186, 189, 190, 204–206, 208, 211, 213, 221, 222, 230

F

Freeze-cracking 172, 176–177

G

γ-glutamyl transferase (GGT) 190
Gibson assembly 7, 8, 10
Glutamyl endoproteinase (GluC) 118, 120, 122
Glutaraldehyde (GTA) 22, 24, 27–29, 31, 33–35, 42, 48, 130

H

Herovici staining 171, 175, 177
Histopathology ..... v, 135–144
Hybridization 135–144
Hydroxyprolines 14, 21, 60, 61, 63, 69, 70, 82–84, 87, 88, 136, 170, 171, 177, 178, 181

I

Immature crosslinks 80, 83–85
Immunostaining 137
In situ 40, 135–144, 158
Integrins ..... v, 157–164, 205, 208, 211, 231
Interactomes ..... v, 3, 95–112
Isobaric Tag for Relative and Absolute Quantitation (iTRAQ) 112, 116, 117

L

Liver fibrosis ..... v, 189–200, 209
Lung fibrosis 204
Lung metastases 204
Lysyl oxidase (LOX) 23, 204, 209
  like-1 79
  like-2 205
  like-3 79
  like-4 79

Irit Sagi and Nikolaos A. Afratis (eds.), *Collagen: Methods and Protocols*, Methods in Molecular Biology, vol. 1944, https://doi.org/10.1007/978-1-4939-9095-5, © Springer Science+Business Media, LLC, part of Springer Nature 2019

M

Macrophages 24, 29, 31, 33, 203–213
Mass spectrometry ..... v, 57, 61, 79–93, 95–112, 115, 117, 122, 123, 236, 244
Matrix metalloproteinases (MMPs) ..... v, 136, 190, 206, 210, 231–234, 245
Matrix superstructures 4
Mature crosslinks 80, 83–85
Multiphoton microscopy ..... v, 145–154

P

Peptide-based drugs 231
Procollagen C-proteinase enhancer-1 (PCPE-1) 189–200
Proteomics ..... v, 95–112, 122, 207, 213

R

Radio frequency (RF) 58, 68, 71, 85, 86

S

Scaffolds ..... v, 23–35, 95, 130, 203–205, 210, 213
Scanning electron microscope (SEM) 129–132
Second harmonic generation (SHG) 135, 145, 146, 148–153
Single reaction monitoring (SRM) 85, 86
Skin ..... v, 4, 18, 20, 21, 34, 70, 80, 83–85, 91, 95, 145–154, 170, 171, 173, 209, 224, 229
Solid phase extraction (SPE) 80, 81, 84, 85, 92
Stochastic optical reconstruction microscopy (STORM) 40, 48–51, 53

T

Tandem mass tag (TMT) 112, 115–126
Terminal amine isotopic labeling of substrates (TAILS) 115–126
Tissue ..... v, 11, 19–21, 23, 24, 29, 31, 33, 39, 57, 60, 61, 63, 65, 66, 71, 73, 79–93, 95, 129, 135–137, 139–142, 145, 151–153, 169–186, 189, 190, 204, 206, 208, 210–212, 222, 225, 229, 230, 234
Transition state analog 231, 232
Transmission electron microscopy (TEM) 40, 42–47, 51, 52, 161–164
Triple-helical inhibitor 229–249
Tumor-associates macrophages (TAMs) 208–213
Tumor microenvironment ..... v, 203–213, 221

U

Ultra-high performance liquid chromatography-triple quadrupole mass spectrometry (UHPLC-MS/MS) 80, 82–83, 85–90